

Agnieszka Weronika Lach

Hydrogen safety in confined spaces





Agnieszka Weronika Lach

Hydrogen safety in confined spaces

A PhD dissertation in

Process, Energy and Automation Engineering

© 2022 Agnieszka Weronika Lach
Faculty of Technology, Natural Sciences and Maritime Studies
University of South-Eastern Norway
Porsgrunn, 2022

Doctoral dissertations at the University of South-Eastern Norway no. 130

ISSN: 2535-5244 (print)
ISSN: 2535-5252 (online)

ISBN: 978-82-7206-677-1 (print)
ISBN: 978-82-7206-678-8 (online)



This publication is, except otherwise stated, licenced under Creative Commons. You may copy and redistribute the material in any medium or format. You must give appropriate credit provide a link to the license, and indicate if changes were made.
<http://creativecommons.org/licenses/by-nc-sa/4.0/deed.en>

Dedication

Dedicated to my boys Joachim and Jørgen

and to my best friend Aleksandra

Preface

This work was fulfilled at the University in South-Eastern Norway (USN) to obtain the degree of Doctor of Philosophy at the Faculty of Technology, Natural Science and Maritime Science. The dissertation presents my doctoral research on hydrogen safety with a special focus on hydrogen releases in closed and semi-closed enclosures. The collection of scientific journals is the main contribution to this thesis and is included in Part II. This project has been part of the European research project HyTunnel-CS to perform pre-normative research for the safety of hydrogen-driven vehicles and transport in confined spaces like tunnels, covered carparks and private garages.

I would like to thank my main supervisor Dr André Vagner Gaathaug (Associate Professor at USN) for his devotion to my scientific development and support throughout the whole period of this project. His expert guidance and provoking techniques were inspirational and keeps me busy, leading to my professional improvement. I am also very grateful for all feedback, discussions and excellent guidance from my co-supervisor professor Dr Knut Vågsæther. My gratitude is extended to the rest of my research group Joachim Lundberg, Per Morten Hansen, Dag Bjerketvedt, Mathias Henriksen, Prasanna Welahettige for discussions and advice.

Further, I am grateful to Øyvind Johansen for his technical guidance, Fredrik Hansen and Bjørn Vegard Tveraaen for explaining to me and helping with the electrical part of my experimental setup. I would also thank Knut Ove Hauge for his help and support in conducting experiments at the Norwegian Defence Research Institute in Horten.

A special thanks to my new family, Jørgen who keeps me laughing and Joachim for the endless support. Helena Brožek, all my friends and the rest of my wonderful family, thank you for all your support and for believing that I can do it.

Enjoy your reading!

7th January 2022, Porsgrunn

Agnieszka Weronika Lach

Acknowledgments

I wish to acknowledge funding from the Fuel Cells and Hydrogen 2 Joint Undertaking (JU) under grant agreement No 826193. The JU receives support from the European Union's Horizon 2020 research and innovation programme and United Kingdom. Germany. Greece. Denmark. Spain. Italy. Netherlands. Belgium. France. Norway. Switzerland.

This work was performed within MoZEES, a Norwegian Centre for Environment-friendly Energy Research (FME), co-sponsored by the Research Council of Norway (project number 257653) and 40 partners from research, industry, and the public sector.

Abstract

Unwanted hydrogen releases in confined spaces can be significantly more dangerous compared to open-air scenarios. The transition towards a zero-emission system results in a growth of hydrogen-driven vehicles which increases hazards and risk of accidents. Implementing hydrogen technologies into applications that are available to the public needs investigations of the many possible accidental scenarios. The knowledge should be disseminated to specialists, first responders and end-users. The experimental campaigns presented in this study are part of a pre-normative research project to develop a recommendation for Regulation, Codes, and Standards (RCS) and an engineering tool for hydrogen safety engineers.

Four experimental campaigns were conducted during this work to investigate the results from hydrogen releases in the worse case scenarios. The large and full-scale experimental setups were designed to investigate ignited and unignited hydrogen releases. The 15 m³ explosive chamber was used to investigate overpressures – from Pressure Peaking Phenomena in an enclosure similar to private garages. The 40 ft ISO container was used for the investigation of hydrogen dispersion and thermal effects from hydrogen jet fires in enclosures similar to carparks. The hydrogen releases were performed with mass flow rates from 1.4 g/s to 13 g/s from reservoir pressures from 27 bar to 700 bar through nozzle diameters 0.5 mm – 4.0 mm, depending on the experiments and experimental campaign.

The first two campaigns investigated the Pressure Peaking Phenomena from unignited and ignited releases. The experimental results were in good agreement with the developed analytical models, where the perfect mix assumption was confirmed. The model allows estimating the minimum ventilation area for the given mass flow rate and conversely. For the unignited hydrogen releases, the mass flow rate had to be relatively high and the ventilation area relatively small to observe the Pressure Peaking Phenomena. For the ignited releases the much lower mass flow rate will result in much higher overpressure compared to unignited releases for a similar ventilation size. The highest obtained overpressure for unignited releases was 8.1 kPa, resulted from the

mass flow rate of 4.75 g/s and 0.0006 m² vent area. The highest measured overpressure during ignited releases was 48.1 kPa which resulted from the mass flow rate of 8.62 g/s and 0.0055 m² vent area.

Experimental campaigns in the 40 ft ISO container were imitating hydrogen releases from the car – hydrogen jets impinging on the floor (90° - unignited jets and 90° and 45° - ignited jets). During the first experimental campaign in the 40 ft ISO container, the mechanical ventilation was investigated for 6 and 10 air changes per hour. The results showed influence on the time when the cloud is flammable but not for the maximum concentration in the cloud. The second experimental campaign in the 40 ft ISO container investigated thermal effects from hydrogen jet fires. The temperature results showed safe access to the car in case of an accident and the most dangerous areas. The temperature in the ventilation pipe did not exceed 300 °C from all releases. While inside the container, under the ceiling, this temperature limit of 300 °C was not exceeded only from releases through a 0.5 mm diameter.

Keywords: Hydrogen safety, Pressure Peaking Phenomena, Large scale experiments, Hydrogen dispersion, Hydrogen jet fires, Overpressures, Mechanical ventilation, Thermal effects.

List of papers

Article A

A.W. Lach, A.V. Gaathaug, K.Vågsæther, *Pressure peaking phenomena: Unignited hydrogen releases in confined spaces – large-scale experiments*, International Journal of Hydrogen Energy, Volume 45, Issue 56, November 2020, Pages 32702-32712, doi: <https://doi.org/10.1016/j.ijhydene.2020.08.221>

Article B

A.W. Lach, A.V. Gaathaug, *Large scale experiments and model validation of Pressure Peaking Phenomena-ignited hydrogen releases*, International Journal of Hydrogen Energy, Volume 46, Issue 11, February 2021, Pages 8317-8328, doi: <https://doi.org/10.1016/j.ijhydene.2020.12.015>

Article C

A.W. Lach, A.V. Gaathaug, *Effect of Mechanical Ventilation on Accidental Hydrogen Releases—Large-Scale Experiments*, Energies, Volume 14, Issue 11, May 2021, Pages 3008, doi: <https://doi.org/10.3390/en14113008>

List of Conference proceedings

Proceeding A

A.W.Lach, T.G. Østby, *Parameter estimation using Bayesian approach for a model of Pressure Peaking Phenomena-ignited H₂ releases*. Proceedings of The 61st SIMS Conference on Simulation and Modelling SIMS 2020, September 21-24, Virtual Conference, Finland 2020. doi: <https://doi.org/10.3384/ecp20176>

Proceeding B

A.W. Lach, A.V. Gaathaug, *Pressure peaking phenomena: Large-scale experiments of ignited and unignited hydrogen releases*, pp. 813 - 826. In: Proceedings of the 13th International Symposium on Hazards, Prevention and Mitigation of Industrial Explosions (ISHPMIE 2020), Braunschweig, Germany, 2020. doi: [10.7795/810.20200724](https://doi.org/10.7795/810.20200724)

Proceeding C

A.W. Lach, A.V. Gaathaug, *Effect of Mechanical Ventilation on Accidental Hydrogen Releases—Large-Scale Experiments*, Proceedings of the 9th International Conference on Hydrogen Safety (ICHS 2021), 21-24 September, On-line Conference, Edinburg, Scotland 2021

Proceeding D

A.W. Lach, A.V. Gaathaug, K.Vågsæther, *Thermal effects from downwards hydrogen impinging jet flame – experimental results from high-pressure releases in a carpark*, It was submitted to the 10th International Seminar on Fire and Explosion Hazards on the 10th January 2022 and accepted 4th March 2022.

List of Published Supplementary Data

Supplementary Data A

A.W. Lach, A.V. Gaathaug, *Hydrogen Safety: Pressure Peaking Phenomena-unignited releases*. The University of South-Eastern Norway. Dataset, doi: [10.23642/usn.17932439](https://doi.org/10.23642/usn.17932439)

Supplementary Data B

A.W. Lach, A.V. Gaathaug, *Hydrogen Safety: Pressure Peaking Phenomena-ignited releases*. The University of South-Eastern Norway. Dataset, doi: [10.23642/usn.17934047](https://doi.org/10.23642/usn.17934047)

Supplementary Data C

A.W. Lach, A.V. Gaathaug, *Experimental data – Hydrogen Safety- mechanical ventilation*. The University of South-Eastern Norway. Dataset, doi: [10.23642/usn.14405903](https://doi.org/10.23642/usn.14405903)

Supplementary Data D

A.W. Lach, A.V. Gaathaug, *Experimental data – Hydrogen Safety- thermal effects*. The University of South-Eastern Norway. Dataset, doi: [10.23642/usn.17695082](https://doi.org/10.23642/usn.17695082)

List of Co-authorship

Co-Article A

D. Cirrone, D. Makarov, A.W. Lach, A.V. Gaathaug, V.Molkov, *The Pressure Peaking Phenomenon for Ignited Under-Expanded Hydrogen Jets in the Storage Enclosure: Experiments and Simulations for Release Rates of up to 11.5 g/s*. *Energies*, Volume 15, Issue 1, December 2021, Pages, 271, doi: <https://doi.org/10.3390/en15010271>

Table of contents

Dedication	I
Preface	III
Acknowledgments	V
Abstract	VII
List of papers	IX
List of Conference proceedings	IX
List of Published Supplementary Data	X
List of Co-authorship	XI
Table of contents	XIII
Part I	1
1 Introduction	3
1.1 Background	3
1.1.1 Hydrogen driving vehicles	4
1.1.2 Regulation codes and standards (RCS) for hydrogen driven vehicles	5
1.1.3 Accidents with hydrogen applications	6
1.2 Research objectives	8
1.3 Outline of the thesis.....	9
2 Literature review	10
2.1 Gas releases	11
2.2 Hydrogen dispersion – in confined spaces	14
2.2.1 Effect of ventilation.....	16
2.2.2 Effect of discharge parameters.....	19
2.2.3 Effect of enclosure geometry.....	22
2.3 Jet fires	23
2.3.1 Ignition mechanism.....	25
2.3.2 Flame length.....	26
2.3.3 Blow off	30
2.3.4 Thermal effects and separation distances.....	31
2.4 Pressure Peaking Phenomena	34

3 Experimental work	39
3.1 Pressure Peaking Phenomena (PPP).....	40
3.1.1 Geometry	41
3.1.2 Instrumentation and logging	44
3.1.3 General Procedure	45
3.1.4 Analytical models	46
3.1.5 Results and analysis	48
3.2 Hydrogen releases in covered carpark	59
3.2.1 Geometry	61
3.2.2 Instrumentation and logging	65
3.2.3 General Procedure	73
3.2.4 Results and analysis	74
4 Summary	88
4.1 The upper limit of hydrogen release rate that will not require change in the ventilation system.....	89
4.2 Effectiveness of regulated ventilation systems in case of hydrogen release accident.....	89
4.3 Thermal effects of hydrogen non-premixed turbulent combustion on a vehicle, structure and evacuation in covered carpark	90
4.4 Pressure effects from ignited and unignited hydrogen releases in a private garage.....	90
References	93
Part II.....	103
Article A.....	105
Article B.....	119
Article C.....	133
Proceedings A.....	149
Proceedings B.....	159
Proceedings D	175
Co-Article A	189
Errata	211

Part I

Overview

1 Introduction

Hydrogen is playing a significant role in changing the transport industry in order to minimize/eliminate greenhouse gas emissions. The development of hydrogen applications has grown very fast in the last years and relevant hazards have been investigated. The consequences of indoor hydrogen releases differ significantly from outdoor releases and can affect people, structures, and the environment. Due to differences in chemical and physical parameters of hydrogen from other fuels, safety engineering tools must be developed. The hydrogen properties lead to specific challenges that the transport industry needs to face. The advantage of hydrogen is its buoyancy, allowing gas to escape very rapidly from the place of release/accident and disappear in the air. For confined spaces, it can accumulate in a flammable cloud near the ceiling. The accumulation of the cloud creates a risk of high hydrogen concentration and hence explosion hazards. Due to hydrogen's high diffusion coefficient in air and wide flammability range, the new safety hazards have to be identified and mitigated [1].

1.1 Background

The challenge of implementing a hydrogen system among the public is safety regulation codes and standards that reflect relevant hazards and acquainting the community with the technology and safety parameters. One hazard of compressed hydrogen storage is the accidental release of hydrogen. This could be a result of a component leak or a sudden release of a thermally-activated pressure relief device (TPRD). Different application manufacturers use different TPRD diameters, which reflects a variety of expected mass flows in the case of a failure or release. It is suggested that a TPRD diameter of 0.5 mm would be inherently safe for hydrogen cars in naturally vented car parks [2]. The relationship between the hydrogen discharge ratio and the enclosure ventilation is a crucial parameter to avoid or significantly reduce the risk of the enclosure's collapse. Pressure peaking phenomena (PPP) is the effect of introducing a light gas into a vented volume of denser gas. This will result in a nonequilibrium pressure

as the light gas pushes the dense gas out at the vent. This pressure can reach destructive levels for buildings and compartments. This effect was first observed by Brennan et al. [3] as they used CFD to investigate an unignited PRD release from 350 bar through a 5.08 mm nozzle inside a 30.4 m³ volume. For unignited releases of gas, this phenomenon is only observed for gases lighter than air, and it is most relevant for hydrogen.

1.1.1 Hydrogen driving vehicles

The transport sector is one of the biggest emissions source in Norway accounting for 17%, while 8.6 % comes from domestic shipping [4]. The Norwegian Government's hydrogen strategy is part of a plan to meet zero-emissions goals in the transport sector by 2050 (Table 1). In 2019, 149 hydrogen driven cars, 1 light van, 5 buses and 1 hydrogen truck were registered in Norway[4,5]. It's over 100 hydrogen-powered vehicles (HPV) more compared to 2016. In Europe 1300 hydrogen driving vehicles have been registered. Comparing Norway (156 HPV) to Germany (600 HPV) per capita, results in 29 HPV/1mln capita and 7.2 HPV/1mln capita respectively. More than 200 Toyota Mirais will be delivered to Denmark by end of 2022, scaling up hydrogen taxis significantly contributing to the decarbonisation of Copenhagen [6]. The cost for hydrogen fuel per 01/2022 was ca. 90 NOK¹/kg making it cost-competitive to conventional cars (~0.77 NOK/km for hydrogen cars and ~1.09 NOK/km for 45 l gasoline tank with 17 NOK/l) [7,8]. Planned and invested actions for hydrogen development among European countries leads to rapid development in the hydrogen road map in Europe (Table 1). The pessimistic scenario listed in Table 1 will not allow to reach the EU's climate goals by 2050.

Table 1: Zero-emissions strategies: a hydrogen road map for Europe [9] and Norwegian targets [4].

	Europe	Norway
By 2030	1 in 22 passenger cars (of 3.7 mln)	50% reduction in emissions from the transport sector (compared to 2005)

¹ NOK – Norwegian krone

	1 in 12 light commercial vehicles, LCV (of 500,000) 45,000 trucks 570 trains 3,700 hydrogen refuelling stations (HRS) in Europe		50 % reduction in emissions from domestic shipping Zero-emission transport: 75% of new long-distance buses, 50% of trucks and all goods distribution in the urban centres
By 2050	Ambitious: 45 mln passenger cars 6.5 mln LCV 1.7 mln trucks 250,000 buses	Pesysmistic 1.4 mln passenger cars 700,000 LCV 380,00 trucks 60,000 buses	Transport must be virtually zero emissions

Hydrogen driven passenger cars are equipped with one or more hydrogen tanks (350 bar or 700 bar), trucks, trains and ferries have more than one hydrogen tank (200-700 bar). The hydrogen system has installed TPRD for safety purposes, but the diameter is not publicly accessible. The diameter varies from 2.0 mm up to 6.0 mm. The importance of the TPRD activation is to allow hydrogen to escape in case of fire, hence reducing pressure in the tank to prevent rupture. However, rapid hydrogen discharges may lead to catastrophic consequences when they occur in confined spaces. The activation of a TPRD may also happen by a mechanical failure and the possible consequences need to be investigated in order to secure safe hydrogen discharge.

1.1.2 Regulation codes and standards (RCS) for hydrogen driven vehicles

The lack of RCS with recognition of Hydrogen Powered Vehicles (HPV) became an issue for the transport sector with hydrogen application development. The existing RCS considering hydrogen as a fuel (not only as a dangerous gas) are related mostly to Hydrogen Refueling Station (HRS). The vehicles with alternative fuel (i.e. hydrogen) are not part of RCS for confined spaces like a tunnel, covered carpark, private garages. The first responder's action plan is not prepared for HPV – not allowing the immediate entry to the enclosure (tunnel) with accidents classified in dangerous goods class 2. Norway

is an exceptional country with regulations for ferries but road transport remain an issue like other EU countries. The existing standards used for fire protection and safety in confined spaces, relevant for the thesis work are listed below with their specifics:

- *The application of fire safety engineering principles to fire safety design of buildings - Human factors. Life safety strategies. Occupant evacuation, behaviour and condition (Sub-system 6)*, British Standards Institution, BSI PD 7974-6: 2004 – min 3 air change per hour (ACH) ventilation rate for carpark with natural ventilation (2.5 % of the floor area), min 6 ACH for carpark without natural ventilation and 10 ACH in carpark where cars stay in a queue with a running engine. The temperature limitation is classified as class F300 i.e. temperature limit for the structure of the building and ventilation system is 300 °C [10].
- *Calculation of areas and volumes of buildings*, Norwegian Standard, NS 3940: 2012 – accordingly to the Norwegian Building Authority: “Rooms with polluting activities and processes must have sufficient exhaust to maintain satisfactory air quality” [11]; ventilation rate for special rooms are given accordingly to a floor gross area: carpark for long-term parking – 3 m³ per hour per m² gross area, carpark for short-term parking – 6 per hour per m² gross area.
- *Components for smoke and heat control systems. Code of practice on functional recommendations and calculation methods for smoke and heat control systems for covered car parks*, British Standard Institution, BSI 7346-7: 2013 – the exposure time limits to convected heat with < 10 % H₂O is 5 min for 115 °C and 1 min for 180 °C. For a 100% saturated atmosphere the exposure time limit is up to 30 min for <60 °C [12].

1.1.3 Accidents with hydrogen applications

The well known incidents involving hydrogen are listed below.

- 1937 – Hindenburg disaster, Germany; when the airship was landing the combustible zeppelin's structure got ignited. As the consequence, the hydrogen

(used for lifting the zeppelin) ignited. The diffusive combustion of hydrogen in the air was not a cause of the disaster as has been presented over the years [13].

- 1985 – Explosion at N1 ammonia plant, Norway; a large amount of hydrogen leaked due to valve faulty gasket. Undetected on time hydrogen leak mixed with air. The unknown source of ignition caused a big explosion killing two people [14].
- 2011 – Fukushima nuclear accident, Japan; the explosion at the nuclear power plant was the final consequence caused by the chain of events initiated by a tsunami. First, the tsunami caused failure in the cooling system (loss of coolant accident – LOCA) which led to hydrogen production in the reactor. The safety system vented the hydrogen to avoid overpressure inside the reactor. First, from primary containment to secondary containment where it mixed with air and eventually ignited [15].
- 2019 – Hydrogen tank explosion in Gangwon technopark, South Korea; hydrogen produced by the water electrolysis was stored outdoor in a steel tank at the P2G testing site of the research centre. The oxygen permeated to the tank (storage capacity 1 MPa). An unknown source of ignition caused the ignition of the H₂/O₂ mixture and tank explosion killing two people [16].

Some of the recent accidents in the transport sector:

- 2019 – Explosion in Uno-X fueling station in Norway; an error in a plug assembly in a high-pressure storage tank caused the leakage, which was undetected. The mass flow rate continued to grow, leading to a large mass flow of hydrogen into the air. The source of ignition of the H₂/air mixture is unknown [17].
- 2020 – Explosion of hydrogen tanker, Taiwan; road accident of the hydrogen tanker (collision with construction's elevation) resulted in the dispatch of the hydrogen unit from the rest of the vehicle. The impact of the fall on a second road (20 m below) resulted in an explosion [18].
- 2021 – Explosion in Medupi Power Station, South Africa; the coal plant with a hydrogen generator. During preparation for the leak test, the procedures were

not followed resulting in purging air into the generator while a fair amount of hydrogen was still present. The hydrogen-air mixture ignited leading to explosion [19].

Hydrogen applications are very well developed in many industry sectors like petrochemical, metallurgy or nuclear. However, safety precautions used in the industry were established for experts and trained workers. When introducing hydrogen application into the public sector (transport), more conservative safety measures are needed.

1.2 Research objectives

This PhD project was pre-normative research for hydrogen releases and fires in confined spaces, which will contribute to increasing the safety of hydrogen energy systems. The work goal is closely related to cooperation with the EU project: HyTunnel-CS, to make integral recommendations related to the risk associated with hydrogen vehicles in tunnels and confined spaces. The work will focus on hydrogen dispersion, ventilation prospects, and pressure peaking phenomenon for unignited and ignited hydrogen releases in enclosures. The experimental work was designed to answer the research question with the goal of filling the knowledge gaps:

1. The upper limit of hydrogen release rate that will not require change in the ventilation system.
2. Effectiveness of regulated ventilation systems in case of hydrogen release accident.
3. Thermal effects of hydrogen non-premixed turbulent combustion on a vehicle, structure and evacuation in covered carpark.
4. Pressure effects from ignited and unignited hydrogen releases in a private garage.

Figure 1.1 presents the author's experimental approach for the investigation of the presented objectives.

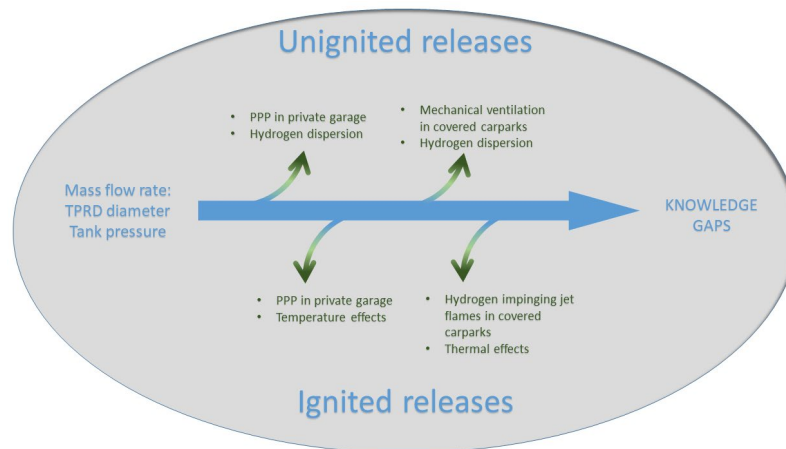


Figure 1.1: Illustration of research contributions and 'work path' included in this thesis.

Three scientific journal articles and four scientific conference proceedings documented answers for the thesis objectives. Article A and B and conference proceedings A and B investigated the first two and the last objective. Article C and conference proceeding C investigated the first three objectives and conference proceedings D investigated objective 4.

1.3 Outline of the thesis

The PhD thesis consists of two parts. Part I is divided into four chapters providing a broad overview of the research project. The research problem and main objectives are described in Chapter 1. The literature review presented in Chapter 2 includes the general information and previous work on hydrogen dispersion, natural and mechanical ventilation, hydrogen jet fires and pressure peaking phenomena. This chapter serves the reader as necessary background and scientific information relevant to unignited and ignited hydrogen releases in confined spaces. A detailed description of the experimental work and a summary of its results, presented in the attached articles, are given in Chapter 3. Finally, a short summary of all findings is presented in chapter 4. Part II of the thesis is a collection of published and submitted scientific articles. Before each article, the author's contribution is presented.

2 Literature review

This chapter presents the selected review on related phenomena giving the necessary background knowledge as shown in Figure 2.1.

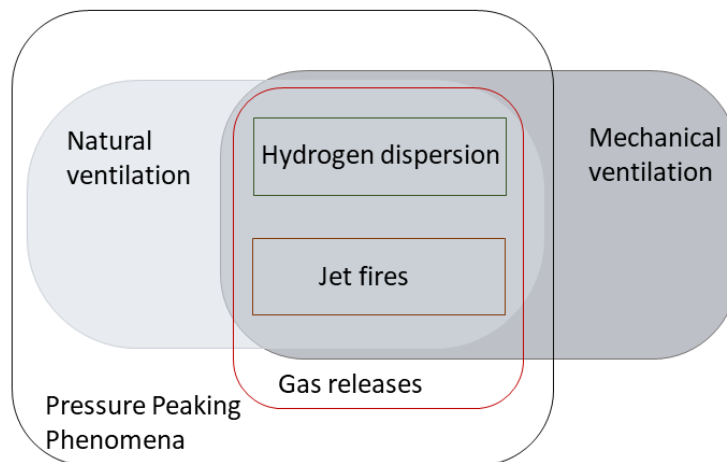


Figure 2.1: Pictorial form of the literature overview.

Unwanted hence accidental hydrogen discharge from a TPRD may occur at different scenarios:

- Unignited discharge
- Unignited discharge and delayed ignition
- Immediate ignition
- Catastrophic failure of the vessel – tank rupture.

Mechanical and natural ventilation systems can be used as mitigation techniques to avoid the formation of flammable cloud (hydrogen concentration under low flammability limit (LFL) – 4%). Hot combustion products from jet fires pose a great threat due to the low visibility of a hydrogen flame and its thermal and pressure effects. This work focuses on effects and phenomena from unignited and immediate ignited non-premixed hydrogen jets in different types of enclosures. Nevertheless, the explosion hazards are described as well as the worst-case scenario which may result from hydrogen-related accidents.

2.1 Gas releases

Hydrogen can be stored in liquid or gaseous form. The research in this thesis focuses on high compressed hydrogen used in hydrogen powered vehicles (HPV) and hydrogen refuelling stations (HRS). The storage pressure in the onboard tank-type IV is up to 700 bar which in case of accidental release creates a hazardous turbulent jet at the first stage of the release.

Gas leaks through a crack, hole or TPRD from high pressure expands, changing its pressure, density and temperature. The isentropic expansion is with the assumption of free expansion (pressure energy is converted into kinetic without friction losses and heat and matter transfer) without heat transfer and constant entropy. An adiabatic expansion is with the assumption of no heat or mass transfer. Since the system is thermally isolated the total internal energy consist only of the work. Both are simplified scenarios being useful for the engineering models and comparison purposes for the real releases. Often adiabatic flow through pipes is assumed and then since no friction is assumed instead of the Reynold number the Mach (Ma) number is used to define the ratio of the gas velocity to the velocity of sound. Due to safety precautions, the maximum flow rate through the opening is mandatory. The maximum flow rate is called choked flow and the maximum pressure at the opening when the flow is choked is a function of a heat capacity ratio only (for hydrogen $\gamma \cong 1.405$ at STP and $\gamma \cong 1.39$ at NTP). For hydrogen, the pressure ratio (Eq.2.1) for choked flow is 1.91 (STP) and 1.89 (NTP).

$$\frac{p_{choked}}{p_0} = \left(\frac{\gamma + 1}{2}\right)^{\gamma(\gamma-1)} \quad Eq. 2.1$$

The choked flows are characteristic for under expanded turbulent jet resulting from unexpected hydrogen releases from high-pressure storage. Eq.2.1 can be used to estimate the pressure at the hydrogen leak source. In the near-nozzle exit, the complex shock structure is formed ([20–22]. When hydrogen exits the nozzle, its density and pressure decrease caused by a rapid expansion ($Ma > 1$) as is shown in the schematic illustration in Figure 2.2.

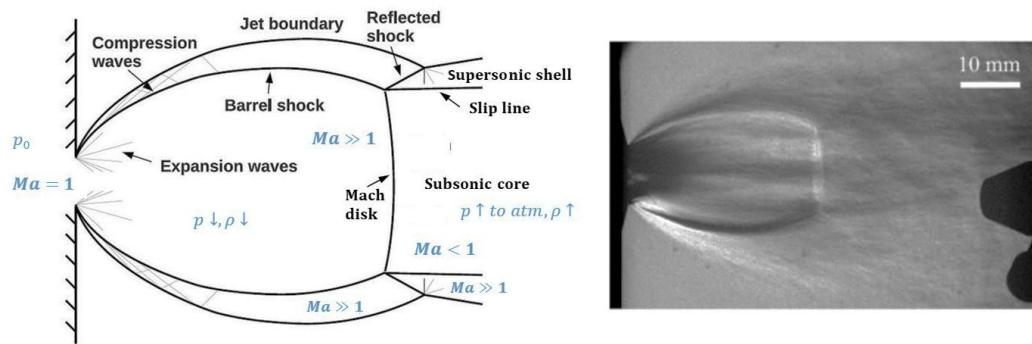


Figure 2.2: Left – A schematic of the near-nozzle structure of an under-expanded jet (based on [23]), Right – Schlieren images of an earlier release stage of under expanded jet (nitrogen in air) from a reservoir with an initial 40 pressure ratio [20].

The shock structure has a characteristic diamond shape which is formed when the ratio of the nozzle exit to the atmospheric pressure is below 40 [20,24]. The diamond structure was captured and investigated with schlieren photography by Ruggles and Ekoto [24]. The Mach disk and following subsonic core with a supersonic shell were clearly visible as is shown in Figure 2.3.

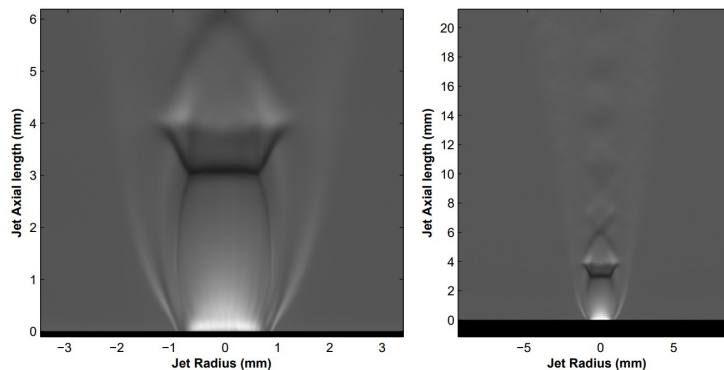


Figure 2.3: Corrected schlieren images of the Mach disk structure – left, and diamond shock structure – right [24].

The engineering calculations of the shock structure are highly advanced and time-consuming. The notional nozzle theory is used as a convenient method to surrogate the under-expanded jets from a real (actual) nozzle. Several notional nozzle theories were developed over the years:

- 1984, Model by Birch et al. [25] – ideal gas equations of state; Assumption of uniform sonic flow (speed of sound) through the notional nozzle. Not applicable for H_2 storage pressure above 10-20 MPa.

- 2007, Model by Schefer et al. [26]– non-ideal behaviour of highly compressed H₂; Abel-Noble equation; Relaxed assumption of the speed of sound at the notional nozzle; Predicts supersonic velocities at the notional nozzle exit at a high storage pressure
- 2009, Molkov et al. [27]– alternative to [25,26]; Applied mass and energy conservation equations; Assumption of uniform sonic flow through the notional nozzle

Before discharge to the surroundings, hydrogen can flow through the pipes, fittings valves etc. Hence the leak may happen at different pressures and leak diameters. Two types of flow at the leak, characterized by the Reynolds number (*Re*), are important in fluid dynamics since they effect heat and mass transfer. *Re* is the ratio of an internal to the viscous forces dividing flows as presented in Figure 2.4. Heat transfer is considerably higher for turbulent flows due to much improved mixing in turbulent boundary layer.

Reynolds number		<i>Re</i> < 2000	Laminar
$Re = \frac{\rho U D}{\mu}$	ρ	Density	2000 < <i>Re</i> < 4000 <i>Re</i> > 4000
	U	Velocity	
	D	Leak diameter	
	μ	Viscosity	
		2000 < <i>Re</i> < 4000	Transitional
		<i>Re</i> > 4000	Turbulent

Figure 2.4: Laminar and turbulent flow- Reynolds number.

Theory by Molkov et al. [27] assumed the same uniform sonic flow through the notional nozzle as Birch et al. but for the Abel Noble equation of state where he replaces momentum conservation equation used by Schefer et al. with energy conservation equation. The notional nozzle theory (with and without losses) by Molkov et al. is well documented and published elsewhere [23,28]. Figure 2.5 presents a scheme of an under-expanded jet [23]. Both theories applied isentropic expansion from vessel (1) to nozzle exit (3). The diameter of the notional nozzle (4) is calculated with a system of equations, using Abel Nobel equation of state, the equations for the speed of sound (choked flow) (3) and local speed of sound (4)) and energy and mass conservation equation, resulted in Eq 2.2.

$$d_4 = d_3 \sqrt{\frac{\rho_3 \cdot u_3}{\rho_4 \cdot u_4}} \quad \text{Eq. 2.2}$$

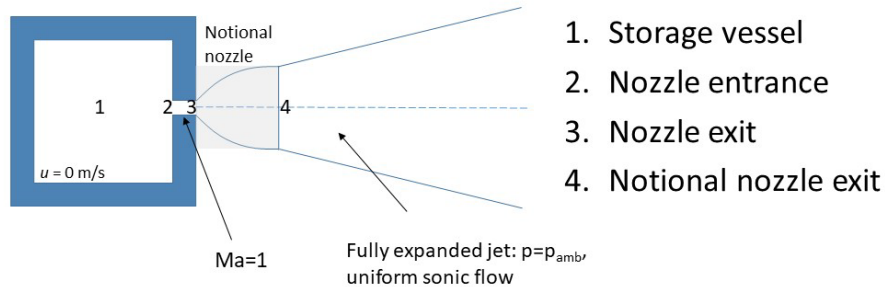


Figure 2.5: Illustration of notional nozzle scheme (based on [23]) for an under-expanded jet.

Theory with losses includes minor losses by using loss coefficient, K (energy losses due to valves, fittings, bends etc.), and frictional losses (between 2-3) subjected to the nozzle/pipe length its diameter and friction factor. Comparing those two theories to the Large Eddy Simulation (LES) show the overprediction of the mass flow rate for the theory without losses while the theory with losses showed a good agreement with LES. Not each hydrogen application has a large 2-3 section, but if the minor and friction losses are justified important, the most accurate separation distance should be estimated (to avoid economical misuse).

2.2 Hydrogen dispersion – in confined spaces

Information on hydrogen dispersion and stratification of a hydrogen leak is essential for effective prevention from ignition possibilities and explosion hazards in case of accidental releases. The fundamental knowledge of hydrogen properties was used to study hydrogen behaviour in confined spaces over the past decades. In Table 2 the main properties of gaseous hydrogen are summarized, commonly used in engineering calculations.

Table 2: Properties of gaseous hydrogen [29–32].

Physical and chemical properties		Combustion and ignition properties	
Density, ρ	0.0838 kg/m ³ NTP	Low flammability limit, LFL	4 %
	42 kg/m ³ at 700 bar		
Molecular mass, M	2.016 kg/mol	Upper flammability limit, UFL	75 %
Diffusivity in air, De	0.61 cm ² /s	Minimum ignition energy, MIE	0.017 mJ
Viscosity μ	89.48 μ Poise NTP	Autoignition temperature, AIT	572 °C
Specific heat capacity, Cp	14.29 J/g/K NTP	Lower heating value, LHV	119.93 MJ/kg
Heat capacity ratio, γ	1.39 NTP	Higher heating value, HHV	141 MJ/kg
Thermal conductivity, k	0.1825 W/m/K NTP	Adiabatic flame temperature in air, T	2390 K
Hydrogen gas constant, R_{H_2}	4124.24 J/kg/K	Latent heat of vaporization	446 kJ/kg
Co-volume constant, b	7.69e-3 m ³ /kg		
Speed of sound in H₂	1270 m/s NTP		

The ideal gas law for applications with high pressures often can not be applied due to high overestimation of the mass flow in calculations. The compressibility factor, $Z = 1/(1 - b \cdot \rho)$, in Abel Noble equation of state ($p = Z \cdot \rho \cdot R_{H_2} \cdot T$) shows an overestimation of around 50% in hydrogen discharge rate for pressures above 700 bar [23]. The focus on the generation of flammable hydrogen cloud was due to its large range of flammability in the air (4%-75%) [30] and low density [33]. Both factors are depending on temperature. An increase in temperature increases the flammability range and decreases the density. The combination of such a low density and viscosity with small hydrogen molecules results in high buoyancy and diffusivity which increases the risk of leakage through fittings, o-rings, materials, etc. It is hydrogen's great advantage in an open environment, allowing gas to rise and rapidly disperse in the air. In closed and semi-closed enclosures the hydrogen can accumulate under the ceiling creating a flammable cloud as is schematically shown in Figure 2.6.

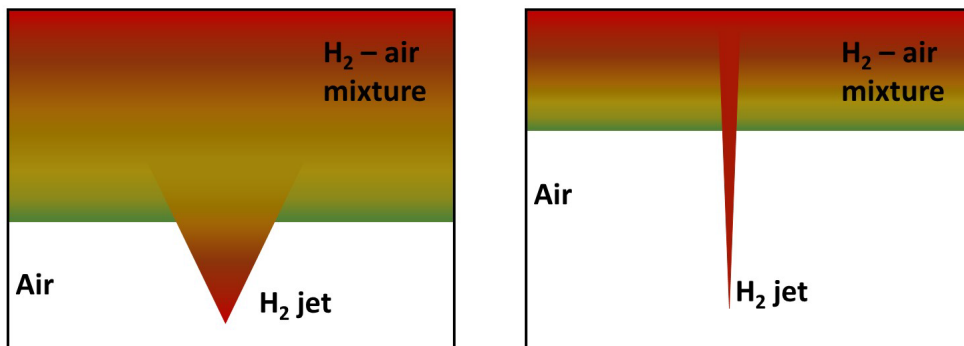


Figure 2.6: A sample sketch of a graphical illustration of a dispersion in a closed room.

Hydrogen dispersion in an enclosure is affected by:

- Ventilation: size and location
- Discharge parameters: flow rate, location, direction, pressure, nozzle size
- Enclosure's geometry: size, shape, presence of obstacles
- Atmospheric conditions: inside and outside

Helium shows a strong similarity to hydrogen [34,35] and experimental investigation of hydrogen dispersion very often used helium due to safety concerns. Nevertheless, the pre-normative research requires experiments in different scales with hydrogen to provide quality data for the recommendation of Regulations, Codes, and Standards (RCS).

2.2.1 Effect of ventilation

Previous studies show that the presence of ventilation may rapidly reduce the concentration of the accumulated flammable cloud [36,37]. The larger the vent, the faster the hydrogen concentration will decline [38,39]. Vent location has no or little effect on the well-mixed hydrogen characteristics for turbulent flows. For the laminar flow with stratification effect, the vents located close to the ceiling show better effectiveness than vents located close to the floor [40]. Two types of ventilation: natural and mechanical are described in more detail below.

Unignited hydrogen releases in a confined space (like private garages), which do not have large enough ventilation size, may lead to high overpressures which can cause

enclosure collapse. The phenomenon is called Pressure Peaking Phenomena (PPP) and is described in detail further in Chapter 2.4.

2.2.1.1 Natural ventilation

To avoid hydrogen accumulation in case of an unwanted release, the enclosure can be equipped with passive/natural ventilation – reliable and cheaper than mechanical ventilation. Natural ventilation is when a neutral plane (a horizontal transition plane) is in the middle of the vent (when the pressure inside an enclosure is equal to the pressure outside). Passive ventilation is when the neutral plane is located below the $\frac{1}{2}$ of the vent (characteristic for gas lighter than air). Vents should be located close to the floor and to the ceiling to provide a ventilation cycle and ensure the safe dissipation of hydrogen. The area of the vents should meet the requirements provided by RCS. In the case of passive ventilation, the minimum total area required by the USA Code of Federal Regulations, standard number 1910.106 – Flammable liquids, is $0.003 \text{ m}^2/\text{m}^3$ [41]. The standard is for Hazardous Materials – Flammable Liquids, since the lack of standards for a building where hydrogen is recognized as a fuel.

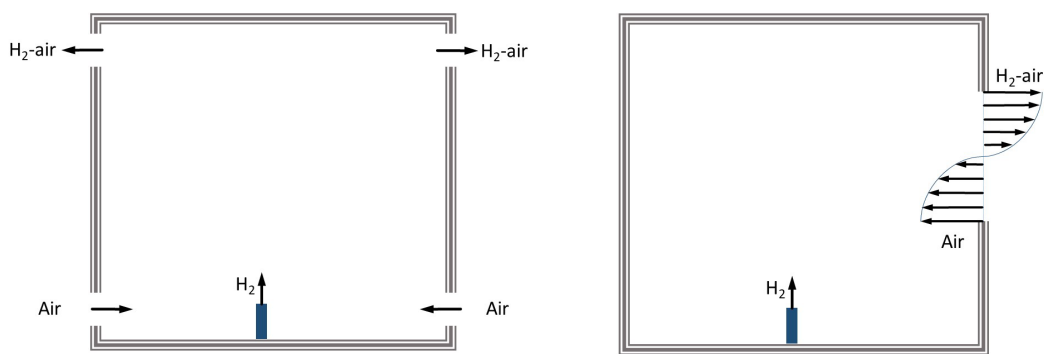


Figure 2.7: Example of passive ventilation geometry (left) and illustration of flow in natural ventilation (right). Based on [42].

In enclosures where hydrogen is stored over a long time, the permeation needs to be considered and proper ventilation applied. The permeation is the penetration in the molecular scale through solid materials, here hydrogen molecules permeate through the storage vessel's walls. Permeation is well documented elsewhere [23,43,44] and since hydrogen tanks used in HPV are type IV (carbon fibre walls with an inner liner of plastic like polyethylene or polyamide), the permeation rate is considered negligible.

Nevertheless, the storage room (with many hydrogen vessels) should be designed with sufficient ventilation. If passive/natural ventilation will not provide enough air change mechanical ventilation should be installed.

2.2.1.2 Mechanical ventilation

To prevent the accumulation of hydrogen in the enclosure and keep the concentration under LFL in enclosures where passive ventilation is insufficient, mechanical ventilation is implemented.

Assessing the ventilation rate where hydrogen applications are present needs to be done accordingly to the hydrogen release rate. With the assumption of a perfect mix in an enclosure the steady-state hydrogen concentration ($C_{\%}$) can be estimated for a given volumetric flow rate, m^3/h of hydrogen release (Q_g) and air (Q_a) [45,46].

$$C_{\%} = \frac{100 * Q_g}{Q_a - Q_g} \quad Eq. 2.3$$

The air volumetric flow rate can be calculated for the given enclosure's volume V, m^3 and air change per hour, ACH, specified by RCS (Chapter 1.1.2):

$$Q_a = ACH \cdot V \quad Eq. 2.4$$

The location of the hydrogen leak in an enclosure can affect the amount of accumulated flammable cloud [47]. Ehrhart et al. [47] presented an investigation of the hydrogen leak from a light-duty HPV with a tank containing 2.5 kg hydrogen in a repair garage. The leak was assumed 61 cm above the floor as a vertical impinging jet from 150 bar pressure through 0.86 mm leak diameter. The CFD simulation results showed that when the hydrogen leak was in the path of the ventilation airflow the flammable hydrogen mixture was reduced and occurred only near the leak's exit. The maximum amount of flammable mass with a ventilation rate of 3 m/s from a box fan was 0.055 g and occurred 180 s after releases rate compared to 2 g (500 s after the release) in the case with no ventilation. The study suggested the use of direct ventilation can be a satisfactory

solution to improve safety without major changes in the structure or ventilation system in the enclosure.

Effective ventilation systems have to be assessed and implemented where passive ventilation is insufficient. In case of the pipe/storage vessel rupture or blowdown with high mass flow rates, neither passive nor mechanical ventilation can effectively disperse hydrogen and keep concentration under LFL. Therefore, finding the most optimal solution is crucial in the worst-case scenarios, to keep concentration under high burning velocity (under 11%). In case of a failure of the ventilation system, the hydrogen equipment and system should be shut down.

2.2.2 Effect of discharge parameters

Increasing storage pressure and/or nozzle diameter results in higher mass flow rates hence a larger amount of released hydrogen. The large release rate characteristic for turbulent flows is dominated by kinetic energy resulting in faster dispersion of hydrogen in the air compared to laminar flow controlled by buoyant forces [1]. Previous studies show that vertical stratification may appear when buoyant forces dominate the flow [48] while well hydrogen mixing in the air can occur for flow dominated by momentum forces [49,50], justifying the assumption of the perfect mix for under-expanded jets [51]. Dimensionless Froude number (Fr) measures the strength of momentum forces to the buoyant force and can be used to classify hydrogen jets into 3 types (Figure 2.8): momentum controlled jet ($Fr > 1000$), Buoyancy controlled jet ($Fr < 10$) and transitional jet from momentum to buoyancy [52]:

$$Fr = \frac{U_{nozzle}}{\left(\frac{g \cdot D_{nozzle} \cdot (\rho_{amb} - \rho_{nozzle})}{\rho_{nozzle}} \right)^{\frac{1}{2}}} \quad Eq. 2.5$$

Where U_{nozzle} is the velocity at the nozzle exit, g is the gravitational acceleration, D_{nozzle} is the nozzle diameter and ρ_{amb} and ρ_{nozzle} is the ambient density and density of the hydrogen at the nozzle respectively. For under expanded jet the parameters with subscript 'nozzle' needs to be calculated with a notional nozzle model.

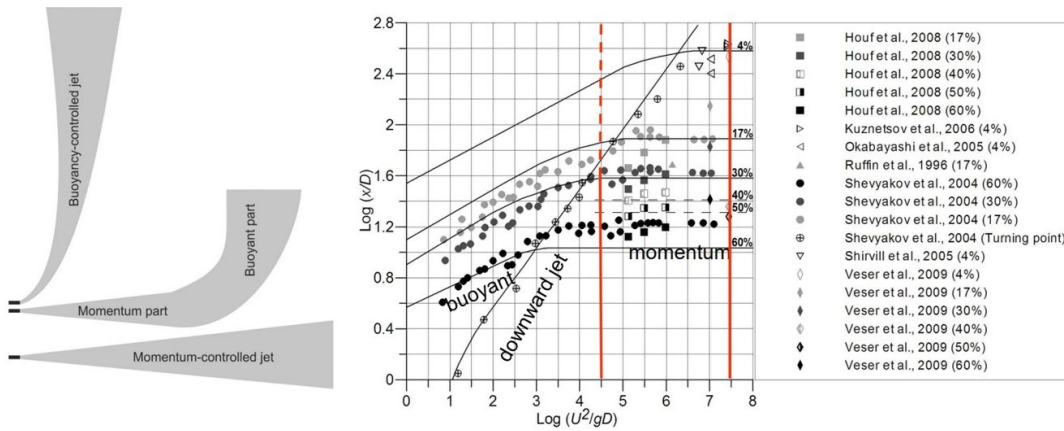


Figure 2.8: (left) Scheme of momentum vs buoyancy controlled jet; (right) relation between Fr and ratio of distance for specific concentration to nozzle diameter. Dash red line-buoyant part, solid red line-momentum part of the jet [23].

Chen C and Rodi W. [53] studied the concentration field for turbulent jets where they investigated and documented concentration field calculations for subsonic, momentum-controlled jets. The model presented by Houf W and Schefer R. [54] for concentration decay (mean mole fraction) of unignited under-expanded hydrogen jet is based on the similarity laws for round jets [23,53]. In accordance with the similarity law the ratio $D_{nozzle}/x = const$, where x is a distance along the central line of the jet to a fixed concentration, \bar{C} (mean mole fraction). That means decreasing the nozzle diameter (TPRD diameter) the concentration at the distance x will be lower (Eq.2.6). The system of equation 2.6 – 2.7 [54] used in the model of Houf W and Schefer calculated concentration decay at axial and radial variation (Eq 2.7). The notional nozzle calculation (Eq 2.8 and 2.9) was based on the model by Birch [25].

$$\bar{C}(x) = \frac{K \cdot d_{eff}}{x + x_0} \left(\frac{\rho_{amb}}{\rho_{H_2}} \right)^{\frac{1}{2}} \quad Eq. 2.6$$

$$\bar{C}(x, r) = \bar{C}(x) \cdot e^{-K_c \cdot (r/(x+x_0))^2} \quad Eq. 2.7$$

$$d_{eff} = d_{nozzle} \sqrt{\frac{\rho_{nozzle} \cdot u_{nozzle}}{\rho_{eff} \cdot u_{eff}}} \quad Eq. 2.8$$

$$u_{eff} = u_{nozzle} + \frac{p_{nozzle} - p_{amb}}{\rho_{nozzle} \cdot u_{nozzle}} \quad Eq. 2.9$$

In Figure 2.9 the results of concentration decay with axial and radial variation for release from 700 bar through 1 mm with the notional model by Molkov et al. [55] and concentration decay by Houf W and Schefer R. [54] are presented. Using similarity law for under expanded jet and notional nozzle approach allowed them to estimate the concentration decay of the unignited jet, hence mass fraction which can be used further in the calculation of overpressures resulted from possible explosion scenarios. Decreasing the leak diameter may results in reduce of the non-ignited jet by half of its length as is shown in Figure 2.9. Model results with notional nozzle by Birch et al. resulted in an underprediction of 4 % contour decay of 3 m for the release conditions presented by Houf W and Schefer R. (207.85 bar through 3.175 mm nozzle).

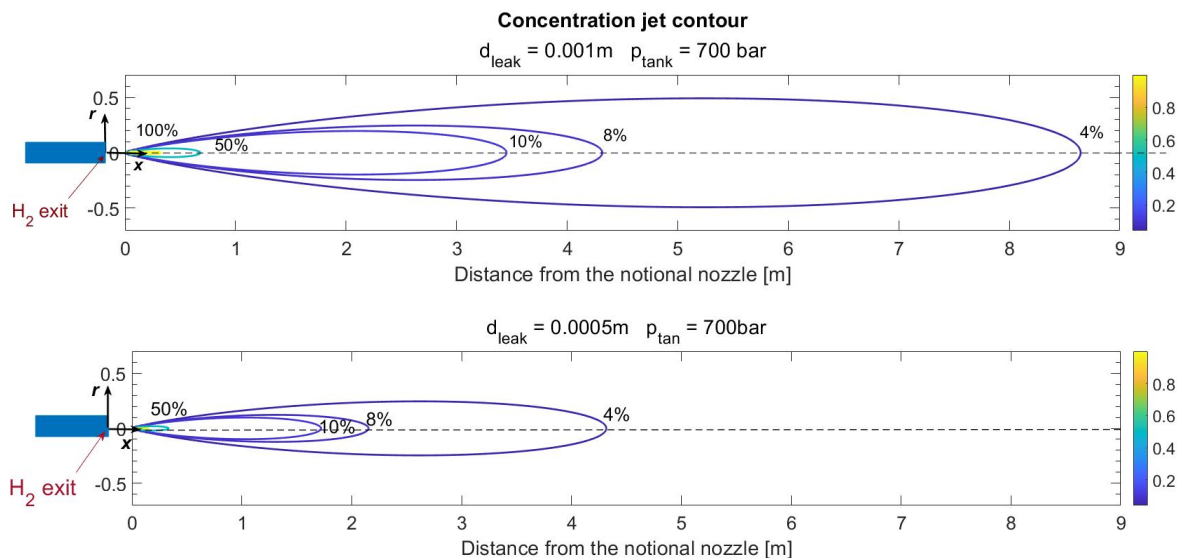


Figure 2.9: Contour of concentration decay for unignited under-expanded hydrogen jet from 700 bar tank through 1 mm exit nozzle (top) and 0.5 mm nozzle (bottom).

A typical HPV is equipped with a TPRD with an exhaust pipe (located around 25 cm above the ground) directed downwards, resulting in impinging with the floor jet [56]. Comparing hazard distances from 90° impinging jets of hydrogen and methane using Computational Fluid Dynamic (CFD) simulation showed the largest flame envelopes for methane. Simulations with 45° jets were done only for methane and resulted in twice longer flames. The study by Hussein et al. [2] investigated dispersion envelopes resulting from under-expanded hydrogen jets in a naturally vented enclosure using CFD. Comparison of hydrogen dispersion from blowdown releases through different nozzle

diameters (0.5 mm, 2.00 mm and 3.34 mm), and nozzle directions (0° upwards, 0°, 30° and 45° downwards). Their results showed stratification of hydrogen in the air resulting from upwards releases shown in Figure 2.10. Investigation of nozzle angle during impinging jets resulted in accumulation of hydrogen around the car for 90° nozzle and long flammable cloud behind the car from 30° and 45° nozzles. For all cases, reducing the nozzle diameter to 0.5 mm decreased the size of the flammable hydrogen cloud.

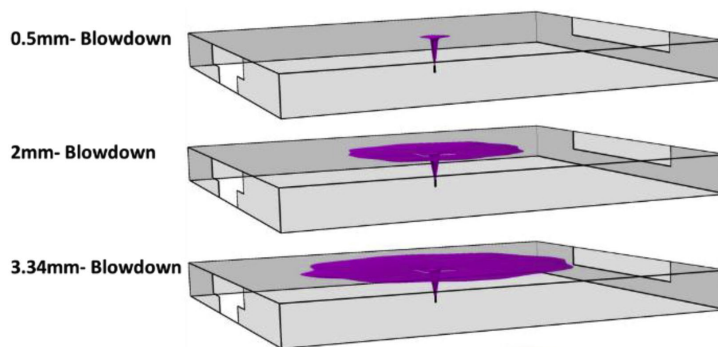


Figure 2.10: 4% vol of hydrogen mole fraction for upwards releases through 0.5 mm, 2.0 mm and 3.34 mm. 20 seconds flow time [2].



Figure 2.11: 4% vol of hydrogen mole fraction for downwards releases through 2.0 mm (left) and 0.5 mm (right) TPRD diameter for three release angles (0°,30°,45°). 20 seconds flow time [2].

2.2.3 Effect of enclosure geometry

The enclosure geometry is an important factor for hydrogen dispersion. The dimensionless Morton number (Mo) characterises a bubbles under the gravitational and viscous forces was used by Denisenko et al. [57]. In their work is describing the relation between the distance from the hydrogen leak to the ceiling and the distance of the momentum specifying domination of buoyancy forces. Based on experimental data when $Mo < 1$ stratification occurs and for $Mo \gg 1$ the uniform hydrogen distribution can be expected. As was mentioned earlier the non-uniform distribution is formed when the hydrogen jet is dominated by buoyancy forces and hydrogen accumulated under the ceiling. Pitts et al. [58] study the presence of obstacles in an enclosure. For constant

buoyancy controlled hydrogen releases (mass flow rate, $mfr \sim 1.39 \text{ g/s}$) into 113.5 m^3 enclosure with natural ventilation (ventilation rate, 3-4.5 air change per hour, ACH) without obstacles the stratification was observed. Placing the car above the release show the uniform hydrogen distribution in the enclosure. The hydrogen released in an enclosure without obstacles is controlled by the motion leading to accumulation under the ceiling [1]. The slow homogenization is the consequence since the concentration first increases under the ceiling and slowly dilutes downwards the floor. The motion is lost in collision with obstacles resulting in faster homogenization.

Some enclosures like covered car parks may have a complex structure of the ceiling which may create pockets for hydrogen to accumulate. The proper ventilation needs to be applied to avoid flammable concentrations.

In Chapter 2.4 the enclosure volume will be discussed regarding the overpressures occurring during rapid hydrogen releases in an enclosure with an inefficient ventilation area.

2.3 Jet fires

Jet fires can be described as diffusion or non-premixed flames – combustion of released hydrogen pointed in a particular direction with significant momentum. Hydrogen jet fires in an enclosure, same as the other fuels, endanger to thermal and pressure hazards. The flames in daylight are hardly visible which may increase the hazards of skin burns. On the other hand, hydrogen jet fires have much lower heat radiation (compare to other fuels). The advantage is that a person can get close to the flame without getting hurt. The intensive study on hydrogen flames in the past decades was focusing on both types (Figure 2.12):

- Premixed – air and hydrogen are mixed prior to combustion (not a diffusion flame).
- Non-premixed – air and hydrogen were not mixed prior to combustion

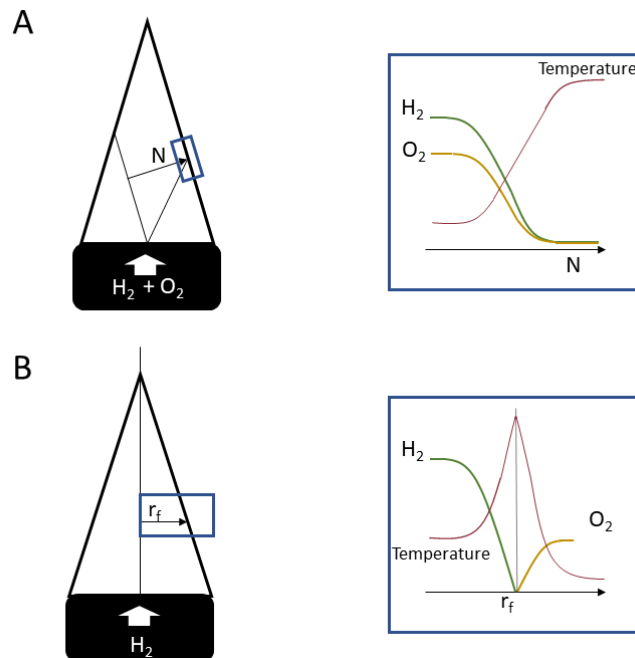


Figure 2.12: Example of the structure of A – premixed flame and B – non-premixed flame. Illustration based on [21].

Hydrogen flames can be categorized based on the:

- Reynolds number: laminar diffusion or turbulent non-premixed flames (Figure 2.14)
- Jet type: buoyancy or momentum controlled
- Condition at the leak's exit: subsonic ($Ma < 1$), sonic ($Ma = 1$) and highly under-expanded supersonic ($Ma > 1$)
- Event: fireballs (during tank rupture), impinging flames (TPRD, short distance to the wall, barrier walls)

The hydrogen can burn with very low mass flow rates (10^{-9} kg/s) – micro-flames, being hard to detect – i.e. through fittings in a compressed system and can burn for a very long time. The momentum-controlled jet fires are considered to be the most hazardous flames and were the subject of interest in this thesis. The presence of obstacles may significantly affect the flame. Barrier walls can be used to shorten the flame or its direction [59] but obstacles like pillars will increase the flame propagation which may result in deflagration increasing the hazards of detonation. Explosions, deflagration, detonation deflagration transition (DDT) it's very well documented elsewhere and here it is just mentioned for information purposes.

Three dimensionless numbers are commonly used for jet fires calculations and classifications:

Table 3: Dimensionless numbers for jet flames classification

Reynolds number (Re) $Re = \frac{\rho_N \cdot d_N \cdot U_N}{\mu_N}$	Froude number (Fr) $Fr = \frac{U_N^2}{d_N \cdot g}$	Mach number (Ma) $Ma = \frac{U_N}{c}$
Laminar or turbulent jet flames	Momentum or buoyancy controlled jet flames	Subsonic, sonic or supersonic jet flames

Further in this chapter, the ignition mechanisms are discussed first. Then the literature study on the flame length and thermal effects will be presented. The focus will be on the under expanded jet fires. The investigation of the hydrogen jet flames is essential for flame length calculation and hence separation distance is discussed further in this chapter.

2.3.1 Ignition mechanism

Understanding the possible ignition mechanisms is one of the fundamental methods for mitigation techniques to prevent the event with uncontrolled/unwanted hydrogen fires.

Due to very low minimum ignition energy (Table 2) very often finding the source of ignition for the accidents with hydrogen is very difficult or impossible. In Figure 2.13 the possible ignition sources are listed. The hot surface ignition is the convective heat transfer from a hot surface with a temperature higher than AIT (Table 2). Electrostatic ignition can occur due to sparks, brush or corona discharges. The ignition due to adiabatic compression may be caused by the equipment geometry which may lead to a shock wave and then result in the ignition. The released heat is called heat of compression - the work done by the gas is transformed to the heat. Diffusion ignition can be observed in the pipe units (from high-pressure to the downstream pipeline). The temperature of the hydrogen-air mixture in the pipe may increase reaching autoignition temperature and can cause pipe rupture. The most common technique (next to the

generated spark) in the experimental investigation to ignited hydrogen is the presence of flames.

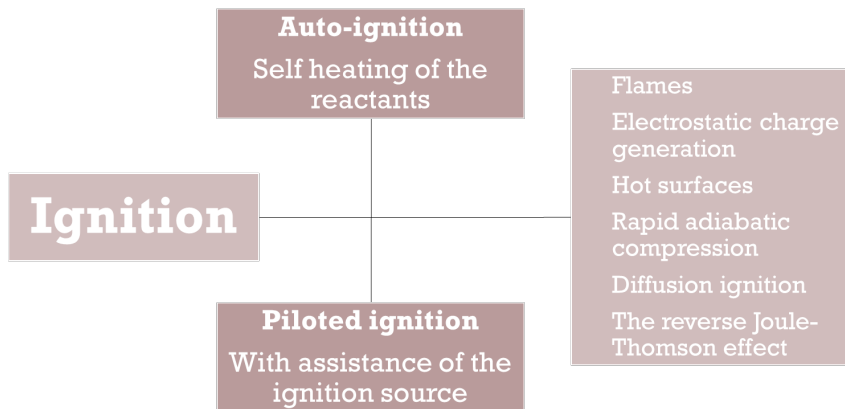


Figure 2.13: Ignition mechanisms.

2.3.2 Flame length

One of the safety concerns for hydrogen applications is the length of the hydrogen jet flame which leads to determining a separation distance. The separation distance defined in ISO 19880 [60,61] describes it as a minimum distance between the source of hazard (jet fire) and the targets (human, structure, equipment). The regulation or physical/numerical modelling are used to determine physical values (temperature, heat flux, pressure, etc) which may lead to harm – the consequences of a potential incident.

The flame length correlations are based on the Re and Fr numbers as shown in Figure 2.14 and Figure 2.15. Figure 2.14 shows that the increase in the velocity at the nozzle in the laminar flames results in an increase of flame length until reaches its maximum. After that, the flame length decreases and stabilizes when the flame becomes turbulent. The study of Hawthorne [62] concluded the flame length is proportional to the leak diameter only (L_F/D), independent of the mass flow rate as long as the fully developed turbulent flame is ensured.

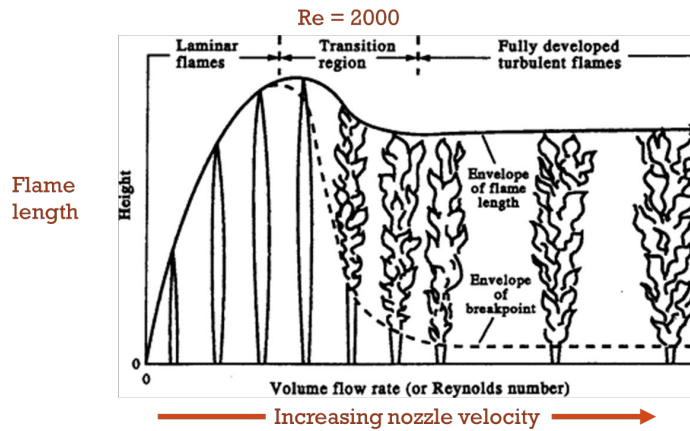


Figure 2.14: Flame categorization based on the Reynolds number (Re). Illustration of flame height/length with a velocity at the nozzle [62].

The derived equation (Eq. 2.10) presented by Hawthorne et al [62] was validated with experiments in a room with daylight, resulting in $L_F/D = 134$ for rounded nozzle ($\phi 4.76$ mm) and $L_F/D = 147$ for sharp nozzle ($\phi 4.62$ mm). The experiments were repeated in a darkened room resulting in flame visibility 10 % greater.

$$\frac{L_F - s}{D} = \frac{5.3}{C_{st}} \sqrt{\frac{T_{ad}}{\alpha_T T_N} \left(C_{st} + (1 - C_{st}) \frac{M_S}{M_N} \right)} \quad Eq. 2.10$$

Further studies show deviations in L_F/D [63,64]. It's important to notice that the turbulent regime described by Hawthorne [62] did not explicitly separate the regime for under-expanded jets. This results in an investigation of flame length in the range from forced convection to natural convection, jets and plums respectively were done by performing 70 experiments with different diameters for subsonic and supersonic flow [63]. Further theoretical studies resulted in a characteristic peak for $L_F(Re)$ showing dependency on the density and viscosity [64]. The theoretical relation between Fr and $L_F(Re)$ for different regimes was showed that when Fr number increases the L_F/D will increase but only for the buoyancy controlled jets [65]. This relation is not applicable for the momentum controlled jets as is graphically presented in Figure 2.15. The theory was confirmed experimentally concluding the increase in L_F/D when Re is approaching the transitional region from laminar to turbulent flames and the L_F/D decreases when the diameter of the leak decreases for the same Re .

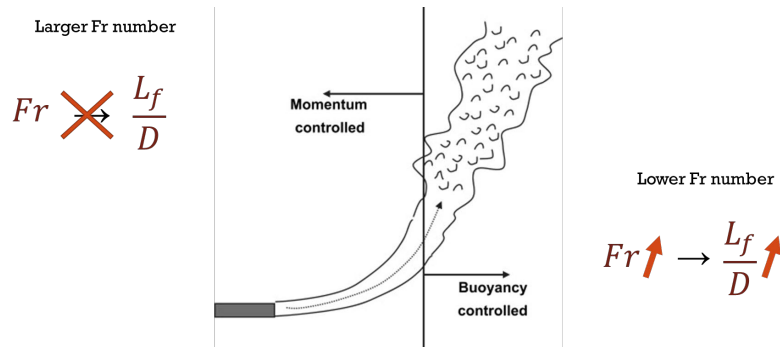


Figure 2.15: Regimes for expanded jets based on Fr number. Illustration based on work by Kim et al. [66].

One of the most important works on flame length was done by Kalghatgi in 1984 [67] which was confirmed experimentally by Schefer in 2006 [68]. Their study proved dependence on the mass flow rate (\dot{m}) showing that L_F/D increases: a) with the increase of \dot{m} for the same leak diameter and b) with larger diameters for constant \dot{m} . The studies contradicted the theory of independence of \dot{m} by Hawthorne and theory where dependence was only on the \dot{m} [69]. Investigating the under-expanded jets led to substituting effective nozzle diameter and scattering the experimental data collected over the years resulting in the dimensional correlation $L_f - (\dot{m} \cdot D)^{1/2}$ where D is the actual nozzle diameter. The best fit line for the collected experimental data: $L_f = 76 \cdot (\dot{m} \cdot D)^{1/2}$ result only with +/- 20% predictive capability [55]. The study by Molkov [55] presented for the first time novel dimensionless flame length correlation for for subsonic, sonic and supersonic hydrogen jets using all three dimensionless numbers (Re, Fr, Ma).

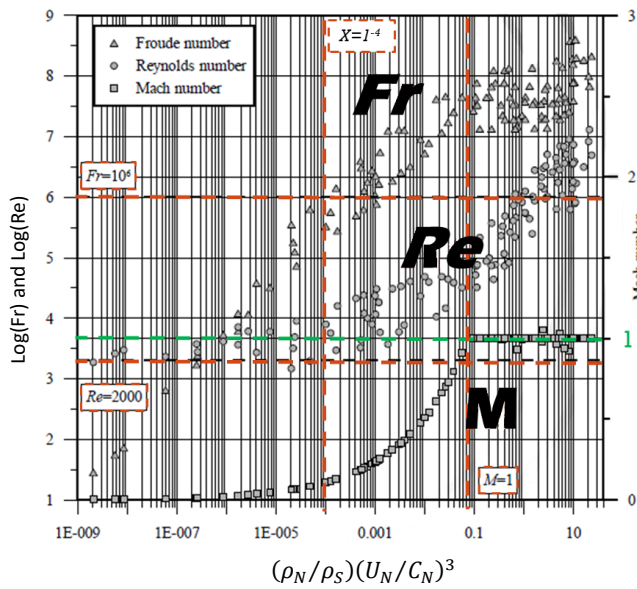


Figure 2.16: Changes of dimensionless numbers Fr , Re , and Ma as a function of the $(\rho_N/\rho_S)(U_N/C_N)^3$. Taken from [23].

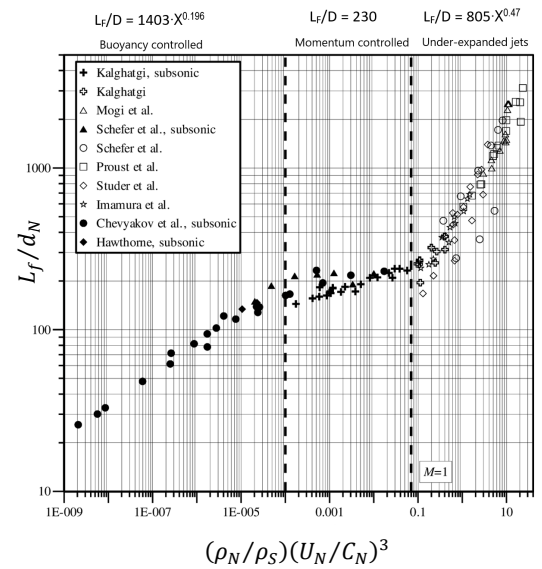


Figure 2.17: Three flame regimes distinct by the novel dimensionless hydrogen flame correlation. Taken from [55].

The novel dimensionless hydrogen flame length correlation (Figure 2.17):

- Normalized flame length (of the experimental data) by the actual nozzle diameter
- Experimental data were correlated with parameter 'X' -the density ratio (ρ_N/ρ_S) and the Mach number cubed $((U_N/C_N)^3)$

This correlation, by using the notional nozzle approach to calculate density at the nozzle for under-expanded jets, allows distinguishing between all three flow regimes (buoyancy/momentum controlled jet flames and expanded and under-expanded jet fires). The 'X' in the equation given in Figure 2.17 for buoyancy dominated jets is $< 1^{-4}$, for momentum dominated jet is between $1^{-4} < X > 0.07$ and for the new under-expanded regime the X is > 0.07 .

The experimental work of Henriksen et al. [70] showed the influence of the downstream and upstream diameter of the nozzle. For low mass flow rates, the increase in upstream nozzle diameter increased the flame jet length. For the safety design of a TPRD, this effect should be considered and investigated in the future.

2.3.3 Blow off

The non-premixed hydrogen jet with a significant velocity at the nozzle will be lifted leading to blow off (turbulent flame speed < flow velocity) or blow out (flame extinguished) [23,30]. Blow off can be often observed for premixed flames when the fuel concentration is low (lean fuels) [21]. For the highly under-expanded hydrogen jet flames, the blow-off phenomena is closely dependent on the storage pressure and the nozzle diameter (Figure 2.18).

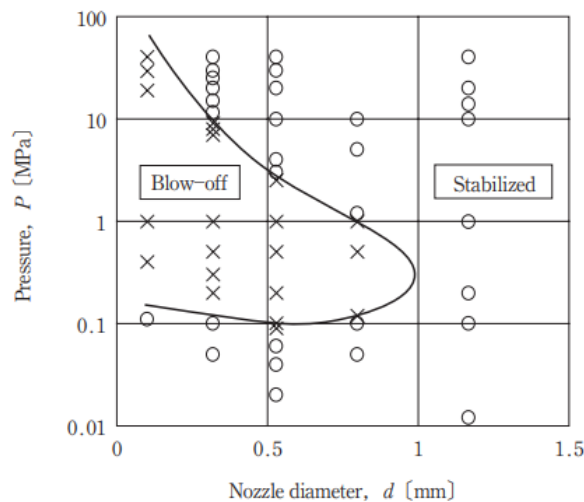


Figure 2.18: Non-premixed hydrogen flame stabilization regimes [71,72].

The experimental investigation of the under-expanded hydrogen jet flame confirmed the results presented above. In case of the tank blow down the large enough nozzle diameter can sustain the flame. In the case of smaller nozzle diameters, the blow-off was observed and stabilized when the pressure drop to a particular pressure [73]. The blow-out was experimentally achieved in work presented by Mogi and Horiguchi [74]. The study concluded the blow off at the lower pressure limit is independent of the nozzle diameter. However for the upper pressure limit the blow-off occurs with decrease of pressure and an increase of the nozzle diameter. Hydrogen jet mixed with other hydrocarbons and CO_2 increases the lift height increasing the chance of the blow-off and blow-out [75].

2.3.4 Thermal effects and separation distances

Thermal effects

The flame length calculations can be used for the estimation of the resulting thermal effects leading to improvement of the fire protection measures like separation distances. When considering hydrogen jet fires that may occur during releases through TPRD (obligatory implemented with onboard hydrogen storage in HPV) the flame length can exceed 10 m depending on the storage pressure and TPRD diameter. The hardly visible hydrogen flame [68] and the thermal radiation can result in hazardous conditions.

The important flame characteristics for the radiant emission are the flame length, discussed in Chapter 2.3.2 and the total heat released during combustion depending on the hydrogen mass flow rate, \dot{m}_{H_2} , and heat of combustion, ΔH_c [76]. The radiant fraction of the total heat released, where Q_{rad} is the total radiant power emitted from the flame, can be then expressed as:

$$X_{rad} = \frac{Q_{rad}}{\dot{m}_{H_2} \cdot \Delta H_c} \quad Eq. 2.11$$

In studies of radiative properties of hydrogen jet flames [54,68], the model for calculation radiative heat flux calculations, $q_{rad}(x, r)$, (eq.2.13) at particular axial, x , and radial, r , is presented based on the non-dimensional radiant power, C^* [76] shown in Figure 2.19.

$$C^*(x/L_f, r/L_f) = 4 \cdot \pi \cdot r^2 \cdot \frac{q_{rad}(x/L_f, r/L_f)}{Q_{rad}} \quad Eq. 2.12$$

Where r is the radius from the central line to the radiant flux measurement's location and L_f is the flame length.

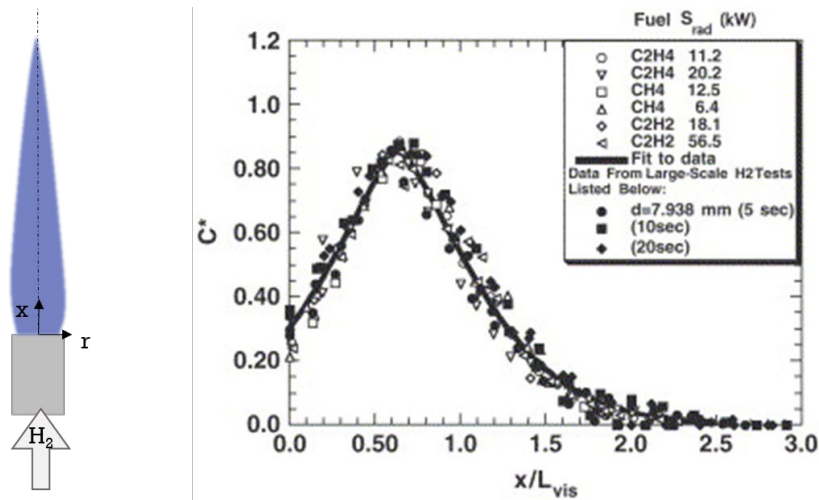


Figure 2.19: (left) radial and axial coordinate system of turbulent jet flame, (right) Axial variation of normalized radiative heat flux [54,76].

$$q_{rad}(x, r) = C^* \cdot \frac{Q_{rad}}{4 \cdot \pi \cdot r^2} \quad \text{Eq. 2.13}$$

The comparison of the experimental data from hydrogen blowdown and results from the presented model [54] showed good agreement. The radiant heat flux from hydrogen releases through 3.175 mm leak diameter and storage pressure of 208 bar resulted in 25 kW/m² 3.5 m from the nozzle at the axial location. The radiant heat flux decreases (at the same axial location) with radial position (further from axial position). It's important to notice the authors calculated flame length based on the model by Birch et al. [77]. Flame length calculation methods can affect the further calculations of radiant heat, especially for under-expanded hydrogen jet flames. The CFD study of the thermal hazards from under-expanded hydrogen jets [78] showed good agreement of the flame length simulation with the experimental study used for validation [79]. The notional model approach was applied. Nevertheless, the reproduced hydrogen releases from 900 bar through 2 mm leak diameter results in underestimation of radiation in the early stage. Due to uncertainties in the basic information of the experiment, the authors suggested the need for more experimental data.

Separation distances

Exposure to high radiation heat fluxes in a particular period will lead to 3rd-degree burns and/or death for humans and fires or significant damage to structures. Determination of the separation distance and possible hazards related to hydrogen jet fires in enclosures (like carpark) is still a challenge for RCS, car manufacturers and relevant actors. In case of hydrogen-related incidents, the proper guidance of safe evacuation of passengers together with their guarding by the first responders has to be available.

The separation distance in the case of the free jet fires can be estimated based on the tenability limits for heat exposure (exposure thresholds that may lead to injuries, incapacity of organ functions and unsuccessful evacuation). There are two types of threshold criteria based on thermal transfer given in BS Standards [10] used and referred in research studies [80,81] and guidelines [82]:

• Radiative heat transfer:	< 2.5 kW/m ²	> 300 s
	2.5 kW/m ²	30 s
	10 kW/m ²	4 s
• Convective heat transfer:	< 60 °C at 100 % saturated	> 30 min
	100 °C	8 min
	110 °C	6 min
	120 °C	4 min
	130 °C	3 min
	150 °C	2 min
	180 °C	1 min

In ISO standard [83] the pain limit of 45 °C is given as the exposure limit. The same pain limits are given in other sources [84–86]. The thermal dose (function of thermal intensity and exposure time) can be calculated with equation 2.14 [87] and then classified with harm criteria (Table 4).

$$\text{Thermal Dose (TD)} = I^{\frac{4}{3}} \cdot t \quad \text{Eq. 2.14}$$

Where I is the radiative heat flux, kW/m², and t is the exposure time, s. The 4/3 is accepted as the best available due to natural and ethical issues with performing experiments with skin burning involved.

Table 4: Example of the thermal dose criteria

Source	Thermal dose	
	2 nd -degree burn	3 rd -degree burn
UKAEA 1983 [88]	1200	2600
BS 2004 [10] HSE 1996[89]	240-730	1000

To present the probability of the consequences related to a particular thermal dose the probit function (Eq.2.15) can be used as a method to calculate the probability of 2nd, 3rd skin burn or death [29].

$$Y = 14.9 + 2.56 \cdot \ln(TD) \quad \text{Eq. 2.15}$$

The important factors which affect the separation distance are the nature of the hazard, the type of the ‘target’, the environment between them and the operating and facility conditions and design.

A CFD study by Hussein et al. [81] compared the temperature envelope resulting from the hydrogen releases from the 700 bar storage tank through different nozzle diameters with its angle variation in an enclosure. The convective heat limits were used as a reference. The best (safe) results were obtained for 0.5 mm nozzle diameter at 45° [81].

2.4 Pressure Peaking Phenomena

Rapid hydrogen releases into an enclosure will cause overpressures unlike other fuels/gases (Figure 2.20). The overpressure peak decreases with the increasing molecular mass of the released gas into denser gas (i.e. air $M= 0.29$ kg/mol): hydrogen – 0.002 kg/mol, helium – 0.004 kg/mol, methane – 0.016 kg/mol and propane 0.044 kg/mol. The high overpressure resulting from hydrogen releases has a characteristic peak (in an early stage of the release for both unignited and ignited releases) and the phenomenon is called Pressure Peak Phenomena (PPP). The PPP was first observed by

Brennan et al. [3] during the CFD investigation of the unignited hydrogen releases from high-pressure storage through a Pressure Relieve Device (PRD) into an enclosure with a single vent (brick size 0.25 m x 0.05 m).

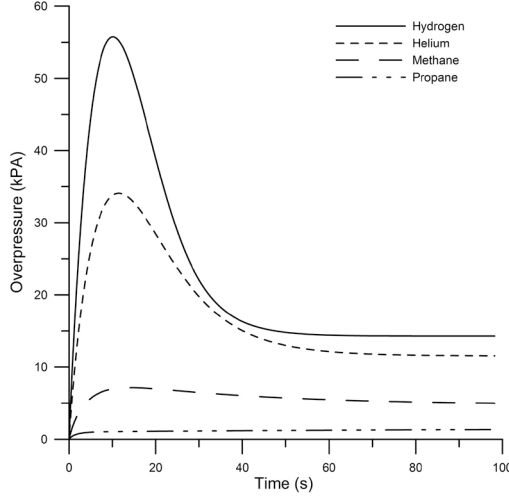


Figure 2.20: Overpressure estimations from gas releases: hydrogen, methane and propane into a 30.4 m³ enclosure with a single vent. Releases from 350 bar storage pressure with mass flow rate 0.39 kg/s through 5.08 mm nozzle, vent size 0.0125 m² [90].

The basis of this phenomenon is the density difference causing the lower flow at the vent than at the leak diameter at the beginning of the release [91]. The density at the vent is assumed to be equal to the density in the enclosure and the overpressure calculation, based on the ideal gas law (Eq.2.18) can be solved with the system of equations presented by Brennan and Molkov [90,91], given below:

$$m_{en}^{t+\Delta t} = m_{en}^t + (\dot{m}_n^t - \dot{m}_v^t)\Delta t \quad Eq. 2.15$$

$$n_{en}^{t+\Delta t} = n_{en}^t + \left(\frac{\dot{m}_n^t}{M_{H_2}} - \frac{\dot{m}_v^t n_{en}^t}{m_{en}^t} \right) \Delta t \quad Eq. 2.16$$

$$\dot{m}_v^{t+\Delta t} = C \frac{m_{en}^{t+\Delta t} A}{V} \sqrt{\frac{2(p_{en}^{t+\Delta t} - p_0)V}{m_{en}^{t+\Delta t}}} \quad Eq. 2.17$$

$$p_{en(t_a+1)} = \frac{n_{en}^{t+\Delta t} RT}{V} \quad Eq. 2.18$$

- m – mass in en –the enclosure, v – mass at the vent, n –mass at the nozzle
- M_{H_2} – hydrogen molecular mass
- T – temperature
- t – time
- V – enclosure volume
- A – vent area
- R – universal gas constant
- C – discharge coefficient

Looking closer to the flow rates at the nozzle (Eq.2.19) and at the vent (Eq.2.20a) it's clear that with hydrogen low molecular mass the molar flow is very high compared to

the molecular flow rate at the vent (due to the molecular mass in the enclosure M_{en} being a mixture of air and released hydrogen).

$$\dot{n}_n = \dot{m}_{H_2}/M_{H_2} = \rho_{H_2}\dot{V}_{H_2}/M_{H_2} \quad Eq. 2.19$$

$$\dot{n}_v = \dot{m}_v/M_{en} \quad Eq. 2.20a$$

$$\dot{n}_v = CA\sqrt{2n_{en}\Delta p/M_{en}V} \quad Eq. 2.20b$$

$$\dot{V}_v = CA\sqrt{2\Delta p/\rho_{en}} \quad Eq. 2.20c$$

From the start of the hydrogen release, the density in the enclosure decreases hence density at the vent decreases. From Eq.2.20b and Eq.2.20c, it can be seen that the molar flow rate and volumetric flow rate at the vent are inversely proportional to the molecular mass and density in the enclosure respectively. In accordance with ideal gas law (Eq.2.18) – the maximum pressure is when the number of moles in the enclosure reaches its maximum (flows at the leak diameter and the vent are equal). With a higher hydrogen flow rate, the number of moles in the enclosure will be higher leading to higher overpressures. Increasing the vent area A , and decreasing hydrogen flow rate, \dot{n}_n will help to avoid high overpressures and/or minimize the PPP.

$$\frac{dn_{en}}{dt} = \dot{n}_{in} - \dot{n}_{out} \quad Eq. 2.21$$

From the presented equations, the pressure peaking phenomena can be described in one sentence: introducing lighter gas with a relatively high flow rate into an enclosure with a denser gas and relatively low ventilation area will result in destructive overpressures. The influence of the enclosure geometry and discharge parameters can be summarized as below [90,92]:

- Increasing the enclosure volume, the pressure peak will be delayed.
- Increasing ventilation area will decrease the pressure peak (Figure 2.21).
- Decreasing hydrogen flow rate (decreasing leak diameter ie. TPRD and/or storage pressure) will decrease pressure peak (Figure 2.21).

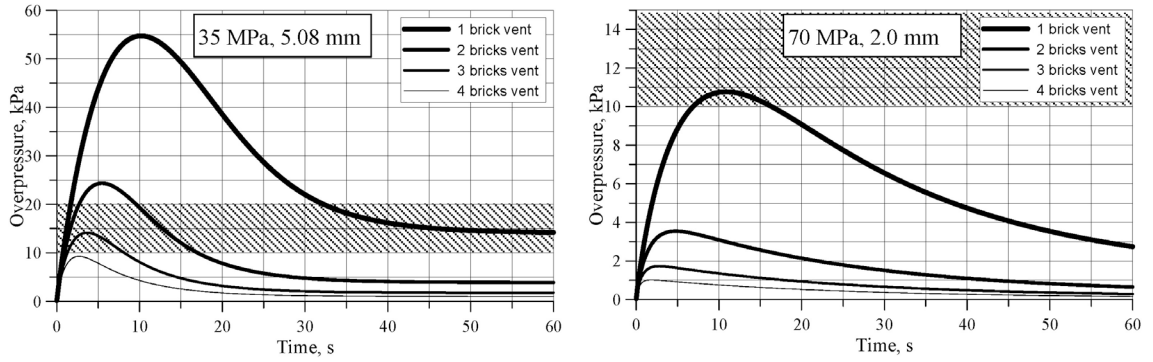


Figure 2.21: Overpressure simulation with 4 different vent sizes resulted from 388 g/s hydrogen release rate (left) and 107 g/s (right). Enclosure volume 30.4 m³, brick size 0.0125 m² [93].

The PPP is much stronger for the ignited hydrogen releases due to the combustion products and released heat [94].

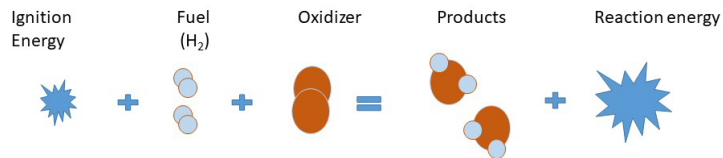


Figure 2.22: Reaction of hydrogen combustion on air.

The calculation's methodology of the PPP resulting from the hydrogen jet flames was presented first with a volumetric flow approach by Makarov et al. [93]. The volumetric balance in an enclosure of the products from full combustion at the adiabatic temperatures and reactants at room temperature can be expressed as

$$\dot{V} = \dot{V}_{\text{H}_2\text{O}|T_{ad}} + \dot{V}_{\text{N}_2|T_{ad}} - \dot{V}_{0.5(\text{O}_2+3.76\text{N}_2)|T_0} - \dot{V}_{\text{H}_2|T_0}$$

Based on the ideal gas law the volumetric flow rate (Eq.2.22), Makarov presented a multiplier (representing the difference between ignited and unignited releases (bold part of Eq.2.22)

$$\dot{V} = \frac{\dot{m}_{\text{H}_2}}{M_{\text{H}_2}} \frac{RT_0}{P} \left(\frac{T_{ad}}{T_0} + \mathbf{1.88} \frac{T_{ad}}{T_0} - \frac{\mathbf{1} + 3.76}{2} - \mathbf{1} \right) \quad \text{Eq. 2.22}$$

The under-expanded jet theory described in Chapter 2.1 was used to calculate hydrogen temperature at the leak diameter. With conservation of enthalpy, the authors calculated the initial temperature of the hydrogen and air (stoichiometric combustion of hydrogen in isobaric conditions). The computed multiplier $\alpha_c = 22 \pm 1$, was used in calculate volumetric flow (Eq2.22) into an enclosure. Then the unignited PPP model was used to estimate overpressures resulting from hydrogen jet fires in an enclosure for different natural ventilation areas, presented in Figure 2.23.

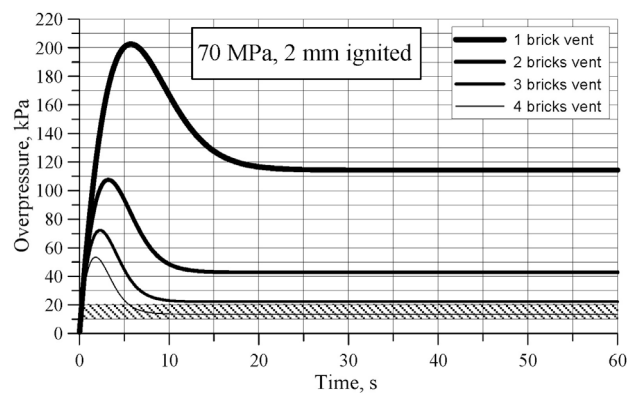


Figure 2.23: Overpressures estimations from non-premix hydrogen jet fires in enclosure. 1 break = 0.0125 m^2 , $\dot{m} = 107 \text{ g/s}$

The model was validated against laboratory-scale experiments in a 1 m^3 enclosure. The enclosure was not sealed properly and during experiments ‘breathing’ was observed. Nevertheless, the performed experiments showed PPP and could be used to validate the model.

Before this thesis work the Pressure Peaking Phenomena was investigated only with analytical and CFD simulation validated based on the experimental results in small scale enclosure [92,93,95]. Experimental data from the large scale experiments with constant and blowdown type releases were needed to validate and improve the models. The new analytical approach for PPP from unignited hydrogen releases and a new analytical model with mass and energy balance for PPP from ignited releases was developed and validated against results from performed experiments on a large scale [96–98].

3 Experimental work

This chapter presents the experimental setups (geometry and instrumentation), the information on data processing, and the results. The chapter is divided into 2 sections, where the first one is representing two experimental campaigns investigating the Pressure Peaking Phenomena, resulting from unignited and ignited hydrogen releases. The large experimental setup imitated enclosures like private garages. The second section describes two experimental campaigns investigating hydrogen dispersion and thermal effects from unignited and ignited releases in a 40 ft container. The large experimental setup imitated enclosures similar to carparks.

The biggest focus during all experimental campaigns was on the relationship between hydrogen mass flow rate and natural ventilation (PPP), mechanical ventilation, and fire effects on vehicle, structure, and evacuation (40 ft container).

The detailed information of the experimental setup and published experimental data from all experiments from all 4 campaigns (Figure 3.1) is given to provide a source for validations of CFD models, with the main goal to the increased safety of hydrogen applications. The large scale of all experimental campaigns is crucial for model validation, and conclusions for the recommendation for RCS.

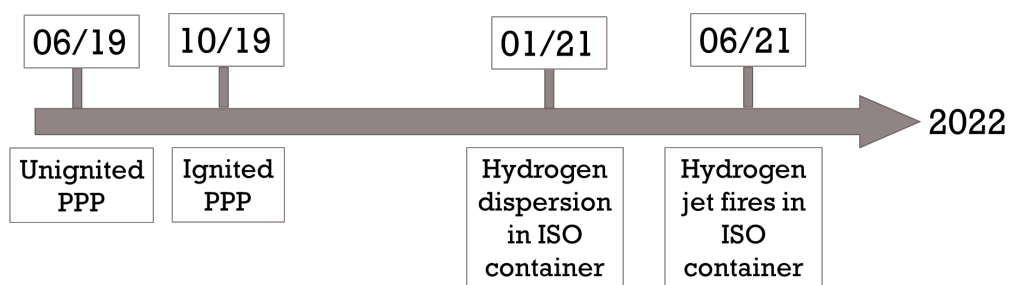


Figure 3.1: Timeline of experimental campaigns.

3.1 Pressure Peaking Phenomena (PPP)

All the experiments were performed in the military area in Horten. The explosion chamber used for the investigation of PPP for both unignited and ignited hydrogen releases was located there and was lent by The Norwegian Defense Research Establishment. The Piping and Instrumentation Diagram (P&ID) of setup and instrumentation for the unignited and ignited campaign is shown in Figure 3.2 and Figure 3.3 respectively.

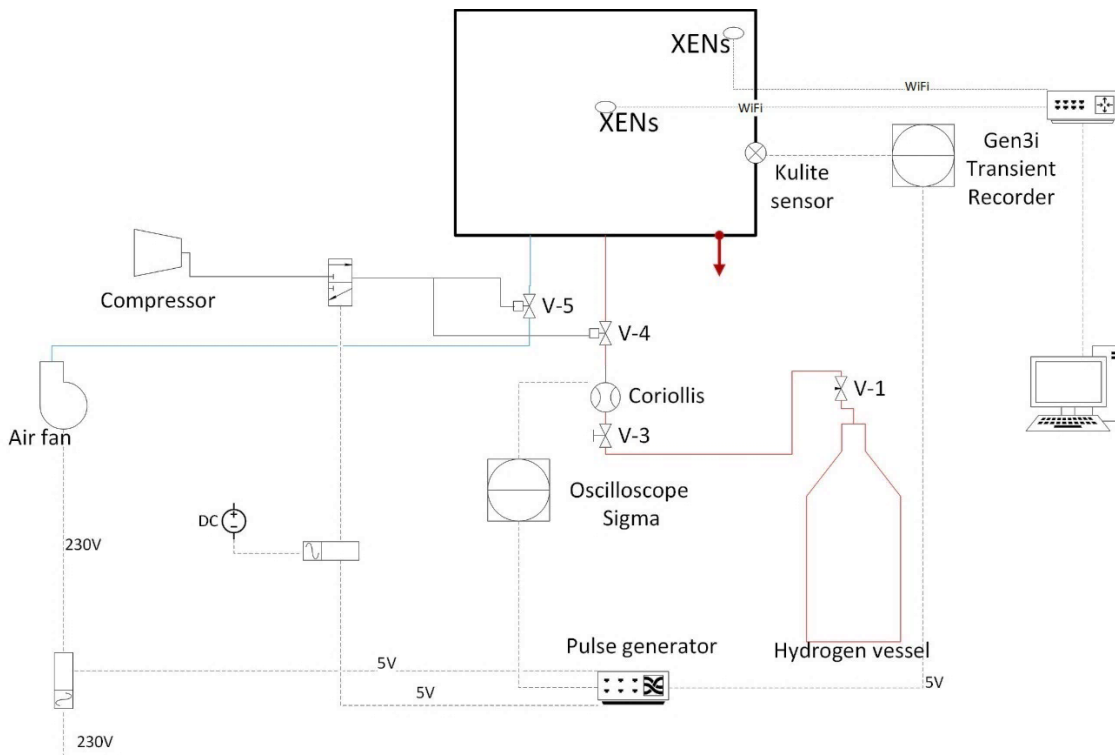


Figure 3.2: P&ID – unignited PPP

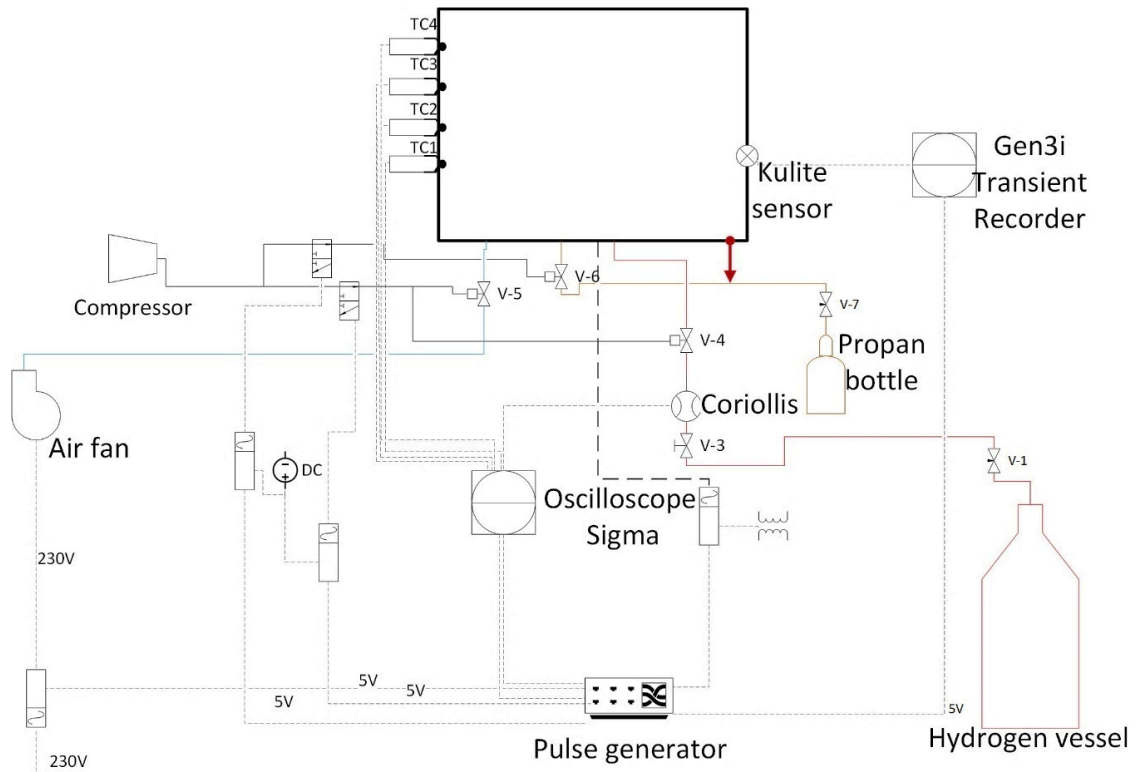


Figure 3.3: P&ID – ignited PPP

3.1.1 Geometry

The explosive chamber (Figure 3.4) has the inner dimensions: $L \times W \times H$: $2.98 \times 2.00 \times 2.50$ m which gives a total volume of 14.9 m^3 . The explosion chamber's walls in total have five vents of 80 mm diameter each. Four of them are located in the lower corners at the front and back wall (Figure 3.4). The fifth is located in the middle of the front wall coming out inside of the chamber floor, used for hydrogen supply and ignition system added after unignited campaign (Figure 3.5, V5). Vent V4 was used for ventilating the chamber with air after each experiment during both campaigns: unignited to blow out the hydrogen and ignited to blow out the hot products. Valves 1-3 was used as the passive ventilation. For the unignited releases, only V1 was used. The constant temperature of the air was ensured with water cooling, which allows performing experiments at the same or very alike initial conditions.

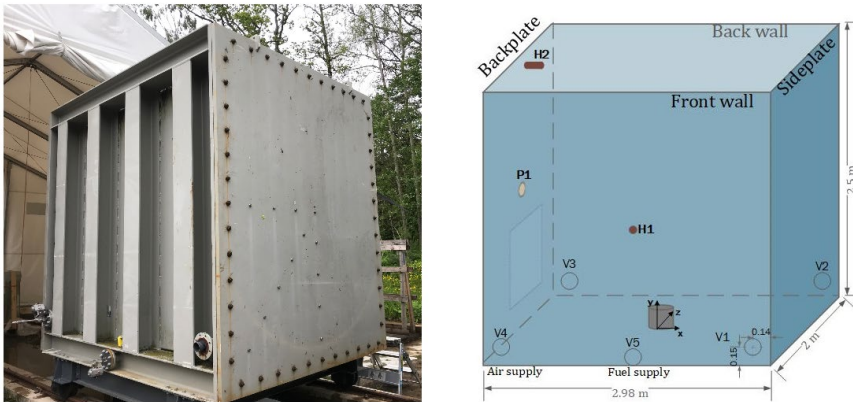


Figure 3.4: Explosive chamber.

Vents V1-V3 were used as natural ventilation during experiments with a total vent area equal to $A_v=0.0151 \text{ m}^2$. For the unignited releases, the area was too large to be able to investigate the PPP and only V1 was used (Figure 3.5). The passive ventilation was placed at the top of the explosive chamber with PVC pipe (diameter 0.075 m) shown in Figure 3.5. Different ventilation areas were obtained by placing the cover on the end of the PVC pipe, outside the explosive chamber (Figure 3.5, V1).



Figure 3.5: Pictures of vents on the front wall (left), ventilation assembly (middle), and the nozzle and PVC pipe-vent outlet inside the explosive chamber (right).

The pressure measurements were of the biggest interest for PPP and the same pressure transducer was used and located at the same location (Figure 3.4 and Table 5). The concentration measurements were added for unignited releases (two WiFi hydrogen sensors, H1 and H2). Sensors were placed in the middle of the front wall and on the backplate (Table 5). For the ignited releases the concentration sensors had to be disassembled due to high temperatures, and four thermocouples were installed instead.

The vents' and sensors' location is presented in Table 5. The point with coordinates (0,0,0) is at the centre of the floor plate and the base of the hydrogen release pipe outlet.

Table 5: Location parameters for sensors and the vents.

Vent/Sensor		x	y	z
V1		1.35	0.15	-1.00
V2		1.35	0.15	1.00
V3		-1.35	0.15	1.00
P1		-1.49	1.24	0.00
Unignited PPP	H1	0.000	1.240	-1.000
	H2	1.430	2.380	0.000
Ignited PPP	T1	1.430	0.035	0.000
	T2	0.000	1.240	-0.940
	T3	-1.430	1.780	0.000
	T4	-1.430	2.380	0.000

The 4 mm diameter nozzle was mounted at the 6mm pipe outlet (Figure 3.5). The nozzle was installed on the floor in the middle of the explosion chamber to upwards discharge hydrogen.

The fuel supply consisted of a hydrogen pack of 12 bottles of hydrogen under 200 bar pressure.

The major changes done in the experimental setup for ignited releases were:

- All three vents were used, without cover.
- The PVC pipe was disassembled for ignited releases.
- The ignition system was added to the nozzle: -isolated wires were placed through the V1, -propane pilot with a 10 kV spark as an ignition source (Figure 3.6).

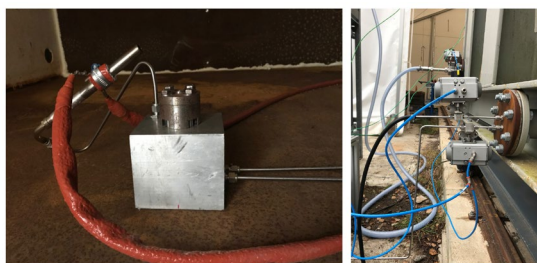


Figure 3.6: Ignition system: nozzle with propane pilot (left), propane valve (right).

3.1.2 Instrumentation and logging

A Quantum Composers pulse generator model 9518 with 8 independent outputs was used to digitally control:

- a trigger for Oscilloscopes SIGMA and GEN3i,
- ignition mechanism: spark and propane valve,
- hydrogen valve and air-fan,

A Micro Motion ELITE coriolis mass flow meter model CMF010M/L was used during both campaigns. Its maximum operating pressure and flow rate are 125 barg and 108 kg/h respectively. Due to the operating pressure limits, and nozzle diameter the maximum experimental hydrogen mass flow rate was limited to a maximum of 11.5 g/s. The pressure of the hydrogen flow was measured at the coriolis mass flow output with a sensor from American Sensor Technologies Inc. model AST4000C00250B4I1000 with operating pressure 0 – 250 bar. The sensor signal was sent through pressure digital transmitter model HD2601V.1 from Delta Ohm. The oscilloscope Sigma has recorded pressure and mass flow rate from Coriolis mass flow meter. The computational signal calculation for mass flow rate (\dot{m} , g/s) and pressure (p , kPa) were obtained with the equations given below

$$\dot{m} = 6.25 \cdot (V - 1) \quad Eq. 3.1$$

$$p = 62.5 \cdot (V - 1) \quad Eq. 3.2$$

Where V is the voltage signal (mV).

The overpressure was measured with Kulite pressure transducer XTM - 190-50A (Figure 3.7) mounted into the 18M screw and installed in the middle of the backplate (Figure 3.4, P1). The experimental data were recorded with HBM Gen3i with a sample rate of 25ks/s.

During unignited releases, the measurements from 5320 XENsonr WiFi hydrogen sensors (Figure 3.7) were stored directly into the software XEN-5320-v3.0.2_WIFI. The

sensors were calibrated each morning before the experiment. Hydrogen concentration was measured each 30 ms.



Figure 3.7: The sensor used during PPP experiments: XENSONR hydrogen sensors (left), Kulite pressure transducer (middle), and Thermocouple type K (right).

During ignited releases, temperatures were recorded with Oscilloscope Sigma. Four thermocouples Type K from Autek-TD20H-KP (Figure 3.7, right) with measurements range $-40^{\circ}\text{C} - 1000^{\circ}\text{C}$ were used. The length and diameter of thermocouples are 500 mm and 1.5 mm respectively. To avoid hot junction the amplifiers were used before the signal was sent to the oscilloscope. The computational signal calculation (T, K) are given below:

$$T = 200 \cdot (V - 1) \quad \text{Eq. 3.3}$$

The uncertainties of measurements are given in Table 6.

Table 6: Measurements uncertainty-PPP.

Equipment	Instrumentation uncertainty	Absolute measurement uncertainty
AST Pressure sensor	$\pm 1\%$	± 2.5 bar
Kulite pressure sensor	$\pm 1\%$ FSO BFSL	± 3.5 kPa
Mass flow	$\pm 0.2\%$ of flow rate	Exp 7 : ± 0.0061 g/s (from 3.05 g/s)
Concentration	$\pm 2\%/%$	$\pm 0.18\%$ (max. conc)
Thermocouples type K	$\pm 0.75\%$	$\pm 2.2^{\circ}\text{C}$ to 4.5°C

3.1.3 General Procedure

All experiments were performed with presence of Andre Vagner Gaathaug, Agnieszka Weronika Lach and Knut Ove Hauge.

Before each experiment, the explosive chamber was ventilated with air to ensure comparable initial conditions. The gate valve at the hydrogen bottle pack was used to obtain desired mass flow rate by setting up the pressure - relevant to the mass flow rate (the constant storage pressure was needed, Figure 3.8 - right). The static pressure was read at the Delta Ohm transmitter to confirm the pressure. The pulse generator with the designed time setup gave the signal to the valves and triggered oscilloscopes to start measurements. The hydrogen release was set up for the desired time after which the pneumatic valve for hydrogen was closed and the air fan was automatically started. The pneumatic valve for the air was closed during experiments and opened after the hydrogen valve was closed.

During unignited hydrogen releases the XENsor software was started first to eliminate the delay measurement time of WiFi sensors.

During ignited hydrogen releases, the mass flow rates were obtained with the opening gate valve at the hydrogen bottle stack on the static pressure based on previous unignited experiments. The pneumatic valves for hydrogen and propane were opening with a signal from the pulse generator. To avoid the premix ignition, the hydrogen valve had a 1s delay time. Therefore hydrogen flux was released into propane flame initiated with ignition system (spark) with a duration of 2 seconds in total.

3.1.4 Analytical models

The analytical models of PPP were developed for both unignited and ignited releases and are published in Article A and Article B respectively. In Table 7 the summary of the governing equations is presented. For the unignited releases, the conservation of mass was applied with flow calculation at the vent based on the choked flows [29]. The overpressure estimation from ignited hydrogen releases was done by solving mass and energy conservation equations. For the calculation, the experimental mass flow rate of hydrogen was used instead of implementing the notional nozzle. The model presented below were developed based on work by Brennan et al. [3].

Table 7: System of equations for ignited and unignited PPP analytical models.

Unignited PPP	Ignited PPP
Mass balance	
$\frac{dn_{en}}{dt} = \dot{n}_{in} - \dot{n}_{out} \quad Eq. 3.4$	$\frac{dn_{H_2}}{dt} = \dot{n}_{in,H_2} - \dot{n}_{out,H_2} + \dot{n}_{rx,H_2} \quad Eq. 3.11$
$\frac{dn_{H_2}}{dt} = \dot{n}_{H_2,in} - X_{H_2} \cdot \dot{n}_{out} \quad Eq. 3.5$	$\frac{dn_{O_2}}{dt} = \dot{n}_{in,O_2} - \dot{n}_{out,O_2} + \dot{n}_{rx,O_2} \quad Eq. 3.12$
	$\frac{dn_{N_2}}{dt} = \dot{n}_{in,N_2} - \dot{n}_{out,N_2} + \dot{n}_{rx,N_2} \quad Eq. 3.13$
	$\frac{dn_{H_2O}}{dt} = \dot{n}_{in,H_2O} - \dot{n}_{out,H_2O} + \dot{n}_{rx,H_2O} \quad Eq. 3.14$
$n_{out} = C \cdot A_v \sqrt{\frac{2 \cdot \Delta p \cdot n_{en}}{V \cdot M_{en}}} \quad Eq. 3.6$	$n_{out,tot} = C \cdot A \sqrt{\frac{2 \cdot \Delta p \cdot n_{tot}}{V \cdot M_{en}}} \quad Eq. 3.15$
$M_{en} = X_{H_2} \cdot M_{H_2} + (1 - X_{H_2}) \cdot M_{air} \quad Eq. 3.7$	$M_{en} = \sum_i \frac{n_i}{n_{tot}} M_i \quad Eq. 3.16$
	$n_{in} = \frac{C \cdot A}{M_{air}} \sqrt{2 \cdot \Delta p \cdot \rho_{air}} \quad Eq. 3.17$
Energy balance	
	$\frac{dU_{en}}{dt} = \dot{H}_{in} - \dot{H}_{out} + \dot{Q}_{rx} - \dot{Q}_{loss} \quad Eq. 3.18$
	$\frac{dT_{en}}{dt} = \frac{1}{\sum_i n_i c_{v,i}} \left(\dot{H}_{in} - \dot{H}_{out} + \dot{Q}_{rx} - \dot{Q}_{loss} - (T_{en} - T_{ref}) \cdot \sum_i c_{v,i} \frac{dn_i}{dt} \right) \quad Eq. 3.19$
$P_{mix}: \quad X_{H_2,p} = \frac{n_{H_2}}{n_{en}} \quad Eq. 3.8$	$\dot{Q}_{loss} = h_{loss} \cdot A_{wall} \cdot (T_{en} - T_{wall}) \quad Eq. 3.20$
$R_{mix}: \quad X_{H_2,R} = \frac{C_{meas}}{100} \quad Eq. 3.9$	$\frac{dT_{wall}}{dt} = \frac{\dot{Q}_{loss}}{m_{wall} \cdot C_{steel}} \quad Eq. 3.21$
Overpressure	
$p_{en} = \frac{n_{en} \cdot R \cdot T_{en}}{V} \quad Eq. 3.10$	$p_{en} = \frac{n_{tot} \cdot R \cdot T_{en}}{V} \quad Eq. 3.22$

The model for PPP resulting from unignited hydrogen releases was solved in Matlab by using the forward Euler method. To calculate the overpressure (Eq.3.10) for a given hydrogen mass flow rate and natural ventilation PPP area the mass balance in the enclosure has to be solved first (Eq. 3.4). The mass flow rate into the enclosure consists only of hydrogen and can be assumed, calculated or taken from measurements. The mass flow rate through the vent (out from the enclosure) consists of air and hydrogen and was calculated based on a steady-state incompressible energy equation- choked flow (Eq.

3.6). To find the solution for Eq. 3.6, the molecular mass in the enclosure has to be calculated first, here, based on the hydrogen mole fraction. The hydrogen mole fraction was calculated for two cases:

- The perfect mix (Pmix) case is when the mole fraction is calculated with Eq. 3.8. It assumes a perfect mixing of hydrogen and air inside the enclosure.
- The real mix (Rmix) case is when the mole fraction of hydrogen is not calculated but extracted from the hydrogen concentration sensor data, (Eq. 3.9).

The model for PPP resulting from ignited hydrogen releases was solved in Matlab using variable time step Runge-Kutta method (MATLAB ode45) [99]. In the calculations the stoichiometric hydrogen combustion was applied where one mole of hydrogen requires 0.5 moles of oxygen: $H_2 + 0.5(O_2 + 3.76N_2) \leftrightarrow H_2O + 1.88N_2$. To calculate the overpressure (Eq. 3.22) the mass and energy balance has to be solved. The mass balance was calculated for each species (Eq. 3.11-Eq. 3.14) for a given hydrogen mass flow rate. The molar flow out (Eq. 3.15) was calculated the same way as in the unignited model. The perfect mix assumption of the mole fraction was used to calculate the molecular mass of the enclosure. The energy balance given by Eq. 3.18 (with neglecting mechanical energy) was calculated in terms of temperature (Eq. 3.19). The NASA polynomials [100] were used to calculate enthalpies and the number of moles: out and into the enclosure, were taken from the mass balance. The energy loss (Eq. 3.20-Eq. 3.21) was calculated with the major assumption of a simple heat transfer through the walls, neglected in the previous work (ref). When the pressure inside the enclosure is lower than outside pressure ($\Delta p < 0.001$ Pa) -end of combustion, the air is flowing in through the vent/s and Eq. 3.17 was used to calculate molar flow instead of hydrogen mass flow rate.

3.1.5 Results and analysis

The Pressure Peaking Phenomena was successfully observed during both unignited and ignited hydrogen releases in the 14.9 m³ explosive chamber. Article A, Article B, Proceeding A and Proceedings B are products of experimental campaigns on PPP. The experimental matrix presented in Table 8 and Table 9 were designed to investigate the

relation between mass flow rate and natural ventilation area and resulting overpressures in the enclosure. In this section the main results from unignited jets are presented first, then the result from the jet fires are followed with a comparison to unignited jets.

Unignited PPP

The hydrogen concentration will increase as long as the enclosure is not 100% filled with hydrogen. The pressure increases until reaching maximum overpressure, which occurs when $\dot{n}_{in} = \dot{n}_{out}$. After that, the overpressure is decreasing since the $\dot{n}_{in} < \dot{n}_{out}$. The results showed as was expected a big dependency on the relation between mass flow rate and size of the vents. In Table 8 the list of measured maximum overpressures (pressure peaks – p_{max}) and maximum concentration is presented in the 2nd column (measured). The simulation results from the analytical model described in section 3.1.4 are presented in the 3rd column.

Table 8: Maximum overpressure and hydrogen concentration results for Experiments 2–11. Unignited releases through a 4 mm nozzle.

Setup					Measured				Simulated			
Exp #	H ₂ release time [s]	Vent area [m ²]	Tank pressure p ₀ [bar]	Mass flow rate [g/s]	To in enclosure [K]	Overpr e-ssure [kPa]	H ₂ conc.at p _{max} [%]	Time of p _{max} [s]	Overpre-ssure R _{mix} [kPa]	Overpre-ssure P _{mix} [kPa]	H ₂ conc at P _{mix} [%]	Time of p _{max} [s]
2	90	0.0012	26.8	1.90	293.00*	0.42	1.5	10	-	0.43	3.0	21
3	120	0.0020	40.0	3.50	293.00*	0.51	0.2	10	-	0.54	4.0	16
4	120	0.0020	104.0	9.05	293.00*	2.86	-	17	-	3.09	15.0	24
5	120	0.0014	110.0	9.90	293.00*	6.45	-	32	-	6.41	26.0	41
6	120	0.0014	11.,5	10.1	296.00	6.74	24.0	37	6.72	6.67	26.0	40
7	180	0.0006	36.0	3.05	292.34	4.07	15.4	80	3.88	3.69	16.5	77
8	180	0.0006	39.7	3.05	291.94	3.96	16.0	77	3.95	3.70	16.5	77
9	200	0.0006	58.5	4.75	293.12	8.05	25.0	89	7.86	7.70	28.0	91
10	200	0.0006	52.6	4.20	289.71	6.70	22.0	89	6.86	6.26	25.0	89
11	1000	0.0006	49.6	4.85	293.57	7.00	21.5	64	7.23	6.58	21.0	89

blowdown

Figure 3.8 show an example of the hydrogen flow measurement: the constant mass flow rate and the constant pressure of the hydrogen flux.

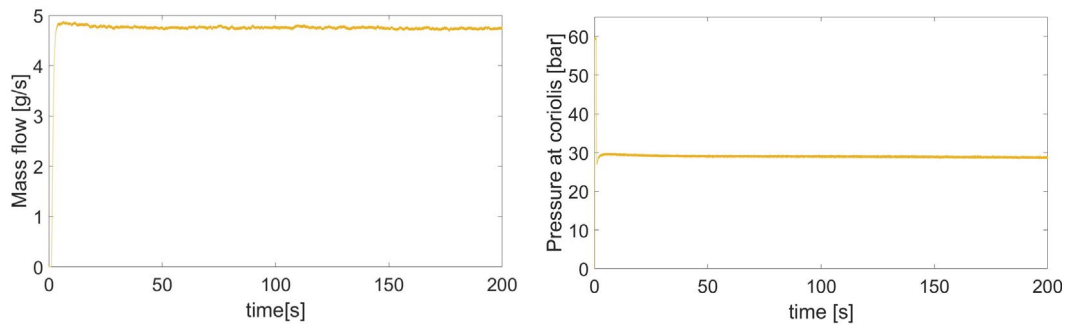


Figure 3.8: Example of the experimental hydrogen flow measurement (Exp 9). Right- mass flow rate, left- pressure at the coriolis output

A significant relation between relatively high mass flow rate and relatively low ventilation area which will result in overpressures was proven. Based on the experimental result shown in Figure 3.9, at constant volume, the pressure peak will be larger for higher mass flow rates and will occur at later times.

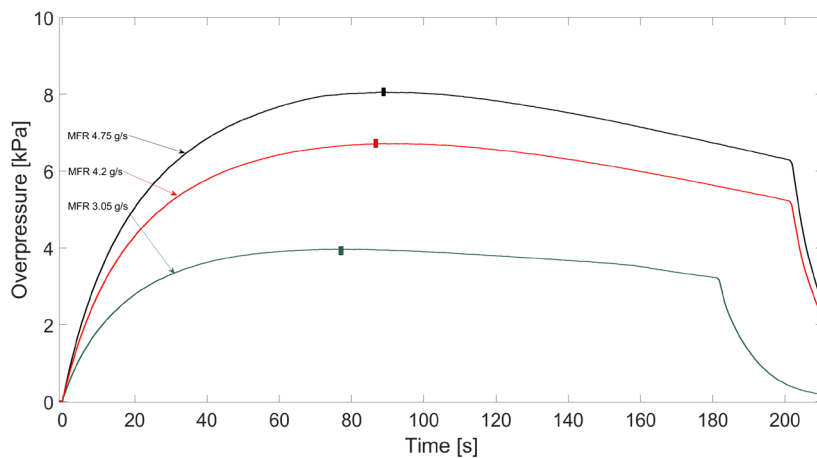


Figure 3.9: Experimental overpressures for varied mass flow rates at the same ventilation area; pressure peak occurrence (rectangle). Vent area 0.0006 m².

The analytical model proved the large dependency on the mass flow rate and vent area but also on the discharge coefficient. Small changes in one of those parameters had a large influence on the overpressure. The discharge coefficient has to be chosen based on the application design. By adjusting the discharge coefficient in both Pmix and Rmix models the value $C=0.7$ gave the best agreement to the experimental result and was used for further computational analysis. The perfect mix assumption showed very good

agreement presented in Article A [101] with the concentration measurements and is used for further analytical calculation on pressure peaking phenomena (ignited as well).

The interconnection of hydrogen mass flow, vent area and enclosure volume presented in Figure 3.10 provide a better understanding of the potential hazards from accidental hydrogen releases in enclosures. Based on the computation result presented in Figure 3.10 for the hydrogen mass flow rate from 1-100 g/s the main correlation between ventilation area, mass flow rate and enclosure volume on overpressure are:

- Decrease of ventilation area will increase the overpressure (confirmed with experiments and simulation)
- An increase in mass flow rate will increase the overpressure (confirmed with experiments and simulations)
- An increase in mass flow rate will cause the pressure peak to occur at a later time (experimental and simulation results). The mass flow rates at which the pressure peak could be observed at an earlier time (at the same ventilation area) are very high and were not part of the experiments.
- Increasing the enclosure volume for the same ventilation area will not influence the maximum overpressure but will delay the time of the pressure peak (simulation results)
- Decreasing ventilation area will cause pressure peak to occur at a later time

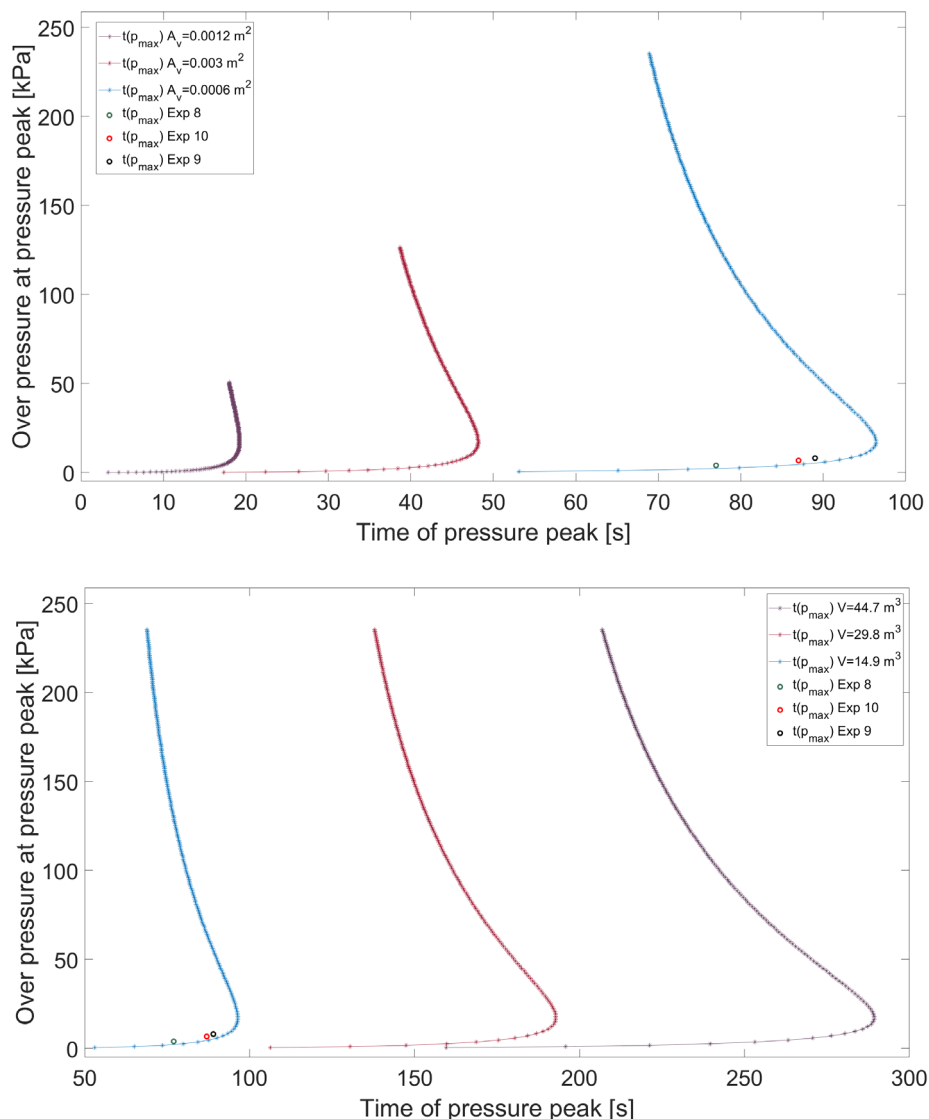


Figure 3.10: (Top) Correlation between the time of overpressure peaks for a constant rate of hydrogen release (1–100 g/s) at different ventilation areas for the same enclosure volume, 14.9 m³. (Bottom) Same as above, but with a different enclosure volume for the same ventilation area, 0.0006 m².

When considering a scenario with an accidental hydrogen release from an HFV, the size of the TPRD diameter directly influences the mass flow rate (as there will be choked flow conditions at the nozzle) and must be designed appropriately to avoid destructive pressure inside enclosures. The safety step for enclosures with a relatively small ventilation area might be an improvement of their ventilation systems. The presented model enables the proper calculation of overpressure as a basis for structural response. This can be used as a design tool to size the proper vent area or the maximum allowed mass flow rate based on the TPRD or process equipment inside enclosures.

Ignited PPP

The expected overpressures from hydrogen jet fires will be much higher. The ventilation area for the next experimental campaign was increased from 0.0006 m² to 0.0055 m² – 0.0164 m². The tests were conducted with different and approximately constant mass flow rates and a combination of three possible vents. For the first 10 experiments, the air fan was used to ventilate hot air and water from the enclosure after the hydrogen jet flame was shut down. Due to the observed underpressure, after the H₂ release was closed, the air fan was disconnected for the rest of the experiments, keeping the vent closed. The overpressure values given in Table 9 are the maximum: positive and negative pressures extracted from the experimental measurements and simulation from the analytical model presented in section 3.1.4. Due to safety measures, the hydrogen releases with a mass flow rate above 11 g/s were done only with 2 and 3 open vents.

Table 9: Experimental results: 31 tests of H₂ releases through a 4 mm nozzle with varying \dot{m} and ventilation area. One open vent = 0.0055 m², two open vents = 0.0109 m², three open vents = 0.0164 m².

Exp #	Setup			Measured							Simulated			
	H ₂ release time [s]	Open vent	Mass flow rate [g/s]	T ₀ in [K]	Overpressure [kPa]	Underpressure [kPa]	Temperature [°C]					Overpressure [kPa]	Underpressure [kPa]	Temp [°C]
							T _{avg}	T1	T2	T3	T4			
1	5.0*	1	1.45	8	4.8	-0.1	58	9	45	86	85	4.96	-0.4	80
2	10.0*	1	1.37	9	4.5	-0.3	93	14	81	128	125	4.54	-0.8	109
3	5.0*	1	3.38	10	16.7	-0.6	129	69	119	171	164	15.69	-1.6	185
4	10.0*	1	3.15	12	15.8	-2.8	195	141	175	251	225	14.30	-2.8	248
5	10.0*	2	3.14	15	5.3	-1.1	199	93	175	270	230	6.14	-1.1	261
6	10.0*	2	3.04	15	5.0	-1.1	192	86	176	258	223	5.92	-1.0	252
7	6.0*	2	7.90	3	22.0	-2.5	260	166	209	353	319	21.83	-3.0	500
8	6.0*	2	7.50	4	20.6	-2.3	250	142	207	348	287	20.28	-2.8	474
9	6.0*	3	8.37	6	13.9	-2.9	297	194	242	403	345	14.3	-1.8	566
10	6.0*	3	8.35	6	13.7	-2.8	292	192	243	389	332	14.26	-1.8	566
11	7.5	3	8.63	7	14.7	-3.3	305	204	249	416	358	14.87	-2.0	610
12	6.0	3	8.90	9	15.1	-2.3	268	176	215	372	322	15.26	-1.7	545
13	6.0	3	11.72	8	21.7	-4.3	345	244	288	458	408	21.48	-2.4	739
14	6.0	3	11.37	4	21.1	-3.8	324	241	274	430	352	21.04	-2.3	701
15	6.0	3	4.00	4	4.3	-0.5	147	40	129	202	194	5.22	-0.5	222
16	6.0	3	4.07	4	4.5	-0.5	148	45	130	209	190	5.39	-0.5	227
17	6.0	2	11.52	5	33.3	-3.2	317	211	263	415	367	33.06	-3.8	661
18	6.0	2	11.47	5	33.0	-3.4	316	205	267	414	367	32.79	-3.8	664
19	6.0	1	8.62	5	48.1	-5.7	254	194	205	359	300	45.75	-4.9	438
20	7.5	1	8.50	5	46.5	-8.2	295	243	247	383	332	45.27	-5.9	505
21	6.0	2	8.52	7	23.7	-2.0	256	166	223	333	294	23.36	-2.7	483
22	6.0	2	2.60	7	4.1	-0.3	104	12	98	142	139	4.87	-0.4	142
23	15.0	2	2.36	6	3.5	-1.1	194	87	174	275	238	4.29	-1.0	212
24	25.0	3	2.38	7	1.8	-1.0	286	195	240	368	331	2.33	-0.6	248
25	25.0	3	3.87	5	4.1	-2.2	395	315	339	481	435	4.99	-1.1	403
26	20.0	3	6.70	9	10.1	-4.6	520	384	467	603	568	10.80	-1.9	677
27	10.0	3	6.65	8	9.9	-2.7	320	213	259	433	391	10.65	-1.7	543
28	10.0	2	6.56	9	16.8	-3.5	314	219	247	419	369	17.22	-3.0	519
29	20.0	2	6.55	8	16.7	-8.7	496	375	474	578	531	17.40	-3.5	659
30	10.0	1	6.65	10	35.9	-14.1	305	246	259	392	349	34.48	-6.1	483
31	20.0	1	6.56	9	35.3	-25.3	477	366	444	556	522	34.44	-8.6	647

The example of the hydrogen flux measurement of constant mass flow is shown in Figure 3.11. The hydrogen releases were at least 20 times shorter than for unignited releases. The pressure drop observed in Figure 3.11 last for 6 s- it is the duration of the experiment after which the pressure came back to its static conditions.

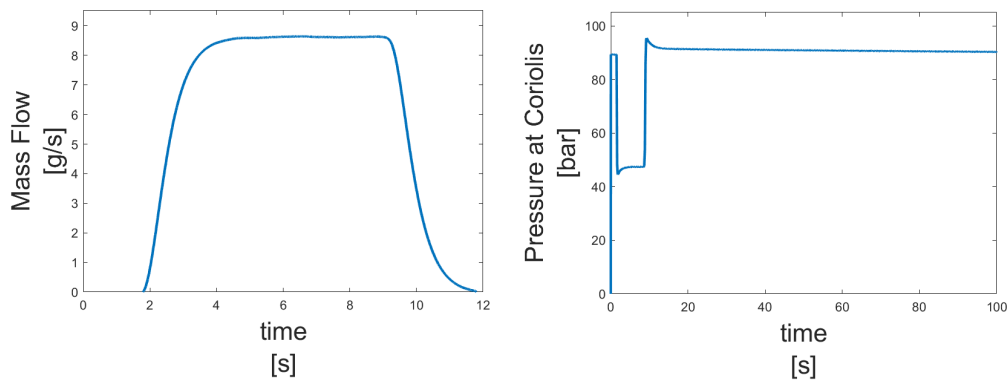


Figure 3.11: Example of the experimental hydrogen flow measurement (Exp 19). Right- mass flow rate, left- pressure at the coriolis output.

The result of hydrogen jet fires showed an increase in pressure and temperature inside the enclosure. The self-extinction due to limited ventilation was not observed in any experiments. The experiments started when the explosive chamber contained only air. When the experiment starts, the immediate combustion of hydrogen resulted in the production of water vapour. The mole fraction inside the enclosure: oxygen depletion and increase of H₂O shown in Figure 3.12. The underpressure effect observed during this campaign occurs when hydrogen stops burning, hence the mole fraction of water vapour starts to decrease. The last six experiments were devoted to the investigation of the dependency of the ventilation area and combustion time on observed underpressures.

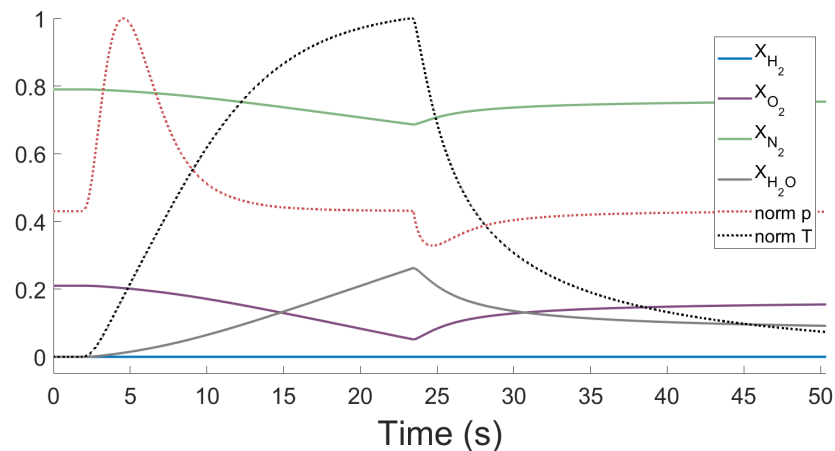


Figure 3.12: Analytical results of exp 26. Mole fractions and normalized pressure and temperature.

The PPP resulting from ignited releases was explained in Article B: “ A light gas is produced inside the volume, but a denser gas (mostly air) flows out at the vent. The mass flow out is given by the density at the vent (Eq. 6), which is relatively higher than the density of the combustion products. This effect of a lighter gas pushing the denser gas is the reason for the transient pressure rise known as the pressure peaking phenomena.” [97]. This is the same effect as for the unignited releases, just the lighter gas is not hydrogen ($M = 2 \text{ g/mol}$) but water vapour ($M = 18 \text{ g/mol}$) which is pushing out the air ($M = 28.97 \text{ g/mol}$).

The overpressure result showed its sensitivity to the mass flow rate and ventilation area (Figure 3.13). For the higher mass flow rates decreased ventilation area results in higher overpressure. The relation can be seen in the right plot in Figure 3.13, where the red line departs from the two other lines.

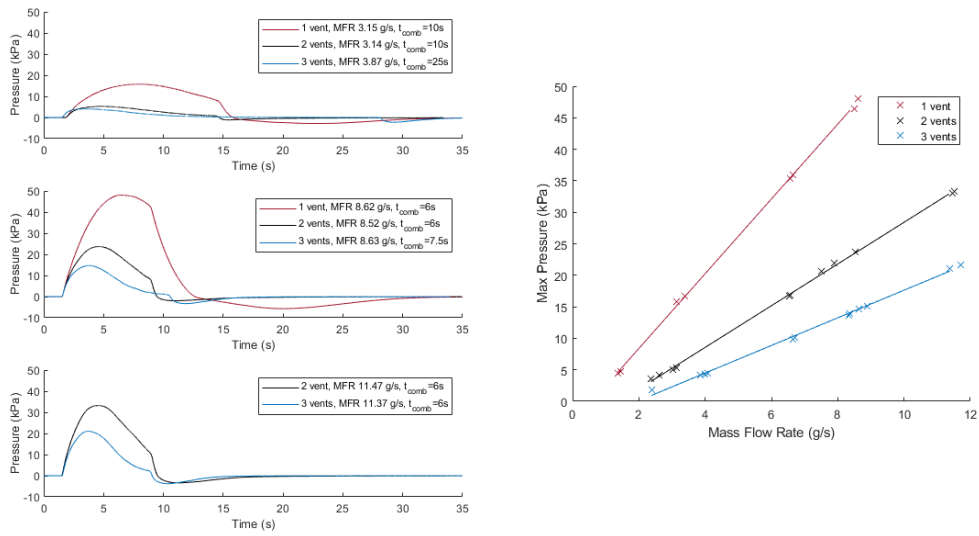


Figure 3.13: (left) The overpressure results from 3 mass flow rate groups (with approximately equal mass flow rate each) top ~3.5 g/s, middle ~8.6 g/s, and bottom ~11.4 g/s for different ventilation areas (red, black, and blue lines). (right) overpressure dynamics for all 31 experiments.

The overpressures resulting from jet fires are much higher than those from unignited releases and occur in only a few seconds. Increasing ventilation area almost 9 times for the hydrogen mass flow almost equal to unignited releases resulted in overpressure 4 times higher and over 73 s faster (Figure 3.14). It can be reasoned with high released combustion energy but also with the molar mass of combustion products. The higher temperature is increasing the density while the molar mass of water is 9 times higher than hydrogen. Higher molecular mass entraining the enclosure is also influencing the molar mass in the enclosure and hence in the vent, causing the $\dot{n}_{in} = \dot{n}_{out}$ (pressure peak) to be reached much faster.

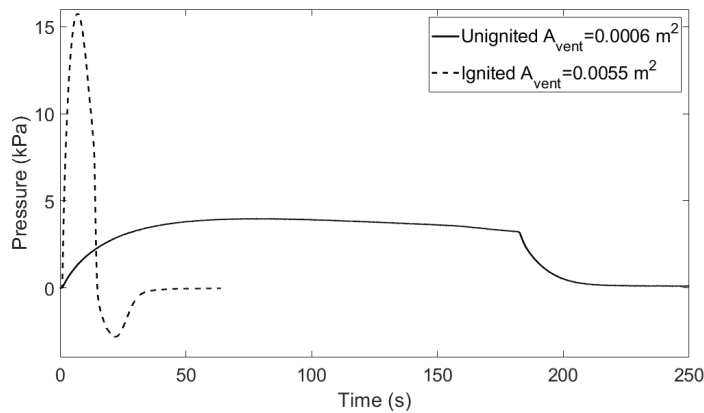


Figure 3.14: Pressure peaking phenomena for unignited (Exp 7), and ignited releases (Exp 4) with $\dot{m} \sim 3.1 \text{ g/s}$ through a 4 mm nozzle.

The analytical model presented in section 3.1.4, has two unknown parameters, the discharge coefficient, C , and heat loss coefficient, h_{loss} , affecting molar flow out \dot{n}_{out} and the underpressure effects respectively. For unignited releases the $C = 0.7$ which due to the different nature of the occurrence may not necessarily be equal for ignited releases. In Proceedings A the Bayesian approach was presented to analyse both coefficients resulting in the best fit to all experiments with $C = 0.9$ and $h_{loss} = 30 \text{ W/m}^2\text{K}$. The analytical model's pressure results are in good agreement with experimental ones within the limit of $\pm 2 \text{ kPa}$, as is shown in Figure 3.15 (both positive and negative peaks). The hydrogen release time (hence combustion time) was the longest for the experiments 26-31. Those experiments with one or two open vents stand out from the $\pm 2 \text{ kPa}$ for the negative peak due to condensation of water which is not included in the analytical model. The accumulated water was not included in the model which caused discrepancies in the underpressure estimation shown in Figure 3.15, middle. Due to the simple assumption of the heat transfer in the analytical model and measurement difficulties (response time) the temperature is not well predicted for most of the experiments. The heat transfer between hot gas and thermocouple is speculated to be the reason. Nevertheless, the temperature measurements are available in Published Supplementary Data B and the results can be used for the improvement and validation of the existing models or to develop a new approach.

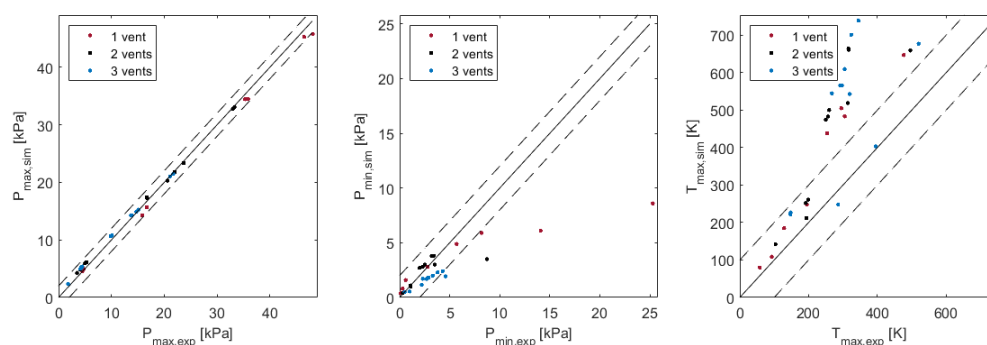


Figure 3.15: Comparison of experimental results and analytical model calculations from 31 experiments: left- positive pressure peak, middle- negative pressure peak, right- maximum temperature.

The pressure peak (positive) does not depend on the total amount of burned hydrogen. It occurs at the first second of the jet fire and rapidly drops to nearly ambient pressure.

The temperature nevertheless is increasing as long the combustion continues (temperature depend on the total amount of burned hydrogen). When hydrogen was stopped, the rapid decrease of temperature was observed which caused the underpressure effect. The underpressure effect depends mostly on the ventilation area and combustion time shown in Figure 3.16. An increase in mass flow rate will automatically affect the combustion and have an obvious effect on the underpressure.

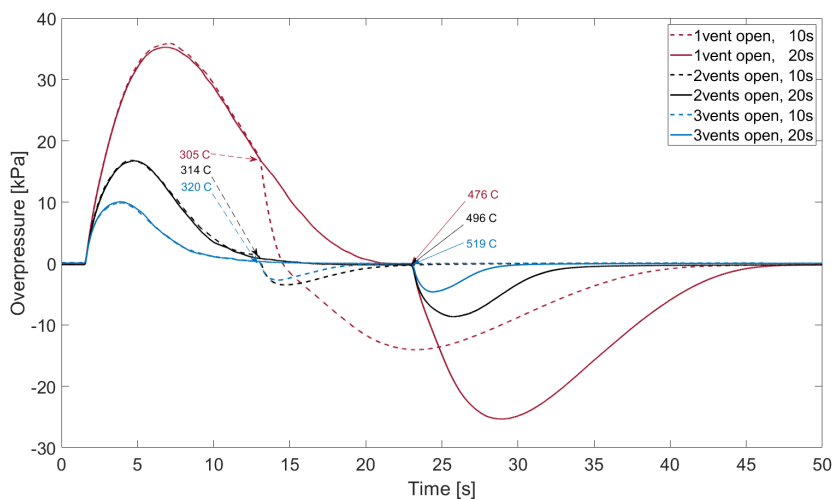


Figure 3.16: Overpressures in the 14.9m³ enclosure during hydrogen releases of 10 s and 20s in three different ventilation area at the same MFR~6.6 g/s, 1 open vent=0.0055 m², 2 vent open= 0.0109 m², 3 vents open= 0.0164 m².

The summary from jet fires:

- Measured and estimated overpressures are much higher compared to unignited jets.
- Overpressure increases with increasing the mass flow rate (larger TPRD diameter), which is the same as for unignited jets.
- The pressure peak occurs earlier with increasing the mass flow rate, which was the opposite for similar mass flow rates for the unignited jets.
- A positive peak is independent of the combustion time.
- The underpressure effect increases with the increase of combustion time and decrease of the ventilation area.
- Underpressure effect was not observed (in experimental nor analytical results) for the unignited jets

3.2 Hydrogen releases in covered carpark

In this chapter, the work of a series of experiments and a summary of the results of hydrogen releases in the semi-confined enclosure is presented. The full-scale experimental setup imitates an enclosure similar to a carpark for both: unignited and ignited releases. The influence of the existing standards of mechanical ventilation on created hydrogen clouds will be tested during unignited releases. The results were published in Article C and Proceedings C. The results from the ignited releases were submitted to the ISFEH – 2022 (Proceedings D) presenting the investigation of fire effects resulting from hydrogen jet fires.

Hydrogen releases were performed on a full scale to investigate the effect of mechanical ventilation on the accumulated hydrogen cloud inside the enclosure. The hydrogen jet fires experiments were conducted to investigate the thermal effects of the non-premixed, impinging on the ground, turbulent jets. To investigate the sufficiency of the existing Regulations, Codes and Standards (RCS) the temperature inside the enclosure and in the ventilation system was measured. Since the 700 bar storage tank pressure is becoming more common, the blowdown type of mass flow were performed full scale from 200 bar to 700 bar. The minimum height of the carpark in Norway is 2.5 m and the required ventilation rate described in Chapter 1.1.2 is 6 or 10 ACH. The releases from the car were imitated with a steel table which had to be 40% of the size of the hydrogen car due to the width limitation of the container.

The full-scale carpark geometry and instrumentation setup are described in detail. The goal of this work is to develop recommendations for the Regulation Codes and Standards (RCS) for the safe use of hydrogen vehicles in the enclosed transportation system. The purpose of the campaigns is to generate data for further model validations and to recommend a safety diameter of the Thermal and Pressure Relief Device with existing ventilation systems.

All experiments were carried out in a 40 ft ISO container. The container was placed at the Norward AS in Bamble. The P&ID of setup and instrumentation is shown in Figure 3.17 and Figure 3.18 for unignited and ignited experiments respectively.

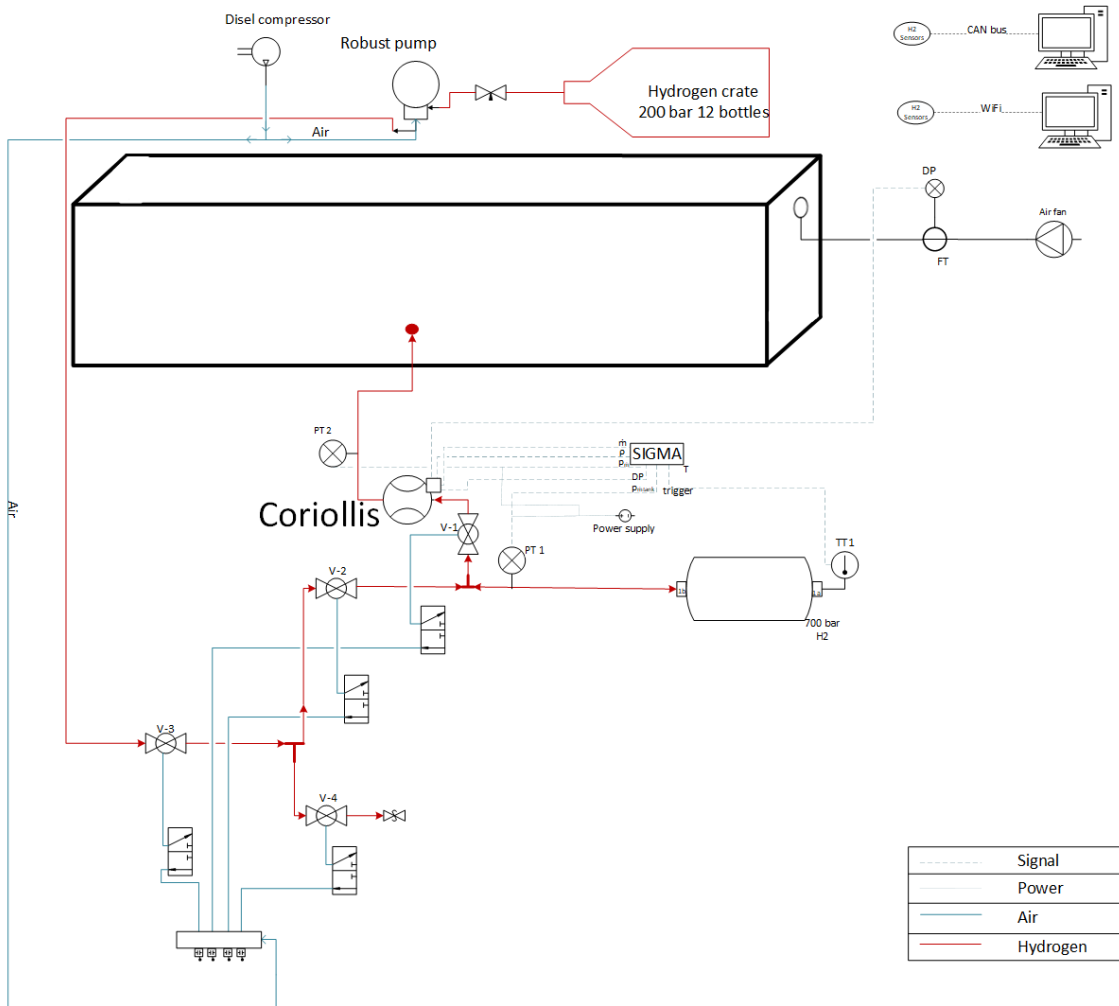


Figure 3.17: P&ID – unignited hydrogen jets.

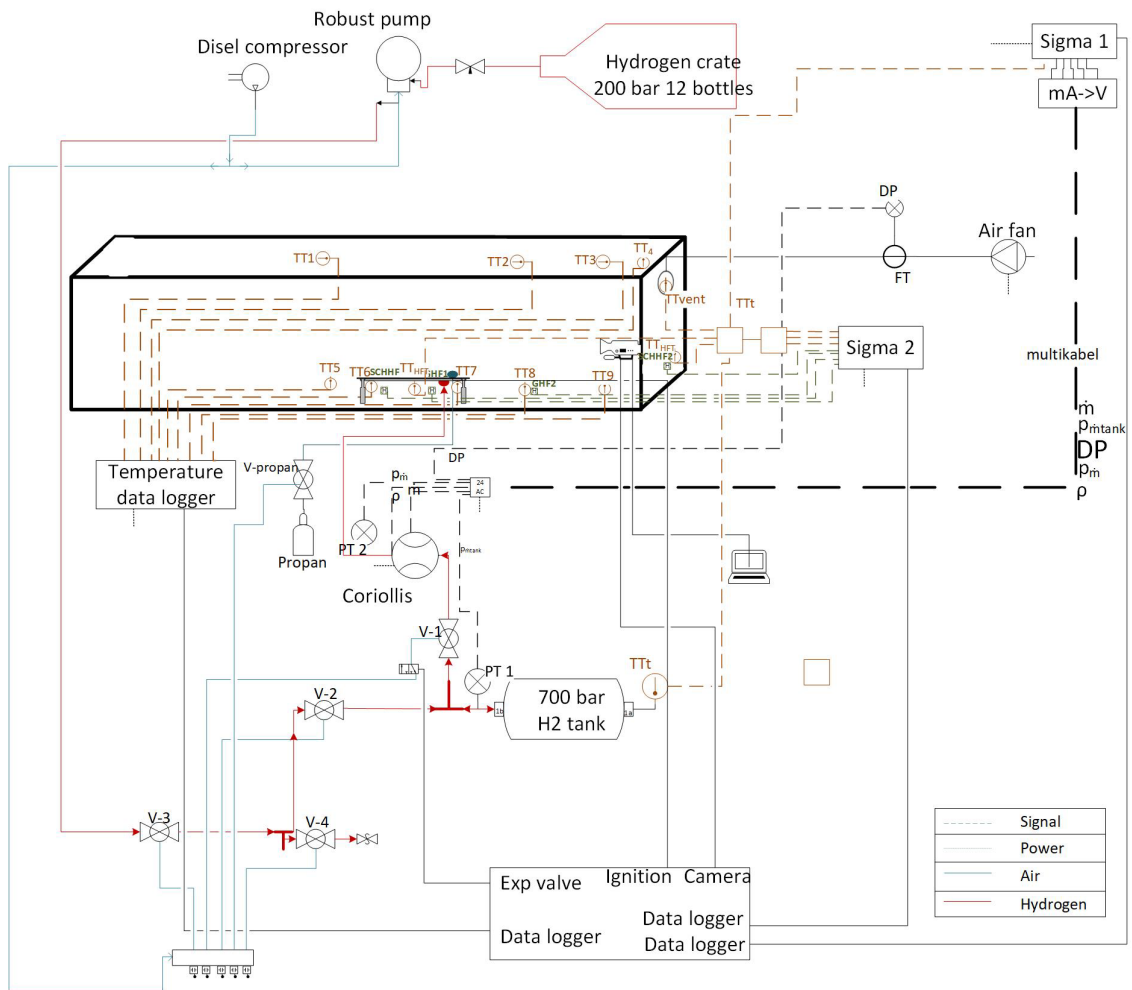


Figure 3.18: P&ID – ignited hydrogen jets.

3.2.1 Geometry

The 40 ft ISO container (Figure 3.19) with isolated walls was used for all experiments with both doors open. Its inner dimension $L \times W \times H$: 11.885 x 2.240 x 2.285 m gives a total volume of 60.8 m³. The insulation thickness was approximately 0.07 m.



Figure 3.19: 40 ft ISO container with installed equipment and instrumentation.

The instrumentation assembled in the:

- Ventilation:
 - The ventilation system consists of ~4 m long pipes with a diameter of 0.315 m and 0.200 m
 - The end of the 0.315 m pipe (outlet) was in the container located 0.05 m from the ceiling at the ventilation wall (0.2075 m to the outlet centre)
 - An air fan, connected with the outlet of 0.200 m pipe
 - Duct damp IRIS 200 with mounted differential pressure transmitter – control over air volume flow.

During unignited releases, the air was blown out from the ventilation and through the container (safety precautions), while during ignited releases the air and hot combustion products were sucked out through the ventilation pipe.

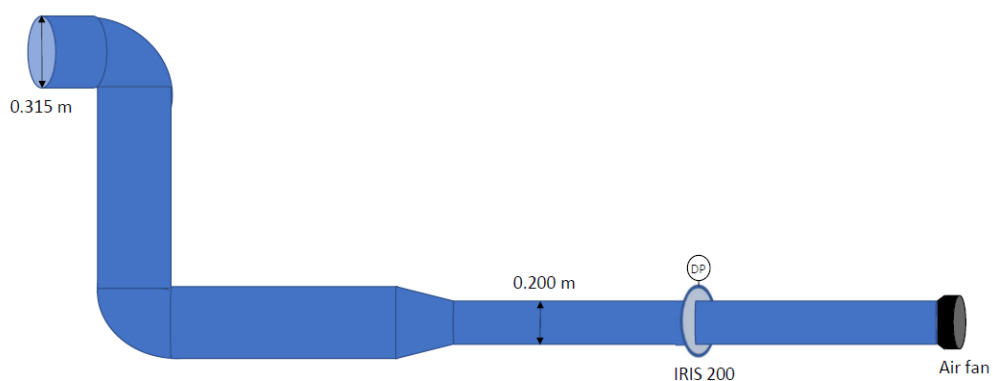


Figure 3.20: Sketch of the ventilation line.

- Hydrogen pipe
 - The pipe with 3 mm ID (6 mm OD) was mounted through the back wall, 5 m from the ventilation wall and 0.6 m above the floor.
 - The H₂ 1 mm or 0.5 mm nozzle was mounted vertically through the steel table 0.25 m above the floor.
 - The unit with 3 mm ID was connected to the nozzle unit to discharge H₂ under the table: 90° for all unignited releases and, 90° and 45° for ignited releases (Figure 3.21).
- Steel table
 - The dimensions $L \times W \times H$: 1.965 x 0.730 x 0.250 m. The table was imitating the hydrogen car (40% of a Toyota Mirai) Figure 3.22.
 - The table was placed in the centre of the container 4.5 m from the ventilation wall.
- Fire plates
 - Placed on the floor under the table with 6.5 m total length: one layer for unignited releases. Two extra layers were added under the nozzle during ignited releases due to the destructive effect on only one layer.



Figure 3.21: Nozzle configurations: left – 90° nozzle, right – 45° nozzle.



Figure 3.22: Picture of the table imitating the Toyota Mirai. Scaling factor 0.4.

- During the unignited releases, 30 Canbus hydrogen sensors were installed inside the container
- During the ignited releases, through the container walls and ceiling, were placed: 9 thermocouples, 4 radiative heat flux sensors, 2 total heat flux sensors, 1 pipe for ignition system (propane pipe) and 1 borescope lens. The isolation blanket FireWrap was used to protect thermocouples (TT6 and TT7) and pipes inside the container. FireWrap was manufactured from Insulfrax low bio-persistence fibres, is made for high temperatures, specifically designed for fire protection applications (128kg/m^3 give the thermal conductivity 0.05 W/mK).

The experiments were performed with two setups:

- One for constant mass flow releases The hydrogen flow started from the hydrogen crate (12 bottles of 200 bar) through coriolis mass flow meter and released through a 1 mm or 0.5 mm nozzle in the container. The total pipe length was 3.84 m (without units) with a starting point from hydrogen storage at 1.75 m height (Figure 3.23, a).
- Second for blowdown type mass flow releases. During experiments, hydrogen flow started from the hydrogen tank, type IV (manufactured by Hexagon Lincoln Inc) with a carbon composite wall and operating pressure up to 700 bar. Then through the coriolis mass flow meter to be released through a 0.5 mm nozzle. The total pipe length was 3.86 m (without units) with starting point from hydrogen storage at 0.3 m height (Figure 3.23, b).

The setup with the constant mass flow was used during unignited releases only. The second setup was expanded with a gas booster pump (Haskel-Proserv operating pressure 1600 bar) which was used to fill hydrogen tank up to 700 bar (from the hydrogen crate)

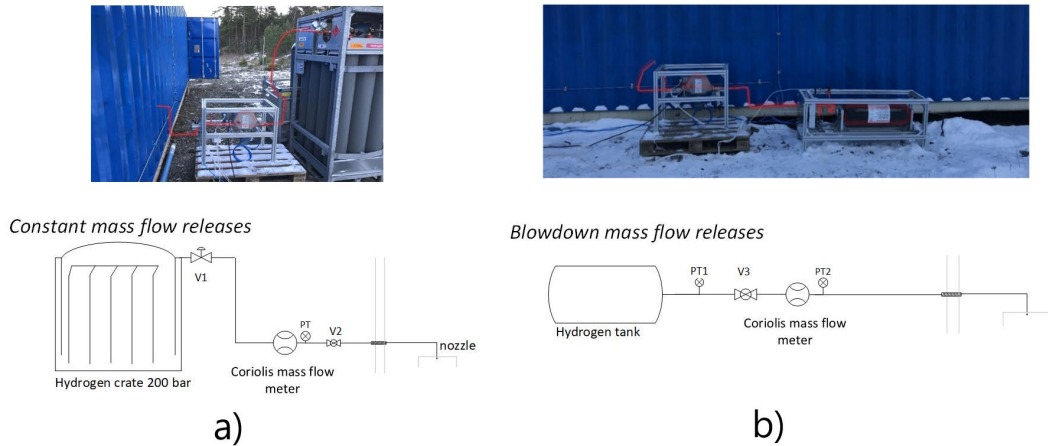


Figure 3.23: Hydrogen path from the hydrogen storage to the release point (inside the container).

3.2.2 Instrumentation and logging

The experiments were performed with constant and blowdown type of mass flow. All experiments were performed with hydrogen flow through Coriolis mass flowmeter model HPC010P ultra-high pressure from Emerson Micromotion with connected transmitter model 5700 with operating pressure up to 1043 bar. The computational signal calculations are given below:

$$\text{Range } 0 - 15 \text{ g/s (all ignited exp) : } \quad \dot{m} = 3.75 \cdot (V - 1) \quad \text{Eq. 23}$$

$$\text{Range } 0 - 15 \text{ g/s (exp20-exp23 unignited releases) : } \dot{m} = 4.006 \cdot (V - 1) \quad \text{Eq. 24}$$

$$\text{Range } 0 - 300 \text{ g/s (unignited exp1-exp19): } \quad \dot{m} = 80.128 \cdot (V - 1) \quad \text{Eq. 25}$$

During all experiments, the same ventilation system was used. The airflow rate was controlled by an IRIS 200 damper and voltage speed controller for the fan. The air change per hour (ACH) for the experiments was according to British Standard [10]: 10 ACH and 6 ACH. The airflow was measured by the differential pressure of the IRIS 200

damper with the GAMS Sensor differential pressure transmitter (DP) model 5266. The computational calculations resulting in pressure unit Pa are given in the equation below:

$$DP = 50 \cdot (V - 3) \quad Eq. 26$$

The airflow for specified ACH was calculated with $q = ACH \cdot V$ (Eq.2.4 in Chapter 2.2.1.2). For the container geometry that means 608 m³/h and 365 m³/h for 10 and 6 ACH respectively. The IRIS damper specification given by the position/diameter was used to calculate resulted airflow with the equation $Q = k\sqrt{DP} \cdot 3,6, m^3/h$.

During blowdown type hydrogen releases the thermocouple type K with measurement range -40 °C – 1000 °C and robust 4-20 mV signal was mounted in the hydrogen tank bolt. To avoid a cold junction the temperature transmitters (1V – 5V) were added with the measurement range 0 – 1000 °C -unignited releases and -15 – 100 °C - ignited releases. The computational calculations are given below:

Unignited releases: $T_{tank} = 250 \cdot (V - 1) \quad Eq. 27$

Ignited releases $T_{tank} = 37.5 \cdot V - 87.5 \quad Eq. 28$

3.2.2.1 Unignited releases

An oscilloscope SIGMA was used to record:

- pressure from sensors (PT1, PT2, DP, Figure 3.17),
- mass flow rate and density from the coriolis mass flow meter and
- temperature from the thermocouple type K mounted at the hydrogen tank (Figure 3.17).

Constant releases were performed directly from the hydrogen crate, through Coriolis mass flow meter, where mass flow, hydrogen pressure (measured at the output) and density were constantly measured. The pressure (p_m , bar) was measured with pressure transmitter ESI model HP1003-1000DE with the pressure range 0- 1000 barg. The same pressure transmitter was installed at the outlet of the hydrogen tank during blowdown releases. During blowdown releases, the pressure transmitter at the tank did not give

accurate signal output. That is why the pressure transmitter at the Coriolis mass flowmeter was placed at the tank (the unworking transmitter was mounted at the Coriolis during the blowdown tests). The solution was applied due to lack of time for ordering new parts and weather conditions which prevented the preparation of new pipes and joints during the experiments. The pressure was calculated from the signal with the equation below:

$$p_{\dot{m}} = 251 \cdot (V - 1) \quad \text{Eq. 29}$$

Along with the container, the 30 Xensornr 5320 CANbus hydrogen sensors (04D) were installed and 8 Xensornr 5320 Wifi sensors (DC). The sensor working temperature range is $-40 - 85$ °C, humidity range $0 - 95$ % RH, and the pressure range $500 - 1200$ mbar. The sensors measure the thermal conductivity of the ambient gas by the temperature elevation of the sensor's element with correction for ambient temperature and humidity. The positions of the sensors are listed in Table 10, according to a reference sketch shown in Figure 3.24 and graphically present in Figure 3.25.

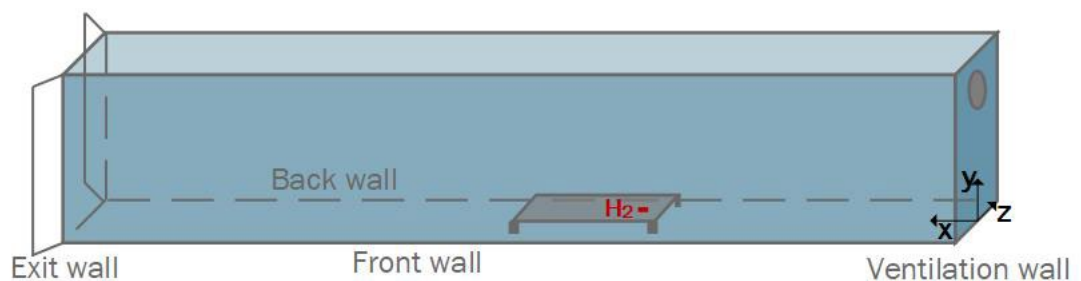


Figure 3.24: Reference sketch- unignited releases.

Table 10: Hydrogen sensors' position.

ID	Sensor Nr	Length	Height	Width
		x	y	Z
04D139	1	-11600	2170	0
04D140	2	-11600	1670	0
04D141	3	-10100	2170	0
04D142	4	-10100	1670	0
04D143	5	-8600	2170	0
04D144	6	-8600	1670	0
04D145	7	-7100	2170	0
04D146	8	-7100	1670	0
04D147	9	-5600	2170	0
04D148	10	-5600	1670	0
04D149	11	-4500	2170	0
04D150	12	-4500	1670	0
04D151	13	-3000	2170	0
04D152	14	-3000	2170	430
04D153	15	-4500	2170	863
04D154	16	-4500	2170	430
04D155	17	-5600	2170	863
04D156	18	-5600	2170	430
04D157	19	-7100	2170	863
04D158	20	-7100	2170	430
04D159	21	-7100	1670	430
04D160	22	-5600	1670	430
04D161	23	-4500	1670	430
04D162	24	-5000	1170	863
04D163	25	-5000	0	370
04D164	26	-5000	250	370
04D165	27	-5010	250	0
04D166	28	-4760	250	0
04D167	29	-6465	250	0
04D168	30	-6465	0	0
DC13	31	-11600	2170	863
DC09	32	-10100	2170	863
DC06	33	-8600	2170	863
DC12	34	-7100	1670	1100
DC11	35	-5600	1670	1100
DC08	36	-4500	1670	1100
DC10	37	-3000	2170	863
DC14	38	-4500	250	0



Figure 3.25: Hydrogen sensors' placement in the container. Red-CANbus sensors, grey-WIFI sensors.

Due to a large number of data points, the noise was reduced with a smoothing method – ‘findpeaks’, Matlab [102]. The method used the maxima of the neighbouring samples, which allowed to avoid averaging the signal output. The resulting hydrogen concentrations are plots with data samples that were larger than the two adjoining samples (an example is presented in Figure 3.26).

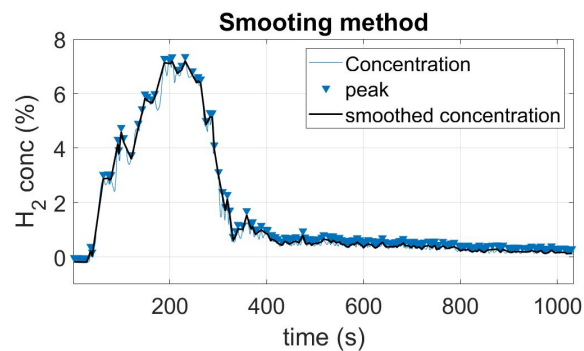


Figure 3.26: ‘Findpeaks’ smoothing method applied for hydrogen concentration results.

3.2.2.2 Ignited releases

The hydrogen sensors were disabled for experiments with hydrogen jet fires. Two oscilloscopes SIGMA were used to record data measured from sensors and transmitters (Figure 3.18). The recording was done with a sample rate of 2 kHz for most of the experiments and sensors. Oscilloscope Sefram model DAS 220 was used to record data from thermocouples TT1-TT9 with a sample rate of 50 Hz. The pressure measured at the

tank outlet and the coriolis outlet were calculated from the signal with the same equation since the sensor parameters were identical:

$$p_{in}, p_{tank} = 250 \cdot (V - 1) \quad Eq. 30$$

10 thermocouples (0.5 mm fast response Type K with grounded hot junction,) were installed to measure the temperature change. Nine thermocouples were placed inside the container: four thermocouples were mounted at the ceiling, 3 at the front wall and 2 thermocouples were mounted in the corners under the car. The 10th thermocouple was mounted inside the ventilation pipe (130 mm from its wall and 510 mm from the top of the ventilation outlet. The location of the thermocouples is listed in Table 11, according to a reference sketch shown in Figure 3.27. The data from the first 9 thermocouples were logged directly in the °C unit by oscilloscope Sefram. The temperature from the ventilation pipe, logged with oscilloscope Sigma 2, was calculated from the signal with the equation below.

$$TT_{vent} = 185.5 \cdot (V - 1) \quad Eq. 31$$

Two types of radiative heat flux sensors were used: Schmidt (range 11.35 kW/m²) and Gardon (range 567.8 kW/m²) from Medtherm Corporation. Three of four radiative heat flux sensors were installed at the front wall: Schmidt (RHF1) on the front of the car, Gardon (RHF2) on the back of the car close to the H₂ nozzle (next to the total heat flux THF1) and Schmidt between thermocouples TT8 and TT9 (RHF3). The fourth, Gardon, was mounted on the ventilation wall close to total heat flux (THF2). Each of the radiative heat flux needs to be cooled with water during the measurements to keep measurements on the same temperature level. Therefore the water pumps were installed close to RHF's outside the container. The specific parameters of the radiative heat flux sensor are given in Table 12. The computational signal calculations for Schmidt and Gardon sensors resulted in kW/m² are given below.

$$RHF_{Schmidt} = V \cdot 0.7463 \cdot 1000 \quad Eq. 32$$

$$RHF_{Gardon} = V \cdot 40.98 \cdot 1000 \quad Eq. 33$$

The total heat flux sensors were made at USN campus Porsgrunn by Andre Gaathaug with help from Øyvind Johansen. The heat flux box was made from a steel plate (2 mm thick). In its centre, the thermocouple type K from Autek was welded and secured around with an insulation blanket FyreWrap. The computational signal calculations for both THF sensors are given below, (°C).

$$T_{THF} = 250 \cdot (V - 1) \quad Eq. 34$$

The total heat flux calculations are based on the thermal resistance theory based on the Newton law: $q \equiv UA\Delta T$, where U is the overall heat transfer coefficient, A is the area and ΔT is the temperature difference. The $UA = 1/R$ where R is the thermal resistance. For total heat flux calculation, the sum of the thermal resistance (container wall, fire isolation inside the container wall, isolation plates inside the container, steel 304, and air gap inside the container's wall) was calculated with temperature difference from the steel box plate (S316) measured by thermocouple and the ambient temperature. The heat transfer at the steel box was calculated with C – specific heat capacity of steel, ρ – steel density, A – area, ΔT – temperature difference measured by a thermocouple in dt time. The equation is given below:

$$Q_{tot} = \frac{1}{A} \cdot (C_i \cdot \rho_i \cdot A_i \cdot \Delta T_{tt} dt - \sum UA \cdot (T_{amb} - T)) \quad Eq. 35$$

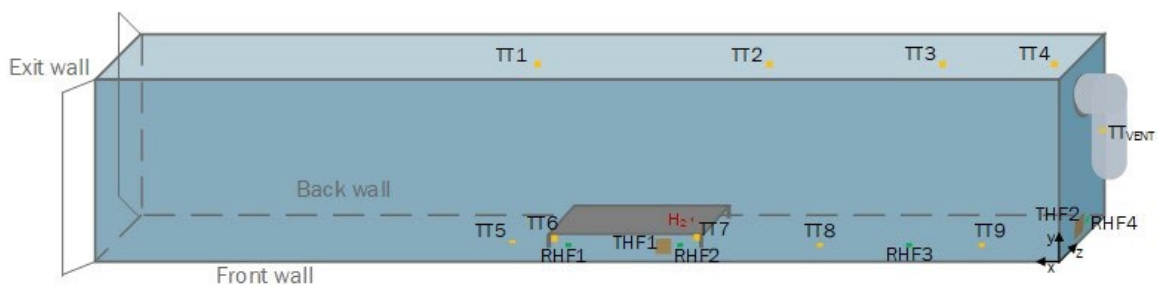


Figure 3.27: Reference sketch – ignited releases.

Table 11: Sensor location parameters [mm].

	y	x	z
TT1	2105	6250	1120
TT2	2105	2320	1120
TT3	2105	1060	1120
TT4	2105	110	1120
TT5	235	7200	80
TT6	198	6330	868
TT7	200	4600	860
TT8	235	3310	74
TT9	235	1030	80
TTvent	1725		130 inside
RHF1	235	6080	40
RHF2	220	4850	0
RHF3	235	2300	40
RHF4	235	40	1100
THF1	75	5020	50
THF2	95	0	750
Nozzle 45	180	4980	1120
Nozzle 90	230	5000	1120
Table	250	4500	755
outlets	2055	0	1120

Table 12: Radiative heat flux datasheet.

HF type	Schmidt	Gardon	Schmidt	Gardon
Chanel/Name	<i>CH5/RHF1</i>	<i>CH6/RHF2</i>	<i>CH7/RHF3</i>	<i>CH8/RHF4</i>
Range	<i>11.35 kW/m²</i>	<i>567.8 kW/m²</i>	<i>11.35 kW/m²</i>	<i>567.8 kW/m²</i>
Uncertainty +/- 2%	<i>+/- 0.227 kW/m²</i>	<i>+/- 11.356 kW/m²</i>	<i>+/- 0.227 kW/m²</i>	<i>+/- 1.356 kW/m²</i>
Serie Nr	<i>169606</i>	<i>169609</i>	<i>169607</i>	<i>169608</i>
Absorbance	<i>0.94</i>	<i>0.92</i>	<i>0.94</i>	<i>0.92</i>
Calibration output [mV]	<i>13.4</i>	<i>12.2</i>	<i>13.96</i>	<i>12.2</i>
	<i>at 10 kW/m²</i>	<i>at 500 kW/m²</i>	<i>at 10 kW/m²</i>	<i>at 500 kW/m²</i>
Responsivity [mV per kW/m²]	<i>1.34</i>	<i>0.0244</i>	<i>1.396</i>	<i>0.0244</i>
Inverse [kW/m² per mV]	<i>0.7463</i>	<i>40.98</i>	<i>0.7163</i>	<i>40.98</i>
Water [C]	<i>14.8</i>	<i>14.8</i>	<i>14.8</i>	<i>14.8</i>
Water [mL/s]	<i>12</i>	<i>12</i>	<i>12</i>	<i>12</i>

The hydrogen jet flames were recorded with Promon 500 high-speed camera from AOS Technologies AG mounted at the ventilation wall. The recording was done continuously to observe if hydrogen ignited and have a visual overview inside the container during

the whole experiment. The second camera – GoPro3 was placed on the floor at the front of the car to record jet flames under the table from a different angle.

The uncertainty of all the instrumentation is listed in the table below. The absolute measurement uncertainty includes the derived uncertainty of the Air Changes per Hour. The data used in the analysis are averages of more than 25 kilo-samples/sec and effectively reducing the uncertainty of the data. The CAN bus network for the XEN-5320 CAN sensors (Xensor catharometres) were used to measure hydrogen concentration. XEN-sensors with a data rate of 3 Hz, gave the concentration measurements pointwise every 0.33 s.

Table 13: uncertainty of measurements.

Equipment	Instrumentation uncertainty	Absolute measurement uncertainty
ESI Pressure transmitter	±1% FSO BFSL	±10 bar
DP transmitter	±1% FS	±15 m ³ /h (±0.2 ACH)
Mass flow	±0.2% of flow rate	
Concentration	±2%/%	±0.18% (max. conc)
Temperature	±0.75%	±2.2 °C to 4.5 °C
Radiative heat flux	+/- 2%	+/- 0.227 kW/m ² - Schmidt +/- 11.356 kW/m ² - Gardon

3.2.3 General Procedure

The experimental campaign with unignited releases was started with constant mass flow releases and a 0.5 mm nozzle due to safety precautions. Both ACHs were tested for three mass flow rates. The static release pressure (hence storage pressure) was set up with a gate valve at the hydrogen bottle stack (the same as for the PPP). The ventilation was tested then for the higher mass flow rates: the same matrix of storage pressure was set up for the releases with a 1.0 mm nozzle. After completing constant mass flow releases, the setup was rebuilt for blowdown mass flow releases, described in section 3.2.1. The same ACHs were tested against hydrogen releases from the three storage pressure: 200 bar, 350 bar and 700 bar. The tank was filled with hydrogen until reached the desired pressure. Blowdown releases were performed only with 0.5 mm.

The experimental campaign with ignited releases started with 0.5 mm and 90° nozzle from the highest storage pressure. Due to fire (floor and walls were partially burned) the next experiments were done with a 0.5 mm 45° nozzle. The last experiment was performed with 1.0 mm and 45° nozzle to investigate and compare the influence of increasing the nozzle diameter as was done for unignited releases. The ignition system was applied similar to the one in PPP. The hydrogen was released to the propane flame (immediate ignition). Shortly after ignition (observed with Promon camera), the propane flame was shut down; the thermal effect from the propane flame is assumed to be negligible.

3.2.4 Results and analysis

The experimental investigations of the hydrogen dispersion and the thermal effects were performed with the combination of two ACH, two nozzle diameters and in the case of hydrogen jet flames two nozzle angles. The results from unignited hydrogen releases were published in Article C, *Effect of Mechanical Ventilation on Accidental Hydrogen Releases—Large-Scale Experiments*, and Proceeding C. All measurements data are available in published Supplementary Data C and Supplementary Data D. The results of the ignited campaign were submitted to ISFEH 2022 with Proceedings D, *Thermal effects from downwards hydrogen impinging jet flame – experimental results from high-pressure releases in a carpark*, and the main results will be presented next, with the heat flux results published in the Supplementary Data D.

In this section, the main results from the unignited releases will be presented first, with the following results from ignited releases.

UNIGNITED HYDROGEN RELEASES

The result presented in this section will show the relation between hydrogen concentration from mass flow rate, reservoir pressure, and ventilation rate.

The increase in hydrogen mass flow rate results with increasing a storage pressure and/or nozzle diameter, which can be already observed in Table 14 where

- experiments 3 – 16 were performed with the setup for constant hydrogen mass flow discharges (exp 16 was a blowdown type since the storage pressure in the hydrogen bottle stack was not low to keep it constant)
- experiments 19 – 23 were performed with setup for blowdown discharges.

Table 14: Experimental parameters.

Exp	Nozzle Diameter [mm]	ACH [1/h]	ACH measured [1/h]	Exp matrix p_0 [bar]	Measured p_0 [bar]	MFR [g/s]	H ₂ release Time [s]	Ambient temp [C]	Wind [m/s]
3	0.5	10	9.5	120	-	1.1	30	-1	10
4	0.5	10	9.8	120	-	0.8	60	-1	10
5	0.5	10	9.8	160	-	1.1	60	-1	10
6	0.5	6	6.0	160	166	1.0	60	-3	6
7	0.5	6	6.0	120	121	0.7	60	-3	6
8	0.5	6	6.0	60	60	0.4	60	-3	6
9	1.0	6	6.0	160	157	6.0	60	-3	6
10	1.0	10	10.0	160	165	6.0	60	-3	10
11	1.0	10	10.0	120	140	5.2	60	-3	10
12	1.0	10	10.0	120	120	4.2	60	-3	10
13	1.0	6	6.0	120	121	4.2	60	-1	6
14	1.0	6	6.0	60	59	2.2	60	-1	6
15	1.0	10	9.8	60	55	2.2	60	-1	10
16	1.0	10	9.8	140	144	5.3*	1000	-1	10
19	0.5	10	10.2	700	721	7.9*	1000	-5	10
20	0.5	6	6.2	700	713	7.8*	1000	-3	6
21	0.5	6	6.2	360	362	4.2*	1000	-4	6
22	0.5	6	6.2	207	209	2.5*	1000	-2	6
23	0.5	10	10.2	360	359	4.2*	1000	-3	10

*mass flow rate at t_0

The example of the mass flow rate and its pressure for constant and blowdown releases is given in Figure 3.28. To empty the tank, as in the case of accidental TPRD activation, release time was over 16 times longer for blowdown releases. The remaining pressure in the tank was 1-3% of the initial pressure.

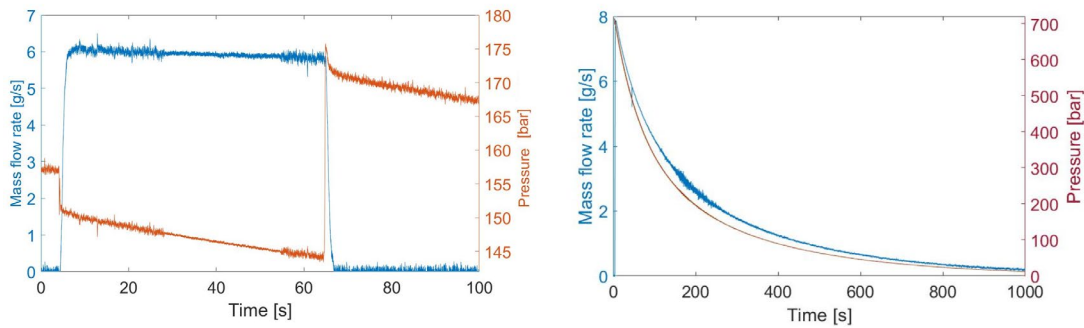


Figure 3.28: (left) Mass flow rate and pressure measured at the coriolis outlet – 60 s constant H_2 mass flow, exp 9 and (right) Mass flow rate and pressure measured at the tank outlet – blowdown H_2 mass flow, exp 20.

Increasing nozzle diameter from 0.5 mm to 1 mm resulted in:

- 6 times higher mass flow rate resulted with releases from the same reservoir pressure
- ~3 times higher hydrogen concentration in the cloud, shown in Figure 3.29- a and b.

Releases through 0.5 mm nozzle diameter but with much higher reservoir pressure (Figure 3.29, c) resulted in concentrations similar to those that resulted from releases through 1 mm (Figure 3.29, a).

The results in Figure 3.29 do not decisively show a decreased concentration with an increased ventilation rate in this particular geometry (red and blue markers). The maximum concentrations from 10 ACH and 6 ACH from releases at the same reservoir pressure overlap with each other showing small differences.

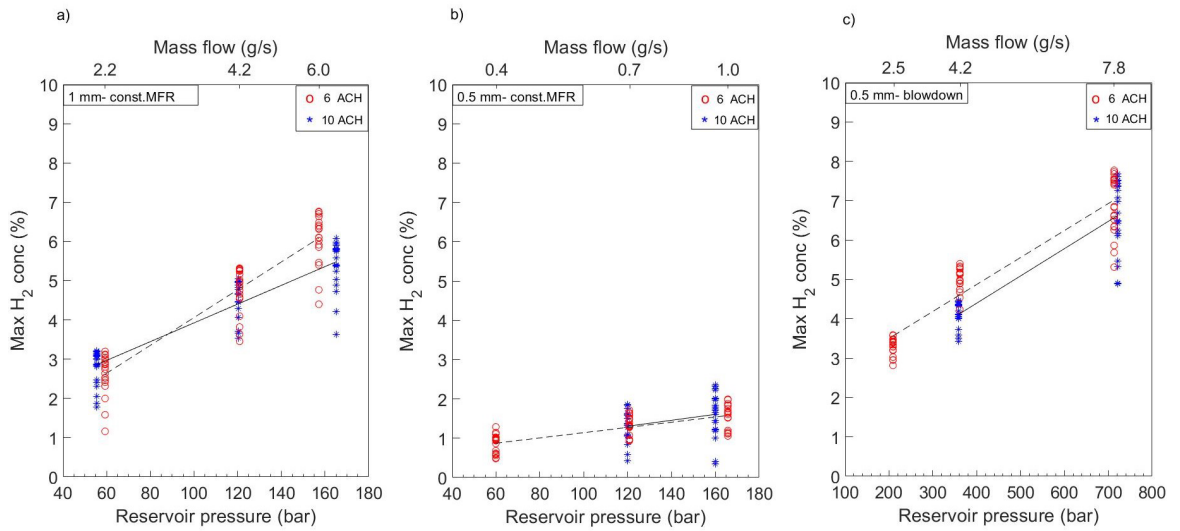


Figure 3.29: Maximum hydrogen concentration resulted with 6 ACH (dash line) and 10 ACH (solid line) during constant mass flow releases (a) through 1 mm diameter nozzle, (b) 0.5 mm diameter nozzle, and (c) blowdown mass flow releases through 0.5 mm nozzle. Maximum concentrations at each sensor during 10 ACH (blue star) and 6 ACH (red circle).

Concentration was measured under and below the ceiling and under the car. Figure 3.30 shows the results from constant mass flow releases measured under and below the ceiling. The concentration results indicate the cloud was at least 50 cm high. More precisely conclusion can not be made since sensors were not mounted on the container's floor (outside the car). The highest measured concentration was behind the car under the ceiling, closest to the ventilation wall (sensor 13). Hydrogen release was shut down after 60 seconds for constant flow hydrogen discharge. For the releases with a 1.0 mm nozzle, the steady-state concentration was not reached compared to releases from a 0.5 mm nozzle. That can be observed from the concentration results from under the car shown in Figure 3.31.

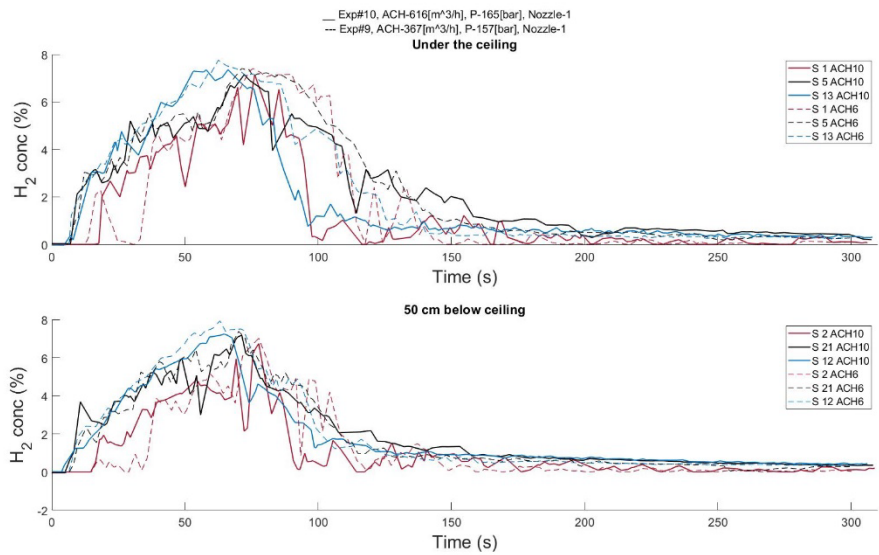


Figure 3.30: Concentration in the cloud and its propagation from hydrogen releases with 10 and 6 ACH.

The blowdown releases were of the biggest interest due to the highest similarity to the accident scenario with the failure of TPRD activation. The duration of the flammable cloud vs two ventilation rates was investigated. The total flammable time of the cloud (the time when the cloud is $\geq 4\%$) is shorter for the higher ventilation rate. In given geometry 10 ACH will decrease the time when the cloud can ignite and/or explode with ~ 2 min for 350 bar and ~ 1 min for 700 bar as shown in Table 15. The impact of ventilation rate on the time when hydrogen cloud starts to be flammable, t_{f0} , (here 4%) was not observed since the 2 s difference between 6 and 10 ACH can be assumed negligible (Table 15, column 7).

Table 15: The flammable time during blowdown releases.

Exp	$P_{0\text{reservoir}}$ [bar]	ACH [h ⁻¹]	Blowdown Time [s]	P_{end} [bar]	Total flammable time t_f [s]	t_{f0} [s]
22	209	6.0	900	6	11	82
23	359	10.2	900	12	83	30
21	362	6.2	900	10	195	32
19	721	10.2	900	16	285	16
20	713	6.2	900	17	336	18

The hydrogen jet was impinging on the floor from a 25 cm distance. The momentum of the jet was different depending on the hydrogen storage pressure and nozzle diameter influencing the plumes rising from under the car (Figure 3.31). For higher mass flow rates

the concentration of the plume at the front of the car was higher (both sensors S29 and S30 showed concentrations near 5%). The presence of the front plume had an impact on the concentrations in the side plumes:

- Constant releases: the concentration of the side plumes was increasing slower compared to 0.5 mm where no front plume was observed
- Blowdown releases: with a decrease of mass flow rate the front plume decreases and disappears which increases the concentration in the side plumes (in this geometry around after 3 min) - the hydrogen escapes closer to the nozzle (Figure 3.32)

The concentration results from the 0.5 mm nozzle (constant- low mass flow rate and blowdown- high mass flow rate) showed similar maxima of reached concentrations. The main hydrogen plumes were at the rear of the car (close to the nozzle) resulting in a concentration above 10% which is the limit for fast flames described by Dorofeev et al [103]. The 10% limit was crossed also for low mass flow rates since the hydrogen escapes slower from under the car. The full-scale car has longer dimensions, which indicates the hydrogen concentration under the car will be higher. The model for impinging jet under the car and its validation is needed to ensure proper mitigation systems.

The effect of the ventilation rate on the concentration under the car was not observed for the constant mass flow rates. However, the concentration results from the blowdown releases indicate that a higher ventilation rate will prevent the accumulation of hydrogen under the car in (S27 and S28) in the last minutes of emptying the tank (Figure 3.32).

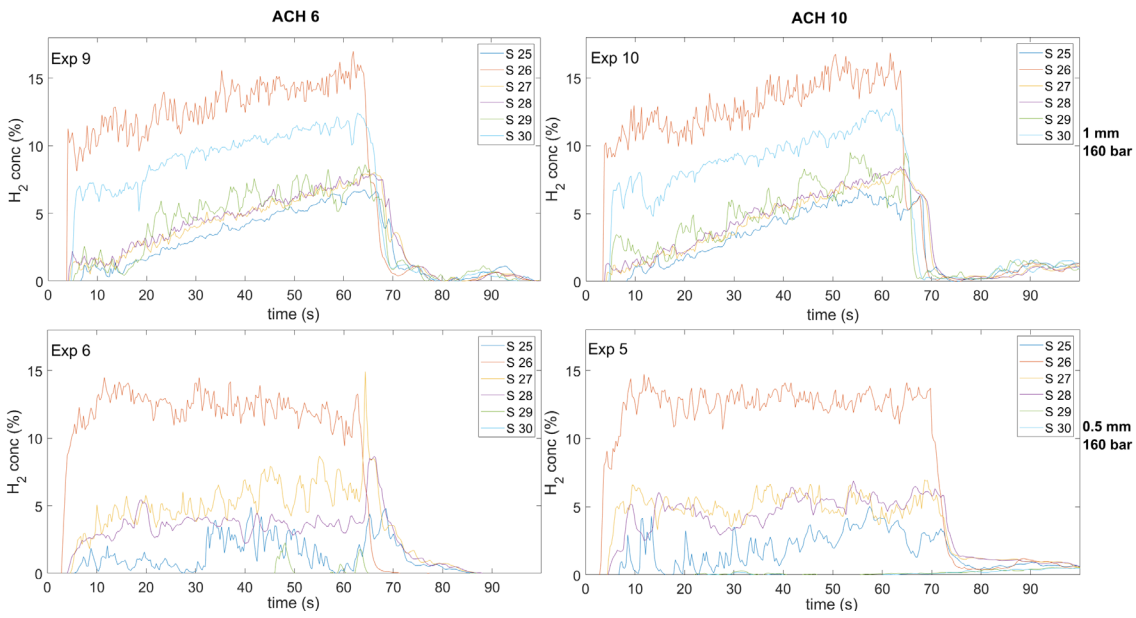


Figure 3.31: Concentration results from sensors mounted under the car for constant releases: experiments 9-10 and 5-6.

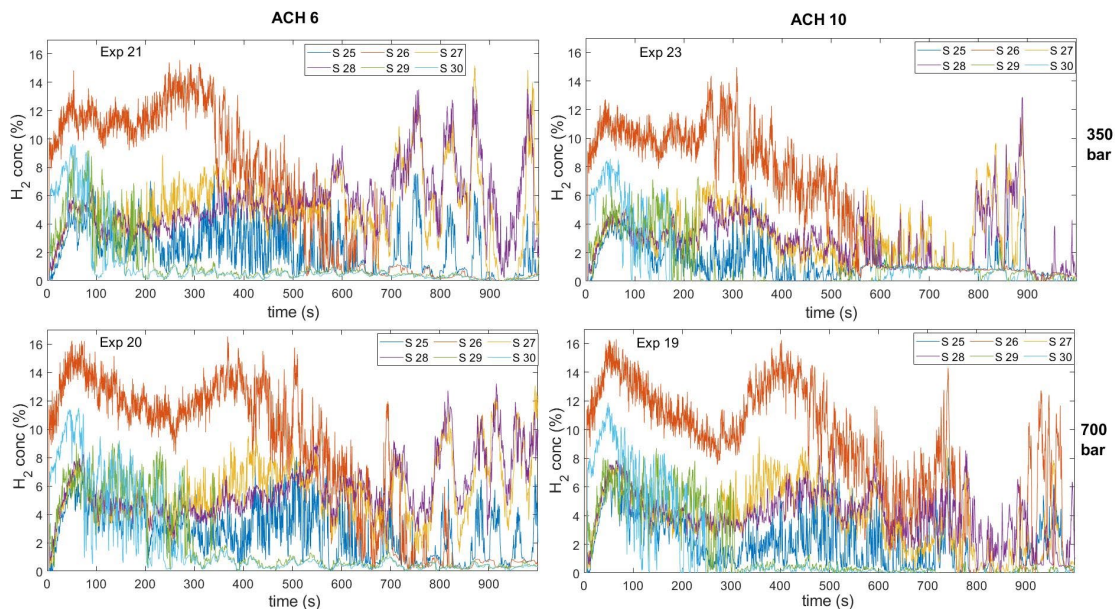


Figure 3.32: Concentration results from sensors mounted under the car for blowdown releases: experiments 19-21 and 23, all through 0.5 mm nozzle.

IGNITED HYDROGEN RELEASES

The results from the last experimental campaign focused on the blowdown releases from high pressurized hydrogen tank. In this section, the main results of thermal effects from the resulting hydrogen jet flames are discussed: the temperature effects-convective heat and heat flux results – radiative heat, are presented in that order.

Due to an insufficient amount of fire-plates under the car during releases through the 90° nozzle, only two experiments were performed. The impact of the nozzle diameter and storage pressure on the mass flow rate is shown once more time in Figure 3.33 and Figure 3.34. A decrease in diameter will result in a lower mass flow rate and pressure drop in the tank but a longer duration of blowdown. In Table 16 the experimental parameters are presented.

Table 16: Parameters of jet fires experiments.

Exp Nr	Nozzle angle [°]	Nozzle diameter [mm]	Air change per hour [1/h]	Ambient temp [°C]	Initial tank pressure [bar]	Initial mass flow rate [g/s]	Blowdown duration [s]
1	90	0.5	10	22	708	7.3	450
2	90	0.5	6	19	695	7.5	80
3	45	0.5	6	23	357	4.0	500
4	45	0.5	6	22	698	7.4	500
5	45	0.5	10	22	690	7.3	500
6	45	0.5	10	19	357	4.1	500
7	45	0.5	6	19	360	4.0	500
8	45	1.0	6	15	357	13	367

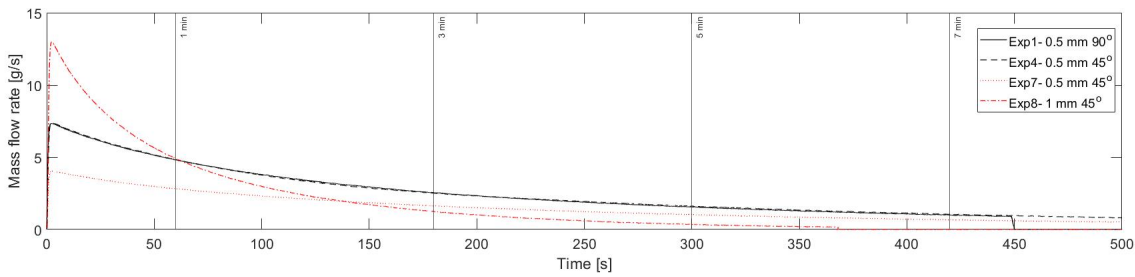


Figure 3.33: Hydrogen mass flow rate during blowdown from Exp.1 (solid line), Exp.4 (dashed line), Exp.7 (dotted line), and Exp.8 (dot-dash line).

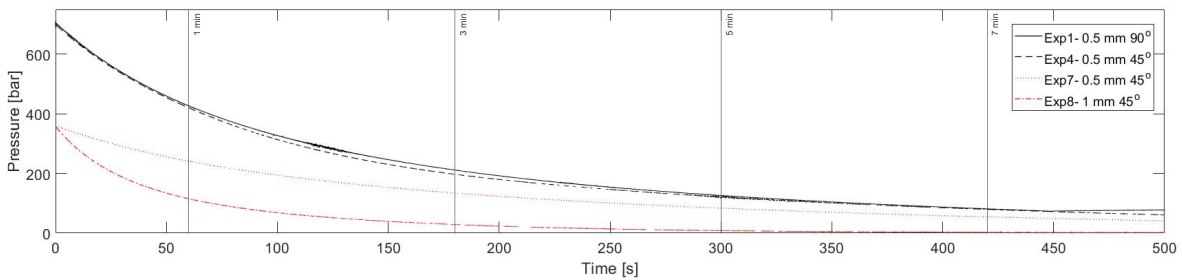


Figure 3.34: Tank pressure during blowdown from Exp.1 (solid line), Exp.4 (dashed line), Exp.7 (dotted line), and Exp.8 (dot-dash line).

The analysis of the temperature effect from releases through the 45° nozzle presented in Figure 3.35 shows no temperature change at the front of the car. Results from the thermocouple mounted under the car, closest to the nozzle, did not exceed 110 °C and were very similar for all three experiments. The experiments with a 45° nozzle angle, which was pointed towards the ventilation wall, showed the highest temperatures behind the car. The deviation between temperature measurements among those experiments was also biggest behind the car, while at the front and under the car measured temperatures were similar. The expected highest temperatures were for experiments with the highest mass flow rate: bigger amount of combusted hydrogen at the same time, hence higher energy released. Experiments 4 and 8 with 7.4 g/s and 13.0 g/s initial mass flow rate respectively had the highest mass flow rates. The releases through a larger nozzle diameter (exp 8) resulted in the temperature 3 times and 12 times higher than exp 4 and 7 respectively in the position closest to the ventilation wall. Nevertheless, the observed temperature drop also decreased faster than the two other experiments at the same position. The temperature measured behind the car (1.68 m from the nozzle) was highest for exp 4. The results indicate the distance where the

temperature is highest is subjected to the nozzle diameter and storage pressure as it is for the flame length calculations described in section 2.3.

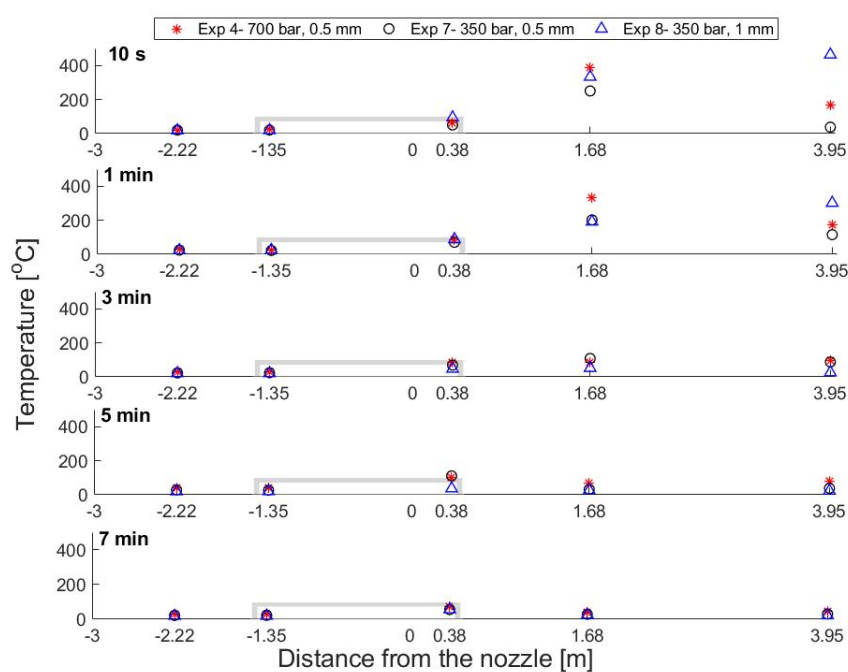


Figure 3.35: Comparison of temperature resulted from different initial tank pressure and nozzle diameter (mass flow rates) at five longitudinal positions with the same 6 ACH.

The temperature measurements under the ceiling did not exceed 300 °C which is the limit given in several standards presented in section 1.1.2. Nevertheless, the temperature obtained during experiments does include only hydrogen jet fires, the thermal effect resulting from the combustion of the car and surroundings are not included in this work. In Proceedings D the presented effect of the ventilation rate on the temperature in the ventilation pipe showed a decrease in temperature with 3.3% and 6.9% for releases from 700 bar and 350 bar respectively (through 0.5 mm nozzle). The highest measured min temperature in the ventilation pipe was for the experiments with the highest mass flow rate. The relation between mass flow rate and the resulting temperature in the ventilation pipe from analysed earlier three experiments (exp 4, exp 7, and exp 8) was investigated, shown in Figure 3.36. The temperature decreases with decreasing mass flow rate resulting in similar temperatures for a given mass flow rate for all three experiments. The fit line with a 95 % prediction interval was added showing that the temperatures are almost constant for given mass flow rates (Figure 3.36).

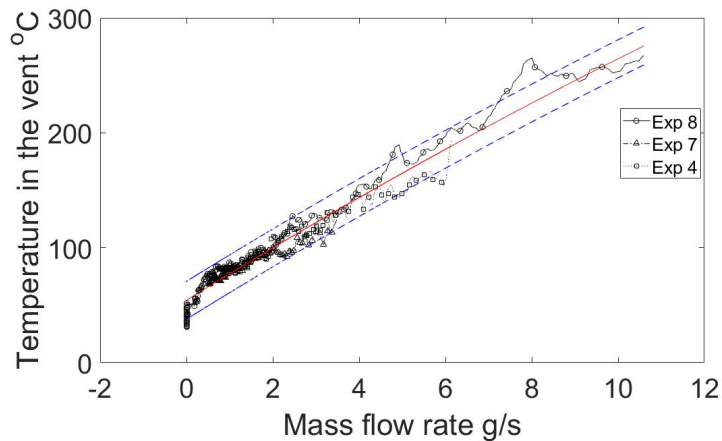


Figure 3.36: Temperature change in the ventilation pipe vs mass flow rate.

Convective heat is one criterion used for RCS and guidelines for harm distances. The radiative heat, presented next, is the second (both discussed in Chapter 2.3.4). The radiation heat from the hydrogen flames decreases with the radial distance from the flame central line. All experiments were recorded with Promon 500 high-speed camera. The video frames from four experiments presented in Figure 3.33 and Figure 3.34 illustrate the flame development during blowdown releases through both: angles, nozzle diameters and storage pressures. The vigorous flames from the experiment with the 1.0 mm nozzle and experiments with 700 bar storage pressure are clearly visible. The recorded hydrogen jets will be used for the flame length calculations for impinging hydrogen jets in the future but are not part of this thesis work.

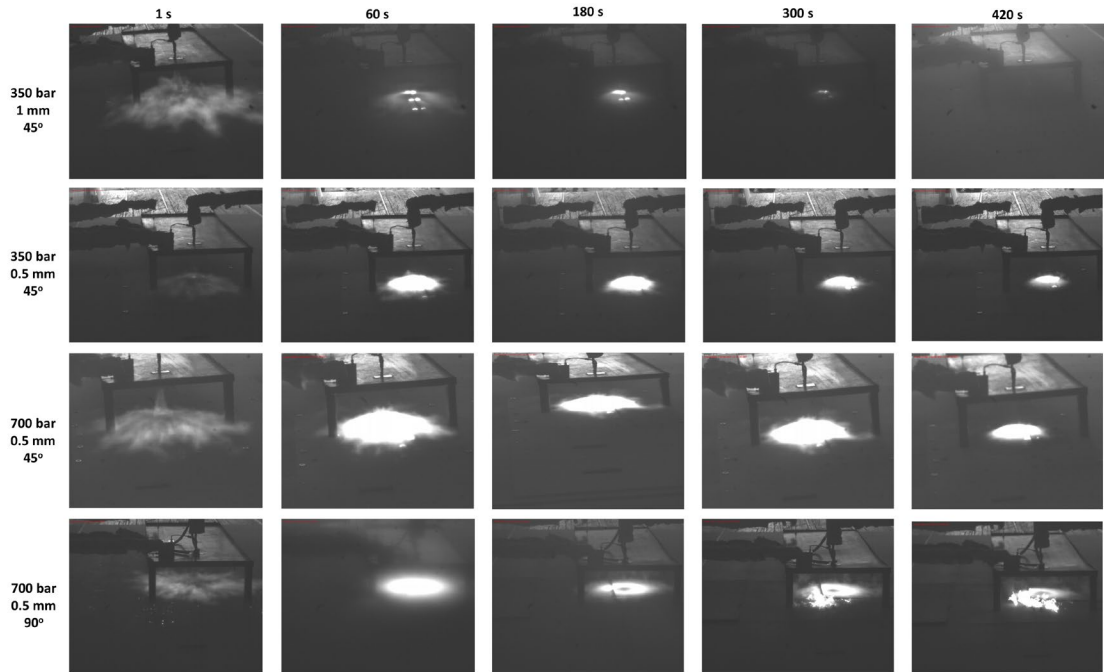


Figure 3.37: Flame development from Exp.8 (top row), Exp.7 (second row), Exp.4 (third row), and Exp.1 (bottom row).

The heat flux sensors used during experiments had uncertainty above the measured values (Table 12). Nevertheless, the results (Figure 3.38) are comparable with the values presented by Houf and Schefer [54]. The direct comparison is not possible due to the nature of the flame. This work presents for the first time heat flux (radiative and total) results from turbulence hydrogen jet flame impinged on the floor in a semiconfined space. While radiative heat flux results presented in previous works [54,79,104–106] resulted from the open flames directed upwards or horizontally. The location of the sensors is the other distinguishing parameter. The sensor location in this work was decided based on places of the possible presence of humans (civil or firefighter) or another vehicle. The flame length calculations have to be modified and validated for downwards impinging with the floor hydrogen jet flames – the one which will appear in case of TPRD activation. The flame length calculations are used to calculate the total heat flux and its radial fraction. This task is not part of this thesis work, but the data will be used for a model development by NCSR Demokritos – a partner of the HyTunnel-CS EU project.

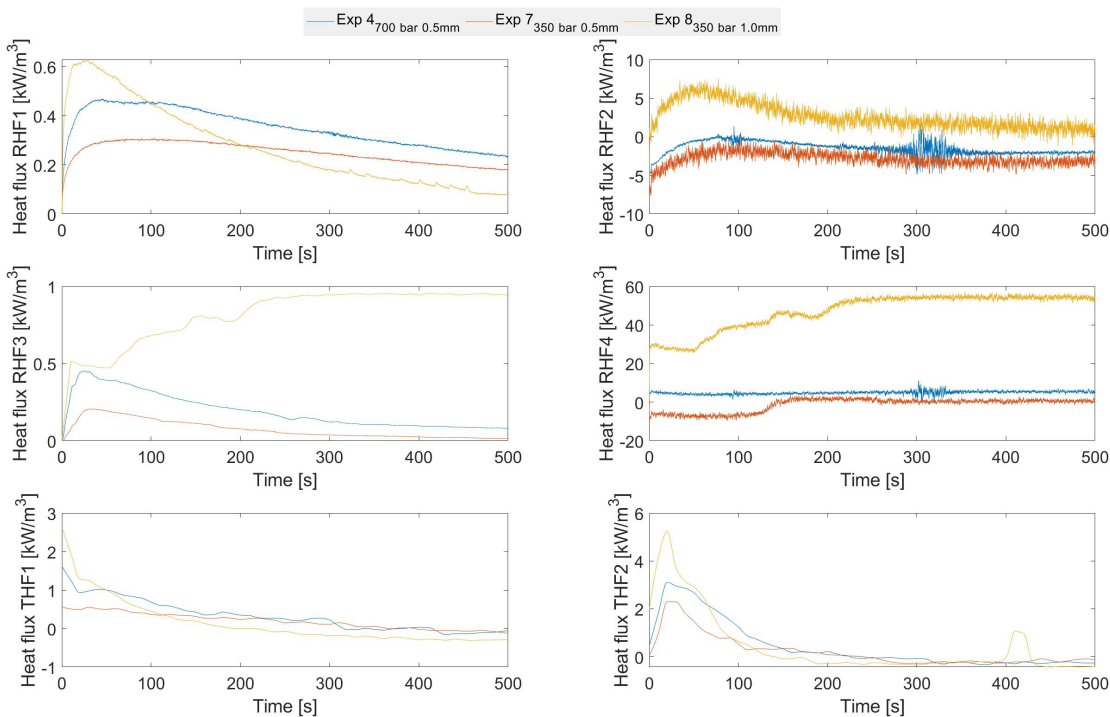


Figure 3.38: Heat flux measurements: radiative (RHF1-RHF4) and total (THF1-THF2) from experiments with 6 ACH and: 700 bar and 350 bar through 0.5 mm nozzle and 350 bar through 1.0 mm nozzle. Exp 4,7,8 respectively.

The heat flux profiles (Figure 3.39) showed dependency on the mass flow rate (nozzle diameter and storage pressure). The main conclusion:

- Lower mass flow rate resulted in shorter radiation distance for the maximum 2.5 kW/m^2 given in BS/PD 7974-6:2004 [10]
- The larger the flame (visually observed exp 4 and exp 8, Figure 3.37) higher the heat flux which can be seen in Figure 3.38 and Figure 3.39
- Mass flow profiles (Figure 3.33) are responding and are surprisingly alike to radiative heat flux results from RHF1 (Figure 3.39), measured closest to the nozzle.
- The temperature decreases with the nozzle diameter and storage pressure (Figure 3.39). The observed decrease in the sharpness of the temperature curve (measured at the longest distance from the nozzle is) was observed also for the heat flux measurement closest to the nozzle. Similar results to those presented by D. Bouix et al. [106]
- Both radiative and total heat flux results decreased with the mass flow rate.

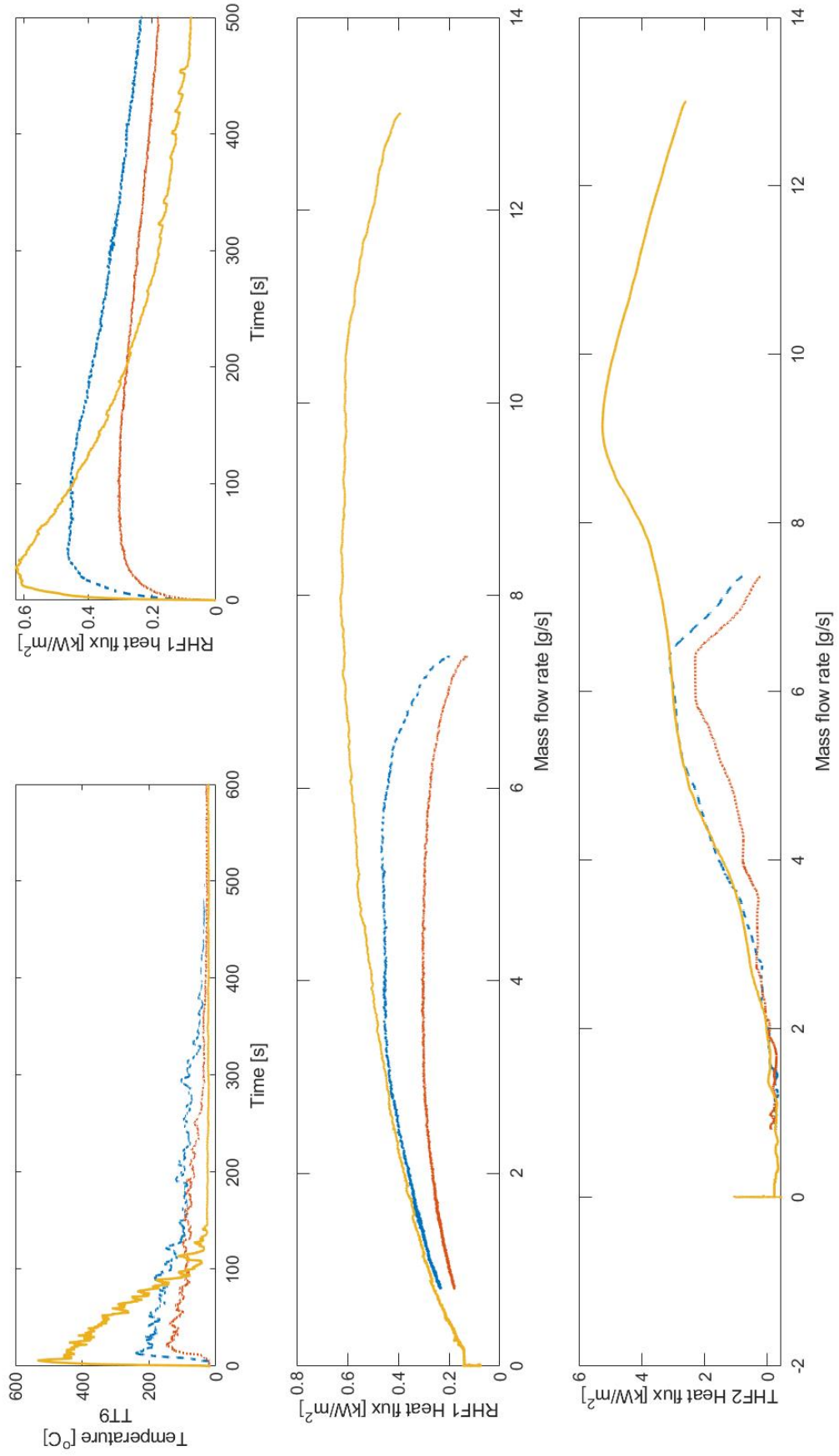


Figure 3.39: Temperature in the container: 3.95 m from the nozzle (left top corner). Radiative heat flux nearest the nozzle. Effect of mass flow rate on: middle – radiative heat flux, bottom – total heat flux.

4 Summary

The work presented in this Ph.D thesis studied the safety aspects of hydrogen releases in confined spaces. Hydrogen safety is an acknowledged challenge to enable the use of hydrogen applications and pursuing infrastructure development as it's critical for public acceptance. The safety application can be added to existing infrastructure like new passive ventilation solutions or forced ventilation systems. Reduction of the mass flow rates is the possibility when the change in the ventilation system is not possible or economically unacceptable. The forced ventilation systems used today operate according to the standards. In parking houses or the storage hall, the recommended air change per hour (ACH) is 6 or 10 depending on the size of the area, and 3 ACH when natural ventilation of 25% of floor area is present, according to British Standards [10]. The thermal characteristics near the hydrogen jet fire resulting from the activation of TPRD are important for the escape possibilities not only for the passengers of the car but people around as well. The investigation presented in this Ph.D thesis focuses on the accidental release of hydrogen from the hydrogen storage tank. The accidental releases occur due to for example a failure of the TPRD with immediate ignition and with no ignition.

Pressure peaking phenomena was investigated in the large-scale experimental setup during two campaigns. 10 unignited experiments and 31 ignited experiments were conducted in the 15 m³ explosive chamber, exemplifying a privet garage. The overpressures were investigated at constant hydrogen flow releases (range 1.9 g/s – 8.1 g/s for unignited and 1.4 g/s – 11.7 g/s for ignited) with a variation of ventilation area.

The full-scale experiments were performed in the 40 ft ISO container to investigate hydrogen dispersion and thermal effects resulting from the high-pressure hydrogen releases. The experimental setup exemplifies an enclosure similar to a carpark with a mechanical ventilation rate of 6 ACH and 10 ACH. Experiments were designed to imitate the scenario of accidental hydrogen release from a car with storage tank pressure up to 700 bar through two different nozzle diameters: 1.0 mm and 0.5 mm. Hydrogen dispersion was investigated with 14 experiments with constant mass flow H₂ releases

(0.8 g/s – 8.0 g/s) and 5 experiments with blowdown releases from 200 bar to 700 bar. The thermal effects were investigated with 8 experiments with blowdown releases from 350 bar to 700 bar. The hydrogen jet was released into propane flame, and hence immediate ignition, resulting in jet fire impinging with the floor. The thermal effects resulting from a 90° and 45° of the TPRD exhaust pipe were tested with the major focus on 45°.

The further summary follows the main knowledge gaps given in Chapter 1.2

4.1 The upper limit of hydrogen release rate that will not require change in the ventilation system

In a real case scenario, the hydrogen leak will be a blowdown type of mass flow. This work presented both constant and blowdown hydrogen flows. The upper limit of the hydrogen leak rate depends on the size of the ventilation system: natural and mechanical, and the enclosure geometry. The results from the given experimental setup showed the upper limit of 4 g/s (blowdown from 200 bar through 0.5 mm) which will not lead to LFL in the accumulated hydrogen cloud. In case of ignited releases the maximum temperature in the ventilation pipe did not exceed allowed 300 °C for all experiments performed with 0.5 mm nozzle diameter (4.0 – 7.5 g/s). Nevertheless, the temperature in the hazardous zone – behind the car for the 45° nozzle, exceed the exposure time limits of 1 min for 180 °C, given by the BSI 7346-7 [12], in the first stage of the jet fire.

4.2 Effectiveness of regulated ventilation systems in case of hydrogen release accident

The effectiveness of the regulated ventilation systems on the concentration of the accumulated cloud was not observed. Nevertheless, the time when the hydrogen cloud is above LFL was reduced with the higher ventilation rate.

4.3 Thermal effects of hydrogen non-premixed turbulent combustion on a vehicle, structure and evacuation in covered carpark

Increasing the mass flow rate (larger TPRD diameter or/and higher storage pressure) results in higher temperatures both in the ventilation pipe and around the car. The releases through the 45° nozzle were mostly investigated. The results around the car showed low temperatures (~30 °C) at the front and higher (~100 °C) at the back of the car, close to the nozzle. The results indicate a possible safe approach to the car in case of hydrogen fire towards the front of the car. With the increase of mass flow rate, the temperature behind the car increases. The higher the mass flow the greater the distance from the nozzle with the increased temperature (from 400 °C at 2 m to 500 °C at 4 m for releases from 350 bar through 0.5 mm and 1 mm nozzle diameter respectively). The highest temperature was measured behind the car in the early stage of the hydrogen release.

The temperature drop depends on the nozzle diameter. The decrease of the nozzle diameter leads to the lower temperature behind the car, but also a longer duration of blowdown-emptying the tank. The prolonged exposure to high temperatures may be the consequence leading to injuries of 1st -3rd burn degrees.

4.4 Pressure effects from ignited and unignited hydrogen releases in a private garage.

Rapidly releases of unignited hydrogen into an enclosure like a private garage are unlikely to cause damages caused by overpressure as long as the enclosure has natural ventilation like crevices around windows and doors or a vent. An increase in the flow rate will increase the overpressure in case of inefficient ventilation.

Ignited releases, on the other hand, can cause 4 times higher overpressures with 3 times higher ventilation area for the same flow rate. The pressure peak occurs in the first few

seconds of the release. An increase in the ventilation area significantly decreases the maximum overpressure but also reduces the time of reaching the pressure peak.

References

- [1] De Stefano M, Rocourt X, Sochet I, Daudey N. Hydrogen dispersion in a closed environment. *Int J Hydrogen Energy* 2018;44:9031–40. <https://doi.org/10.1016/j.ijhydene.2018.06.099>.
- [2] Hussein H, Brennan S, Molkov V. Dispersion of hydrogen release in a naturally ventilated covered car park. *Int J Hydrogen Energy* 2020;45. <https://doi.org/10.1016/j.ijhydene.2020.06.194>.
- [3] Brennan S, Makarov D, Molkov VV. Dynamics of Flammable Hydrogen-Air Mixture Formation in an Enclosure with a Single Vent. *Fire Explos. Hazards*, 2010, p. 493–503. https://doi.org/10.3850/978-981-08-7724-8_07-04.
- [4] Olje- og energidepartementet, Klima- og Miljødepartementet. Regjeringens hydrogenstrategi 2020.
- [5] Statistics Norway. Statistikkbanken 2020. <https://www.ssb.no/statbank/table/11823/tableViewLayout1/> (accessed September 10, 2020).
- [6] Everfuel. Toyota, Everfuel and DRIVR signs agreement on scaling up hydrogen taxis 2022. <https://www.everfuel.com/news/>.
- [7] Hydrogenbil.net. HYDROGENPRISER 2022. <https://www.hydrogenbil.net/hydrogenpriser/>.
- [8] Hydrogenforum N. Hva koster Hydrogen? 2020. <https://www.hydrogen.no/ressurser/ofte-stilte-sporsmal>.
- [9] Remzi Can Samsun LAMRDS. Deployment Status of Fuel Cells in Road Transport: 2021 Update. 2021.
- [10] British Standard PD 7974-6:2004. Application of Fire Safety Engineering Principles to the Design of Buildings. Part 6: Human factors: Life safety strategies — Occupant evacuation, behaviour and condition (Sub-system 6) 2004.
- [11] Vijay P V., Tulasi Gadde K, Gangarao HVS, Kristl Ž, Temeljotov Salaj A, Roumboutsos A, et al. Regulations on technical requirements for construction works (TEK17). *J Archit Eng* 2009;63.
- [12] BSI Standards Publication BS 7346-7:2013. Components for smoke and heat

control systems – Part 7: Code of practice on functional recommendations and calculation methods for smoke and heat control systems for covered car parks 2013.

- [13] Bain A, Van Vorst DW. Hindenburg tragedy revisited: The fatal flaw found. *Int J Hydrogen Energy* 1999;24. [https://doi.org/10.1016/S0360-3199\(98\)00176-1](https://doi.org/10.1016/S0360-3199(98)00176-1).
- [14] Bjerketvedt, D; Mjaavatten A. A Hydrogen-Air Explosion in a Process Plant: a Case History. *Ichs* 2005 2005.
- [15] Tsuruda T. Plenary – Hydrogen Explosion Hazards in Degraded Core Accidents in Nuclear Power Plants, 2013. https://doi.org/10.3850/978-981-07-5936-0_01-02.
- [16] Kim SI, Kim Y. Review: Hydrogen tank explosion in Gangneung, South Korea. *Cent. Hydrog. Saf. Conf.* 2019, 2019.
- [17] 'Løkke JA. THE KJØRBO INCIDENT. *Press Conf* 2019.
- [18] 'Charlier P. Hydrogen tanker crashes and explodes on freeway in Changhua City. *Taiwan English News* 2020. <https://taiwanenglishnews.com/hydrogen-tanker-crashes-and-explodes-on-freeway-in-changhua-city/>.
- [19] Giles Parkinson. World's newest and most expensive coal plant explodes after hydrogen leak. *Renew Econ Clean Energy News Anal* 2021. <https://reneweconomy.com.au/worlds-newest-and-most-expensive-coal-plant-explodes-after-hydrogen-leak/>.
- [20] Orescanin MM, Austin JM. Exhaust of underexpanded jets from finite reservoirs. *J Propuls Power* 2010;26. <https://doi.org/10.2514/1.47673>.
- [21] Law CK. *Combustion physics*. vol. 9780521870528. 2006. <https://doi.org/10.1017/CBO9780511754517>.
- [22] 'Hamzehloo A 'Aleiferis, P. Large Eddy Simulation of Near-Nozzle Shock Structure and Mixing Characteristics of Hydrogen Jets for Direct-Injection Spark-Ignition Engines. *10th Int. Conf. Heat Transf. Fluid Mech. Thermodyn.*, Orlando: 2014.
- [23] Molkov V. *Fundamentals of Hydrogen Safety Engineering I*. vol. 4. 2012. <https://doi.org/10.1016/B978-0-08-087872-0.00418-2>.
- [24] Ruggles AJ, Ekoto IW. Ignitability and mixing of underexpanded hydrogen jets. *Int J Hydrogen Energy* 2012;37. <https://doi.org/10.1016/j.ijhydene.2012.03.063>.

- [25] Birch AD, Brown DR, Dodson MG, Swaffield F. The structure and concentration decay of high pressure jets of natural gas. *Combust Sci Technol* 1984;36. <https://doi.org/10.1080/00102208408923739>.
- [26] Schefer RW, Houf WG, Williams TC, Bourne B, Colton J. Characterization of high-pressure, underexpanded hydrogen-jet flames. *Int J Hydrogen Energy* 2007;32. <https://doi.org/10.1016/j.ijhydene.2006.08.037>.
- [27] Molkov V, Makarov D, Bragin M. Physics and Modelling of Underexpanded Jets and Hydrogen Dispersion in Atmosphere. *Phys Extrem States Matte* 2009:146–9.
- [28] Papanikolaou E, Baraldi D, Kuznetsov M, Venetsanos A. Evaluation of notional nozzle approaches for CFD simulations of free-shear under-expanded hydrogen jets. *Int J Hydrogen Energy* 2012;37:18563–74. <https://doi.org/10.1016/j.ijhydene.2012.09.135>.
- [29] Crowl DA, Louvar JF. *Chemical Process Safety Fundamentals with Applications*. 3rd ed. Prentice Hall 2011; 2011.
- [30] 'McAllister S'Chen, J-Y 'Fernandez-PAC. *Fundamentals of Combustion Processes*. Springer; 2011.
- [31] Molkov V, Saffers JB. The correlation for non-premixed hydrogen jet flame length in still air. *Fire Saf. Sci.*, 2011. <https://doi.org/10.3801/IAFSS.FSS.10-933>.
- [32] Hydrogen Tools. Basic hydrogen properties n.d. <https://h2tools.org/hyarc/hydrogen-data/basic-hydrogen-properties>.
- [33] Battipede M, Gili P, Maggiore P, Vazzola M. Innovative hydrogen storage tank for flying fuel cell power system. 6th Int. Energy Convers. Eng. Conf. IECEC, 2008. <https://doi.org/10.2514/6.2008-5730>.
- [34] Swain MR, Shriber J, Swain MN. Comparison of hydrogen, natural gas, liquified petroleum gas, and gasoline leakage in a residential garage. *Energy and Fuels* 1998;12.
- [35] Agarant V, Cheng Z, Tchouvelev A. CFD modeling of hydrogen releases and dispersion in hydrogen energy station. ... 15Th World Hydrog Energy ... 2004.
- [36] Hooker P, Hall J, Hoyes JR, Newton A, Willoughby D. Hydrogen jet fires in a passively ventilated enclosure. *Int J Hydrogen Energy* 2017;42:7577–88. <https://doi.org/10.1016/j.ijhydene.2016.07.246>.

- [37] Prasad K, Pitts WM, Fernandez M, Yang JC. Natural and forced ventilation of buoyant gas released in a full-scale garage: Comparison of model predictions and experimental data. *Int J Hydrogen Energy* 2012;37:17436–45. <https://doi.org/10.1016/j.ijhydene.2012.04.148>.
- [38] Prasad K. High-pressure release and dispersion of hydrogen in a partially enclosed compartment: Effect of natural and forced ventilation. *Int J Hydrogen Energy* 2014;39:6518–32. <https://doi.org/10.1016/j.ijhydene.2014.01.189>.
- [39] Prasad K, Pitts W, Yang J. Effect of wind and buoyancy on hydrogen release and dispersion in a compartment with vents at multiple levels. *Int J Hydrogen Energy* 2010;35. <https://doi.org/10.1016/j.ijhydene.2010.06.001>.
- [40] Pitts WM, Yang JC, Fernandez MG. Helium dispersion following release in a 1/4-scale two-car residential garage. *Int J Hydrogen Energy* 2012;37:5286–98. <https://doi.org/10.1016/j.ijhydene.2011.12.008>.
- [41] United States department of labor 1910.106 - Occupation safety and Health Administration. Hazardous Materials. Flammable liquids 2016.
- [42] Molkov V, Shentsov V, Quintiere J. Sustained Hydrogen Leak Concentration in Enclosure with One Vent, 2013. https://doi.org/10.3850/978-981-07-5936-0_14-03.
- [43] Saffers JB, Makarov D, Molkov V V. Modelling and numerical simulation of permeated hydrogen dispersion in a garage with adiabatic walls and still air. *Int J Hydrogen Energy* 2011;36. <https://doi.org/10.1016/j.ijhydene.2010.05.085>.
- [44] Fujiwara H, Ono H, Ohyama K, Kasai M, Kaneko F, Nishimura S. Hydrogen permeation under high pressure conditions and the destruction of exposed polyethylene-property of polymeric materials for high-pressure hydrogen devices (2)-. *Int J Hydrogen Energy* 2021;46. <https://doi.org/10.1016/j.ijhydene.2020.12.223>.
- [45] Swaffield J, Jack L, Douglas ' F., Gasiorek J. *Fluid mechanics*. 6th edition. 6th ed. Pearson; 2011.
- [46] Marshall MR. EFFECT OF VENTILATION ON THE ACCUMULATION AND DISPERSAL OF HAZARDOUS GASES. *Inst. Chem. Eng. Symp. Ser.*, 1983.
- [47] Ehrhart BD, Harris SR, Blaylock ML, Muna AB, Quong S. Risk assessment and ventilation modeling for hydrogen releases in vehicle repair garages. *Int J*

- Hydrogen Energy 2021;46. <https://doi.org/10.1016/j.ijhydene.2020.09.155>.
- [48] Kaye NB, Hunt GR. Time-dependent flows in an emptying filling box. *J Fluid Mech* 2004;520. <https://doi.org/10.1017/S0022112004001156>.
- [49] Merilo EG, Groethe MA, Colton JD, Chiba S. Experimental study of hydrogen release accidents in a vehicle garage. *Int J Hydrogen Energy* 2011;36:2436–44. <https://doi.org/10.1016/j.ijhydene.2010.04.056>.
- [50] Zhang J, Delichatsios MA, Venetsanos AG. Numerical studies of dispersion and flammable volume of hydrogen in enclosures. *Int J Hydrogen Energy* 2010;35. <https://doi.org/10.1016/j.ijhydene.2010.03.107>.
- [51] Morton B. Forced plumes. *J Fluid Mech* 1959;5:151–63. <https://doi.org/10.1017/S002211205900012X>.
- [52] Hourri A, Gomez F, Angers B, Bénard P. Computational study of horizontal subsonic free jets of hydrogen: Validation and classical similarity analysis. *Int J Hydrogen Energy* 2011;36. <https://doi.org/10.1016/j.ijhydene.2011.09.044>.
- [53] Chen CJ, Rodi W. Vertical turbulent buoyant jets: a review of experimental data. OXFORD, UK, PERGAMON Press 1980 1980;4).
- [54] Houf W, Schefer R. Predicting radiative heat fluxes and flammability envelopes from unintended releases of hydrogen. *Int J Hydrogen Energy* 2007;32. <https://doi.org/10.1016/j.ijhydene.2006.04.009>.
- [55] Molkov V, Saffers JB. Hydrogen jet flames. *Int J Hydrogen Energy* 2013;38:8141–58. <https://doi.org/10.1016/j.ijhydene.2012.08.106>.
- [56] Li Z, Luo Y. Comparisons of hazard distances and accident durations between hydrogen vehicles and CNG vehicles. *Int J Hydrogen Energy* 2019;44:8954–9. <https://doi.org/10.1016/J.IJHYDENE.2018.07.074>.
- [57] Denisenko V p., Kirillov IA, Korobtsev SV, Nikolaev II. Hydrogen-air explosive envelope behavior in confined space at diferent leak velocities. *Proc. 3rd Int. Conf. Hydrog. Saf.*, 2009.
- [58] Pitts WM, Yang JC, Blais M, Joyce A. Dispersion and burning behavior of hydrogen released in a full-scale residential garage in the presence and absence of conventional automobiles. *Int J Hydrogen Energy* 2012;37. <https://doi.org/10.1016/j.ijhydene.2012.03.074>.

- [59] Schefer RW, Merilo EG, Groethe MA, Houf WG. Experimental investigation of hydrogen jet fire mitigation by barrier walls. *Int J Hydrogen Energy* 2011;36. <https://doi.org/10.1016/j.ijhydene.2010.04.008>.
- [60] ISO 19880-1:2020. Gaseous hydrogen — Fuelling stations — Part 1: General requirements 2020.
- [61] Schneider JM, Dang-Nhu G, Hart N. ISO 19880-1, Hydrogen Fueling Station and Vehicle Interface Technical Specification. *ECS Trans* 2016;71. <https://doi.org/10.1149/07101.0155ecst>.
- [62] Hawthorne WR, Weddell DS, Hottel HC. Mixing and combustion in turbulent gas jets. *Symp. Combust. Flame Explos. Phenom.*, vol. 3, 1948. [https://doi.org/10.1016/S1062-2896\(49\)80035-3](https://doi.org/10.1016/S1062-2896(49)80035-3).
- [63] Golovichev VI, Yasakov VA. Analysis of a reacting submerged hydrogen jet. *Combust Explos Shock Waves* 1972;8. <https://doi.org/10.1007/BF00740282>.
- [64] Baev VK, Kuznetsov PP, Mogil'nyi IA, Tret'yakov PK, Yasakov VA. Length of diffusion flames. *Combust Explos Shock Waves* 1974;10. <https://doi.org/10.1007/BF01465265>.
- [65] Baev VK, Yasakov VA. Influence of buoyant forces on the length of diffuse flames. *Combust Explos Shock Waves* 1974;10. <https://doi.org/10.1007/BF01463817>.
- [66] Kim JS, Yang W, Kim Y, Won SH. Behavior of buoyancy and momentum controlled hydrogen jets and flames emitted into the quiescent atmosphere. *J Loss Prev Process Ind* 2009;22:943–9. <https://doi.org/10.1016/j.jlp.2009.08.018>.
- [67] Kalghatgi GT. Lift-off heights and visible lengths of vertical turbulent jet diffusion flames in still air. *Combust Sci Technol* 1983;41. <https://doi.org/10.1080/00102208408923819>.
- [68] Schefer RW, Houf WG, Bourne B, Colton J. Spatial and radiative properties of an open-flame hydrogen plume. *Int J Hydrogen Energy* 2006;31. <https://doi.org/10.1016/j.ijhydene.2005.11.020>.
- [69] Mogi, T.; Nishida, H.; Horiguchi S. Flame Characteristics of high-pressure hydrogen gas jet. *First Int Conf Hydrog Saf* 2005.
- [70] Henriksen M, Gaathaug AV, Lundberg J. Determination of underexpanded hydrogen jet flame length with a complex nozzle geometry. *Int J Hydrogen Energy*

2019;44:8988–96. <https://doi.org/10.1016/J.IJHYDENE.2018.07.019>.

- [71] Okabayashi K, Takeno K, Hirashima H, Chitose K, Nonaka T, Hashiguchi K. Introduction of Technology for Assessment on Hydrogen Safety. *Mitsubishi Heavy Ind Ltd Tech Rev* 2007;44.
- [72] TAKENO K, HASHIGUCHI K, OKABAYASHI K, CHITOSE K, KUSHIYAMA M, NOGUCHI F. Experimental Study on Open Jet Diffusion Flame and Unconfined Explosion for Leaked High-pressurized Hydrogen. *J Japan Soc Saf Enginennring* 2005;44. https://doi.org/10.18943/safety.44.6_398.
- [73] Yamamoto S, Sakatsume R, Takeno K. Blow-off process of highly under-expanded hydrogen non-premixed jet flame. *Int J Hydrogen Energy* 2018;43:5199–205. <https://doi.org/10.1016/j.ijhydene.2018.01.116>.
- [74] Mogi T, Horiguchi S. Experimental study on the hazards of high-pressure hydrogen jet diffusion flames. *J Loss Prev Process Ind* 2009;22. <https://doi.org/10.1016/j.jlpl.2008.08.006>.
- [75] Wu Y, Lu Y, Al-Rahbi IS, Kalghatgi GT. Prediction of the liftoff, blowout and blowoff stability limits of pure hydrogen and hydrogen/hydrocarbon mixture jet flames. *Int J Hydrogen Energy* 2009;34. <https://doi.org/10.1016/j.ijhydene.2009.01.084>.
- [76] Sivathanu YR, Gore JP. Total radiative heat loss in jet flames from single point radiative flux measurements. *Combust Flame* 1993;94. [https://doi.org/10.1016/0010-2180\(93\)90073-C](https://doi.org/10.1016/0010-2180(93)90073-C).
- [77] Birch AD, Hughes DJ, Swaffield F. Velocity decay of high pressure jets. *Combust Sci Technol* 1987;52. <https://doi.org/10.1080/00102208708952575>.
- [78] Proust C, Jamois D, Studer E. High pressure hydrogen fires. *Int J Hydrogen Energy* 2011;36. <https://doi.org/10.1016/j.ijhydene.2010.04.055>.
- [79] Cirrone DMC, Makarov D, Molkov V. Simulation of thermal hazards from hydrogen under-expanded jet fire. *Int J Hydrogen Energy* 2019;44:8886–92. <https://doi.org/10.1016/j.ijhydene.2018.08.106>.
- [80] Li Z, Luo Y. Comparisons of hazard distances and accident durations between hydrogen vehicles and CNG vehicles. *Int J Hydrogen Energy* 2019;44:8954–9. <https://doi.org/10.1016/j.ijhydene.2018.07.074>.
- [81] Hussein H, Brennan S, Molkov V. Hydrogen Jet Fire from a Thermally Activated

- Pressure Relief Device (TPRD) from Onboard Storage in a Naturally Ventilated Covered Car Park. *Hydrogen* 2021;2. <https://doi.org/10.3390/hydrogen2030018>.
- [82] CFFPA-E Guideline No 19:2009 F. Fire safety engineering concerning evacuation from buildings 2009.
- [83] ISO/TR 16576:2017. Fire safety engineering — Examples of fire safety objectives, functional requirements and safety criteria 2017.
- [84] Loo YL, Haider S, PY YL, Jeffery S. Predictor of the depth of burn injuries: A time and temperature relationship review. *Int J MedicalScience Clin Invent* 2018;5:4119–28. <https://doi.org/10.18535/ijmsci/v5i11.01>.
- [85] Moritz AR, Henriques FC. Studies of Thermal Injury: II. The Relative Importance of Time and Surface Temperature in the Causation of Cutaneous Burns. *Am J Pathol* 1947;23.
- [86] Gottuk, D. R Hall. John, Kazunori, H. Kuligowski, E. Puchovsky, M. Torero, J. Watts J.M. Wieczorek C. SFPE Handbook of Fire Protection Engineering. 5th ed. Springer; n.d.
- [87] LaChance J, Houf W, Middleton B, Fluer L. Analyses to support development of risk-informed separation distances for hydrogen codes and standards. 2009.
- [88] Hymes I. Physiological and pathological effects of thermal radiation. 1985.
- [89] Health and Safety Executive (HSE) CRR/285/2000. Thermal radiation criteria for vulnerable populations . 200AD.
- [90] Brennan S, Molkov V. Pressure peaking phenomenon for indoor hydrogen releases. *Int J Hydrogen Energy* 2018;43:18530–41. <https://doi.org/10.1016/J.IJHYDENE.2018.08.096>.
- [91] Brennan S, Molkov V. Safety assessment of unignited hydrogen discharge from onboard storage in garages with low levels of natural ventilation. *Int J Hydrogen Energy* 2013;38:8159–66. <https://doi.org/10.1016/J.IJHYDENE.2012.08.036>.
- [92] Shentsov V, Kuznetsov M, Mokov V. The pressure peaking phenomenon: validation for unignited releases in laboratory scale enclosure. *Int Conf Hydrog Saf* 2015;(148) 10 pp.
- [93] Makarov D, Shentsov V, Kuznetsov M, Molkov V. Pressure peaking phenomenon:

- Model validation against unignited release and jet fire experiments. *Int J Hydrogen Energy* 2018;43:9454–69. <https://doi.org/10.1016/J.IJHYDENE.2018.03.162>.
- [94] Brennan S, Hussein HG, Makarov D, Shentsov V, Molkov V. Pressure effects of an ignited release from onboard storage in a garage with a single vent. *Int J Hydrogen Energy* 2019;44:8927–34. <https://doi.org/10.1016/J.IJHYDENE.2018.07.130>.
- [95] Hussein HG, Brennan S, Shentsov V, Makarov D, Molkov V. Numerical validation of pressure peaking from an ignited hydrogen release in a laboratory-scale enclosure and application to a garage scenario. *Int J Hydrogen Energy* 2018;43:17954–68. <https://doi.org/10.1016/J.IJHYDENE.2018.07.154>.
- [96] Lach AW, Vagner Gaathaug A, Vaagsaether K. Pressure peaking phenomena: Unignited hydrogen releases in confined spaces- Large scale experiments. *Int J Hydrogen Energy* 2020.
- [97] Lach AW, Gaathaug AV. Large scale experiments and model validation of Pressure Peaking Phenomena-ignited hydrogen releases. *Int J Hydrogen Energy* 2021;46:8317–28. <https://doi.org/10.1016/j.ijhydene.2020.12.015>.
- [98] Lach AW, Vagner Gaathaug A. Pressure peaking phenomena: Large-scale experiments of ignited and unignited hydrogen releases. 13 th Int. Symp. Hazards , Prev. Mitig. Ind. Explos. ISHPMIE2020 Phys. Bundesanstalt, Braunschweig, Germany: Physikalisch-Technische Bundesanstalt (PTB); 2020, p. 813–26. <https://doi.org/10.7795/810.20200724>.
- [99] MathWorks. Ode45.Matlab 2022. <https://se.mathworks.com/help/matlab/ref/ode45.html#bu0200w-3>.
- [100] McBride B, Gordon S, Reno M. Coefficients for Calculating Thermodynamic and Transport Properties of Individual Species. Nasa Tech Memo 1993;4513:98.
- [101] Lach AW, Gaathaug AV, Vaagsaether K. Pressure peaking phenomena: Unignited hydrogen releases in confined spaces – Large-scale experiments. *Int J Hydrogen Energy* 2020. <https://doi.org/10.1016/j.ijhydene.2020.08.221>.
- [102] MathWorks. Findpeaks.Matlab 2022. <https://www.mathworks.com/help/signal/ref/findpeaks.html>.
- [103] Dorofeev SB, Kuznetsov MS, Alekseev VI, Efimenko AA, Breitung W. Evaluation of limits for effective flame acceleration in hydrogen mixtures. *J Loss Prev Process*

Ind 2001;14:583–9. [https://doi.org/10.1016/S0950-4230\(01\)00050-X](https://doi.org/10.1016/S0950-4230(01)00050-X).

- [104] Middha P, Hansen OR. CFD simulation study to investigate the risk from hydrogen vehicles in tunnels. *Int J Hydrogen Energy* 2009;34. <https://doi.org/10.1016/j.ijhydene.2009.02.004>.
- [105] Palacios A, García W, Rengel B. Flame shapes and thermal fluxes for an extensive range of horizontal jet flames. *Fuel* 2020;279. <https://doi.org/10.1016/j.fuel.2020.118328>.
- [106] BOUIX D, SAUZEDDE F, MANICARDI P, MARTIN M, FORERO-MORENO D., STUDER E, et al. FULL-SCALE TUNNEL EXPERIMENTS FOR FUEL CELL HYDROGEN VEHICLES: JET FIRE AND EXPLOSIONS. 9th Int. Conf. Hydrog. Saf., 2021, p. 1197–210.

Part II

Scientific Publications

Article A

Pressure peaking phenomena: Unignited hydrogen releases in confined spaces – large-scale experiments

A.W. Lach, A.V. Gaathaug and K. Vågsæther

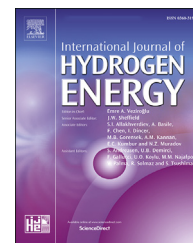
Published in International Journal of Hydrogen Energy, November 2020,
45(56): 32702-32712, doi:<https://doi.org/10.1016/j.ijhydene.2020.08.221>



ELSEVIER

Available online at www.sciencedirect.com

ScienceDirect

journal homepage: www.elsevier.com/locate/he

Pressure peaking phenomena: Unignited hydrogen releases in confined spaces – Large-scale experiments

Agnieszka Weronika Lach*, André Vagner Gaathaug, Knut Vaagsaether

University of South-Eastern Norway, Kjolnes Ring 56, 3918, Porsgrunn, Norway

HIGHLIGHTS

- Hydrogen releases inside an enclosure confirm PPP.
- Description of large-scale experimental setup and instrumentation.
- Overpressures as a consequence of vent size configuration and mass flow rates.
- The model for the unignited hydrogen releases is validated against 10 experiments.
- Two models using either real mix and perfect mix are investigated.

ARTICLE INFO

Article history:

Received 23 June 2020

Received in revised form

11 August 2020

Accepted 26 August 2020

Available online xxx

Keywords:

Hydrogen safety

Pressure peaking phenomenon

Model validation

Passive ventilation

Large-scale experiments

Enclosures

ABSTRACT

The aim of this study was to validate a model for predicting overpressure arising from accidental hydrogen releases in areas with limited ventilation. Experiments were performed in a large-scale setup that included a steel-reinforced container of volume 14.9 m³ and variable ventilation areas and mass flow rates. The pressure peaking phenomenon, characterized as transient overpressure with a characteristic peak in a vented enclosure, was observed during all the experiments. The model description presented the relationship between the ventilation area, mass flow rate, enclosure volume, and discharge coefficient. The experimental results were compared with two prediction models representing a perfect mix and the real mix. The perfect mix assumed that all the released hydrogen was well stirred inside the enclosure during the releases. The real mix prediction used the hydrogen concentration and temperature data measured during experiments. The prediction results with both perfect mix and real mix showed possible hazards during unignited hydrogen releases.

© 2020 The Authors. Published by Elsevier Ltd on behalf of Hydrogen Energy Publications LLC. This is an open access article under the CC BY license (<http://creativecommons.org/licenses/by/4.0/>).

Introduction

Hydrogen-fueled vehicles are becoming increasingly common in today's transportation systems. In such vehicles, hydrogen

is most commonly stored in tanks as a compressed gas at 700 bar. Under EU Commission Regulation requirements, tanks must be equipped with a pressure relief device (PRD) [1]. The PRD activates by pressure, temperature, or combination of both to release hydrogen from the pressurized tank, and

* Corresponding author.

E-mail address: AgnieszkaLach@usn.no (A.W. Lach).

<https://doi.org/10.1016/j.ijhydene.2020.08.221>

0360-3199/© 2020 The Authors. Published by Elsevier Ltd on behalf of Hydrogen Energy Publications LLC. This is an open access article under the CC BY license (<http://creativecommons.org/licenses/by/4.0/>).

this rapid discharge of hydrogen is needed to avoid tank rupture when there is exposure to a fire [2]. The PRDs used in hydrogen vehicles typically have an orifice of 5.08 mm diameter [3], or 4.2 mm [4] providing high mass flow rates that are not specified in regulations, codes, and standards (RCS). High mass flow rates released into confined space creates hazards of enclosure collapse due to high overpressure. This is the main subject of interest in this paper. Thermally activated release devices (TPRDs) with a “typical” diameter will most likely result in acceptable safety for open-air releases (the hydrogen will disperse into the atmosphere). However, new hazards that arise from the rapid discharge of hydrogen in confined spaces must be considered by auto manufacturers and controlled using RCS.

The consequences of indoor hydrogen releases differ significantly from those of outdoor releases and can affect people, structures, and the environment. In past years, several European research projects have focused on hydrogen energy systems and related safety issues. Projects like HyIndoor [5], H2FC [6,7], or HySafe noted that one important issue among others is the possibility of hydrogen leakage inside an enclosure, which, without proper ventilation systems, may result in the formation of explosive clouds [8]. Further study of hydrogen release in a battery room investigated the influence of ventilation systems or its lack in a closed room [9]. The study exposed the risk of explosion hazards when no proper ventilation was assured. The final report of the HyIndoor project [5] directed attention to existing knowledge gaps, which still need to be resolved. The HySafe project studied the non-catastrophic conditions created by release from a hydrogen fuel tank inside a small enclosure [10]. The relationship between the enclosure venting and the hydrogen mass discharge ratio is crucial in reducing the significant risk of the enclosure’s collapse. Those knowledge gaps have to be closed as a part of safety development of hydrogen applications. In particular, an engineering tool for hydrogen safety engineers must be developed and disseminated.

Generally, most studies of hydrogen dispersion and overpressures have been performed for small-scale scenarios that often used helium instead of hydrogen. The studies reported in Ref. [11,12] showed that helium behaves similarly to hydrogen and can be used as a substitute for research purposes. The work reported in Ref. [10] investigated helium dispersion behavior depending on injected helium initial flow regimes (turbulent and laminar flows) in non-catastrophic scenarios. Experiments were performed in a 40.92 m³ well-ventilated enclosure, ensuring atmospheric pressure during the tests. The concentration level of accumulated helium mostly depended on the total volume of helium discharged into the enclosure. Previous work by reported in Ref. [10–13] have investigated hydrogen dispersion in enclosures with natural or passive ventilation. In all of these studies, helium was used instead of hydrogen. Nine experiments and CFD modeling were performed in a real-scale facility to investigate the relationship between leak rate, ventilation design, and hydrogen concentration [13]. The results showed the importance and variability of stratification, and there was good agreement of the CFD model with experiments. Later studies [14,15] investigated the relationships between three ratios

$\dot{m}_{in}/\dot{m}_{out}$, V_{en}/A_{vent} and A_{nozzle}/H_{vent} and the mixture (air-helium) uniformity. The results of 48 experiments on helium releases in an enclosure of ~1 m³ and combinations of three vent sizes and two nozzle diameters were compared to the model of passive ventilation. The discharge coefficient, the only unknown value in the model, was found through a best fit to be 0.85. The different CFD codes were compared with different turbulence models, and satisfactory results were obtained to justify using models to estimate hydrogen concentrations [16].

The following study considers hydrogen releases in a confined space with a limited ventilation area. The investigation of overpressures and hydrogen concentrations at specific conditions is part of a pre-normative research into the safety of hydrogen-fueled vehicles and their transport through tunnels and similar confined spaces.

The rapid discharge of hydrogen from a tank in a confined space may lead to high overpressures, which in turn may cause injury and property damage. This so-called pressure peaking phenomenon (PPP) is characterized as a transient overpressure with a characteristic peak in a vented enclosure. PPP occurs when a light gas (i.e., H₂) flows into an enclosure with a denser gas (in this case, air). The phenomenon is distinct for hydrogen and occurs when the released hydrogen mass flow rate is relatively high and the vent area is relatively small [17]. With these conditions, the flow at the vent area will consist of hydrogen and air. At the beginning it will be mostly air, and the hydrogen content increases with time. At the nozzle, the flow will consist only of hydrogen. This will result in a situation where the light gas will push out the denser gas, hence leading to an accumulation of the number of moles inside the enclosure (air and hydrogen). The overpressure continue to grow until the flow of moles at both the vent and nozzle are equal. Then, the peak pressure will be reached and concurrently the total density of gas inside the enclosure will be lower. The density will continue to decrease until the hydrogen concentration reaches 100% (concentration not achieved during experiments presented in this work). Previous numerical validation studies [18] confirmed that the two major parameters governing the overpressure in an enclosure are the vent size and the hydrogen mass flow rate into the enclosure. These have the most significant roles in creating high overpressures. Brennan and Molkov [19] presented their investigation of “safety” PRD parameters with a correlation of the natural ventilation variables in the enclosure for a tank blowdown scenario. Their study describes the model used during the experiments described in the present work. The study showed that the overpressure drops accordingly with decreasing PRD diameter. Their study presented a correlation between hydrogen concentration and the vent area. With an increasing vent area, the maximum overpressure decreases. But due to the larger vent area the hydrogen concentration increases more rapidly. This leads to a greater hydrogen concentration at the maximum overpressure, under the assumption of no air ingress into the enclosure. A high concentration of hydrogen will also create hazards of asphyxiation and explosion (not part of this study). The hydrogen tanks designed for cars, currently in use, are type 4 [20] with the time limitation of being exposed to high temperatures resulting from a fire. With decreasing PRD diameter, the tank will be

pressurized for a longer time when exposed to a fire, and this must be taken into consideration.

The following study reports the validation of the pressure peaking phenomenon for unignited hydrogen releases in a confined space with a limited ventilation area. The paper first describes the experiments and the model used in the work. This is followed by a discussion of the results and a conclusion.

Experimental setup and methods

This section will first present the experimental setup and second the analytical model used to compare the results.

Experimental setup

The experiments were performed in the explosion chamber shown in Fig. 1. The explosion chamber has the inner dimensions $L \cdot W \cdot H$: $2980 \cdot 2000 \cdot 2500$ mm, which gives a total volume of 14.9 m^3 . The explosion chamber has a total of five vents, each with a diameter of 80 mm. Four of them are located at the lower corners at the front and back wall. The fifth is located in the middle of the front wall (V5 in Fig. 1) and comes out on the inside of the chamber floor. It was used as the hydrogen inlet from a crate of 12·50 l bottles at 200 bar.

Only one vent was used for ventilation (V1 in Fig. 1). To enable passive ventilation 20 cm from the ceiling, a 75 mm diameter PVC pipe was installed from the vent (V1) located at the right corner 15 cm above the floor. The cover with a diameter providing the desired ventilation area was placed at the end of the PVC pipe (outside the explosion chamber; Fig. 2).

The hydrogen pressure was controlled by a valve at the bottle crate that was connected to the mass flow meter by a stainless steel pipe (4 mm ID). From the mass flow meter, the pipe was connected to a ball valve before being connected to the 4 mm release nozzle. The nozzle was placed at the center of the explosion chamber's floor to vertically discharge hydrogen inside the chamber. A Coriolis-type mass flow meter was used to measure the hydrogen mass flow, and the data were logged with an oscilloscope (Sigma, Fig. 3). The mass flow rates of hydrogen discharge were limited by two factors: the 110-bar maximum operating pressure of the mass flow meter

and the decreasing hydrogen pressure in the bottle stack (due to the decreasing amount of hydrogen). The pressure regulator valve mounted at the bottle stack was used to set the pressure of the hydrogen, resulting in the needed mass flow rate. The explosion chamber was equipped with a pressure transducer and hydrogen sensors. To measure the overpressure, a Kulite pressure transducer XTM-190-10A was used that was mounted 1.5 m above the floor in the middle of the wall (Fig. 3). The pressure transducer was connected to an oscilloscope (HBM Gen3i, Fig. 3). Hydrogen concentration measurements were carried out continuously inside the chamber during experiments. Two XEN-3520 wireless concentration sensors (3 Hz) were used to measure the hydrogen concentration. The sensors also measured the temperature inside the enclosure. Due to technical problems for Experiments 6–11, a USB cable was used instead of the wireless connection. Sensors were connected to a laptop computer that stored the data. One sensor (H1) was mounted in the middle of the front wall 1.24 m above the floor. The second sensor (H2) was mounted in the middle of the backplate 2.85 m above the floor (Fig. 1).

The ventilation area was kept constant during the experiment. Several small leaks were identified during preliminary tests and sealed using different sealants.

All instrumentation was controlled via a pulse generator programmed to trigger both oscilloscopes and the hydrogen release valve at the same time. An air fan (Fig. 3) was activated after the release of hydrogen was closed.

After each experiment, the hydrogen concentration in the explosion chamber reached between 13% and 62% (depending on the experiment). To ensure the same conditions without interfering with the applied sealing, air from a fan was introduced to reduce the hydrogen concentration to <2%.

Analytical model

The pressure peaking phenomenon occurs with a relatively small ventilation area and a large hydrogen mass flow, assuring that there is no air mass flow into the enclosure [17]. The model presented in the equations below [3] was used to simulate the overpressure in the enclosure in terms of moles, with $V = 14.9 \text{ m}^3$ and transient molar flow rates \dot{n}_{in} and \dot{n}_{out} . The overpressure inside the enclosure p_{en} depends on the number of moles in the enclosure:

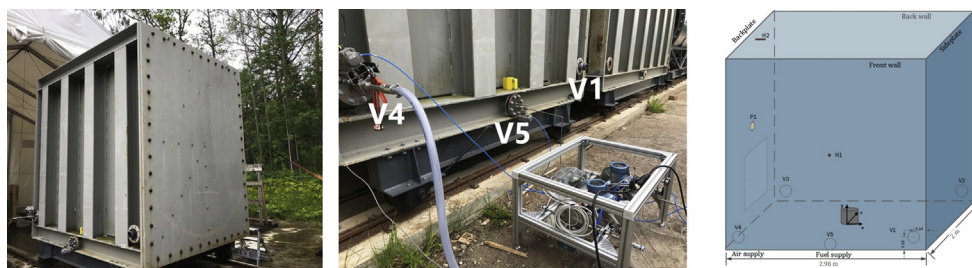


Fig. 1 – (Left) The 14.9 m^3 enclosure. (Middle) Vents used for experiments: V4 air inlet, V5 hydrogen inlet with Coriolis mass flow meter, V1 ventilation. (Right) Enclosure scheme showing sensor placement (x,y,z): H1 (0, 1.24, -1), H2 (-1.43, 2.38, 0), P1 (-1.49, 1.24, 0).

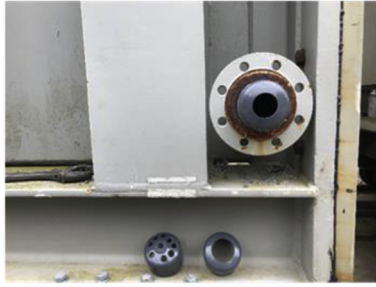


Fig. 2 – Ventilation assembly.

$$\frac{dn_{en}}{dt} = \dot{n}_{in} - \dot{n}_{out} \quad (1)$$

$$\frac{dn_{H_2}}{dt} = \dot{n}_{H_2,in} - X_{H_2} \cdot \dot{n}_{out} \quad (2)$$

$$p_{en} = \frac{n_{en} \cdot R \cdot T_{en}}{V} \quad (3)$$

The initial conditions were $n_{H_2}(0) = 0$ and $n_{en}(0) = p_0 V / RT_0$. The initial pressure in the enclosure was assumed to be equal to the ambient pressure, $p_0 = 101.325$ kPa. By solving this conservation equation, the overpressure inside the enclosure can be calculated with the ideal gas law in Eq. (3). R is the universal gas constant and T is the temperature inside the enclosure (constant for P_{mix} and transient/measured for R_{mix}).

The molar flow into the enclosure consists only of hydrogen, $\dot{n}_{in} = \dot{n}_{H_2,in} = \dot{m}_{in} / M_{H_2}$ (hydrogen mass flow \dot{m}_{in} was measured with the Coriolis mass flow meter). The quantities n_{H_2} and X_{H_2} are the number of moles of hydrogen and the hydrogen mole fraction, respectively, inside the enclosure. The molar flow of air and hydrogen from the enclosure, \dot{n}_{out} , is calculated from Eq. (4) for the mass flow through the vent [21] in terms of moles:

$$\dot{n}_{out} = C \cdot A_v \sqrt{\frac{2 \cdot \Delta p \cdot n_{en}}{V \cdot M_{en}}} \quad (4)$$

where $\Delta p = p_{en} - p_0$, V is the enclosure volume, n_{en} is the number of moles in the enclosure, C is the discharge coefficient, and A_v is the ventilation area. The molecular mass of gases in the enclosure M_{en} depends on the hydrogen mole fraction in the enclosure:

$$M_{en} = X_{H_2} \cdot M_{H_2} + (1 - X_{H_2}) \cdot M_{air} \quad (5)$$

where X is the hydrogen mole fraction and M_{H_2} and M_{air} are the molecular mass of hydrogen and air, respectively.

The overpressure in the enclosure is then a transient pressure with a characteristic peak occurring only for gases lighter than air. The lack of airflow into the enclosure is ensured as long as the pressure in the enclosure is higher than ambient pressure. It can be seen from Eqs. (1) and (3) that, with an increasing number of moles in the enclosure with constant V , the resulting pressure will increase. The pressure will continue to grow as long as \dot{n}_{in} is higher than \dot{n}_{out} . The low density of the entering hydrogen will lead to a decrease in the overall density in the enclosure. Thus, the density inside the enclosure has its maximum value at t_0 and will decrease until hydrogen is the only gas in the enclosure.

Mass flow in

When comparing the analytical model results to the experimental results, the hydrogen molar flow into the enclosure is based on the measured mass flow of hydrogen. This captures the effect of the transient mass flow due to valve operation delays.

Mole fraction inside enclosure

In this study, the analytical model results are presented for two cases in comparison with the experimental results. The

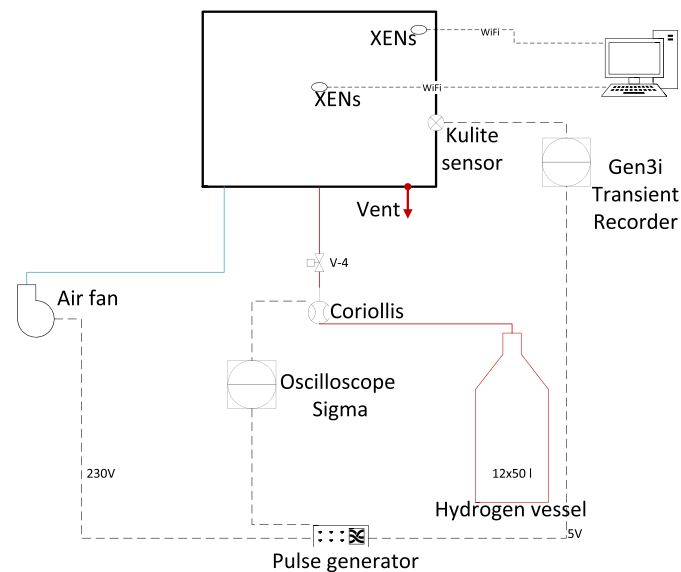


Fig. 3 – Simplified piping and instrumentation diagram (P&ID).

difference between the two cases is the evaluation of the mole fraction of hydrogen. The details follow below.

1. The perfect mix (Pmix) case is when the mole fraction is calculated with Eq. (6). It assumes a perfect mixing of hydrogen and air inside the enclosure.
2. The real mix (Rmix) case is when the mole fraction of hydrogen is not calculated but extracted from the hydrogen concentration sensor data.

Both models are based on Eqs. (1) through (5) and contain parameters crucial for PPP: the hydrogen mass flow into the enclosure, the ventilation area, the enclosure volume, and the discharge coefficient. The shape of the ventilation area and its location are not included in the model.

Perfect mix

The prediction model with a perfect mix scenario includes the process of gas mixing based on the molar balance in the enclosure, given by Eq. (1). The model is based on the system of Eqs. (1), (2) and (4). The molecular mass inside the enclosure changes with time due to the hydrogen discharge, \dot{n}_{in} , with \dot{n}_{out} being a mixture of air and hydrogen. To calculate M_{en} using Eq. (5), the mole fraction of hydrogen is calculated with Eq. (6) below:

$$X_{H_2,p} = \frac{n_{H_2}}{n_{en}} \quad (6)$$

$X_{H_2,p}$ represents the mole fraction for the perfect mix model in the enclosure, where n_{H_2} and n_{en} were calculated with Eq. (2) and Eq. (1), respectively.

Real mix

The hydrogen concentration measurements were used to validate the perfect mix assumption in the model and investigate the influence of non-perfect mixing. The prediction model with a real mix scenario represents the same process of mixing gases in an enclosure as given by Eq. (1). The mole fraction inside the enclosure was not calculated as it had been for Pmix but was measured with hydrogen concentration sensors; (C_{meas}): $X_{H_2,R} = \frac{C_{meas}}{100}$. The number of moles of hydrogen measured during the experiments was implemented into the Rmix model as $n_{en} = n_{H_2} / X_{H_2,R}$, where n_{H_2} was calculated with Eq. (2) and $X_{H_2,R}$ time transient mole fraction. The n_{en} was used in Eq. (4) to calculate molar flow out of the enclosure. The temperature measured with hydrogen sensors was implemented into Eq. (3), while for Pmix, the temperature was constant and equal to T_0 . Then, the number of moles in the enclosure from Eq. (1) was used to calculate the overpressure in Eq. (3).

A discharge coefficient is a non-dimensional number representing flow and pressure loss through the orifice [21]. Therefore varies for different setups. Due to the unknown discharge coefficient for the vents of the explosion chamber and resulting pressure losses, for the overpressure computing, the discharge coefficient (C) must be chosen based on the experimental results.

Results

The measured overpressures (pressure peak) and maximum concentrations are listed in Table 1. In order to observe Pressure Peaking Phenomenon for unignited releases in a 14.9 m³ enclosure with setup for hydrogen releases, described in Section Experimental setup, the small ventilation areas had to be implemented (Table 1, column 4). The pressure at the bottle crate was set up at different values to obtain mass flow rates presented in the experimental matrix (Table 1, column 5). Due to technical issues with XENsensors, no data were stored for Experiments 4 and 5. For Experiments 2 and 3, the temperature data, stored during experiments, had a format with large uncertainty (this was corrected in subsequent experiments). Therefore, the initial temperature for those experiments was assumed to be 293 K (the average temperature of summer days during the experiments). The hydrogen concentration increased until the H₂ discharge stopped, giving maximum values at the end of the H₂ inflow (Table 1).

Experiment 11 was performed with continuously decreasing mass flow (blowdown). It started at a maximum value of 4.85 g/s (see Fig. 4). The hydrogen inflow duration was the longest among all experiments. During Experiment 11, the laptop computer used for collecting the data from the concentration sensors shut down after 122 s (Fig. 4). The maximum pressure was observed after 64 s, and the obtained data allowed further real mix predictions (Table 2). The H₂ concentration varied depending on mass flow rate (MFR) and A_v , showing that, with higher MFR at the same A_v , the concentration at $t_{(p_{max})}$ is higher (Table 2).

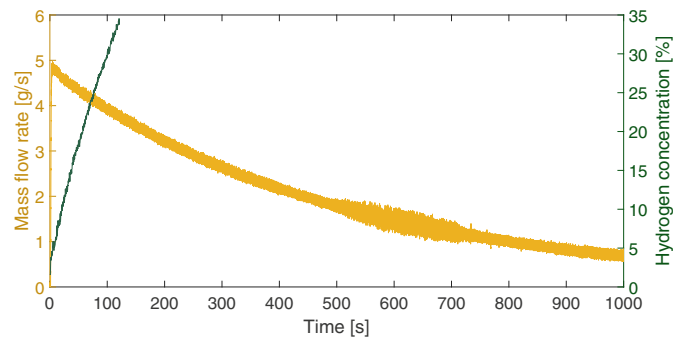
Analysis and discussion

A comparison between experimental results and other studies is presented first, followed by an explanation of the experimental results based on the proposed analytical model. In addition, the predictions with perfect and real mix assumptions are compared to the experimental results.

All experiments were performed successfully and showed the pressure peaking phenomenon. As expected, the results showed the large dependency of PPP on mass flow rate, ventilation area, and discharge coefficient. Even small changes in one of those parameters had a large influence on the overpressures, as was also showed in earlier studies presented in the introduction [22]. The value of the discharge coefficient depends on the ventilation area, its size and shape, the density of gas, and pressure [21]. The discharge coefficient value $C = 0.6$, suggested in other studies [17,19], did not show a good match. Authors of [17] applied $C = 0.85$ to build the nomogram for a graphical calculation at the lower limit of MFR. This value also did not show a good match. By adjusting the discharge coefficient in both predictions (the first with the perfect mix assumption, Pmix, and the second with the real mix assumption, Rmix), a value of $C = 0.7$ gave the best agreement to the experimental results (Table 3).

Table 1 – Maximum overpressure and hydrogen concentration results for Experiments 2–11. Unignited releases through a 4 mm nozzle.

Setup					Measured		
Exp #	T ₀ in enclosure [K]	H ₂ release time [s]	Vent area [m ²]	Mass flow rate [g/s]	Experimental overpressure [kPa]	Experimental max H ₂ conc. [%]	
2	293.00 ^a	90	0.0012	1.90	0.42	13	
3	293.00 ^a	120	0.0020	3.50	0.51	28	
4	293.00 ^a	120	0.0020	9.05	2.86	–	
5	293.00 ^a	120	0.0014	9.90	6.45	–	
6	296.00	120	0.0014	10.10	6.74	62	
7	292.34	180	0.0006	3.05	4.07	35	
8	291.94	180	0.0006	3.05	3.96	35	
9	293.12	200	0.0006	4.75	8.05	53	
10	289.71	200	0.0006	4.20	6.70	47	
11	293.57	1000	0.0006	4.85 _{blowdown}	7.00	–	

^a assumed values.**Fig. 4 – Mass flow rate and hydrogen concentration measurements for Experiment 11.**

As mentioned in previous sections, the maximum overpressure appears at the moment when $\dot{n}_{in} = \dot{n}_{out}$. After that, the molar flow at the vent (\dot{n}_{out}/M_{en}) is higher than the molar flow at the nozzle (\dot{n}_{in}/M_{H_2}), and the overpressure begins to decrease. The measured overpressures inside the enclosure (for the selected experiments) are shown in Fig. 5.

It has been proven that the maximum overpressure $t(p_{max})$ at a given ventilation area does not significantly depend on the enclosure volume but on \dot{n}_{in} [19]. If the incoming molar flow and the ventilation area are kept constant, the time until peak pressure increases [19]. It is a clear consequence, based on the model description, that with the same enclosure volume and ventilation area, p_{max} will increase with increasing \dot{n}_{in} . Based on experimental results with higher \dot{n}_{in} , the p_{max} will be larger, as seen in Fig. 6. By

changing the mass flow rate in the model from a constant release of 1 g/s to 100 g/s, the maximum pressure and the time of maximum pressure are calculated (for each mass flow rate) and plotted in Fig. 7. These predictions are conducted based on a perfect mix assumption. Each point on the curve represents one mass flow rate, where the lowest mass flow rate starts at the lower left part of the curve. The circles on the plot show the same points (maximum p at $t(p_{max})$) as the three experiments plotted in Fig. 6. From the model calculation, one can see that decreasing the ventilation areas causes the pressure peak to reach higher values but at later times (Fig. 7, top). The same model results show that, when increasing the enclosure volume (at constant A_v), the maximum overpressure is the same for the same \dot{n}_{in} , but it occurs later (Fig. 7, bottom).

Table 2 – Hydrogen concentrations at maximum pressures: measured used in Rmix, and calculated with Pmix model.

Exp #		2	3	4	5	6	7	8	9	10	11
MFR [g/s]		1.90	3.50	9.05	9.90	10.10	3.05	3.05	4.75	4.20	4.85 _{blowdown}
A_v [m ²]		0.0012	0.0020	0.0020	0.0014	0.0014	0.0006	0.0006	0.0006	0.0006	0.0006
Measured	H ₂ % at p_{max}	1.5%	0.2%	–	–	24.0%	15.4%	16.0%	25.0%	22.0%	21.5%
	$t(p_{max})$ [s]	10 s	10 s	–	–	37 s	80 s	77 s	89 s	87 s	64 s
Calculated for Pmix with C = 0.7	H ₂ % at p_{max}	3%	4%	15%	26%	26%	16.5%	16.5%	28%	25%	21%
	$t(p_{max})$ [s]	21	16 s	24 s	41 s	40 s	77 s	77 s	91 s	89 s	69 s

Table 3 – Overpressures in the enclosure from unignited hydrogen releases: experimental, P_{mix} prediction, and R_{mix} prediction with C = 0.7.

Setup			Measured			Calculated		
Exp #	H ₂ release time	Vent area [m ²]	Mass flow rate [g/s]	Experimental overpressure [kPa]	Experimental max H ₂ conc. [%]	Calculated overpressure R _{mix} [kPa]	Calculated overpressure P _{mix} [kPa]	Calculated max H ₂ conc P _{mix} [%]
2	90	0.0012	1.90	0.42	13	-	0.43	13
3	120	0.0020	3.50	0.51	28	-	0.54	29
4	120	0.0020	9.05	2.86	-	-	3.09	58
5	120	0.0014	9.90	6.45	-	-	6.41	61
6	120	0.0014	10.10	6.74	62	6.72	6.67	61
7	180	0.0006	3.05	4.07	35	3.88	3.69	35
8	180	0.0006	3.05	3.96	35	3.95	3.70	35
9	200	0.0006	4.75	8.05	53	7.86	7.70	51
10	200	0.0006	4.20	6.70	47	6.86	6.26	47
11	1000	0.0006	4.85 _{blowdown}	7.00	34	7.23	6.58	81

The previous study on hydrogen concentration in a ventilated enclosure showed that increasing the ventilation area increases hydrogen concentration [19]. All the experiments showed that the maximum overpressure occurs before the hydrogen concentration reached its measured maximum value (Fig. 8), which is also seen in the analytical calculations. Experiment 9 has the highest pressure peak of all experiments with $A_v = 0.0006 \text{ m}^2$, and it also has the highest value of hydrogen concentration at the time of peak pressure (Table 2).

The presented close correlation between enclosure volume, MFR, and vent area provides a good understanding of the possible hazards during an accidental hydrogen release through a TPRD inside an enclosure. In the case of a real car, the size of the TPRD diameter directly influences the MFR (as there will be choked flow conditions at the nozzle) and must be designed appropriately to avoid destructive pressure inside enclosures. This conclusion is also found in earlier studies [23]. Enclosures which have a relatively small ventilation area might need improvement of their ventilation systems. The presented model enables the proper calculation of overpressure as a basis for structural response. This can be used as a design tool to size the proper vent area or maximum allowed MFR based on the TPRD or process equipment inside

enclosures. It is important to note that, for ignited releases, the expected overpressures will be much higher. An engineering tool for ignited PPP is necessary to calculate the overpressure from such releases. This is available from Ref. [18].

Pressure peaking phenomena predictions: P_{mix} and R_{mix}

The results showed good similarity for both P_{mix} and R_{mix} (see Table 3). The real mix prediction gave differences between 0.2% and 3.2% and the perfect mix prediction between 0.6% and 7.4% when compared to the experimental overpressures (excluding Experiment 7, which showed 5% and 10% difference, respectively). The comparison can be seen in Fig. 5, which shows that the experimental results of p_{max} are in the range of the results from the perfect mix prediction. This is also the case for the other experiments not shown in Fig. 5. The results of the R_{mix} prediction include the hydrogen concentrations and the temperature data measured during the experiments. Both have an impact on the calculated overpressures, showing their influence on the slope of the overpressure before reaching the pressure peak.

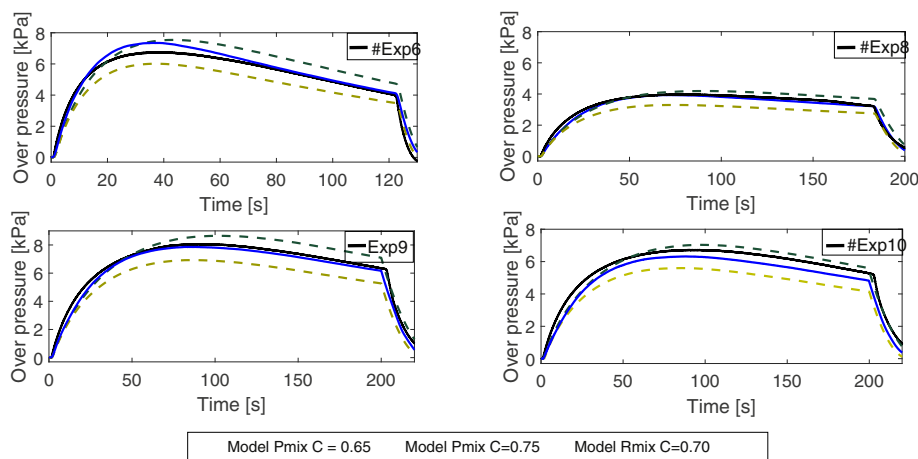


Fig. 5 – Model and experimental overpressures: prediction for real mix with C = 0.7 and perfect mix with C in the range 0.65–0.75; constant mass flow releases.

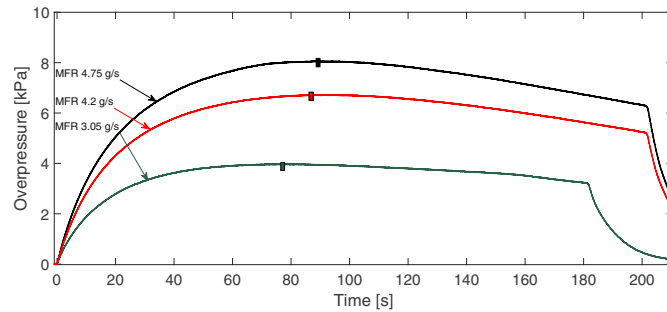


Fig. 6 – Experimental overpressures for varied MFR at the same ventilation area; pressure peak occurrence (rectangle).

The purpose of this comparison is to investigate the validity of the perfect mix assumption. By relaxing the assumption and including real mix data, one can observe that the slope of the overpressure is more accurate. But overall, the perfect mix assumption is a decent approach. The difference between P_{mix} and R_{mix} before $t(p_{max})$ is in the range of 2 s.

The hydrogen concentration was measured at two different locations. The measurements show that, for the chosen enclosure volume, the influence of the sensor locations can be neglected (Fig. 8). For calculations, the data from one sensor was used. For very low momentum jets, this might not be the case. It is important to notice that the ventilation area must be very small in order to observe the pressure peaking phenomenon in this setup, and therefore the concentration change in the enclosure may be similar at two different locations.

The investigation of the hydrogen concentration, both measured and simulated, showed the complexity of the dynamics of the system. Both concentration's growth characteristics were similar before reaching $t(p_{max})$ (see Fig. 8). The concentrations at the $t(p_{max})$ presented in Table 2 show different values which resulted in a variety of maximum overpressures predicted with R_{mix} and P_{mix} model.

The simulated concentration (P_{mix}) is similar to the measured concentration until reaching $t(p_{max})$. However, the calculation results for the overpressure with the perfect mix assumption (which neglects the temperature change) gave larger differences (pressure in Table 3) compared to the R_{mix} predictions. The divergence between the calculated concentration and the measured concentration would suggest a large divergence in pressure as well. This is not observed and is likely due to the compensation of using the measured

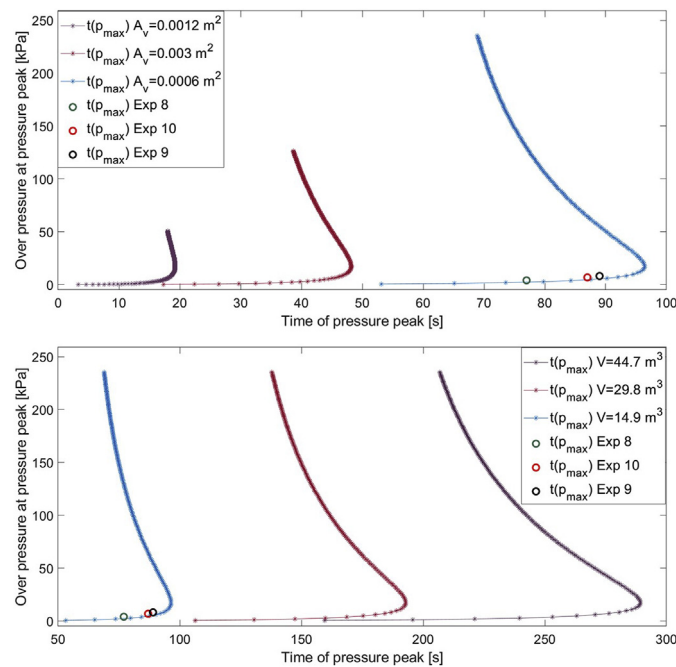


Fig. 7 – (Top) Correlation between time of overpressure peaks for a constant rate of hydrogen release (1–100 g/s) at different ventilation areas for the same enclosure volume, 14.9 m³. (Bottom) Same as above, but with a different enclosure volumes for the same ventilation area, 0.0006 m².

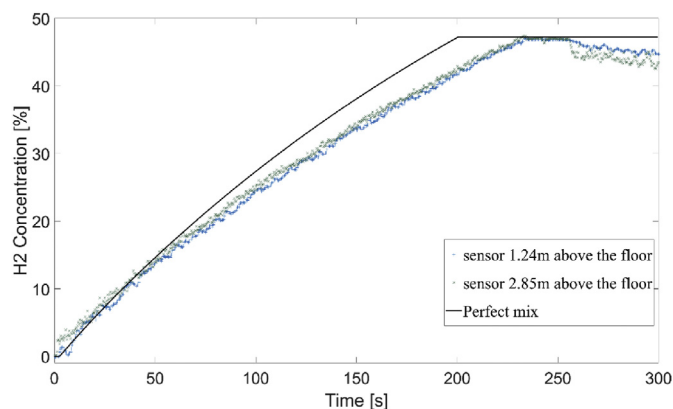


Fig. 8 – Simulated results of hydrogen concentration (perfect mix, solid black line) compared to the measured concentration from Experiment 10.

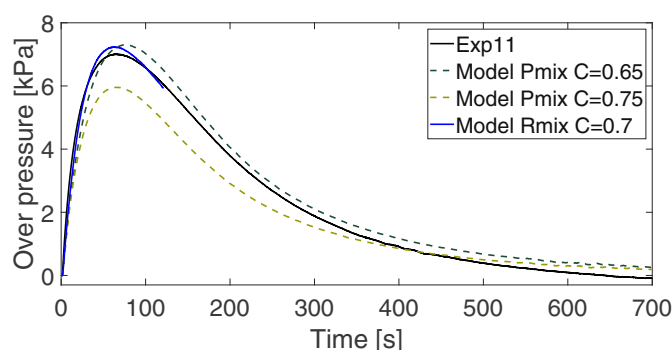


Fig. 9 – Model and experimental overpressures: R_{mix} prediction with $C = 0.7$ and P_{mix} prediction with C in the range 0.65–0.75. See Fig. 4 for the blowdown mass flow release.

temperature data in the R_{mix} predictions. Nevertheless, the perfect mix assumption showed acceptable accuracy and can be used to simulate overpressure as a result of an accidental hydrogen release in an enclosure. In Fig. 5 the dash lines represent P_{mix} predictions for $C = 0.65$ and $C = 0.75$ creating a range for calculation in slightly different setups. The measured pressure and calculated pressure for both P_{mix} and R_{mix} with $C = 0.7$ are in the mentioned range. In order to use the model for overpressure calculation as an engineering tool, the suggested range of discharge coefficient, $C = 0.65$ – 0.75 , provides a safe area for the estimation of overpressures in similar setups (at the given ventilation area, hydrogen inflow rate, and enclosure volume).

Blowdown experiment and prediction

Experiments 2–10 were performed with an (almost) constant mass flow rate of hydrogen, while Experiment 11 had continuously decreasing mass flow rate (Fig. 4). The application of the model was demonstrated earlier for (almost) constant mass flow rates, where $\dot{n}_{in} = \text{const}$. Experiment 9 with $MFR = 4.75$ g/s reached $p_{max} = 8.05$ kPa, and Experiment 11 with the same ventilation area and MFR (Fig. 4) at t_0 equal to 4.85 g/s reached $p_{max} = 7.00$ kPa

(Fig. 9). Experiment 11, performed with blowdown MFR , shows that, with decreasing mass flow into the enclosure, the obtained maximum pressure will be lower (Fig. 9). The mole balance presented in the model description from Eq. (1) shows that dependency. With the blowdown hydrogen inflow ($\dot{n}_{in} \neq \text{constant}$), the time at which $\dot{n}_{in} = \dot{n}_{out}$ occurs earlier and results in a lower overpressure, which confirms the model. The R_{mix} model showed good accuracy for reaching $t(p_{max})$, while the P_{mix} model better estimated the value of p_{max} compared to the experimental results. Nevertheless, the R_{mix} and experimental overpressure are in the range of the P_{mix} predictions, again justifying its applicability as an engineering tool for both blowdown and constant MFR s.

Conclusion

The pressure peaking phenomenon was investigated using large-scale experiments. The experimental setup was sealed, assuring a constant ventilation area. The hydrogen inflow and data from a pressure transmitter and hydrogen concentration sensors were measured continuously during the experiments. Due to the high risk from hydrogen releases in confined

spaces, an explosion chamber was used to ensure the safety and quality of the experiments.

The model description presented the relationship between the ventilation area, mass flow rate, enclosure volume, and the discharge coefficient. The overpressure can be determined by setting a mass flow rate for the hydrogen and specifying the enclosure volume and ventilation area in the model. The analytical calculations were compared with the experimental results to estimate the discharge coefficient at the vent.

The predictions of the analytical model showed that the time of maximum overpressure occurred later with increasing mass inflow (with the same enclosure setup), until a certain point where this time started occurring earlier. The vent area influences the overpressure, as a larger vent results in a lower overpressure. The enclosure volume does not significantly influence the overpressure, but a larger volume will result in the pressure peaking at a later time.

All the experiments showed the phenomenon and were used to validate two prediction models: perfect mix and real mix. The perfect mix assumes that all the released hydrogen is well stirred inside the enclosure during the releases. The real mix predictions use the hydrogen concentration and temperature data measured during experiments. The real mix assumption had a small influence on maximum overpressures but showed its impact on the pressure dynamic before $t(p_{\max})$. Temperature changes measured during experiments influenced the \dot{v}_{out} , providing a better overpressure prediction. Both predictions showed good similarity with experimental results, proving the accuracy of the model and justifying the validity of the perfect mix assumption. One particular hazard of unignited hydrogen releases in confined spaces (with small ventilation areas) has been proved.

Performed largescale experiments demonstrate the relationship between ventilation area, enclosure volume, and release rate which may result in significant overpressures in an enclosure. The maximum release rate, hence TPRD diameter should be regulated in RCS to protect humans and surroundings. The pressure peaking phenomena is relevant for rapid releases of hydrogen into an enclosure with limited ventilation area, which should be considered by other application than hydrogen vehicles as well.

Declaration of competing interest

The authors declare that they have no known competing financial interests or personal relationships that could have appeared to influence the work reported in this paper.

Acknowledgments

The authors wish to thank Knut Ove Hauge and The Norwegian Defence Estates Agency for the experimental facility and support.

The authors wish to acknowledge funding from the Fuel Cells and Hydrogen 2 Joint Undertaking (JU) under grant agreement No 826193. The JU receives support from the

European Union's Horizon 2020 research and innovation programme and United Kingdom, Germany, Greece, Denmark, Spain, Italy, Netherlands, Belgium, France, Norway, Switzerland.

This work was performed within MoZEEs, a Norwegian Centre for Environment-friendly Energy Research (FME), co-sponsored by the Research Council of Norway (project number 257653) and 40 partners from research, industry, and the public sector.

REFERENCES

- [1] Commission Regulation (EU) No 406/2010 of 26 April 2010 on type-approval of hydrogen-powered motor vehicles. [Online]. pp 61–62. Available from: <https://eur-lex.europa.eu/LexUriServ/LexUriServ.do?uri=OJ:L:2010:122:0001:0107:EN:PDF>. [Accessed October 2019].
- [2] Sunderland P. Pressure relief devices for hydrogen vehicles. Belfast, UK: 3rd Eur Summer Sch Hydrog Safety; 2008. p. 1–29.
- [3] Brennan S, Makarov D, Molkov VV. Dynamics of flammable hydrogen-air mixture formation in an enclosure with a single vent. *Fire Explos Hazards* 2010;493–503. https://doi.org/10.3850/978-981-08-7724-8_07-04.
- [4] Li Z, Sun K. Quantified risk assessment on life and property loss from road collision vehicle fires with hydrogen-fueled tank. *Int J Green Energy* 2019;16:583–9. <https://doi.org/10.1080/15435075.2019.1598415>.
- [5] Fuster B, Houssin-Agbomson D, Jallais S, Vyazmina E, Dang-Nhu G, Bernard-Michel G, et al. Guidelines and recommendations for indoor use of fuel cells and hydrogen systems. *Int J Hydrogen Energy* 2017;42:7600–7. <https://doi.org/10.1016/j.ijhydene.2016.05.266>.
- [6] Saffers J-B, Molkov VV. Hydrogen safety engineering framework and elementary design safety tools. *Int J Hydrogen Energy* 2014;39:6268–85. <https://doi.org/10.1016/j.ijhydene.2013.06.060>.
- [7] Stockford C, Brandon N, Irvine J, Mays T, Metcalfe I, Book D, et al. H2FC SUPERGEN: an overview of the hydrogen and fuel cell research across the UK. *Int J Hydrogen Energy* 2015;40:5534–43. <https://doi.org/10.1016/j.ijhydene.2015.01.180>.
- [8] Papanikolaou EA, Venetsanos AG, Heitsch M, Baraldi D, Huser A, Pujol J, et al. HySafe SBEP-V20: numerical studies of release experiments inside a naturally ventilated residential garage. *Int J Hydrogen Energy* 2010;35:4747–57. <https://doi.org/10.1016/j.ijhydene.2010.02.020>.
- [9] Brzezińska D. Ventilation system influence on hydrogen explosion hazards in industrial lead-acid battery rooms. *Energies* 2018;11:1–11. <https://doi.org/10.3390/en11082086>.
- [10] Gupta S, Brinster J, Studer E, Tkatschenko I. Hydrogen related risks within a private garage: concentration measurements in a realistic full scale experimental facility. *Int J Hydrogen Energy* 2009;34:5902–11. <https://doi.org/10.1016/j.ijhydene.2009.03.026>.
- [11] Swain M, Grilliot E, Mn S. Risks incurred by hydrogen escaping containers and conduits. In: *Proc. 1998 U.S. DOE hydrog. Progr. Rev.*; 1998.
- [12] Swain MR, Filoso P, Grilliot ES, Swain MN. Hydrogen leakage into simple geometric enclosures. *Int J Hydrogen Energy* 2003;28:229–48. [https://doi.org/10.1016/S0360-3199\(02\)00048-4](https://doi.org/10.1016/S0360-3199(02)00048-4).
- [13] Barley CD, Gawlik K. Buoyancy-driven ventilation of hydrogen from buildings: laboratory test and model

- validation. *Int J Hydrogen Energy* 2009;34:5592–603. <https://doi.org/10.1016/j.ijhydene.2009.04.078>.
- [14] Molkov V, Shentsov V, Quintiere J. Passive ventilation of a sustained gaseous release in an enclosure with one vent. *Int J Hydrogen Energy* 2014;39:8158–68. <https://doi.org/10.1016/j.ijhydene.2014.03.069>.
- [15] Molkov V, Shentsov V. Numerical and physical requirements to simulation of gas release and dispersion in an enclosure with one vent. *Int J Hydrogen Energy* 2014;39:13328–45. <https://doi.org/10.1016/j.ijhydene.2014.06.154>.
- [16] Giannissi SG, Shentsov V, Melideo D, Cariteau B, Baraldi D, Venetsanos AG, et al. CFD benchmark on hydrogen release and dispersion in confined, naturally ventilated space with one vent. *Int J Hydrogen Energy* 2015;40:2415–29. <https://doi.org/10.1016/j.ijhydene.2014.12.013>.
- [17] Makarov D, Shentsov V, Kuznetsov M, Molkov V. Pressure peaking phenomenon: model validation against unignited release and jet fire experiments. *Int J Hydrogen Energy* 2018;43:9454–69. <https://doi.org/10.1016/j.ijhydene.2018.03.162>.
- [18] Hussein HG, Brennan S, Shentsov V, Makarov D, Molkov V. Numerical validation of pressure peaking from an ignited hydrogen release in a laboratory-scale enclosure and application to a garage scenario. *Int J Hydrogen Energy* 2018;43:17954–68. <https://doi.org/10.1016/j.ijhydene.2018.07.154>.
- [19] Brennan S, Molkov V. Pressure peaking phenomenon for indoor hydrogen releases. *Int J Hydrogen Energy* 2018;43:18530–41. <https://doi.org/10.1016/j.ijhydene.2018.08.096>.
- [20] Stephenson R. *Fire safety of hydrogen-fueled Vehicles : system-level bonfire test*. Ichs; 2005.
- [21] Crowl DA, Louvar JF. *Chemical process safety fundamentals with applications*. 3rd ed. Prentice Hall; 2011. 2011.
- [22] Shentsov V, Kuznetsov M, Molkov V. The pressure peaking phenomenon: validation for unignited releases in laboratory scale enclosure. *Int Conf Hydrog Saf* 2015;148:10.
- [23] Brennan S, Molkov V. Safety assessment of unignited hydrogen discharge from onboard storage in garages with low levels of natural ventilation. *Int J Hydrogen Energy* 2013;38:8159–66. <https://doi.org/10.1016/j.ijhydene.2012.08.036>.

Article B

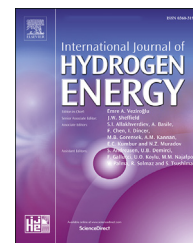
Large scale experiments and model validation of Pressure Peaking Phenomena-ignited hydrogen releases

A.W. Lach and A.V. Gaathaug

Published in International Journal of Hydrogen Energy, February 2021,
46(11): 8317-8328, doi: <https://doi.org/10.1016/j.ijhydene.2020.12.015>

Available online at www.sciencedirect.com

ScienceDirect

journal homepage: www.elsevier.com/locate/he

Large scale experiments and model validation of Pressure Peaking Phenomena-ignited hydrogen releases

Agnieszka Weronika Lach*, André Vagner Gaathaug

University of South-Eastern Norway, Kjolnes Ring 56, Porsgrunn, 3918, Norway

HIGHLIGHTS

- Large scale experimental pressure peaking phenomena.
- Constant volume with pressure and temperature measurements.
- Peak pressure was measured above 45 kPa.
- Model predicts the pressures within ± 2 kPa.
- Increasing the \dot{m}_{in,H_2} - increase p_{peak} , increasing A_{vent} - decreases p_{peak} .

ARTICLE INFO

Article history:

Received 1 October 2020
 Received in revised form
 1 December 2020
 Accepted 2 December 2020
 Available online 2 January 2021

Keywords:

Hydrogen safety
 Pressure peaking phenomena
 Model validation
 Large-scale experiments
 Ignited releases

ABSTRACT

The Pressure Peaking Phenomena (PPP) is the effect of introducing a light gas into a vented volume of denser gas. This will result in a nonequilibrium pressure as the light gas pushes the dense gas out at the vent. Large scale experiments have been performed to produce relevant evidence. The results were used to validate an analytical model. Pressure and temperature were measured inside a constant volume, while the mass flow and vent area were varied. The analytical model was based on the conservation of mass and energy. The results showed that increasing the mass flow rate, the peak pressure increases and with increasing the ventilation area, the peak pressure decreases. Peak pressure was measured above 45 kPa. Longer combustion time resulted in higher temperatures, increasing an underpressure effect. The experimental results showed agreement with the analytical model results. The model predicts the pressures within reasonable limits of ± 2 kPa. The pressure peaking phenomena could be very relevant for hydrogen applications in enclosures with limited ventilation. This could include car garages, ship hull compartments as well as compressor shielding. This work shows that the effect can be modeled and results can be used in design to reduce the consequences.

© 2020 The Author(s). Published by Elsevier Ltd on behalf of Hydrogen Energy Publications LLC. This is an open access article under the CC BY license (<http://creativecommons.org/licenses/by/4.0/>).

* Corresponding author.

E-mail addresses: agl@usn.no, lachagnie@gmail.com, AgnieszkaLach@usn.no (A.W. Lach).

<https://doi.org/10.1016/j.ijhydene.2020.12.015>

0360-3199/© 2020 The Author(s). Published by Elsevier Ltd on behalf of Hydrogen Energy Publications LLC. This is an open access article under the CC BY license (<http://creativecommons.org/licenses/by/4.0/>).

Introduction

In 2019 Norway had a total of 153 hydrogen passenger cars [1] (143 in 2018 [2]), while a total of 822 cars were in Europe in 2018 [2]. This number is expected to increase to 10–15 million in 2030 [3]. 120 large hydrogen refueling stations (HRS) were operating in Europe in 2019 and are expected to increase up to 3700 HRSs in 2030 [4]. The first hydrogen fueled ferries will be in operation in 2021 [5–7]. The safe implementation of these technologies will require regulations, codes, and standards that reflect relevant hazards. One hazard of compressed hydrogen storage is the accidental release of hydrogen. This could be a result of pipe rupture or a sudden release of a thermally-activated pressure relief device (TPRD). Different application manufacturers use different TPRD diameters, which reflects a variety of expected mass flows in the case of a leakage. It is suggested that a TPRD diameter of 0.5 mm would be inherently safe for hydrogen cars in naturally vented car parks [8]. Besides the well know hazards of explosions and fires, there is also the pressure peaking phenomena (PPP).

Pressure peaking phenomena (PPP) is the effect of introducing a light gas into a vented volume of denser gas. This will result in a nonequilibrium pressure as the light gas pushes the dense gas out at the vent. This pressure can reach destructive levels for buildings and compartments. This effect was first observed by Brennan et al. [9], as they used CFD to investigate an unignited PRD release from 350 bar through a 5.08 mm nozzle inside a 30.4 m³ volume. For unignited releases of gas, this phenomenon is only observed for gases lighter than air, and it is most relevant for hydrogen. Brennan et al. found the pressure peaking phenomena to be destructive as pressure increased above 50 kPa within 10 s, without any ignition. Brennan et al. [9–11], developed an engineering model, based on conservation of mass to estimate the pressure. Based on the engineering model, they developed nomograms for the safe design of indoor hydrogen systems. The model was validated against CFD calculations and experimental investigation [12]. Makarov et al. [12] present the engineering model validated against 19 unignited experiments [13] and 21 ignited experiments [14]. An increasing amount of brick vents resulted in lower overpressure dynamics of hydrogen jet fires (calculation methodology). The overpressures for 1 brick vent was approximately 4 times higher compared to overpressures resulted in the same conditions of mass flow rates to 4 brick vents [12]. The experimental results [13] showed that with higher mass flow rates (x5) at the same ventilation area the resulted overpressures were approximately 9 times higher. The small scale experimental setup was a 1 m³ volume with transparent walls. The hydrogen release nozzle was 5 mm and unignited mass flow rates from 0.1 to 2.8 g/s, both helium and hydrogen. The vent areas were $9.5 \cdot 10^{-5} \text{ m}^2$ and $21.3 \cdot 10^{-5} \text{ m}^2$. The ignited PPP model presented uses the unignited PPP model with a correction to the volume flow rate due to combustion and nozzle expansion. They found that the vent location did not influence the overpressure. But contradicting results are shown in Ref. [15], where the authors presented a dependency of pressure from the vent location. The vent located at the top of the volume will result in lower overpressures than in the case of the vent located at the bottom of

the volume. The fire dynamics and formation of the hydrogen cloud are presented in the work of Brennan et al. [16]. Their work investigates CFD results of hydrogen releases in 30.4 m³ volume from 700 bar tank through 3.34 mm TPRD (mass flow 299.3 g/s) with a single vent – 0.1925 m². The main focus was on the pressure increase from both ignited and unignited releases. The results shows potentially destructive hazards from the pressure rising during ignited hydrogen releases which were two order of magnitude higher than from the unignited releases. The study of Xiao et al. [14] in the laboratory scale experiments showed that the heat transfer was an important parameter in ignited hydrogen releases in confined spaces. Their work presented evidence of an underpressure effect due to heat loss.

The authors of the paper [16] pointed out the need for large scale experimental studies of ignited hydrogen releases in confined spaces. The studies on hydrogen flame behavior were missing which was highlighted by Molkov et al. [17]. The CFD study [17] revealed the effect of passive ventilation on the hydrogen jet fires in an enclosure. The flame regimes were investigated exposing dependency from the mass flow rate of hydrogen. Small flow rates showed a ventilated fire while increasing the flow rate resulted in an external fire at the vent. When the mass flow is increased and the vent area is decreased the study showed the extinction of the fire as the result. The authors of this paper performed large scale experiments for unignited releases and investigated it with an analytical model presented in Ref. [18]. The detailed experimental work and the results of both ignited and unignited hydrogen releases are presented in Ref. [19]. The analytical model for ignited releases will be presented further in this paper for the first time. The results of jet fires in the enclosure with limited ventilation area are discussed in more detail.

This work will produce large scale evidence of pressure peaking phenomena. This will be used as validation data for analytical models discussed in this paper and can be used for CFD model validation. As pointed out by Tolia et al. [20] in their CFD best practice guidelines paper: “... benchmark exercise, in which numerical models are evaluated against experiments, are necessary, in order to ensure that the numerical model reproduces the physical phenomenon with the required accuracy.”

Consequence models, such as models for PPP can be used in risk assessments [21–23]. The PPP is a relevant hazard for private parking garages and ship hull compartments [24]. It is also relevant for compressor shielding and fuel cell enclosures.

The main scientific approach in this work is experimental investigations. A constant volume chamber will be used, and the pressure and temperature inside will be measured. The mass flow in (to the chamber) will be controlled and measured and the vent area will be varied. An analytical model will be developed based on the conservation of mass and energy, coupled with a heat transfer model.

Methods

This section describes the experimental methods and setup with geometry and instrumentation. Then follows a section

with a description of the analytical model based on conservation of mass and energy. It is a zero dimensional model.

Experimental setup

Large scale experiments were performed in the 14.9 m³ explosion chamber in autumn 2019. The chamber was equipped with fuel supplies (V5 Fig. 1) and a variety of passive ventilation areas (V1–V3 Fig. 1). 1 open vent gave ventilation area $A_v = 0.0055 \text{ m}^2$, 2 open vents gave $A_v = 0.0109 \text{ m}^2$ and 3 open vents resulted in $A_v = 0.0164 \text{ m}^2$. A more detailed description of the experimental work and setup can be found in Ref. [19]. The pressure of hydrogen releases was controlled by a valve at the hydrogen bottle crate and the resulting mass flows were measured at the Coriolis-type mass flow meter. The stainless steel pipe with a 4 mm ID was used to vertically released hydrogen in the center of the explosion chambers' floor. For the ignition of the hydrogen jet, a propane pilot was mounted close to the hydrogen nozzle and controlled by a pulse generator. The hydrogen release was immediately ignited at the start of the experiment. The investigation of the pressure effect from the pilot flame shows the negligible effect.

The explosion chamber was equipped with a pressure transducer and thermocouples for transient measurements. To measure overpressures, a Kulite pressure transducer XTM-190-50A was used (Fig. 1 P1). Its accuracy was calibrated and data was logged at 25 kHz which gave measurement precision of $\sigma = 0.07 \text{ kPa}$. To measure temperature inside the chamber, four thermocouples Type K Autek-TD20H-KP were used with a measurement range $-40 \text{ }^\circ\text{C} - 1000 \text{ }^\circ\text{C}$ (Fig. 1, T1-T4). The locations of sensors are listed in Table 1. Thermocouples were mounted 6 cm from the chamber walls to exceed the boundary layer. The size of the thermocouple was 1.5 mm diameter with a shielded bead. This shield was made of Inconel.

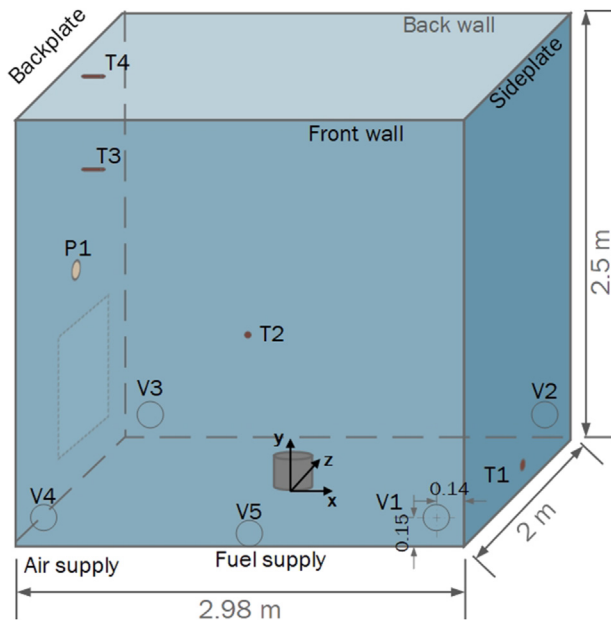


Fig. 1 – Sensor locations on the explosion chamber walls: T1–T4–thermocouples type K and P1–Kulite pressure transducer. V1–V3 passive vents.

Table 1 – Sensors and vents locations.

Sensor	X [m]	Y [m]	Z [m]
Nozzle	0.00	0.00	0.00
T1	1.43	0.04	0.00
T2	0.00	1.24	-0.94
T3	-1.43	1.78	0.00
T4	-1.43	2.38	0.00
P1	-1.49	1.25	0.00
V1 centre	1.35	0.15	-1.00
V2 centre	1.35	0.15	1.00
V3 centre	-1.35	0.15	1.00

An average volume-weighted temperature, T_{avg} , was estimated from the thermocouples. The method was chosen to compare experimental temperatures with calculated temperatures.

The uncertainties of instrumentation used in experiments are listed in Table 2.

The ventilation area was kept constant during each experiment. Several small leaks were identified during preliminary tests and sealed using different sealants. An air fan (Fig. 1. V4) was connected to the chamber to flush the hot combustion products out after the conducted experiment. The air fan was used only for the first 10 experiments. It was removed to investigate an observed underpressure effect. After each experiment, the explosion chamber was dried to remove the accumulated liquid water. Drying was done with a fan or additional manual water removal.

All experiments were controlled by a pre-programmed pulse generator. This was done to ensure equal conditions for all the experiments as well as for safety precautions.

Analytical model

The analytical model for pressure peaking phenomena is based on a mass and energy balance of a constant volume open system. It is assumed no condensation effects and all species are in a gaseous state. A perfect mix assumption is used, as it is shown in Ref. [18] to be reasonable for unignited releases.

The mass balance for each species in the volume is described with the system of Eqs. (1)–(6). The number of moles in the volume n_{tot} is a sum of the number of moles of each species in the volume $n_{tot} = \sum n_i$:

$$\frac{dn_{H_2}}{dt} = \dot{n}_{in,H_2} - \dot{n}_{out,H_2} + \dot{n}_{rx,H_2} \quad (1)$$

$$\frac{dn_{O_2}}{dt} = \dot{n}_{in,O_2} - \dot{n}_{out,O_2} + \dot{n}_{rx,O_2} \quad (2)$$

$$\frac{dn_{N_2}}{dt} = \dot{n}_{in,N_2} - \dot{n}_{out,N_2} + \dot{n}_{rx,N_2} \quad (3)$$

Table 2 – Uncertainties of instrumentations.

Pressure sensor	±1% FSO BFSL 250 point (0.025 s) filter	±3.5 kPa ±0.07 kPa
Mass flow sensor	±0.5% of flow rate	
Thermocouples type K	±max(2.2 C, 0.75%)	2.2°C to 4.5°C

$$\frac{dn_{H_2O}}{dt} = \dot{n}_{in,H_2O} - \dot{n}_{out,H_2O} + \dot{n}_{rx,H_2O} \quad (4)$$

Given the initial conditions (at $t = 0$) $n_{H_2,0} = 0$, $n_{O_2,0} = 0.21 \cdot n_{tot,0}$, $n_{N_2,0} = 0.79 \cdot n_{tot,0}$, $n_{H_2O,0} = 0$ and $n_{tot,0} = p_0 \cdot \frac{V}{RT_0}$.

The molar flow into the system is given at the nozzle and the vent. Only hydrogen flows at the nozzle. It can be fixed to a value or taken from experimental measurements. The air can flow into the system (through the vents) when the pressure inside is lower than the outside pressure ($\Delta p < 0.001$ Pa).

The total molar flow in \dot{n}_{in} at the vent, is given by Eq. (5)

$$\dot{n}_{in} = \frac{C \cdot A}{M_{air}} \sqrt{2 \cdot \Delta p \cdot \rho_{air}} \quad (5)$$

And then $\dot{n}_{in,H_2} = 0$, $\dot{n}_{in,O_2} = 0.21 \cdot \dot{n}_{in}$ and $\dot{n}_{in,N_2} = 0.79 \cdot \dot{n}_{in}$ and $\dot{n}_{in,H_2O} = 0$.

Where M_{air} is the molecular mass of air and ρ_{air} is the density of air outside. A is the vent cross-section area. The C is the discharge coefficient of the vent and represents the energy loss of the flow. It is a geometrical specific value (assumed to be independent of the flow) and has to be given for each particular setup. The C is also uncertain in the model and is estimated based on the experimental results [25,26].

Eq. (6) based on a steady-state incompressible energy equation gives the molar flow out $\dot{n}_{out,tot}$.

$$\dot{n}_{out,tot} = C \cdot A \sqrt{\frac{2 \cdot \Delta p \cdot n_{tot}}{V \cdot M_{en}}} \quad (6)$$

where $n_{tot} = \sum_i n_i$ is the number of moles in the volume, the molecular mass in the volume is then $M_{en} = \sum_i X_i M_i$ where $X_i = n_i/n_{tot}$ and $\dot{n}_{out,i} = X_i \cdot \dot{n}_{out,tot}$ can be calculated.

In the calculations, the stoichiometric hydrogen combustion was assumed. By balancing the combustion reaction equation, to burn all hydrogen $\dot{n}_{rx,H_2} = -\dot{n}_{in,H_2}$ the oxygen needed will be: $\dot{n}_{rx,O_2} = 0.5 \cdot \dot{n}_{rx,H_2}$. The produced water vapor then will be $\dot{n}_{rx,H_2O} = -\dot{n}_{rx,H_2}$, and $\dot{n}_{rx,N_2} = 0$.

To calculate the pressure in the volume (10) the temperature has to be solved first. The internal energy U_{en} (neglecting mechanical energy) for the system is equal to:

$$\frac{dU_{en}}{dt} = \dot{H}_{in} - \dot{H}_{out} + \dot{Q}_{rx} - \dot{Q}_{loss} \quad (7)$$

Giving $T_{ref} = 298.15$ K and $c_{v,i}$ as the molar heat capacity in a constant volume. Changing the energy balance into the temperature equation result in:

$$\frac{dT_{en}}{dt} = \frac{1}{\sum_i n_i c_{v,i}} \left(\dot{H}_{in} - \dot{H}_{out} + \dot{Q}_{rx} - \dot{Q}_{loss} - (T_{en} - T_{ref}) \cdot \sum_i c_{v,i} \frac{dn_i}{dt} \right) \quad (8)$$

The $\dot{H}_{in} = \sum \dot{n}_{in,i} \hat{H}_i$ is the sum of enthalpies of each species calculated at $\hat{T} = T_{in}$. Using a perfect mixing assumption the enthalpy out of the volume is the sum of enthalpies: $\dot{H}_{out} = \sum_i \dot{n}_{out,i} \cdot \hat{H}_i$ at $T_{out} = T_{en}$. The $c_{v,i}$ was calculated with NASA polynomials [27]. The \dot{Q}_{rx} is the heat of formation. Since the

water vapor is the only product $\dot{Q}_{rx} = \dot{Q}_{rx,H_2O} = \dot{n}_{rx,H_2O} \cdot (-\Delta \hat{H}_{f,H_2O})$ where the \hat{H}_{f,H_2O} is the enthalpy of formation of water vapor.

The \dot{Q}_{loss} is the heat loss calculated with the major assumption of a simple heat transfer: $\dot{Q}_{loss} = h_{loss} \cdot A_{wall} \cdot (T_{en} - T_{wall})$ where A_{wall} is the surface area inside the volume and h_{loss} is the heat transfer coefficient. When the pressure inside the volume will be lower than ambient pressure $\Delta p < 0.001$ the air flows into the system ($T_{en} > T_{outside}$) and the heat transfer coefficient is assumed to be $h_{loss,2} = 0.5 \cdot h_{loss}$. The h_{loss} is uncertain in the model, it depends on the setup material, its geometrics, and most likely the water condensation.

The change of the number of moles in the system causes temperature change, expressed in Eq. (8) with $\left((T_{en} - T_{ref}) \cdot \sum_i c_{v,i} \frac{dn_i}{dt} \right)$. The temperature of the wall T_{wall} , was calculated with the major assumption that the whole wall is one thermal mass with the same temperature inside (i.e. no temperature gradient in the wall):

$$\frac{dT_{wall}}{dt} = \frac{\dot{Q}_{loss}}{m_{wall} \cdot C_{steel}} \quad (9)$$

where m_{wall} is the mass of walls and C_{steel} is the heat capacity of the wall.

Solving the PPP model of state-space Eqs. (1)–(4), (8), (9) gives the pressure inside the volume from ideal gas law (10):

$$p_{en} = \frac{n_{tot} \cdot R \cdot T_{en}}{V} \quad (10)$$

A variable time step Runge-Kutta method (MATLAB ode45) was used to solve the system of equations [28].

When comparing the experimental and predicted (analytical model) pressures, the hydrogen inflow in the model is given by $\dot{n}_{in,H_2} = \dot{m}_{in}/M_{H_2}$. The hydrogen mass flow \dot{m}_{in} was the transient mass flow from the experiments. The pressure inside the enclosure is compared to the analytical model prediction of the constant volume.

Results

Experimental results

Table 3 gives the list of setup parameters and experimental results from all 31 experiments. The initial temperature in the enclosure is measured with T_{avg} at t_0 . The hydrogen release time is the duration of the open valve control signal equal to hydrogen burning time. The open vents number refers to how many vents were open during the experiment (the passive ventilation area). The pressure regulator valve was used to set up a desired mass flow rate (MFR), measured with the coriolis mass flow meter. The mass flows were almost constant during the experiments. The experimental overpressures given in Table 3 are the values of the pressure peak, the maximum value. The experimental underpressure analogically is the negative pressure peak, the maximum negative value (the pressures presented in Table 3 are the gauge pressures). The temperatures are measured in Celcius at the positions given in

Table 3 – Results from experiments and analytical model: 31 test of H₂ releases through 4 mm nozzle with different MFR and ventilation area: 1 open vent = 0.0055 m², 2 vent open = 0.0109 m², 3 vents open = 0.0164 m².

Setup					Measured							Calculated		
Exp nr	T ₀ in enclosure (K)	H ₂ release Time (s)	Open Vents	Mass flow Rate (g/s)	Exp Over Pressure (kPa)	Exp Under pressure (kPa)	Temp (°C)					Calc Over Pressure (kPa)	Calc Under Pressure (kPa)	Temp (°C)
							T1	T2	T3	T4	T _{avg}			
1	281	5.0 ^a	1	1.45	4.8	-0.1	9	45	86	85	58	4.96	-0.4	80
2	282	10.0 ^a	1	1.37	4.5	-0.3	14	81	128	125	93	4.54	-0.8	109
3	283	5.0 ^a	1	3.38	16.7	-0.6	69	119	171	164	129	15.69	-1.6	185
4	285	10.0 ^a	1	3.15	15.8	-2.8	141	175	251	225	195	14.30	-2.8	248
5	288	10.0 ^a	2	3.14	5.3	-1.1	93	175	270	230	199	6.14	-1.1	261
6	288	10.0 ^a	2	3.04	5.0	-1.1	86	176	258	223	192	5.92	-1.0	252
7	276	6.0 ^a	2	7.90	22.0	-2.5	166	209	353	319	260	21.83	-3.0	500
8	277	6.0 ^a	2	7.50	20.6	-2.3	142	207	348	287	250	20.28	-2.8	474
9	279	6.0 ^a	3	8.37	13.9	-2.9	194	242	403	345	297	14.3	-1.8	566
10	279	6.0 ^a	3	8.35	13.7	-2.8	192	243	389	332	292	14.26	-1.8	566
11	280	7.5	3	8.63	14.7	-3.3	204	249	416	358	305	14.87	-2.0	610
12	282	6.0	3	8.90	15.1	-2.3	176	215	372	322	268	15.26	-1.7	545
13	281	6.0	3	11.72	21.7	-4.3	244	288	458	408	345	21.48	-2.4	739
14	277	6.0	3	11.37	21.1	-3.8	241	274	430	352	324	21.04	-2.3	701
15	277	6.0	3	4.00	4.3	-0.5	40	129	202	194	147	5.22	-0.5	222
16	277	6.0	3	4.07	4.5	-0.5	45	130	209	190	148	5.39	-0.5	227
17	278	6.0	2	11.52	33.3 ^b	-3.2	211	263	415	367	317	33.06	-3.8	661
18	278	6.0	2	11.47	33.0	-3.4	205	267	414	367	316	32.79	-3.8	664
19	278	6.0	1	8.62	48.1	-5.7	194	205	359	300	254	45.75	-4.9	438
20	278	7.5	1	8.50	46.5	-8.2	243	247	383	332	295	45.27	-5.9	505
21	280	6.0	2	8.52	23.7	-2.0	166	223	333	294	256	23.36	-2.7	483
22	280	6.0	2	2.60	4.1	-0.3	12	98	142	139	104	4.87	-0.4	142
23	279	15.0	2	2.36	3.5	-1.1	87	174	275	238	194	4.29	-1.0	212
24	280	25.0	3	2.38	1.8	-1.0	195	240	368	331	286	2.33	-0.6	248
25	278	25.0	3	3.87	4.1	-2.2	315	339	481	435	395	4.99	-1.1	403
26	282	20.0	3	6.70	10.1	-4.6	384	467	603	568	520	10.80	-1.9	677
27	281	10.0	3	6.65	9.9	-2.7	213	259	433	391	320	10.65	-1.7	543
28	282	10.0	2	6.56	16.8	-3.5	219	247	419	369	314	17.22	-3.0	519
29	281	20.0	2	6.55	16.7	-8.7	375	474	578	531	496	17.40	-3.5	659
30	283	10.0	1	6.65	35.9	-14.1	246	259	392	349	305	34.48	-6.1	483
31	282	20.0	1	6.56	35.3	-25.3	366	444	556	522	477	34.44	-8.6	647

^a The air fan was used after hydrogen release (duration time).

^b pressure sensor signal saturation. Real pressure assumed to be higher.

section [Experimental setup](#) representing the maximum measured values. The maximum average volume-weighted temperature (T_{avg}) is given for each experiment as well.

The times of the positive and negative peaks of pressure are listed in [Table 4](#). Both measured and calculated results are given.

Pressure results

The overpressure results from the experiments are shown in [Fig. 2](#). The left column shows overpressures and the right column the temperatures. In the first row the exp 4, exp 5, and exp 25 are presented. The middle row shows exp 19, exp 21, and exp 11, and the bottom row exp 18 and exp 14. Each subfigure has approximately the same MFR. Each line in the subfigure represents the overpressure from experiments with 1 (red), 2 (black), or 3 (blue) open vents. For the first two MFR (the top and the middle subfigure) experiments were performed for all three vent configurations. Experiment 19 (middle plot, red line, MFR = 8.62 g/s, one open vent) resulted in overpressure over 45 kPa. Due to safety measures, the

hydrogen releases with MFR~11.4 g/s were done only with 2 and 3 open vents.

The last 6 experiments (Exp 25–31) were devoted to the investigation of an observed underpressure effect. All 6 experiments had approximately equal MFR~6.6 g/s. The time of hydrogen release (hydrogen burning time) was set up on 10 s (dashed line) and 20 s (solid line) for each ventilation area red- 1 open vent, black- 2 open vents, and blue- 3 open vents. The measured temperatures at $t = 10$ s and $t = 20$ s are marked at the plot with respective colors to the open vent number.

The temperature from each thermocouple, listed in [Table 3](#), shows the maximum measured temperature at each position. The location of thermocouple 1 (T1) and thermocouple 4 (T4) were located close to the corners of the explosion chamber (see [Fig. 1](#)) and show lower values than thermocouples located in the middle of the wall/backplate. Typically T3 (position 0.72 m from the ceiling) shows higher temperatures than T4 (0.12 m from the ceiling). [Fig. 2](#) shows the experimental temperatures. When the hydrogen release time is kept the same, the maximum temperatures are equal (first row: 1 and 2 vents open, second row: 1 and 2 vents open, third row: 2

Table 4 – The time of maximum pressure (positive pressure peak) and minimum pressure (negative peak): experimental and calculated.

Exp nr	\dot{m} (g/s)	A_v Open vents	$t_{p(max)exp}$ (s)	$t_{p(max)calc}$ (s)	$t_{p(min)exp}$ (s)	$t_{p(min)calc}$ (s)
1	1.45	1	5.9	5.6	10.6	12.6
2	1.37	1	5.8	5.5	15.4	17.1
3	3.38	1	6.5	5.9	13.5	13.6
4	3.15	1	6.7	5.9	21.0	18.2
19	8.62	1	5.2	5.6	18.6	14.0
20	8.50	1	5.3	5.6	19.1	15.5
30	6.65	1	5.7	5.6	21.7	17.2
31	6.56	1	5.4	5.6	27.5	26.2
5	3.14	2	3.4	4.0	14.1	15.5
6	3.04	2	3.7	4.1	14.0	15.5
7	7.90	2	3.6	4.1	10.9	12.0
8	7.50	2	3.5	4.1	10.7	12.0
17	11.52	2	3.1	3.8	10.0	10.9
18	11.47	2	3.2	3.8	9.8	11.0
21	8.52	2	3.2	3.8	9.6	10.8
22	2.60	2	2.7	3.7	8.6	10.1
23	2.36	2	2.5	3.6	17.5	18.0
28	6.56	2	3.2	3.9	13.2	14.3
29	6.55	2	3.4	3.8	24.4	24.1
9	8.37	3	2.7	3.4	10.2	11.0
10	8.35	3	2.6	3.4	10.2	11.2
11	8.63	3	2.4	3.2	10.5	11.1
12	8.90	3	2.3	3.1	8.7	9.7
13	11.72	3	2.3	3.1	9.0	9.7
14	11.37	3	2.3	3.2	9.0	9.8
15	4.00	3	2.4	3.1	8.2	9.5
16	4.07	3	2.2	3.1	8.2	9.6
24	2.38	3	1.5	3.0	27.3	27.9
25	3.87	3	2.0	3.1	27.8	28.2
26	6.70	3	2.5	3.2	23.0	23.3
27	6.65	3	2.5	3.2	12.9	13.5

and 3 vents open). Longer hydrogen release time gives a higher maximum temperature when comparing similar mass flow rates.

Analytical model results

The results from the analytical model are listed in Table 3. Calculations were done with the boundary condition of the molar flow in: \dot{n}_{in,H_2} , calculated from the experimentally measured mass flow. The initial temperature was set equal to the experimentally measured average volume-weighted temperature at time $t = 0$ s.

The calculated pressures represent the maximum positive and negative value for each experiment. The calculated temperature gives the maximum temperature in the system. Fig. 4 presents the calculated results for conditions equal to the experiments showed in Fig. 2. The colors were chosen accordingly to the number of open vents, as presented before.

The maximum temperature calculated for each experimental condition is listed in Table 3. It is the constant-volume temperature of the system. The right column in Fig. 4 shows the calculated temperatures for the chosen experimental conditions (the same as Fig. 2). The calculated temperatures showed the same maximum values while the hydrogen

release time was equal (for similar MFR). Longer release time resulted in higher temperatures when comparing similar mass flow rates.

Analysis and discussion

The presented experimental results from 31 tests were used to validate the analytical model of pressure peaking phenomena for ignited hydrogen releases.

The experimental results were produced in fall 2019 in south Norway, where temperatures are stable ~ 10 °C. When hydrogen burns inside the volume (jet fire) the pressure and temperature increase. The jet fires are considered to be limited-ventilated fires as the complete hydrogen combustion leads to oxygen depletion in the volume. This may result in the self-extinction of the flame as the H_2 -air mixture inside the enclosure is beyond the flammability limits [14]. This was not observed in these experiments.

Initially, the volume consists of air. When the experiments start the oxygen reacts with hydrogen and produce water vapor. The mole fractions in the volume are changing, this can be seen in Fig. 5. The figure shows the results from the calculation of conditions equal to exp 26. The hydrogen mole fraction is 0 due to complete combustion and stopping the experiment before all the oxygen was consumed. The figure also shows the mole fraction of water increasing until the combustion stops, then the air flows into the volume.

By looking only at stoichiometric products, the pressure should decrease (3.38 mol $H_2/O_2/N_2$ to 1.88 mol H_2O/N_2). But the temperatures increases due to the combustion of hydrogen which increases the pressure. The combustion products are also lighter than air and this is the main reason for the observed pressure peak. A light gas is produced inside the volume, but a denser gas (mostly air) flows out at the vent. The mass flow out is given by the density at the vent (Eq. (6)), which is relatively higher than the density of the combustion products. This effect of a lighter gas pushing the denser gas is the reason for the transient pressure rise known as the pressure peaking phenomena. This effect is previously observed in the numerical work of [9–13,15–17] and small scale experiments [12–14]. The previous study by the authors of the large scale set up reported results for unignited pressure peaking phenomena [18]. All previous work confirmed the same result of overpressure.

Both experimental and calculated pressure results showed a dependency on mass flow rate (MFR) and ventilation area (A_v), similar to results in Refs. [12,13]. By comparing experiment 4 (1 open vent) with experiment 25 (3 open vents), first row in Fig. 2 (approximately the same MFR), it is shown that the overpressure increases 4 times while the vent area decreases 3 times. For higher MFR that difference is slightly less-3 times lower overpressure (second row in Fig. 2). While comparing overpressures resulted from different MFR but at the same A_v (exp 5, exp 21 and exp 18- black line Fig. 2) the significant, visible growth can be observed. The overpressure is 6 times larger for 3.5 higher MFR with 2 open vents. This relation is presented in Fig. 6 for all 31 experiments. Increasing the mass flow rates results in higher overpressures (at the same ventilation area) while increasing ventilation area

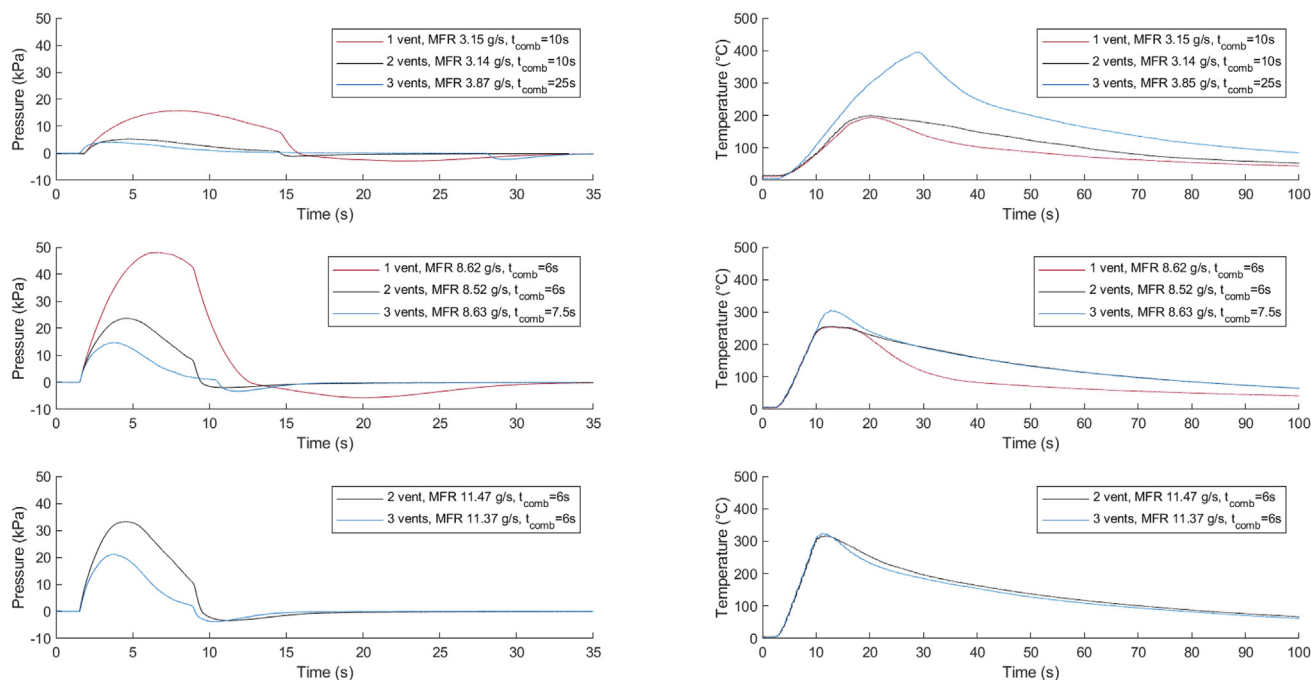


Fig. 2 – The overpressure and temperature results from experiments with approximately equal MFR: top ~3.5 g/s, middle ~8.6 g/s, and bottom ~11.4 g/s for different ventilation areas (red, black, and blue lines). (For interpretation of the references to color in this figure legend, the reader is referred to the Web version of this article.)

results in lower overpressures (at the same mass flow rates) (Figs. 2 and 4). The relation is shown in the analytical model as well (Fig. 6). It is due to increased molar flow out at the vent (Eq. (6)). The resulted experimental overpressures could be lower if the location of the vent will be placed at the top of the explosion chamber, according to Ref. [15].

Experimental results showed expected values based on previous studies on PPP. The ignited hydrogen releases result in higher overpressures compare to unignited [18]. Overpressure results from ignited and unignited releases, at approximately the same MFR, showed almost 4 times higher overpressure while the ventilation area was 9 times larger (Fig. 7). The results

showed higher hazards of enclosure collapse for ignited releases when the ventilation area is not large enough. This is also shown in the study by Brennan et al. [16].

The pressure peak occurs 73.3 s faster for ignited releases than unignited when comparing two almost equal mass flow rates and volume, see Fig. 7. For ignited releases, the pressure peak occurs in the first few seconds (Table 4). With increasing the ventilation area the pressure peak is reached in a shorter time: below 3 s for experiments with all 3 open vents, below 4 s for 2 open vents and below 7 s for one open vent (Table 4). This is the same as the unignited PPP results.

When comparing the time of pressure peak with the mass flow rate, one can observe that increasing the MFR results in an earlier pressure peak. This is contradicting the unignited PPP results (when comparing similar MFR) but in line with the analytical model calculations. The unignited PPP could observe a similar time-MFR effect only for very high mass flow rates, as shown in Ref. [18].

In real hydrogen applications, the MFR is given by the pipe or TPRD diameters and reservoir pressure. In such applications, one must consider the maximum expected hydrogen releases together with a proper design of the ventilation area. These results show the importance of such design, and the analytical model can be used in the design for overpressure predictions.

The temperature results are given in Table 3. They are not compared to other experimental results as the only relevant literature [14] (to the knowledge of the authors) does not present any comparable experimental setup. The paper by Makarov et al. [12] presents a model without an explicit energy balance, hence the temperature effect, as well as heat transfer, is thus neglected. When comparing the experimental

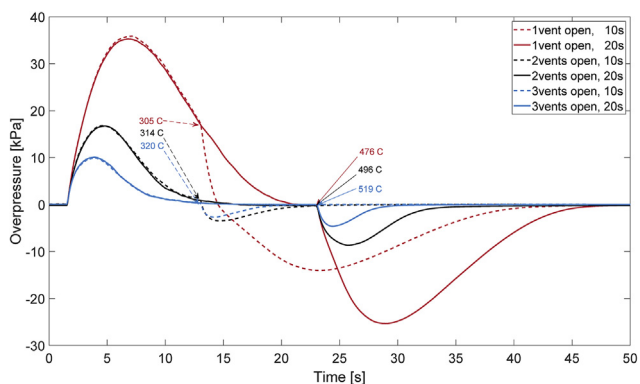


Fig. 3 – Overpressures in the 14.9 m³ enclosure during hydrogen releases of 10s and 20s in three different ventilation area at the same MFR~6.6 g/s, 1 open vent = 0.0055 m², 2 vent open = 0.0109 m², 3 vents open = 0.0164 m².

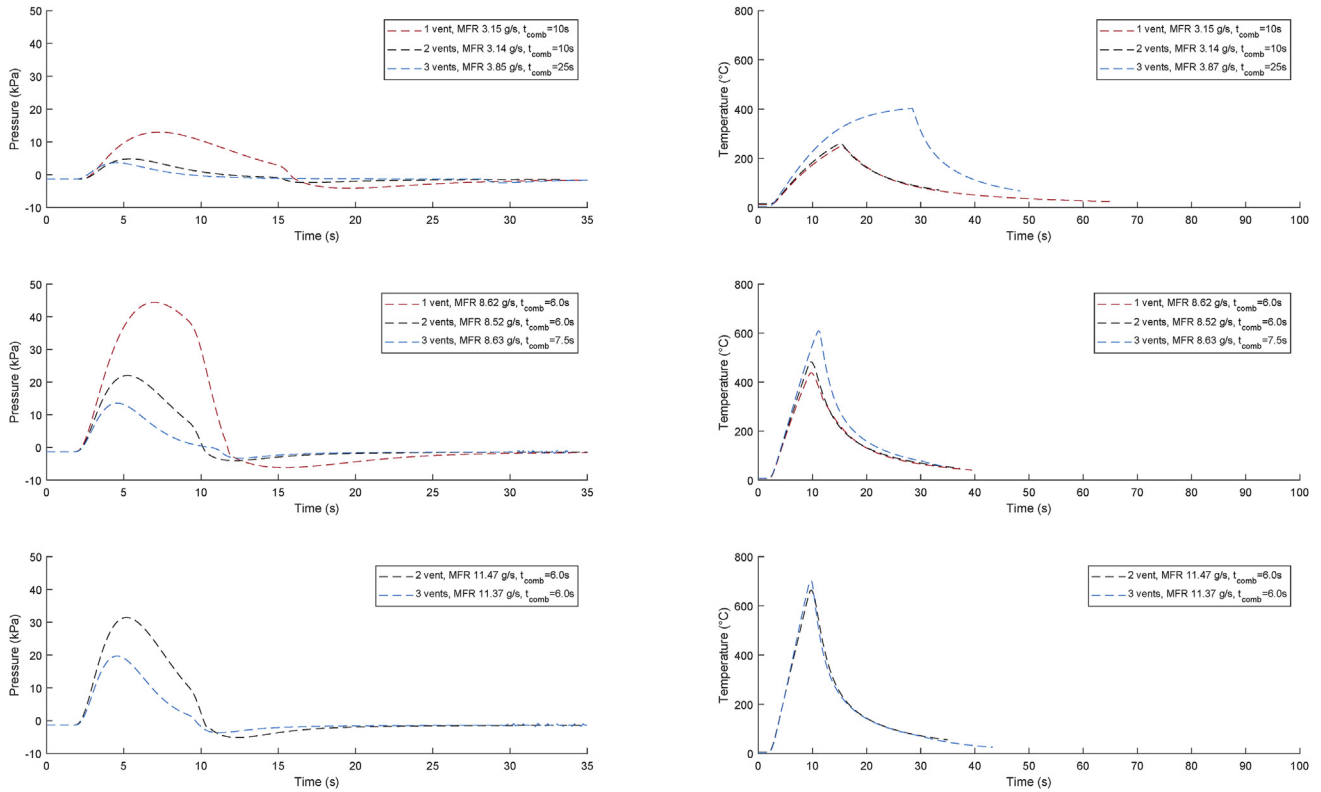


Fig. 4 – The overpressure and temperature results from the analytical model with approximately equal MFR: top ~3.5 g/s, middle ~8.6 g/s, and bottom ~11.4 g/s for different ventilation areas.

temperature data to the analytical model calculations (in this work), the volume average temperature is used. The data shows that the measured temperature results are between 10 and 385 °C lower predicted results. The reason for this discrepancy is speculated to be due to the heat transfer between the gas and the thermocouple. This will affect the thermal response time of the thermocouple. One method to compensate the heat loss at the thermocouples was presented by Zhao and Zhang [29] where they developed an inverse problem approach to correct the conductive heat transfer at the bead of the thermocouple. They do not include the convective heat transfer, important in this work. Liu et al. [30] applied a model with conduction, convection and radiation heat transfer into the thermocouple model. The convective

heat transfer is based on a Nusselt number approach, which is not possible in this study due to unknown velocities inside the system. To compensate the discrepancy from the thermocouples one can apply a correction algorithm based on the time constant of the system [31]. The thermocouples do not measure temperature in the surrounding gas. The measured temperature at the thermocouple's bead is a result of a heat transfer: conduction, convection and radiation at the bead and shielding. Then the dynamic errors of the signal have to be solved. The response time is dependent on the thermocouple bead diameter. That is why the measured temperature are time-average temperatures [31].

Another reason for the temperature difference between measured and predicted by the model is due to the condensation of water on the steel walls of the explosion chamber. This condensation affects heat transfer through the walls as it increases heat transfer. The condensation was observed after the experiments, like droplets on the walls and water on the floor. Residual liquid water inside the chamber would also influence the temperature as it would evaporate inside during the experiments. The phase transition of water was not included in the analytical model, while the experimental results suggest that this should be improved in further work on ignited pressure peaking phenomena. Due to the mentioned considerations, the temperature profiles are not compared with each other. The focus was based on the relation among the experiments (measured and predicted) and further analysis will include the relations only.

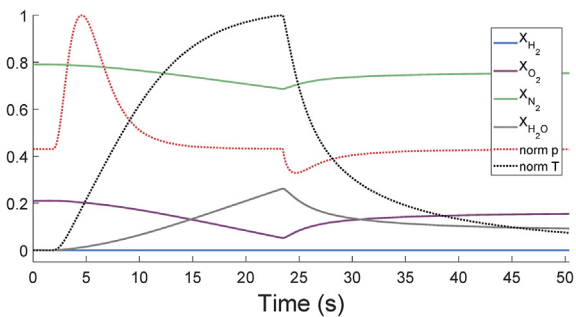


Fig. 5 – Analytical results of exp 26. Mole fractions and normalized pressure and temperature.

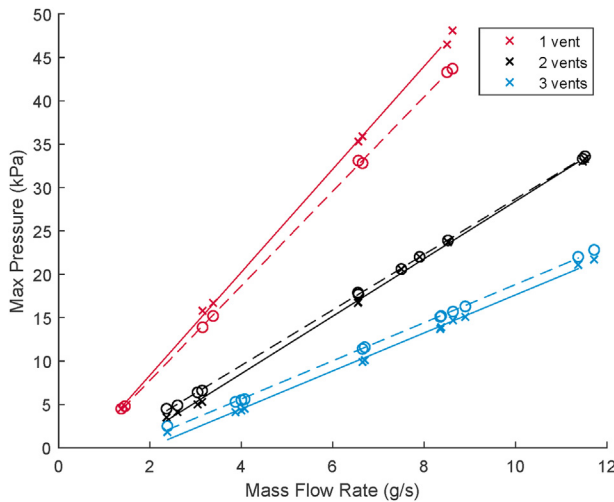


Fig. 6 – Overpressure dynamics: the relation between MFR and number of vents open- 31 experiments. Solid line-experimental result, dash line-calculated result.

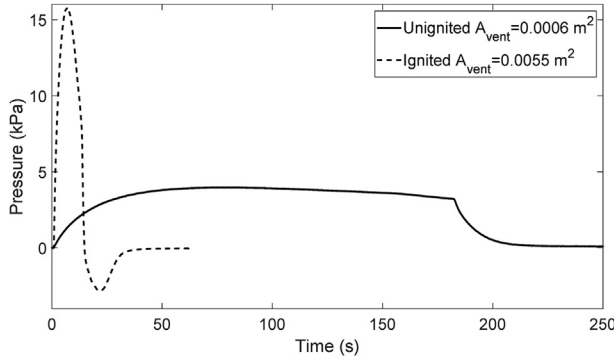


Fig. 7 – Pressure peaking phenomena for unignited ([18], exp 7), and ignited releases (exp 4) with $\dot{m} \sim 3.1$ g/s through a 4 mm nozzle.

Fig. 2 shows that for 1 and 2 open vents (1st row) the maximum pressure differs while the maximum temperature is the same. The exp 25, with 3 open vents in the 1st row, showed higher temperature. It was due to 25 s of combustion time compare to 10 s combustion time for two other experiments with the same MFR. The temperature increased 200C during 15 s. The same results can be observed in the 2nd row when the combustion time changes. The experiment with 3 open vents was performed 1.5 s longer (combustion time) than the two other experiments with similar MFR. The change in the temperature is shown. For the shorter time of change in combustion 1.5 s the temperature increased 50C. One can compare experiments with the same combustion time but with different MFR (experiment 21 blackline 2nd row and experiment 18 blackline 3rd row). The temperature increased 60C for higher MFR. The experimental results show that the temperature increase as the mass flow rate increase and/or the hydrogen burning time increases. This is as expected as both will increase the total energy released from combustion. The temperature is not

significantly influenced by the vent area, this is seen in both experimental (Fig. 2) and analytical results (Fig. 4). While comparing temperature profiles: measured and predicted, the higher temperature difference between measured and calculated temperatures were observed with increasing the MFR. Fig. 8 shows the relation between maximum average-volume weighted temperature and the total mass of hydrogen burned. It can be seen that the maximum temperature is independent of the vent area. The pressure peak occurs earlier than the maximum temperature as they are dependant on separate factors. The overpressure depends on temperature, MFR, and A_v , while the maximum temperature depends on the total mass of hydrogen burned ($\int \dot{m}_{in,H_2} dt$). The pressure is given by the temperature, but as the peak pressure occurs early, the model is still capable of predicting it accurately.

The underpressure effects observed in the experiments are mostly dependant on the temperature inside the chamber and the vent area. This suggests that the heat transfer through the walls is the most prominent factor in the effect. The experiments by Makarov et al. [12] showed a significant underpressure, but it was not mentioned by the authors. It was investigated simultaneously by Xiao et al. [14] based on detailed numerical models for the heat loss to the walls and mass loss due to condensation. As the hot gas inside the chamber is cooled by the walls, the pressure inside decreases. The vent area affects the mass flow of air into the chamber from the outside. This is seen in the experimental results in Fig. 3 as the peak pressure is equal for long and short hydrogen burning time, while the underpressure is significantly different. The same discrepancy between experimental and calculated temperatures are also found in the results of underpressures, showing that the underpressure is also dependant on the total mass of hydrogen burned ($\int \dot{m}_{in,H_2} dt$). Following this reasoning, the heat transfer through the wall will then be an important parameter to the underpressure effect.

Model validation

The main unknown parameters in the analytical model are the discharge coefficient, C , and the heat loss coefficient, h_{loss} . The first mainly affects \dot{n}_{out} and the latter the underpressure. Both coefficients were analyzed with a Bayesian approach [25] resulting in $C = 0.9$ and $h_{loss} = 30 \text{ W/m}^2\text{K}$ as the best fit to all the experimental results. The parameters are kept constant for all calculations. The coefficients affect each other and must be estimated together. The uncertainty of the chosen parameters results in $\delta p_{\pm peak} = 0.06 \text{ kPa}$. The work by Ref. [12] showed that the best fit of the discharge coefficient was $C = 0.72$ for unignited releases and for ignited releases $C = 0.68$ to $C = 0.79$. This was also related to a problem with leakage during the experiments. The assumption of the simple heat transfer represents the heat loss to the walls only. The cooling effect from the continuous release of hydrogen, mentioned in numerical studies in Ref. [17] is not included in the model (in this work). The detailed CFD simulations by Hussein et al. [15] showed that the main heat transfer mechanism in laboratory-scale experiments was radiation. It is also suggested by Xiao [14], in the detailed CFD study, together with the effect of water

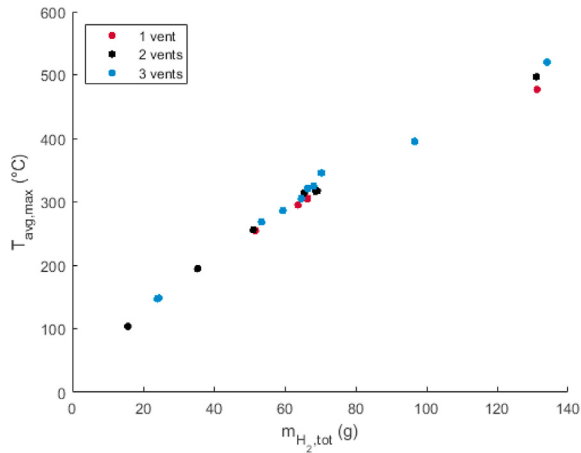


Fig. 8 – The relation between maximum average volume-weighted temperature and the total burned mass of hydrogen.

condensation. This is not included in the model presented in this paper.

The experimental pressure results are in good agreement with the analytical model results within limits of ± 2 kPa. This is shown in Fig. 9 (dashed line, left, and middle). For the positive pressure peak, the average difference between experimental and analytical model results is 0.3 kPa and 0.35 kPa for the negative pressure peak (without exp 28–31). The times of positive pressure peaks were calculated in ~ 1 s later time for experiments with 2 and 3 open vents, and ~ 1 s faster for experiments with 1 open vent. This can be seen in Table 4. The results of the negative pressure peaks for exp 1–27 showed good agreement within ± 2 kPa. The last 4 experiments were affected by accumulated condensed water during experiments, which resulted in significant discrepancies. The temperatures are given with ± 100 K. The measured temperature results are not accurately predicted with the numerical model. As discussed earlier, this is partly due to the heat transfer to the thermocouples.

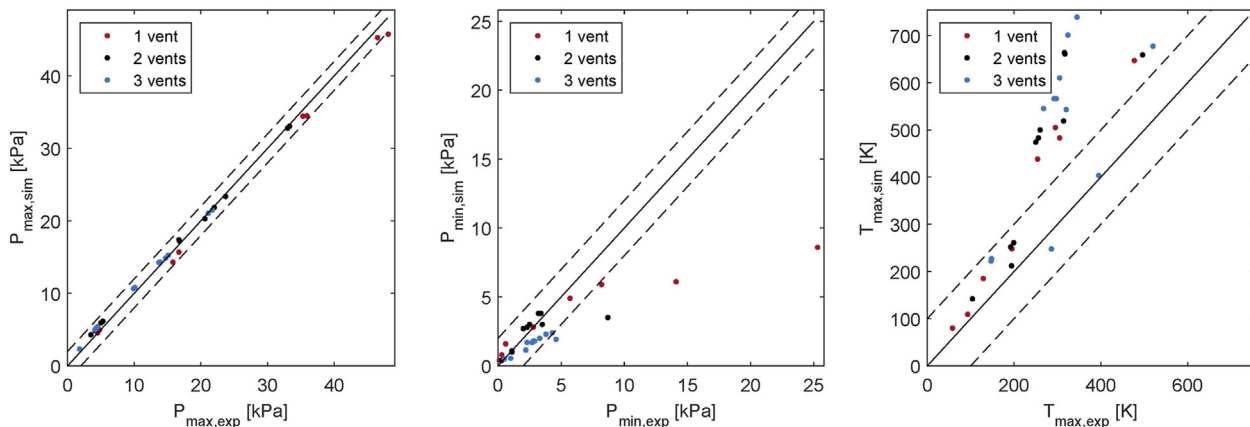


Fig. 9 – Comparison of experimental results and analytical model calculations from 31 experiments: left-positive pressure peak, middle-negative pressure peak, right-maximum temperature.

Conclusion

The large scale experiments (14.9 m^3) of ignited hydrogen releases were performed for the first time and were used to validate an analytical model of Pressure Peaking Phenomena (PPP). The experimental results confirmed that with increasing the mass flow rate, the peak pressure increases, and with increasing the ventilation area, the peak pressure decreases. The large scale experiments revealed an underpressure phenomenon. This was dependent on the total energy released from the combustion of hydrogen. Longer combustion time resulted in higher temperatures, increasing the underpressure effect. Hence it is the heat transfer through the walls that leads to the underpressure.

The overpressure peak occurs within the first few seconds of the experiments. When increasing the mass flow rate of hydrogen, the time of the pressure peak decreases. This is contradicting the experimental results of the unignited pressure peaking phenomenon (at similar flow rates).

The experimental results showed agreement with the analytical model results. The model predicts the pressures within reasonable limits of ± 2 kPa. The temperature is not well predicted. This is discussed in the paper, as it is a result of a simple assumption of heat transfer and no water condensation. The physical size and shielding of the type K-thermocouple also influence the temperature results.

In this work the main parameters of the analytical model have been estimated to be $C = 0.9$ (discharge coefficient) and $h_{\text{loss}} = 30 \text{ W/m}^2\text{K}$ (heat transfer coefficient). These parameters are geometry and material dependant and should be assessed for each application.

The pressure peaking phenomena could be very relevant for hydrogen applications in enclosures with limited ventilation. This could include car garages, ship hull compartments as well as compressor shielding. This work shows that the effect can be modeled and results can be used in design to reduce the consequences.

Declaration of competing interest

The authors declare that they have no known competing financial interests or personal relationships that could have appeared to influence the work reported in this paper.

Acknowledgments

The authors wish to thank Knut Ove Hauge for valuable support in conducting the experimental work.

The authors wish to acknowledge funding from the Fuel Cells and Hydrogen 2 Joint Undertaking (JU) under grant agreement No 826193. The JU receives support from the European Union's Horizon 2020 research and innovation programme and United Kingdom. Germany. Greece. Denmark. Spain. Italy. Netherlands. Belgium. France. Norway. Switzerland.

This work was performed within MoZEES, a Norwegian Centre for Environment-friendly Energy Research (FME), co-sponsored by the Research Council of Norway (project number 257653) and 40 partners from research, industry, and the public sector.

REFERENCES

- [1] Statistics Norway. Statistikkbanken; 2020. <https://www.ssb.no/statbank/table/11823/tableViewLayout1/>. [Accessed 10 September 2020].
- [2] Eurostat. Passenger cars, by type of motor energy. 2020. <https://appsso.eurostat.ec.europa.eu/nui/submitViewTableAction.do>.
- [3] SINTEF, IFPEN. Hydrogen for Europe - final report of the pre-study. 2019.
- [4] Fuel cells and hydrogen Joint undertaking (FCH). Hydrogen Roadmap Europe 2019:50–3. <https://doi.org/10.2843/249013>.
- [5] World's Norled. First ship driven by LH2, vol. 1. Florø; 2019.
- [6] Vegvesen Statens. En stille revolusjon i norske fjorder. 2019.
- [7] Norwegian Ministry of Petroleum and Energy, Norwegian Ministry of Climate and Environment. The Norwegian Government's hydrogen strategy towards a low emission society. 2020.
- [8] Hussein H, Brennan S, Molkov V. Dispersion of hydrogen release in a naturally ventilated covered car park. *Int J Hydrogen Energy* 2020;45:23882–97. <https://doi.org/10.1016/j.ijhydene.2020.06.194>.
- [9] Brennan S, Makarov D, Molkov VV. Dynamics of flammable hydrogen-air mixture formation in an enclosure with a single vent. *Fire Explos. Hazards* 2010;493–503. https://doi.org/10.3850/978-981-08-7724-8_07-04.
- [10] Brennan S, Molkov V. Safety assessment of unignited hydrogen discharge from onboard storage in garages with low levels of natural ventilation. *Int J Hydrogen Energy* 2013;38:8159–66. <https://doi.org/10.1016/j.ijhydene.2012.08.036>.
- [11] Brennan S, Molkov V. Pressure peaking phenomenon for indoor hydrogen releases. *Int J Hydrogen Energy* 2018;43:18530–41. <https://doi.org/10.1016/j.ijhydene.2018.08.096>.
- [12] Makarov D, Shentsov V, Kuznetsov M, Molkov V. Pressure peaking phenomenon: model validation against unignited release and jet fire experiments. *Int J Hydrogen Energy* 2018;43:9454–69. <https://doi.org/10.1016/j.ijhydene.2018.03.162>.
- [13] Shentsov V, Kuznetsov M, Molkov V. The pressure peaking phenomenon: validation for unignited releases in laboratory scale enclosure. *Int Conf Hydrog Saf* 2015;148:10.
- [14] Xiao J, Kuznetsov M, Travis JR. Experimental and numerical investigations of hydrogen jet fire in a vented compartment. *Int J Hydrogen Energy* 2018;43:10167–84. <https://doi.org/10.1016/j.ijhydene.2018.03.178>.
- [15] Hussein HG, Brennan S, Shentsov V, Makarov D, Molkov V. Numerical validation of pressure peaking from an ignited hydrogen release in a laboratory-scale enclosure and application to a garage scenario. *Int J Hydrogen Energy* 2018;43:17954–68. <https://doi.org/10.1016/j.ijhydene.2018.07.154>.
- [16] Brennan S, Hussein HG, Makarov D, Shentsov V, Molkov V. Pressure effects of an ignited release from onboard storage in a garage with a single vent. *Int J Hydrogen Energy* 2019;44:8927–34. <https://doi.org/10.1016/j.ijhydene.2018.07.130>.
- [17] Molkov V, Shentsov V, Brennan S, Makarov D. Hydrogen non-premixed combustion in enclosure with one vent and sustained release: numerical experiments. *Int J Hydrogen Energy* 2014;39:10788–801. <https://doi.org/10.1016/j.ijhydene.2014.05.007>.
- [18] Lach AW, Vagner Gaathaug A, Vaagsaether K. Pressure peaking phenomena: unignited hydrogen releases in confined spaces- Large scale experiments. *Int J Hydrogen Energy* 2020;45(56):32702–12. <https://doi.org/10.1016/j.ijhydene.2020.08.221>.
- [19] Lach AW, Vagner Gaathaug A. Pressure peaking phenomena: large-scale experiments of ignited and unignited hydrogen releases. In: 13 th int. Symp. Hazards , prev. Mitig. Ind. Explos. ISHPMIE2020 phys. Bundesanstalt. Braunschweig, Germany: Physikalisch-Technische Bundesanstalt (PTB); 2020. p. 813–26. <https://doi.org/10.7795/810.20200724>.
- [20] Toliás IC, Giannisi SG, Venetsanos AG, Keenan J, Shentsov V, Makarov D, et al. Best practice guidelines in numerical simulations and CFD benchmarking for hydrogen safety applications. *Int J Hydrogen Energy* 2019;44:9050–62. <https://doi.org/10.1016/j.ijhydene.2018.06.005>.
- [21] Hansen OR. Hydrogen infrastructure - efficient risk assessment and design optimization approach to ensure safe and practical solutions. *Process Saf Environ Protect* 2020;143:164–76. <https://doi.org/10.1016/j.psep.2020.06.028>.
- [22] Markert F, Marangon A, Carcassi M, Duijm NJ. Risk and sustainability analysis of complex hydrogen infrastructures. *Int J Hydrogen Energy* 2017;42:7698–706. <https://doi.org/10.1016/j.ijhydene.2016.06.058>.
- [23] Li Z, Sun K. Quantified risk assessment on life and property loss from road collision vehicle fires with hydrogen-fueled tank. *Int J Green Energy* 2019;16:583–9. <https://doi.org/10.1080/15435075.2019.1598415>.
- [24] Aarskog FG, Hansen OR, Strømgren T, Ulleberg Ø. Concept risk assessment of a hydrogen driven high speed passenger ferry. *Int J Hydrogen Energy* 2020;45:1359–72. <https://doi.org/10.1016/j.ijhydene.2019.05.128>.
- [25] Lach AW, Grande Østby T. Parameter estimation using Bayesian approach for a model of Pressure Peaking Phenomena-ignited H2 releases. *Proc 61th SIMS Conf Simul Model SIMS* 2020, Sept 21-24:443–50. <https://doi.org/10.3384/ecp20176>. Finl 2020.
- [26] Crowl DA, Louvar JF. Chemical process safety fundamentals with applications. 3rd ed. Prentice Hall; 2011. 2011.

-
- [27] McBride B, Gordon S, Reno M. Coefficients for calculating thermodynamic and transport properties of individual species. NASA Tech Memo 1993;4513:98.
- [28] Shampine LF, Gladwell I, Thompson S. Solving ODEs with MATLAB. Cambridge: Cambridge University Press; 2003.
- [29] Zhao C, Zhang Z. Dynamic error correction of filament thermocouples with different structures of junction based on inverse filtering method. Micromachines 2020;11. <https://doi.org/10.3390/mi11010044>.
- [30] Liu B, Huang Q, Wang P. Influence of surrounding gas temperature on thermocouple measurement. Case Stud Therm Eng 2020;19:100627. <https://doi.org/10.1016/j.csite.2020.100627>.
- [31] Konopka K. Thermocouple dynamic errors correction for instantaneous temperature measurements in induction heating. 19th IMEKO TC4 Symp - Meas Electr Quant 2013 17th Int Work ADC DAC Model Test 2013:508–14.

Article C

Effect of Mechanical Ventilation on Accidental Hydrogen Releases—Large-Scale Experiments

A.W. Lach and A.V. Gaathaug

Published in Energies, May 2021, 14(11), Pages 3008, doi:

<https://doi.org/10.3390/en14113008>

Article

Effect of Mechanical Ventilation on Accidental Hydrogen Releases—Large-Scale Experiments

Agnieszka W. Lach * and André V. Gaathaug

Department of Process, Energy and Environmental Technology, University of South-Eastern Norway, Faculty of Technology, Natural Science and Maritime Science, Campus Porsgrunn, 3918 Porsgrunn, Norway; Andre.V.Gaathaug@usn.no

* Correspondence: Agnieszka.Lach@usn.no; Tel.: +47-400-43-514

Abstract: This paper presents a series of experiments on the effectiveness of existing mechanical ventilation systems during accidental hydrogen releases in confined spaces, such as underground garages. The purpose was to find the mass flow rate limit, hence the TPRD diameter limit, that will not require a change in the ventilation system. The experiments were performed in a 40 ft ISO container in Norway, and hydrogen gas was used in all experiments. The forced ventilation system was installed with a standard 315 mm diameter outlet. The ventilation parameters during the investigation were British Standard with 10 ACH and British Standard with 6 ACH. The hydrogen releases were obtained through 0.5 mm and 1 mm nozzles from different hydrogen reservoir pressures. Both types of mass flow, constant and blowdown, were included in the experimental matrix. The analysis of the hydrogen concentration of the created hydrogen cloud in the container shows the influence of the forced ventilation on hydrogen releases, together with TPRD diameter and reservoir pressure. The generated experimental data will be used to validate a CFD model in the next step.

Keywords: hydrogen safety; dispersion; mechanical ventilation; ACH; large-scale experiments



Citation: Lach, A.W.; Gaathaug, A.V. Effect of Mechanical Ventilation on Accidental Hydrogen Releases—Large-Scale Experiments. *Energies* **2021**, *14*, 3008. <https://doi.org/10.3390/en14113008>

Academic Editor: Hoi Dick Ng

Received: 13 April 2021

Accepted: 18 May 2021

Published: 22 May 2021

Publisher's Note: MDPI stays neutral with regard to jurisdictional claims in published maps and institutional affiliations.



Copyright: © 2021 by the authors. Licensee MDPI, Basel, Switzerland. This article is an open access article distributed under the terms and conditions of the Creative Commons Attribution (CC BY) license (<https://creativecommons.org/licenses/by/4.0/>).

1. Introduction

Existing mechanical ventilation systems used in semiconfined spaces are designed for conventional fuels only. The increasing number of hydrogen-driven vehicles requires investigation if a change in those ventilation systems is needed.

Hydrogen releases in semiconfined spaces can be significantly more dangerous than in the open air. The released hydrogen can form a cloud/layer under the ceiling and build up its concentration, increasing hazards of ignition and explosion. The wide range of the hydrogen flammability limit (4–75%) [1,2] obliges investigation in the mitigation system to keep concentration within safety limits. There are many studies on hydrogen dispersion in semiconfined enclosures [1,3–8]. The concentration levels in the enclosure mainly depend on the hydrogen leakage source (mass flow rate, its pressure, location, and direction) and the ventilation area [4,6,7]. Insufficient ventilation results in higher concentrations and requires a longer time to reduce it under the flammability limit [6]. A study by Merilo et al. [5] investigated the risks of deflagration in a private garage as a result of leakage from the car. The concentration from a mass flow rate from 1.52 kg/h to 9.22 kg/h resulted in well-mixed layers under the ceiling (with natural and mechanical ventilation). The results showed a decrease in concentration with an increase in ventilation rate. Tests with the highest mass flow rates, 4.92 kg/h and 6.7 kg/h, and the lowest ventilation rate, resulted in average concentration (at the ignition time) over 10% increasing hazards of deflagration.

When hydrogen is released with a low-momentum jet (low Fr number) [9], the formed cloud will be a result of buoyancy motion. As a consequence, the stratification of hydrogen will form hydrogen layers in the enclosure. The buoyancy effect is less significant from the releases from the high pressurized reservoir when the high-momentum jets (high Fr number) are occurring [9,10]. It results in a well-mixed system where hydrogen will

mix with surrounding gases [11]. The authors developed a simple analytical model to investigate the consequences of hydrogen releases from high pressurized releases with natural and forced ventilation. The releases from a 40 MPa container with 1 to 5 ACH were studied through a 6, 3, and 1 mm nozzle. The overpressures that occurred during the releases were much higher for releases through a 6 mm nozzle. The analytical model results showed that with increasing forced ventilation the duration of flammable H₂–air mixture will decrease. A similar study [12] was performed in a full-scale residential garage to validate the analytical model. The model resulted in overpredicting 1% of forced ventilation. The study showed a significant effect of forced ventilation on the reduction in flammable concentration in an enclosure.

The level of hydrogen concentration is crucial to limit flame acceleration [13,14]. The limits for slow flame acceleration have been developed by Dorofev et al. [15], to be under 10% hydrogen in air. Minimum ignition energy (MIE) for 10% H₂–air mixture significantly decreases from 0.052 mJ for 10% to 0.017 mJ for 20% air mixture [14]. The MIE of hydrogen–air mixtures compared to other fuels (order of 0.1 mJ [16]) has higher ignition risks. Therefore, the hydrogen concentration in the enclosure has to be kept under flammability limits, or at least under 10% vol, above which the flame propagation is more violent.

A numerical investigation of hydrogen release in the naturally ventilated enclosure was performed by Hussein et al. [17]. The study examined the hydrogen concentrations that resulted from blowdown type releases from 700 bar, through different diameters of TPRD (Thermal and Pressure Relief Device). The release source was located under the car, between the back wheels. TPRDs with diameters larger than 0.5 mm resulted in a flammable cloud, filling the major part of the enclosure in less than 20 s. The author outlined the unacceptable large diameters of TPRD, which lead to high concentrations in a short time, and may result in pressure peaking phenomena described in previous studies, also by authors of this article [18–21]. Forced ventilation as a mitigation method in the semiclosed space was investigated by Malakhov et al. [22]. The computational fluid dynamics (CFD) methods and conducted experiments resulted in concentration distribution from horizontal hydrogen release. The results show the effect of mechanical ventilation on the hydrogen jet behavior, its length, and on the reduction in hydrogen concentration in a tested compartment.

In this study, series of experiments were conducted to investigate the effect of existing standards of ventilation rates on concentration in the hydrogen cloud. The 40 ft ISO container was used to create a scenario of accidental hydrogen releases in a parking garage, with a release source under the car (placed 4.5 m from the ventilation). The hydrogen concentrations from blowdown and constant mass flow releases from low- and high-pressurized reservoirs are presented. The authors put a major focus on the releases through 0.5 mm TPRD diameter as proposed by Hussein et al. [17]. The experimental results will be used to validate the CFD model in further work developed within the HyTunnel consortium (<https://hytunnel.net/>, accessed on 20 May 2020).

2. Materials and Methods

The 40 ft ISO container (Figure 1) with isolated walls was used for all experiments with open exit doors. Its inner dimension (L × W × H: 11885 × 2240 × 2285 mm) gives a total volume of 60.8 m³.

For all experiments, the Coriolis mass flowmeter for high-pressure flows (up to 1043 bar) was used, and forced ventilation with an outer diameter of 315 mm was installed at the ventilation wall. The ventilation was a blowing type ventilation (exit at the open doors) instead of sucking type, typical for underground parking garages. The choice was made due to safety reasons. The air fan used during experiments was not certified for explosive atmospheres. Nevertheless, the ventilation rate used in underground parking garages was applied in experiments to investigate if the rate is sufficient to limit the hydrogen concentration during accidental releases in confined spaces. The ventilation rate (air change

per hour ACH) was measured by airflow at an IRIS damper with a GAMS differential pressure transmitter.

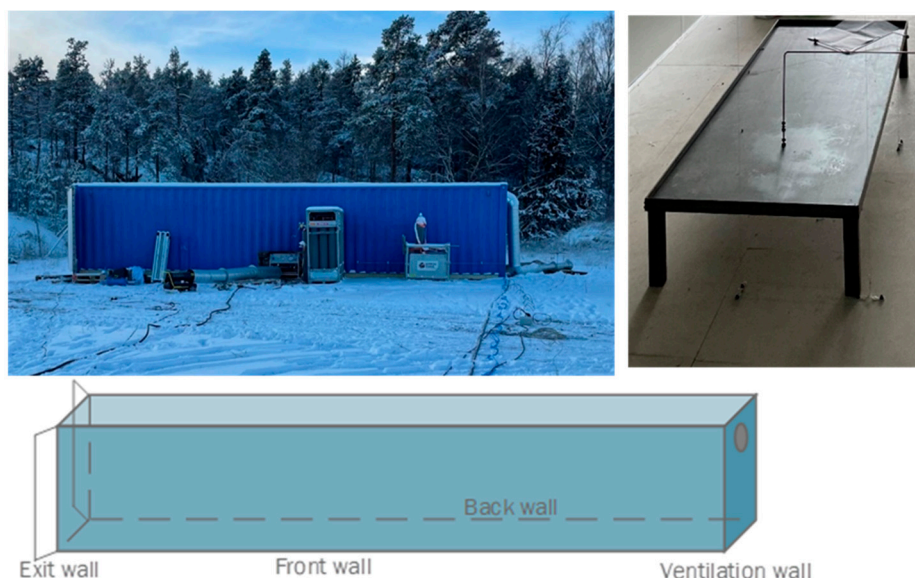


Figure 1. 40 ft ISO container with installed equipment and instrumentation.

Inside the container, a steel table (scaled 1:4 of a hydrogen car) with dimensions $L \times W \times H$: $1965 \times 730 \times 250$ mm was placed 4500 mm from the ventilation wall. The hydrogen was discharged vertically downwards through the steel table. The nozzle outlet was placed 250 mm above the floor and 5000 mm from the ventilation wall.

The experiments were performed with constant and blowdown type of flow with two hydrogen supply setups (Figure 2):

1. Constant mass flow releases. The hydrogen flowed from the hydrogen crate (12 bottles with 200 bar) through the Coriolis mass flow meter and was released through a 1 mm or 0.5 mm nozzle inside the container. The inner diameter of the discharge line was 4 mm outside the container and 3 mm inside (1370 mm), with a total length of 3840 mm (1620 mm before the Coriolis mass flow meter and 2220 mm after). The initial pressure was set by a pressure regulator (V1) at the H₂ crate and kept constant. The release pressure was constantly measured at the exit of the Coriolis mass flow meter with an ESI pressure transmitter (PT). The pneumatic valve (V2) was used to discharge hydrogen during experiments.
2. Blowdown-type mass flow releases. The hydrogen was pumped from the hydrogen crate by a gas booster pump (Haskel-Proserv operating pressure 1600 bar) to the hydrogen tank (Hexagon, Type 4 composite high-pressure tank-carbon fiber). During experiments, hydrogen flowed from the tank through the Coriolis mass flow meter and was released through a 0.5 mm nozzle. The inner diameter of the discharge line was 3 mm with a total length of 3860 mm (1510 mm before the Coriolis mass flow meter and 2350 mm after). The release pressure was constantly measured at the exit of the tank (PT1) with an ESI pressure transmitter. Due to technical issues, the signal from the PT2 was not measured.

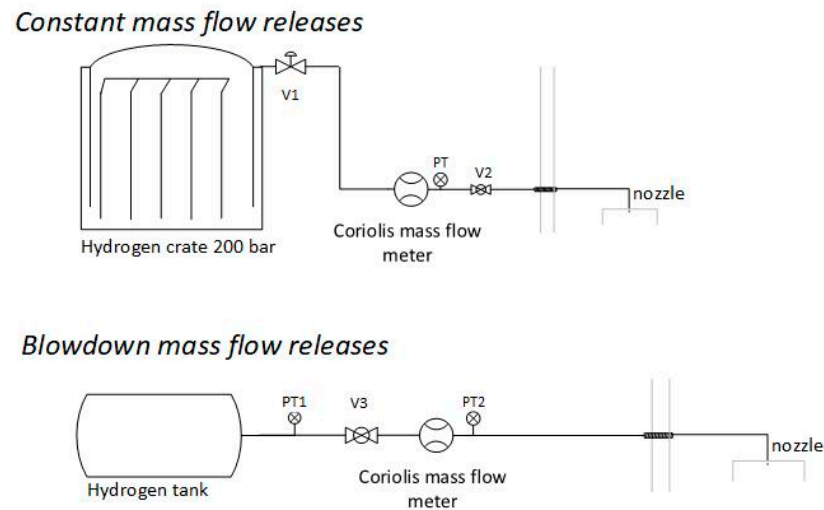


Figure 2. P and ID for hydrogen releases during experiments with constant and blowdown mass flow releases.

The uncertainty of all the instrumentation is listed in the Table 1. The absolute measurement uncertainty includes the derived uncertainty of the air changes per hour. The data used in the analysis are averages of more than 25 kilo-samples and effectively reduce the uncertainty of the data. The concentration sensors with a data rate of 3 Hz gave the concentration measurements pointwise, every 0.33 s.

Table 1. Uncertainty of measurements.

Equipment	Measurement Uncertainty	Absolute Measurement Uncertainty
ESI Pressure transmitter	$\pm 1\%$ FSO BFSL	± 10 bar
GAMS Differential pressure transmitter	$\pm 1\%$ FS	± 15 m ³ /h (± 0.2 ACH)
Mass flow	$\pm 0.2\%$ of flow rate	
Concentration	$\pm 1\%$ FS	$\pm 1\%$

The hydrogen concentration was measured in the container with the 30 CANbus hydrogen sensors (mounted under the ceiling, 500 mm under the ceiling, and under the table) and 8 WIFI hydrogen sensors (mounted on the back wall of the container). Sensor location is illustrated in Figures 3 and 4.

The experiments were designed for two ventilation volumetric airflow rates according to British Standard for 10 ACH and 6 ACH. The needed airflow rate was calculated to be 608 m³/h and 365 m³/h for 10 ACH and 6 ACH accordingly. The effect of the forced ventilation (ACH) on the hydrogen cloud concentration and duration was tested. The hydrogen was released through a 1 mm and 0.5 mm diameter nozzle from 60, 120, and 160 bar reservoir pressures (constant releases), and through a 0.5 mm diameter nozzle from 200, 350, and 700 bar reservoir pressures (blowdown). The pressure at the hydrogen crate and nozzle diameter were the controlling methods for mass flow rates during constant mass flow releases, while the pressure at the hydrogen tank, obtained during the filling process, was the controlling method for blowdown releases.

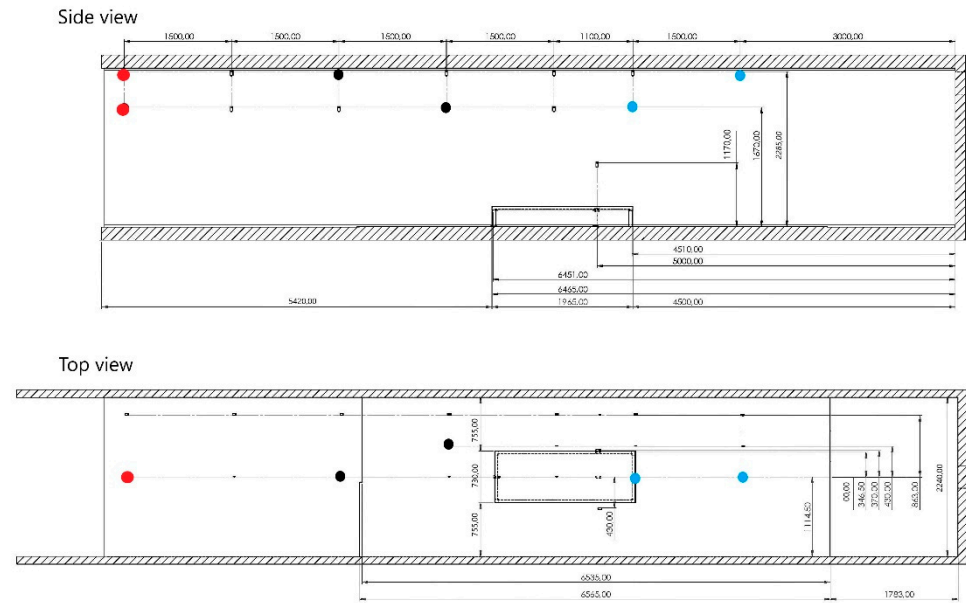


Figure 3. Location of the hydrogen sensors. Circle markers: red—S1, S2; black—S5, S21; blue—S13, S12.

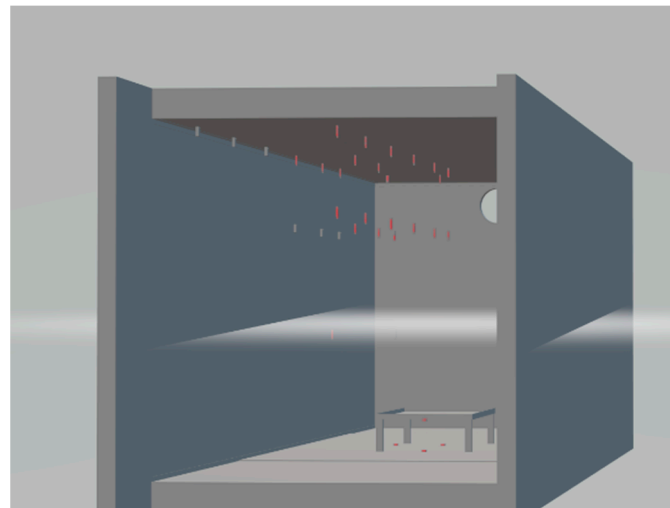


Figure 4. Hydrogen sensors' placement in the container. Red—CANbus sensors, grey—WIFI sensors.

3. Results and Discussion

Experiments were performed in January 2021, regardless of weather conditions. The results and parameters of each experiment are listed in Table 2. Due to low temperatures (up to $-19\text{ }^{\circ}\text{C}$) freezing issues occurred during experiments. For this reason, Exp. 1–3 and Exp. 17–18 do not have representative data and are not included in Table 2. The volumetric airflow was constantly measured during experiments, and the averaged ACH is listed in Table 2 (column 4). The initial pressure was read by the pressure transmitter (Table 2, column 6), and the mass flow rate (MFR) by the Coriolis mass flow meter (Table 2, column 7).

Table 2. Experimental parameters.

Exp	Nozzle Diameter (mm)	ACH (1/h)	ACH Measured (1/h)	Exp Matrix p_0 (bar)	Measured p_0 (bar)	MFR (g/s)	H2 Release Time (s)	Out Temp. (°C)
3	0.5	10	9.5	120	-	1.1	30	-1
4	0.5	10	9.8	120	-	0.8	60	-1
5	0.5	10	9.8	160	-	1.1	60	-1
6	0.5	6	6.0	160	166	1.0	60	-3
7	0.5	6	6.0	120	121	0.7	60	-3
8	0.5	6	6.0	60	60	0.4	60	-3
9	1.0	6	6.0	160	157	6.0	60	-3
10	1.0	10	10.0	160	165	6.0	60	-3
11	1.0	10	10.0	120	140	5.2	60	-3
12	1.0	10	10.0	120	120	4.2	60	-3
13	1.0	6	6.0	120	121	4.2	60	-1
14	1.0	6	6.0	60	59	2.2	60	-1
15	1.0	10	9.8	60	55	2.2	60	-1
16	1.0	10	9.8	140	144	5.3 *	1000	-1
19	0.5	10	10.2	700	721	7.9 *	1000	-5
20	0.5	6	6.2	700	713	7.8 *	1000	-3
21	0.5	6	6.2	360	362	4.2 *	1000	-4
22	0.5	6	6.2	207	209	2.5 *	1000	-2
23	0.5	10	10.2	360	359	4.2 *	1000	-3

* mass flow rate at t_0 .

The higher hydrogen mass flows occurred with increasing reservoir pressure and/or nozzle diameter. The mass flow rates during all experiments were choked at the nozzle. Hence, the non-reacting hydrogen jets (formed under the table) were momentum-dominated jets. Nevertheless, with a higher MFR the concentration in the cloud increased (Figure 5). Increasing nozzle diameter to 1 mm resulted in an MFR 6 times higher than the MFR that resulted during releases through a 0.5 mm diameter nozzle from the same reservoir pressure (Figure 5). The hydrogen concentration in the cloud, accordingly, was ~3 times higher. Decreased diameter with much higher reservoir pressure (Figure 5c) resulted in concentrations similar to those that resulted from releases through 1 mm (Figure 5a). Merilo et al. [5] pointed out the risk of deflagration for hydrogen releases with high mass flow rates when the ventilation rate was kept too low. Therefore, the mass flow rate limits have to be determined for the ventilation rate to keep hydrogen concentration under 10% to limit flame acceleration [13].

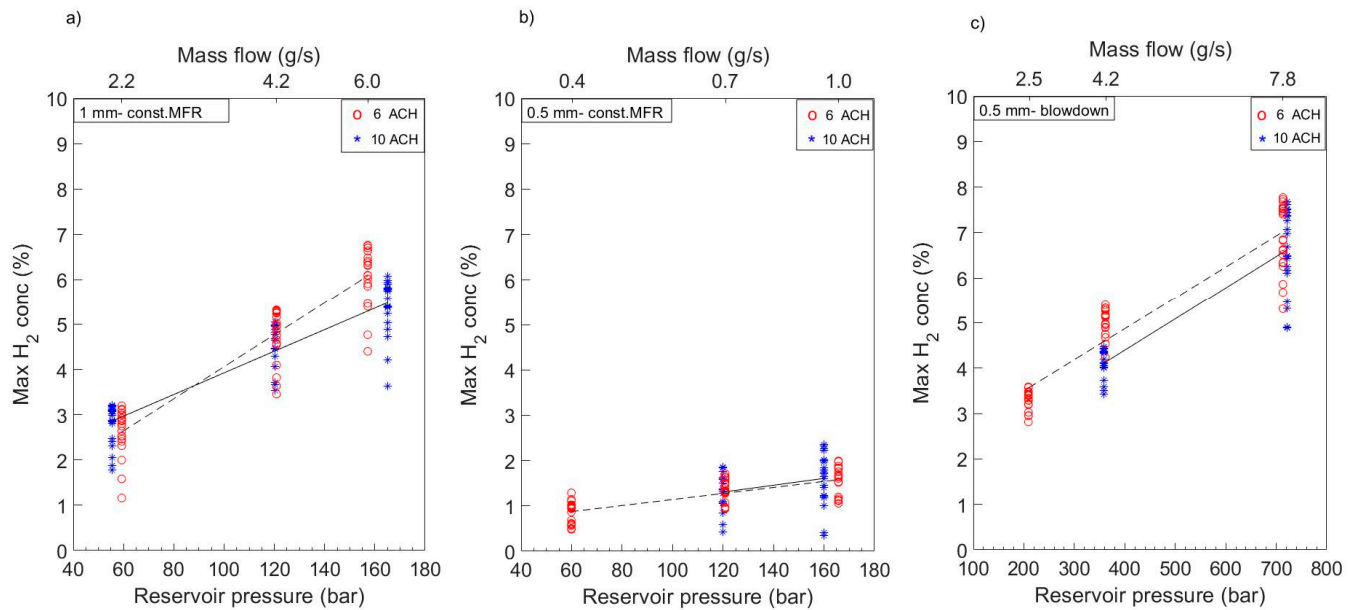


Figure 5. Maximum hydrogen concentration resulted with 6 ACH (dash line) and 10 ACH (solid line) during constant mass flow releases (a) through 1 mm diameter nozzle, (b) 0.5 mm diameter nozzle, and (c) blowdown mass flow releases through 0.5 mm nozzle. Maximum concentrations at each sensor during 10 ACH (blue star) and 6 ACH (red circle).

The effect of the mechanical ventilation on the concentration is shown in Figure 5. The red-circle markers represent the maximum concentration from each sensor above the car during the experiment with 6 ACH. The blue-star marker, accordingly, represents the maximum concentration with 10 ACH. The results of maximum concentration (constant mass flow releases (a) and (b) and blowdown releases (c)) with 6 ACH and 10 ACH were compared in Figure 5. The dashed line demonstrated a straight line fit to the experimental data with 6 ACH, as did the solid line with 10 ACH. The results in Figure 5 do not decisively show a decreased concentration with increased ventilation rate in this particular geometry. The maximum concentrations from 10 ACH and 6 ACH from releases at the same reservoir pressure overlapped with each other, showing small differences.

The concentration results from experiments with 10 ACH (Exp. 10, solid lines) and 6 ACH (Exp. 9, dash lines) are shown in Figure 6. The color of the line corresponds to the sensor's location marked (with the same color) in Figure 3. The top plot shows concentration results from sensors mounted under the ceiling, as does the bottom plot for chosen sensors mounted 50 cm below the ceiling. The results from sensors mounted under the ceiling showed similar concentrations to sensors mounted 50 cm below the ceiling (Figure 6). Since sensors were not mounted closer to the container floor, the results indicate the cloud was at least 50 cm high, as the concentrations were more or less equal. By following line colors, the cloud propagation was observed from sensors closest to the nozzle—blue line (3.0 m and 4.5 m from the ventilation wall), black line (7.1 m and 8.6 m from the ventilation wall), and red line (11.6 m from the ventilation wall). The highest concentration was observed under the ceiling, closest to the ventilation wall (behind the table, upstream the ventilation flow). The hydrogen plume from under the table (car) rises towards the ceiling, and the increased concentration is measured simultaneously on both the blue and the black sensors. This indicates that there are plumes rising in front and behind (as well as along the sides) the table. For lower mass flows, the plumes are mostly at the rear of the table (closest to the nozzle). During blowdown releases, the plume at the front of the table decreases and disappears as the mass flow rate (and tank pressure) decreases.

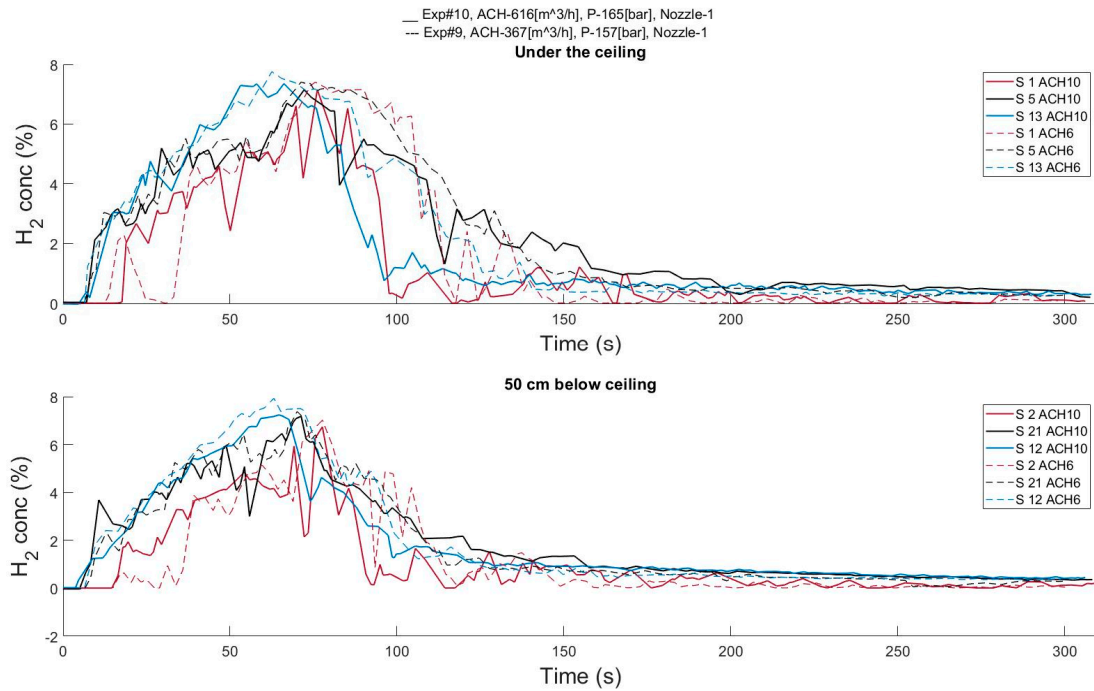


Figure 6. Concentration in the cloud and its propagation from hydrogen releases with 10 ACH and 6 ACH.

The effect of the ventilation on the duration of the flammable cloud was investigated further for the blowdown hydrogen releases. The blowdown experiments recorded the mass flow rate for a total of 900 s (Figure 7), after which the remaining pressure in the tank was 2–3% of the initial pressure. A hydrogen–air cloud can ignite when the concentration is within 4–75% by volume.

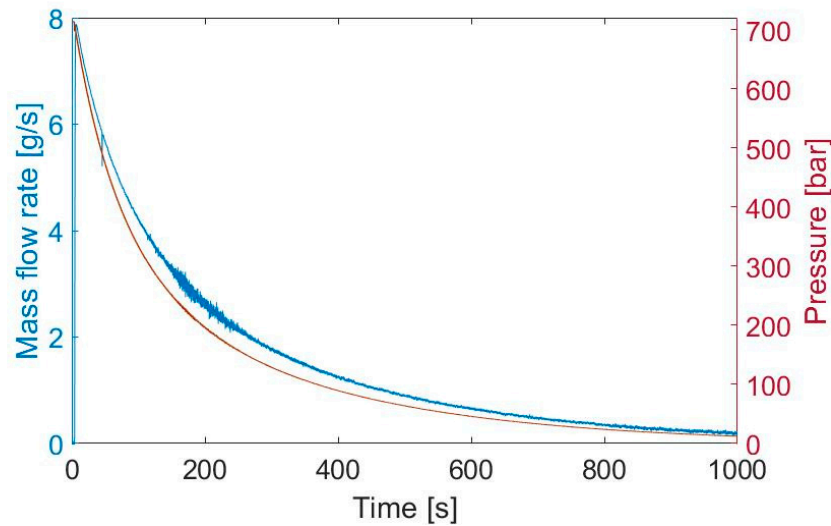


Figure 7. Mass flow rate and pressure at the tank measured during Exp. 20: 700 bar.

In Table 3, the total time, t_f (column 6), when the cloud is flammable is presented together with the time when the concentration in the cloud reached 4% for the first time, t_{f0} (column 7).

Table 3. The flammable time during blowdown releases.

Exp. Nr	$P_{\text{reservoir}}$ (bar)	ACH (h^{-1})	Blowdown Time (s)	P_{end} (bar)	Total Flammable Time t_f (s)	t_{f0} (s)
22	209	6.0	900	6	11	82
23	359	10.2	900	12	83	30
21	362	6.2	900	10	195	32
19	721	10.2	900	16	285	16
20	713	6.2	900	17	336	18

The total time when the hydrogen cloud is flammable was longer when the ventilation rate was lower (6 ACH), see Figure 8 and Table 3. When we compare Exp. 23 ($p_0 = 359$, 10.2 ACH) with Exp. 21 ($p_0 = 362$, 6.2 ACH), we observe that the total flammable time was almost 2 min longer. A 1 min increase in duration was observed when we compared the 700 bar experiments (Exp. 20 and Exp. 19). Since the MFR from reservoirs with higher pressure is higher, the natural consequence is that the flammable cloud occurs faster from those releases. Nevertheless, the ventilation rate has no (or very little) effect on the time when the cloud starts to be flammable. It is important to notice that the flammable time presented in Table 3 and Figure 8 is only for the geometry used during the experiments. However, the difference between flammable time resulting from the releases with 6 ACH and 10 ACH demonstrate the effect of higher ventilation rate on the time of risk of ignition or explosion. The shorter flammable time as an effect of increasing forced ventilation rate was presented earlier by Prasad et al. [12].

The concentration results from all experiments did not exceed 9%. This is below the 10% limit for fast flames described by Dorofeev et al. [15]. The authors, nevertheless, cannot state that it was due to applied ventilation rates since a ‘no-ventilation’ case was not performed. However, the concentrations were above the 4% lower flammability limit. The flame propagation in a slow regime is regarded to result in minor consequences.

Six concentration sensors were placed under the car (Table 4) to measure hydrogen concentration in formed hydrogen plumes. During the releases, the main hydrogen plumes were on the sides, close to the nozzle (Figure 9, S 26). At the first 3–4 min of the release, the strong hydrogen plume was observed at the front of the table (S 29 and S 30). With decreasing mass flow, the hydrogen was eluding on the sides of the table. This can be observed in Figure 9, looking at the orange curve (S 26), which increased after the green (S 29) and light blue (S 30) curves decreased. The accumulation of the hydrogen under the table was observed at the end, where the purple curve (S 28) and the yellow curve (S 27) increased. The higher ventilation rate shows a decrease in hydrogen concentration at the end of the blowdown releases for both experiments with 350 bar and 700 bar initial pressure. Nevertheless, the influence of mechanical ventilation on the concentration under the car needs more investigation in further work.

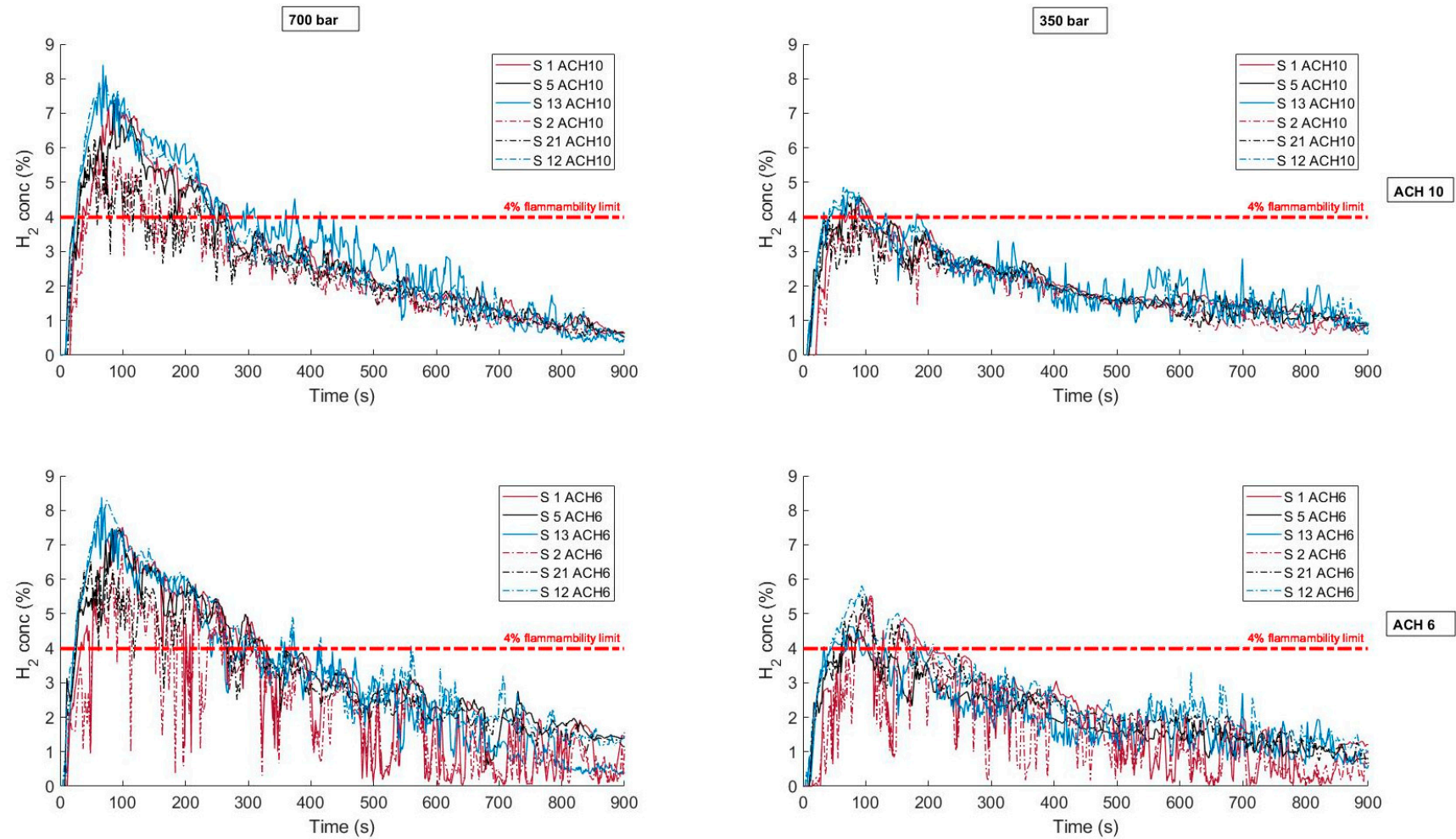
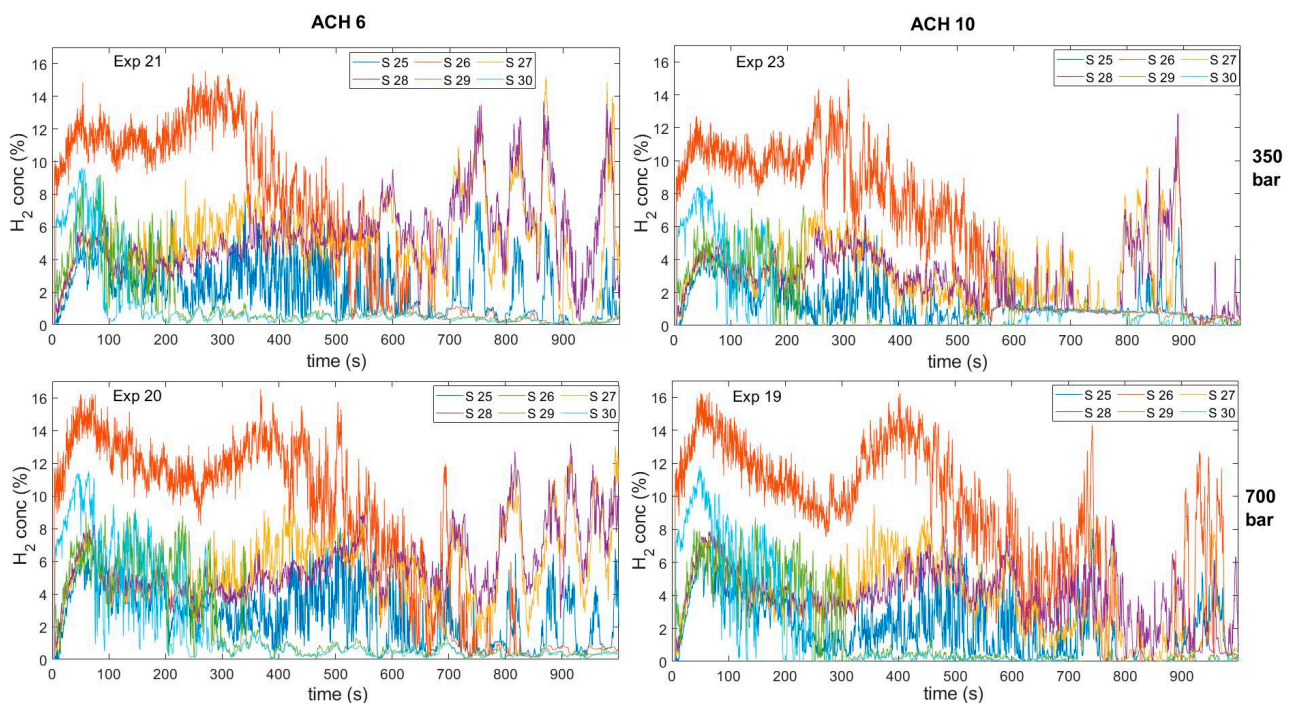


Figure 8. Concentration results from blowdown hydrogen releases with ventilation 10 ACH and 6 ACH. Solid lines-sensors mounted under the ceiling, dash lines-sensors mounted 50 cm under the ceiling.

Table 4. Hydrogen sensor location under the car.

Sensor Nr	x	y	z
25	−5000	0	370
26	−5000	250	370
27	−5010	250	0
28	−4760	250	0
29	−6465	250	0
30	−6465	0	0

**Figure 9.** Concentration results from sensors mounted under the car for Experiments 19–21 and 23.

4. Conclusions

The effect of the forced ventilation was investigated. The results of the presented experiments show the relation between hydrogen concentration from mass flow rate, reservoir pressure, and ventilation rate.

The maximum concentration results for 6 ACH and 10 ACH did not show a significant difference. The time when the cloud becomes flammable (reaches the minimum flammability limit 4%) has been observed differently for hydrogen releases with the same mass flow rate and different ventilation rates. The strongest effect observed during the experiments is on the duration of the flammable cloud, which reduces the duration twice for a ventilation rate with 10 ACH. The sufficiency of forced ventilation, used today, on hydrogen concentration was not conclusive in geometry used during experiments.

As per the recommendation for regulation codes and standards, it is recommended to keep the TPRD diameter small. A 0.5 mm diameter is preferred since the releases through 1 mm TPRD resulted in 3 times higher maximum concentrations. In the case of unintended hydrogen releases in the parking garage, the ventilation rate should be 10 ACH (or higher). Lower ventilation rates will result in a longer duration of a flammable cloud.

The experimental results will be used to validate the model in further work. The model will be an important tool to estimate the required forced ventilation rate for given hydrogen mass flow rates in a geometry.

Author Contributions: A.W.L. and A.V.G. devised the main conceptual ideas and methodology, A.W.L. conceived and planned experimental matrix, A.W.L. and A.V.G. carried out the experiments, A.V.G. developed and performed computation of raw data with A.W.L. assistance, A.W.L. possessed the experimental data, A.W.L. and A.V.G. analyzed the data and performed visualization, A.W.L. took the lead in writing the manuscript., A.V.G. supervised the project and reviewed the manuscript. All authors have read and agreed to the published version of the manuscript.

Funding: This research was funded by the Fuel Cells and Hydrogen 2 Joint Undertaking (JU) under grant agreement No. 826193. The JU receives support from the European Union's Horizon 2020 research and innovation programme and United Kingdom, Germany, Greece, Denmark, Spain, Italy, Netherlands, Belgium, France, Norway, Switzerland.

Institutional Review Board Statement: Not applicable.

Informed Consent Statement: Not applicable.

Data Availability Statement: Data supporting reported results are available in public USN repository that issues datasets with doi:10.23642/usn.14405903.

Acknowledgments: This work was performed within MoZEEES. A Norwegian Centre for Environment-friendly Energy Research (FME), co-sponsored by the Research Council of Norway (project number 257653) and 40 partners from research, industry, and the public sector.

Conflicts of Interest: The authors declare no conflict of interest.

References

1. Dadashzadeh, M.; Ahmad, A.; Khan, F. Dispersion modelling and analysis of hydrogen fuel gas released in an enclosed area: A CFD-based approach. *Fuel* **2016**, *184*, 192–201. [[CrossRef](#)]
2. De Stefano, M.; Rocourt, X.; Sochet, I.; Daudey, N. Hydrogen dispersion in a closed environment. *Int. J. Hydrogen Energy* **2018**, *44*, 9031–9040. [[CrossRef](#)]
3. He, J.; Kokgil, E.; Wang, L.L.; Ng, H.D. Assessment of similarity relations using helium for prediction of hydrogen dispersion and safety in an enclosure. *Int. J. Hydrogen Energy* **2016**, *41*, 15388–15398. [[CrossRef](#)]
4. Pitts, W.M.; Yang, J.C.; Fernandez, M.G. Helium dispersion following release in a 1/4-scale two-car residential garage. *Int. J. Hydrogen Energy* **2012**, *37*, 5286–5298. [[CrossRef](#)]
5. Merilo, E.G.; Groethe, M.A.; Colton, J.D.; Chiba, S. Experimental study of hydrogen release accidents in a vehicle garage. *Int. J. Hydrogen Energy* **2011**, *36*, 2436–2444. [[CrossRef](#)]
6. Gupta, S.; Brinster, J.; Studer, E.; Tkatschenko, I. Hydrogen related risks within a private garage: Concentration measurements in a realistic full scale experimental facility. *Int. J. Hydrogen Energy* **2009**, *34*, 5902–5911. [[CrossRef](#)]
7. Cariteau, B.; Brinster, J.; Studer, E.; Tkatschenko, I.; Joncquet, G. Experimental results on the dispersion of buoyant gas in a full scale garage from a complex source. *Int. J. Hydrogen Energy* **2011**, *36*, 2489–2496. [[CrossRef](#)]
8. Beard, T.; Bragin, M.; Malalasekera, W.; Ibrahim, S.S. Numerical Simulation of hydrogen discharge in a partially enclosed space. *Energy Procedia* **2015**, *66*, 153–156. [[CrossRef](#)]
9. Kim, J.S.; Yang, W.; Kim, Y.; Won, S.H. Behavior of buoyancy and momentum controlled hydrogen jets and flames emitted into the quiescent atmosphere. *J. Loss Prev. Process Ind.* **2009**, *22*, 943–949. [[CrossRef](#)]
10. Veser, A.; Kuznetsov, M.; Fast, G.; Friedrich, A.; Kotchourko, N.; Stern, G.; Schwall, M.; Breitung, W. The structure and flame propagation regimes in turbulent hydrogen jets. *Int. J. Hydrogen Energy* **2011**, *36*, 2351–2359. [[CrossRef](#)]
11. Prasad, K. High-pressure release and dispersion of hydrogen in a partially enclosed compartment: Effect of natural and forced ventilation. *Int. J. Hydrogen Energy* **2014**, *39*, 6518–6532. [[CrossRef](#)]
12. Prasad, K.; Pitts, W.M.; Fernandez, M.; Yang, J.C. Natural and forced ventilation of buoyant gas released in a full-scale garage: Comparison of model predictions and experimental data. *Int. J. Hydrogen Energy* **2012**, *37*, 17436–17445. [[CrossRef](#)]
13. Hu, P.; Zhai, S. Experimental study of lean hydrogen-air mixture combustion in a 12 m³ tank. *Prog. Nucl. Energy* **2021**, *133*, 103633. [[CrossRef](#)]
14. Ono, R.; Nifuku, M.; Fujiwara, S.; Horiguchi, S.; Oda, T. Minimum ignition energy of hydrogen-air mixture: Effects of humidity and spark duration. *J. Electrostat.* **2007**, *65*, 87–93. [[CrossRef](#)]
15. Dorofeev, S.B.; Kuznetsov, M.S.; Alekseev, V.I.; Efimenko, A.A.; Breitung, W. Evaluation of limits for effective flame acceleration in hydrogen mixtures. *J. Loss Prev. Process Ind.* **2001**, *14*, 583–589. [[CrossRef](#)]
16. Kumamoto, A.; Iseki, H.; Ono, R.; Oda, T. Measurement of minimum ignition energy in hydrogen-oxygen-nitrogen premixed gas by spark discharge. *J. Phys. Conf. Ser.* **2011**, *301*, 012039. [[CrossRef](#)]
17. Hussein, H.; Brennan, S.; Molkov, V. Dispersion of hydrogen release in a naturally ventilated covered car park. *Int. J. Hydrogen Energy* **2020**, *45*, 23882–23897. [[CrossRef](#)]
18. Brennan, S.; Molkov, V. Pressure peaking phenomenon for indoor hydrogen releases. *Int. J. Hydrogen Energy* **2018**, *43*, 18530–18541. [[CrossRef](#)]

19. Makarov, D.; Shentsov, V.; Kuznetsov, M.; Molkov, V. Pressure peaking phenomenon: Model validation against unignited release and jet fire experiments. *Int. J. Hydrogen Energy* **2018**, *43*, 9454–9469. [[CrossRef](#)]
20. Lach, A.W.; Vagner Gaathaug, A.; Vaagsaether, K. Pressure peaking phenomena: Unignited hydrogen releases in confined spaces—Large scale experiments. *Int. J. Hydrogen Energy* **2020**, *45*, 32702–32712. [[CrossRef](#)]
21. Lach, A.W.; Gaathaug, A.V. Large scale experiments and model validation of Pressure Peaking Phenomena—ignited hydrogen releases. *Int. J. Hydrogen Energy* **2021**, *46*, 8317–8328. [[CrossRef](#)]
22. Malakhov, A.A.; Avdeenkov, A.V.; du Toit, M.H.; Bessarabov, D.G. CFD simulation and experimental study of a hydrogen leak in a semi-closed space with the purpose of risk mitigation. *Int. J. Hydrogen Energy* **2020**, *45*, 9231–9240. [[CrossRef](#)]

Proceeding A

Parameter estimation using Bayesian approach for a model of Pressure Peaking Phenomena-ignited H2 releases

A.W. Lach and T.G. Østby

This paper was presented at the 61st International Conference of Scandinavian Simulation Society, SIMS 2020 – Virtual Conference on Simulation and Modelling, Finland, 443-450, doi:

<https://doi.org/10.3390/en14113008>

Parameter estimation using Bayesian approach for a model of Pressure Peaking Phenomena-ignited H₂ releases.

Agnieszka Weronika Lach Torbjørn Grande Østby

Process, Energy and Environmental Technology, University of South-Eastern Norway, Kjølnes Ring 53 3916 Norway,
 Agnieszka.Lach@usn.no
 Torbjorn.G.Ostby@usn.no

Abstract

The aim of this paper is to estimate the parameters of the model of Pressure Peaking Phenomena (PPP). This project focuses on the investigation of the overpressures arising from the ignited hydrogen releases in 14.9m³ enclosure (explosive chamber) through a 4mm nozzle. The various ventilation areas and mass flow rates were applied in 31 tests. The controlled variables for experiments are mass flow rate (MFR, g/s), ventilation area (A_v , m²) and time of hydrogen releases (t , s). The Bayesian approach was implemented in the parameter estimation using Markov chain Monte Carlo method for simulations. The discharge coefficient and heat loss coefficient has been analyzed and gave by posterior distribution.

Keywords: pressure peaking phenomena, hydrogen safety, Bayesian analysis, parameter estimation, MCMC.

1 Introduction

Hydrogen releases in confined spaces are bringing new hazards into underground transportation systems. Unexpected hydrogen releases in confined spaces can result in dynamic overpressures with characteristic peaks. The phenomenon called pressure peak phenomena is distinct for hydrogen and occurs while introducing gas with lower density than the gas inside the enclosure (Brennan and Molkov, 2018). The characteristic transient pressure can be observed during releases with a high molar flow in combination with a relatively low ventilation area.

In a study by Makarov et al. (2018) a model for hydrogen jet fires from the TPRD (Thermal activated Pressure Relief Devices) was presented, which was demonstrated to be consistent with the experimental observations on in ~1m³ enclosure. The model predicted much higher overpressures compared to the unignited releases. The model consists of the volumetric mass balance of the gasses in the enclosure during a combustion process. They applied a perfect mix assumption and included adiabatic temperature in the calculations. The results of their simulation for garage-like enclosures showed the risk of enclosure collapse in a few seconds. The parameters used for the simulation were typical TPRD diameter and low ventilation area

(commonly used in UK and France). Further numerical study of pressure peaking from ignited hydrogen releases was performed by Hussein et al. (2018). Their simulations were performed for small scale enclosures (experimental result from 1m³ enclosure) and real scale (garage-like) for the common use of TPRD diameters. The model used ANSYS ICEM CFD (Computational Fluid Dynamics) to generate geometries for both studied cases. The RANS (Reynolds-Average Navier-Stokes) conservation equations were used for solving energy, mass, species and momentum, turbulent model, radiation, and combustion model. The EDC (Eddy Dissipation Concept) model was used to solve the combustion process and DO (Discrete Oridantes) model to include the radiation process. Results demonstrated the relation between vent area and release rate. The big impact of heat transfer mechanisms in the prediction of the pressure peaking phenomenon was acknowledged. It was concluded that the current TPRD diameters may result in a significantly dangerous situation in under-ventilated enclosures. The heat transfer mechanisms (radiation and conduction) has been investigated (Hussein et al., 2018). The assumption of adiabatic walls showed high over predictions compared to simulations where both radiation and conduction were included. The heat transfer has been computationally demonstrated but due to the small scale of experiments (2 s experimental run) couldn't be physically observed. The heat transfer in the system is found to be important and needs further investigation.

In this study, the model of ignited hydrogen releases developed at USN (University of South-East Norway) is presented for the first time. It is based on the problem approach presented by Brennan et al. (2010). The model was validated against large scale experiments in the explosion chamber, allowing to observe high overpressures (over 45 kPa). In this study, we use the Bayesian parameter estimation approach to estimate the model parameters, the discharge coefficient and the heat loss. The Bayesian method combines the information on a discrepancy between the model and the measurements given a set of parameter values (described by the likelihood) and the information available in the literature (described by the prior) through use of the Bayes rule to determine the probable values of the unknown parameters. An important distinction between

the Bayesian method and other classical methods is that it can explicitly and consistently incorporate all the existing knowledge about the unknown parameters. The results of each parameter consistent with the measurements are represented by a posterior distribution. We use a Markov Chain Monte Carlo (MCMC) method to generate samples from the posterior, which can be used for estimation of the unknown parameters. In recent years, the popularity of the MCMC methods has been on the rise (Vrugt, 2016). The prior distribution is chosen based on information found in the literature in order to impose bounds on the parameter space. The prior and posterior densities have been graphically presented as a normal distribution function as in studies on combustion kinetics models (Wang et al., 2020).

The main goal is to create a probability density function (pdf) for parameters giving the most accurate model.

Using Bayesian analysis allows us to understand the parameters' influence on pressure dynamics in the system hence improve the model. The pressure peaking model is designated to be an engineering tool for safety engineers. The accurate parameter estimation plays a significant role in its development.

The investigation of occurring overpressures from ignited hydrogen releases in confined spaces is part of pre-normative research for the safety of hydrogen fuel vehicles and transport through tunnels and similar confined spaces (Hy-Tunnel CS).

2 Case set up and methodology

2.1 Experimental setup and materials

All experiments were performed in a steel explosion with a total volume of 14.9 m³. The explosion chamber's walls in total have five vents of 80 mm diameter each (0.005027m²). The vent in the middle of the front wall was used for the hydrogen and propane pipes. Three of the vents were used to vary the passive ventilation area. The flanges were used to fully close/open the vents with gasket ensuring no leakage. The specifics of the releases were obtained with hydrogen mass flow through a stainless pipe outlet located in the center of the chamber's floor to vertically discharge hydrogen jets fires.

The Coriolis mass flow meter and the pneumatic valve were mounted to measure and control hydrogen releases. Oscilloscope Sigma has recorded pressure and

mass flow rate from Coriolis mass flow. The complete overpressure development was measured with Kulite pressure transducer XTM - 190-50A. Oscilloscope Gen3i recorded the overpressure constantly with parallel measurement initiated by the voltage signal (with 25 ks/s). In the table below are listed the uncertainties of measurement.

Table 2. Standard deviations of instruments

Pressure sensor	±1% FSO BFSL 250 point (0.025 sec) filter
Mass flow sensor	±0.5% of a flow rate
Thermocouples type K	±0.75%

2.1.1 Data set

The experiments were designed for three different ventilation areas and with a variety of mass flow rates. The purpose of those experiments was to validate the model of PPP. To observe overpressure the mass flow rate of discharged hydrogen into an enclosure has to be relatively high while the ventilation area has to be relatively small (Makarov et al., 2018). The chosen combination of vent area and mass flow rates is based on previous unignited experiments (Lach, 2019) and studies on PPP (Hussein et al., 2018). The pressure peak phenomenon for hydrogen jet fires in the 14.9m³ enclosure was successfully observed during all 31 experiments. Experiment 11 described in Table 1 will be used to present methods of the Bayesian approach for parameter estimation.

The measured pressure of experiment 11 is presented in Figure 1. The uncertainty of the Kulite sensor together with the sampling time, result in uncertainty +/- 0.22 kPa.

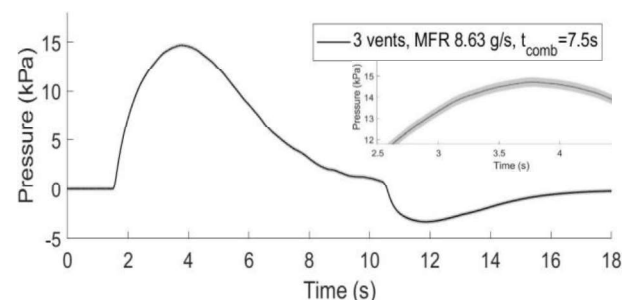


Figure 1. Exp 11; Overpressure for MFR 8.63 g/s with 3 open vent with total vent area 0.0164 m². Measurement uncertainty 0.22kPa.

Table 1 Experimental results: H₂ releases through 4mm nozzle in 14.9m³ enclosure with ventilation area: 1 open vent=0.0055m², 2 vent open= 0,0109m², 3 vents open= 0.0164m².

Setup					Measured	
Exp nr	T ₀ in enclosure [K]	H ₂ release time [s]	Open vent	Mass flow rate [g/s]	Experimental overpressure (max) [kPa]	Experimental underpressure (max) [kPa]
11	280	7.50	3	8.63	14.70	-3.30

2.2 Model of Pressure Peaking Phenomena-governing equation

The model of pressure dynamics in the enclosure during ignited hydrogen releases (jet fires) is presented. In the calculations, the stoichiometric hydrogen combustion was applied where one mole of hydrogen requires 0.5 moles of oxygen: $H_2 + 0.5(O_2 + 3.76N_2) \leftrightarrow H_2O + 1.88N_2$. The system of conservation equations described in this chapter provides a solution for the PPP model explaining mass balance and temperature based on the internal energy in the enclosure.

The mass balance for each species in the enclosure is described with the system of equations (1)-(6). The number of moles in the enclosure n_{tot} is a sum of the number of moles of each species in the enclosure $n_{tot} = \sum n_i$:

$$\frac{dn_{H_2}}{dt} = \dot{n}_{inH_2} - \dot{n}_{outH_2} + \dot{n}_{rxH_2} \quad (1)$$

$$\frac{dn_{O_2}}{dt} = \dot{n}_{inO_2} - \dot{n}_{outO_2} + \dot{n}_{rxO_2} \quad (2)$$

$$\frac{dn_{N_2}}{dt} = \dot{n}_{inN_2} - \dot{n}_{outN_2} + \dot{n}_{rxN_2} \quad (3)$$

$$\frac{dn_{H_2O}}{dt} = \dot{n}_{inH_2O} - \dot{n}_{outH_2O} + \dot{n}_{rxH_2O} \quad (4)$$

Where $\dot{n}_{in,H_2} = \dot{m}_{in}/M_{H_2}$ (hydrogen mass flow \dot{m}_{in} was measured with coriolis mass flow meter), given the initial conditions (at $t=0$) $n_{H_2,0} = 0$, $n_{O_2,0} = 0.21 \cdot n_{tot,0}$, $n_{N_2,0} = 0.79 \cdot n_{tot,0}$, $n_{H_2O,0} = 0$ and $n_{tot,0} = p_0 \cdot \frac{V}{RT_0}$. If the pressure inside the enclosure will be lower than ambient pressure $\Delta p < 0.001$ that means the hydrogen mass flow into the enclosure was closed and $\dot{n}_{in,H_2} = 0$. Then the air from outside the chamber starts to flow into the enclosure through the vent area, means the $\dot{n}_{out,i} = 0$ and:

$$\dot{n}_{in,i} = \frac{C_{in} \cdot A}{M_{air}} \sqrt{2 \cdot \Delta p \cdot \rho_{air}} \quad (5)$$

Where M_{air} is the molecular mass of air and ρ_{air} is the density of air. The C_{in} and A is the discharge coefficient and the vent area, respectively. Using equation (5) the $\dot{n}_{in,i}$ can be calculated: $\dot{n}_{in,O_2} = 0.21 \cdot \dot{n}_{in}$ and $\dot{n}_{in,N_2} = 0.79 \cdot \dot{n}_{in}$ given the assumption that $\dot{n}_{in,H_2O} = 0$.

By balancing the combustion reaction equation, to burn all hydrogen $\dot{n}_{rx,H_2} = -\dot{n}_{in,H_2}$ the oxygen needed will be: $\dot{n}_{rx,O_2} = 0.5 \cdot \dot{n}_{rx,H_2}$. The produced water vapor then will be $\dot{n}_{rx,H_2O} = -\dot{n}_{in,H_2}$, and $\dot{n}_{rx,N_2} = 0$.

Equation (6) based on the steady-state in a compressible energy equation (Bernoulli equation) gives the molar flow out $n_{out,tot}$, which contains all the species in the enclosure from the initial stage and combustion products (no condensation of the water on the walls inside the chamber):

$$n_{out,tot} = C \cdot A \sqrt{\frac{2 \cdot \Delta p \cdot n_{tot}}{V \cdot M_{en}}} \quad (6)$$

Where $n_{tot} = \sum_i n_i$ is the number of moles in the enclosure, the molecular mass in the enclosure is then $M_{en} = \sum_i X_i M_i$ where $X_i = n_i/n_{tot}$ and $\dot{n}_{out,i} = X_i \cdot n_{out,tot}$ can be calculated. The C is the discharge coefficient and A is the ventilation area.

To calculate the pressure in the enclosure (12) the temperature has to be solved first. The internal energy U for the system is equal to:

$$\frac{dU}{dt} = \dot{H}_{in} - \dot{H}_{out} + \dot{Q}_{rx} - \dot{Q}_{loss} \quad (7)$$

And

$$\frac{dU}{dt} = \frac{dn\bar{U}}{dt} \quad (8)$$

With the assumption of specific internal energy \bar{U} :

$$\bar{U}_i = \bar{U}_{ref,i} + \int_{T_{ref}}^T c_{v,i} dt \quad (9)$$

Where $\bar{U}_{ref,i} = 0$ at $T_{ref} = 298.15K$ and $c_{v,i}$ is the molar heat capacity in a constant volume. Changing the internal energy to the temperature will result in a governing equation of temperature in the enclosure T_{en} :

$$\frac{dT_{en}}{dt} = \frac{1}{\sum_i n_i c_{v,i}} \left(\dot{H}_{in} - \dot{H}_{out} + \dot{Q}_{rx} - \dot{Q}_{loss} - (T_{ref}) \cdot \sum_i c_{v,i} \frac{dn_i}{dt} \right) \quad (10)$$

The $\dot{H}_{in} = \sum_i \dot{n}_{in,i} \hat{H}_i$ is the sum of enthalpies of each species at $T = T_{in}$. Using the same analogy the enthalpy of the system at $T = T_{en}$ is the sum of enthalpies: $\dot{H}_{out} = \sum_i n_{out,i} \cdot \hat{H}_i$.

The $c_{v,i}$ was calculated by reducing the heat capacity at constant pressure by the universal gas constant $c_{v,i} = c_{p,i} - R$. The $c_{p,i}$, $\hat{H}_{in,i}$ and $\hat{H}_{out,i}$ where calculated with NASA polynomials (Mcbride et al., 1993) which includes thermodynamic data coefficients and enthalpy of formation $\hat{H}_{f,i}$.

The \dot{Q}_{rx} is the heat of formation. Since the water vapor is the only product $\dot{Q}_{rx} = \dot{Q}_{rx,H_2O} = \dot{n}_{rxH_2O} \cdot (-\Delta \hat{H}_{f,H_2O})$ where the \hat{H}_{f,H_2O} is the enthalpy of formation of water vapor.

The \dot{Q}_{loss} is the heat loss calculated with the major assumption of a simple heat transfer with no condensation of water: $\dot{Q}_{loss} = h_{loss} \cdot A_{wall} \cdot (T_{en} - T_{wall})$ where A_{wall} is the surface area inside the enclosure and h_{loss} is the heat transfer coefficient. When the pressure inside the enclosure will be lower than ambient pressure $\Delta p < 0.001$ the cold air is entering into enclosure and heat transfer coefficient is assumed to be $h_{loss,2} = 0.5 \cdot h_{loss}$.

The change of the number of moles in enclosure causes temperature change, expressed in equation (10) with $((T - T_{ref}) \cdot \sum_i c_{v,i} \frac{dn_i}{dt})$. The temperature of the wall T_{wall} , was calculated with the major assumption that the whole wall is one thermal mass with the same temperature inside (i.e. no temperature gradient in the wall):

$$\frac{dT_{wall}}{dt} = \frac{\dot{Q}_{loss}}{m_{wall} \cdot c_{steel}} \quad (11)$$

Where m_{wall} is the mass of walls and C_{steel} is the heat capacity of the wall.

Solving the PPP model with conservation equations (1), (2), (3), (4), (10), (11) then allows to calculating pressure inside the enclosure with the ideal gas law (12):

$$p_{en} = \frac{n_{tot} \cdot R \cdot T_{en}}{V} \quad (12)$$

2.3 Bayesian framework

A Bayesian approach with Monte Carlo simulation was used in estimating the parameters: the discharge coefficient, C , and the heat transfer coefficient, h_{loss} . The purpose of using Bayesian inference is to obtain new recognition about the parameters θ . Whereas standard optimization techniques would estimate the optimal value for these parameters, Bayesian simulation instead estimates a distribution of probable values (based on including observed data and prior knowledge). Using a Bayesian approach makes sense given the uncertainties inherent in experiments and measurements.

The relationship between $\theta = [C, h_{loss}]$ and the measurement data d is given according to Bayes' theorem, equation (13). C and h_{loss} are assumed to be independent.

$$p_{post}(\theta|d, M, I) = \frac{\mathcal{L}(d|\theta, M, I)p_{prior}(\theta|M, I)}{\int \mathcal{L}(d|\theta, M, I)p_{prior}(\theta|M, I)d\theta} \quad (13)$$

$$\propto \mathcal{L}(d|\theta, M, I)p_{prior}(\theta|M, I)$$

Here $p_{post}(\theta|d, M, I)$ is the posterior probability for parameters θ given the measurement data d , M representing the previously described model, and I represents other unspecified information given in this paper, such as the experimental setup. The $p_{post}(\theta|d, M, I)$ expresses the updated knowledge of the θ given the d, M, I . Further, $p_{prior}(\theta|M, I)$ represents the prior probability distribution for parameters θ given the model M and the information I —the initial belief about the θ . Preliminary testing suggested that the value of h_{loss} was between 20 and 40, while the value of C was between 0.6 and 1. The prior distributions used are further detailed in the next subchapter. Finally, $\mathcal{L}(d|\theta, M, I)$ represents the likelihood (probability) of seeing the measurement data d given the parameters θ , the model M , and other information I . The Bayesian calculation will confront the simulation results of the earlier described model as a function of θ and d, M, I to gather the pdf (probability density function) of the θ for the observed data.

Assuming the measurement uncertainties are normally distributed, the likelihood is given by the Gaussian function (Daly et al., 1995). As experiments consist of multiple measurements, this gives us equation (14), where d_i (experimental overpressure) and m_i (simulated overpressures) represent measurement data

and model data at index i (step), respectively. The sigma, σ is the standard deviation of the measurement uncertainty (constant σ , Table 2).

$$\mathcal{L}(d|\theta, M, I) = \prod_{i=1}^n \frac{1}{\sqrt{2\pi\sigma^2}} \exp\left(-\frac{(d_i - m_i)^2}{2\sigma^2}\right) \quad (14)$$

Having the priors and likelihood allows the posterior pdf to be estimated through Monte Carlo simulation. This was done using the standard Metropolis Markov Chain Monte Carlo algorithm, which is further detailed in algorithm 1.

Algorithm 1

The Metropolis algorithm (adapted from (Kruschke, 2015))

1. **Given:** data d ; prior distribution $p_{prior}(\theta|M, I)$; likelihood function $\mathcal{L}(d|\theta, M, I)$; step standard deviation σ ; number of steps T
2. Initialize θ^0
3. **For** $i = 1$ **to** T :
4. Sample $\theta' \sim \mathcal{N}(\theta^{i-1}, \sigma_2)$
5. Sample $u \sim \mathcal{U}(0,1)$
6. $p_{move} = \min\left(1, \frac{\mathcal{L}(d|\theta', M, I)p_{prior}(\theta'|M, I)}{\mathcal{L}(d|\theta^{i-1}, M, I)p_{prior}(\theta^{i-1}|M, I)}\right)$
7. **If** $p_{move} \geq u$: $\theta^i = \theta'$; **else**: $\theta^i = \theta^{i-1}$

This is a sampling algorithm where samples producing a higher probability than the current sample is always accepted, while samples producing a lower probability than the current sample is sometimes accepted, depending on a randomly sampled value. This process is then repeated for a limited number of steps.

However, with high numbers of measurements, the likelihood has a tendency to vanish, as many values between 0 and 1 are multiplied. Using the natural logarithm is a natural way of overcoming this. Using the natural logarithm changes steps 6 and 7 of algorithm 1 in the following way. The fraction in step 6 is changed as shown in equation (15). Here ℓ refers to the loglikelihood, and \mathcal{P}_{prior} refers to the logarithm of the prior. Due to a high number of steps (100000) needed to describe our physical event the Gaussian distributions were assumed for the loglikelihood and the logprior. Then ℓ and \mathcal{P}_{prior} can be calculated as shown in equation (16) and (17). In equation (16), as in equation (14), d_i and m_i represent measurement data and model data at index i , respectively, and σ is the standard deviation of the measurement uncertainty. In equation (17) θ_j represents the j -th parameter in θ , and μ_j and σ_j represent the expected value and standard deviation, respectively, for the prior for this parameter. Equation (17) is only valid if the parameters of θ are independent. The final change that needs to be made is to alter step 7 to compare p_{move} to the value of $\ln(u)$ instead of u .

$$\ln\left(\frac{\mathcal{L}(d|\theta', M, I)p_{prior}(\theta'|M, I)}{\mathcal{L}(d|\theta^{i-1}, M, I)p_{prior}(\theta^{i-1}|M, I)}\right) =$$

$$\ell(d|\theta', M, I) + \mathcal{P}_{prior}(\theta'|M, I)$$

$$- \ell(d|\theta^{i-1}, M, I) - \mathcal{P}_{prior}(\theta^{i-1}|M, I) \quad (15)$$

$$\ell(d|\theta, M, I) = k + \sum_{i=1}^n -\frac{(d_i - m_i)^2}{2\sigma^2} \tag{16}$$

$$p_{\text{prior}}(\theta^{i-1}|M, I) = l + \sum_{j=1}^m -\frac{(\theta_j - \mu_j)^2}{2\sigma_j^2} \tag{17}$$

2.3.1 MCMC Setup

There are parameters that must be set for the MCMC algorithm, including the number of steps T , the standard deviation of the step σ_2 . Additionally, the prior distributions for θ must be specified. Based on this the MCMC was run with the parameters and priors shown in Table 3. The prior probability distributions for C and h_{loss} are also shown in Figure 2.

Table 3. MCMC parameters and prior distributions

T	100000
σ_C	0.01
$\sigma_{h_{\text{loss}}}$	0.1
$p_{\text{prior}}(\theta M, I)$	$p_{\text{prior}}(C M, I) \cdot p_{\text{prior}}(h_{\text{loss}} M, I)$
$p_{\text{prior}}(C M, I)$	$\mathcal{N}(0.8, 0.05)$
$p_{\text{prior}}(h_{\text{loss}} M, I)$	$\mathcal{N}(30, 5)$

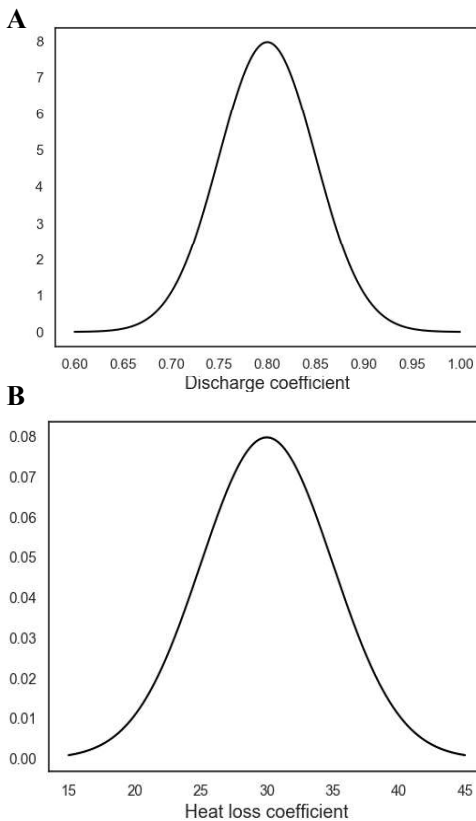


Figure 2. The prior probability distributions for A: discharge coefficient C and B: heat loss coefficient h_{loss} .

Additionally, some lead/lag compensation was implemented due to a time offset between the experimental and simulated data of approximately 4000 time-steps, consistent between experiments. It resulted

in a significant difference during the rise and fall of the pressure response in the experiments.

The model was solved using solve nonstiff differential equations- medium order method ode45 (MathWorks, 2020), with a maximum time step of 0.5 s.

2.3.2 Evaluation of MCMC representativeness

The representativeness and performance of the MCMC chains that were run were evaluated as described by Kruschke (2015). In this subchapter “the chains” refers to four chains run on experiment 11.

A visual inspection of the chains’ trajectory shows that after a burn-in period, all the chains had converged to the same area. The first 3000 steps of each chain were then removed, considered to be part of burn-in. With these steps removed the chains were seen to overlap and mix well, and distinguishing the different chains from one another was basically impossible. This indicates that none of the chains are stuck with all the chains sampling from the same region. The convergence of chains with the starting position given by the X marker is presented in Figure 3.

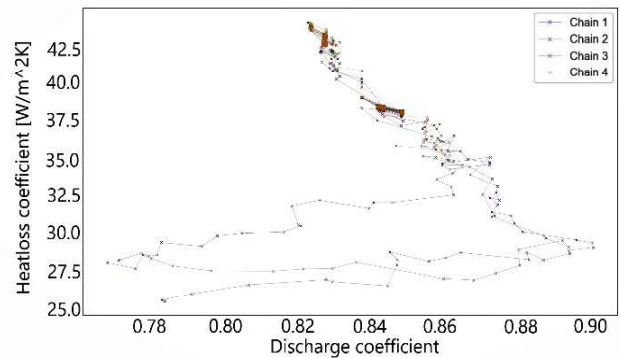


Figure 3. Convergence of 4 chains run in MCMC; exp 11.

The plots of marginal distributions were then created for the sampled parameter values for each chain, shown in Figure 4 and Figure 5. These density plots show high overlap, though with some difference in the peaks. Some difference in the density plot is to be expected, due to the finite number of samples drawn. The overlap between chains suggests the chains sample representative values from the posterior distribution.

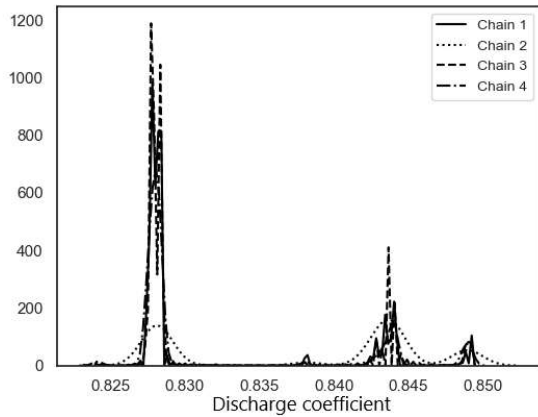


Figure 4. Density plot for parameter C for chain 1 through 4 for experiment 11.

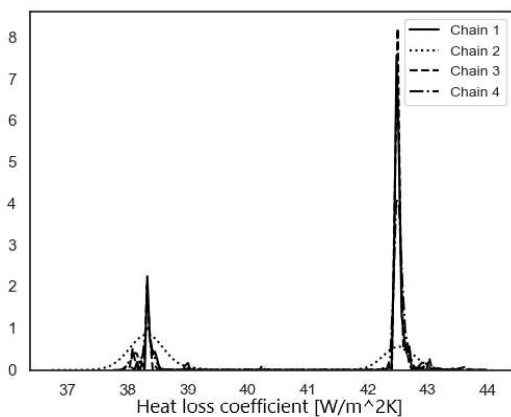


Figure 5. Density plot for parameter h_{loss} for chain 1 through 4 for experiment 11.

This evaluation of the MCMC gives us confidence in the results produced by the simulation. The evaluation shows no indication of poor representativeness nor low accuracy.

2.3.3 Posterior predictive check

If our model is adequate, then replication of the current experiment should generate data that are similar to the predictions made by the model. Let $y_t = y(t; \theta)$ denote the predicted pressure given $\theta = (C, h)$. We are interested in $p(y_t|D, m, I)$, where D and m denote the experimental data from the previous run and the model output (section 2.2), respectively. It follows from the marginalization and the product rules that

$$p(y_t|D, m, I) = \int_{\Omega} p(y_t, \theta|D, m, I) = \int_{\Omega} p(y_t|D, \theta, m, I)p(\theta|D, m, I)d\theta \quad (18)$$

In case we know m and θ , it is reasonable to assume that previously acquired data and the prediction y_t are conditionally independent. This means that

$$p(y_t|D, \theta, m, I) = p(y_t|\theta, m, I) \quad (19)$$

Thus, the posterior predictive density is given by

$$p(y_t|D, m, I) = \int_{\Omega} p(y_t|\theta, m, I)p(\theta|D, m, I)d\theta \quad (20)$$

The second term of the integrand, $p(\theta|D, m, I)$ is the posterior density, which has been previously determined. The first term of the integrand, $p(y_t|\theta, m, I)$, is the model density which depends on the model and the measurement noise. The model density has the same functional form as the likelihood for a single data point. Note that, in the case of model density, this function is a probability density with respect to y_t , with the parameter θ assumed to be known.

The expression for the posterior predictive density (20) shows that the uncertainty in the predicted pressure is due to two processes. The first one is contributed by the posterior density, which expresses the uncertainty about the true value of θ . The second contribution is due to the measurement noise. Although, more experimental evidence can reduce the uncertainty about θ , nevertheless, the measurement noise cannot be eliminated. In the maximum likelihood approach, it is assumed that the inferred value θ_{ML} for the unknown parameter is the true value and therefore the only source of uncertainty is the measurement noise. Indeed, in the context of eq. (20), in the maximum likelihood approach one claims that

$$p(\theta|D, m, I) = \delta(\theta - \theta_{ML}) \quad (21)$$

and hence, the integral in (20) reduces to

$$p(y_t|D, m, I) = p(y_t|\theta_{ML}, m, I) \quad (22)$$

As the evidence grows, we will become more confident about the true value of θ and hence the posterior density becomes narrower and in the limit it converges to (21). Nevertheless, as long as the uncertainty about the true value of θ is large, the Bayesian and maximum likelihood approaches will differ.

Due to difficulties to find an analytical expression for y_t , in general, a Monte Carlo based approach is more viable. The algorithm below describes the steps.

Algorithm 1

Generating y_t ; for $i = 1, \dots, N$ repeat the following steps

1. $\theta_i \sim p(\theta|D, m, I)$
2. $y_i \sim p(y|\theta_i, m, I)$

Applying this algorithm for large N (equal to the number of MCMC samples), the empirical distribution of the samples y_i will approximate $p(y_t|D, m, I)$.

3 Results and discussion

Hydrogen jet fires are causing high overpressure due to the high amount of released energy in a very short time. The molar balance and temperature in the enclosure described in the methodology explained the pressure dynamic.

In the model, the mass balance is crucial for the accuracy of overpressure prediction. Therefore the discharge coefficient used in the calculation of molar flow through the vents (in and out) needs to be

investigated. A discharge coefficient is a dimensional number representing flow and pressure loss through the orifice. Is a function of Reynold number $C = f(Re)$ while the Re is a function of the flow rate, hence the $E_{loss} \sim u^2$. Some assumptions have been used for different scenarios but when the discharge coefficient is unknown or uncertain it has to be found experimentally. For the computing methods, it is recommended to assume $C=1$ (Crowl and Louvar, 2011). From the previous study on PPP it is known that $C=1$ is an assumption that can't be applied, and lower values showed better accuracy. The reasoning of choosing the values of C in the work of Hussein et al., (2018) and Makarov et al., (2018) was based on the literature knowledge and validated against their experiments. The values presented in their work are not. It can be due to different experimental setups and mass flow rates. In the mentioned studies the heat transfer shows its importance for the pressure dynamics. Nevertheless, the heat loss has been neglected in the model (due to the small scale of experiments).

In the model presented in this paper a simple solution of the heat loss is used. The water condensation hasn't been included in the numerical simulations. The heat loss described in section 2.2 determines the rate of heat transfer through the walls.

The MCMC evaluation results in the posterior distributions. Experiment 11 has been chosen to presents the parameter estimation analysis. In the figure below (Figure 6) the posterior pdf is presented. The clusters you can see on the plots represent the area of 'the best' θ . Experiment 11 resulted in bimodal posterior distributions. By looking into the density plots of C and h_{loss} (Figure 4 and Figure 5) the two major peaks are clearly visible. Two clusters represent two areas of θ value which are consistent with the experimental results.

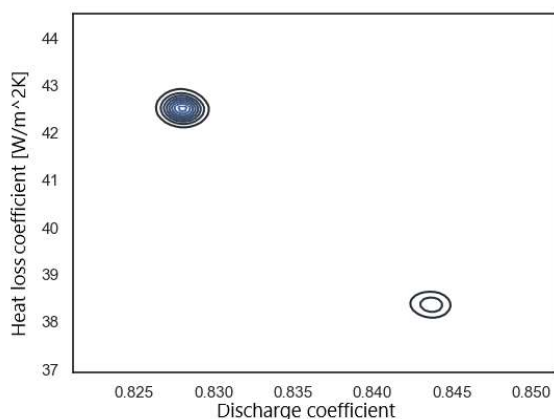


Figure 6. Bivariate posterior distributions for experiment 11.

Due to uncertainty in measurements, in general, it is not possible to uniquely determine the values of the

unknown parameters. In the Bayesian approach, this problem is addressed by the posterior distribution. The posterior distribution summarizes the belief in the probable range of the values for the unknown parameters (Kruschke, 2015). Models are simplified versions of reality. In this context, the simplification means that we only take into account certain aspects of the reality and assume that the other aspects either cancel out each other or have no significant influence on the description or predicted behaviour of the system of interest. One way to evaluate how good these simplifications are is to check how accurately the model mimics the data. Therefore, it is important to not confuse the model inadequacies with the uncertainty due to inference. Thus, it is important to keep track of the sources of uncertainty. One way to do this is by conducting the so called posterior predictive check.

The MCMC results have been applied into the PPP model (Figure 7). Both experimental and simulation results have their uncertainty, included in curves. For experimental results, the uncertainty is $\pm 1\%$ FSO BFSL (grey area around black line Figure 1). For the simulation, the uncertainty was calculated at the specific time for each sample (vertical red lines from blue dots Figure 7). The simulation overestimates the actual pressure with 0.6 kPa in maximum pressure and underestimates in minimum pressure is 0.6 kPa as well which is acceptable.

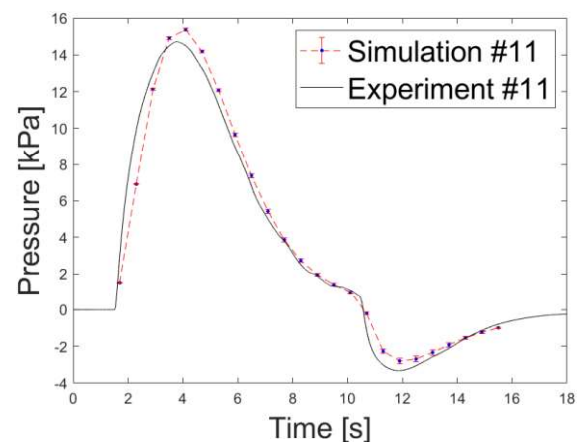


Figure 7. Pressure dynamics in 14,9 m³ the enclosure during experiment 11: experimental (black line), simulation with estimated θ individually for each time step (blue dots). The standard deviation is represented by error bars (red lines with caps).

The simulation result shows good accuracy with experiments (Figure 8).

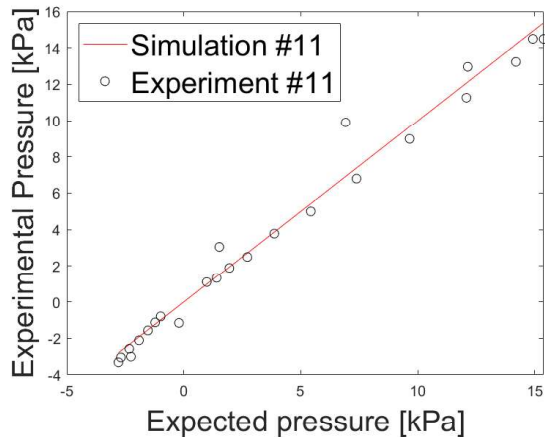


Figure 8. Exp11 pressure predicted (red line) vs. measured (black circles).

4 Summary

In this paper, we have used a Bayesian approach to estimate parameters in a PPP model. The intended use for this model is to simulate overpressures from accidental hydrogen releases in confined spaces. The parameters of interest were the heat loss coefficient and the discharge coefficient. The data used in creating the model, and used when estimating the parameters, was collected from large scale experiments performed by the University of South-Eastern Norway.

Markov Chain Monte Carlo was used to generate samples from the posterior distribution. The performance of the MCMC algorithm was evaluated, and seen to perform well.

In this analysis, we found that a discharge coefficient of $C = 0.9$ and a heat loss coefficient of $h_{loss} = 30$ are the most likely values which capture the results across all the experiments. The Bayesian analysis of the model gave the most probable values for performed experiments (set up dimension and flow rates).

Acknowledgements

The authors wish to acknowledge the European Union Fuel Cells and Hydrogen 2 Joint Undertaking (JU) under grant agreement No 826193 with support from European Union's Horizon 2020 for funding and supporting the HyTunnel project.

This work was performed within MoZEES, a Norwegian Centre for Environment-friendly Energy Research (FME), co-sponsored by the Research Council of Norway (project number 257653) and 40 partners from research, industry and public sector.

We thank Andre V. Gaathuag for his work on the PPP model and Ali Ghaderi for comments and supervision that greatly improved the manuscript

References

S. Brennan, D. Makarov, and V.V. Molkov. Dynamics of Flammable Hydrogen-Air mixture Formation in an

Enclosure with a Single Vent. In *Proceedings - Fire and Explosion Hazards 6, 11.-16. April, Leeds, UK*, 493–503, 2010. doi: 10.3850/978-981-08-7724-8_07-04.

S. Brennan and V.V. Molkov. Pressure peaking phenomenon for indoor hydrogen releases. *International Journal of Hydrogen Energy*, 43(39), 18530–18541, 2018. doi: 10.1016/J.IJHYDENE.2018.08.096

D.A. Crowl and J.F. Louvar. *Chemical Process Safety Fundamentals with Applications*, 3rd ed.; In B. Goodwin, J. Fuller and E. Ryan, editor. Prentice Hall 2011.

F. Daly, D. Hand, M. Jones, A. Lunn, and K. McConway. *Elements of Statistics (1st ed.)*. Addison Wesley, The Open University, 1995.

H.G. Hussein, S. Brennan, V. Shentsov, D. Makarov, and V.V. Molkov. Numerical validation of pressure peaking from an ignited hydrogen release in a laboratory-scale enclosure and application to a garage scenario. *International Journal of Hydrogen Energy*, 43(37), 17954–17968, 2018. doi: 10.1016/J.IJHYDENE.2018.07.154.

J.K. Kruschke. Doing Bayesian Data Analysis, A tutorial with R, JAGS and Stan. In *Becoming a Brilliant Trainer (2nd ed.) 2015*. doi: 10.4324/9781315627960-16.

A.W. Lach. Pressure Peaking Phenomena-unignited releases. *Internal Report experiments, 2019*.

D. Makarov, V. Shentsov, M. Kuznetsov, and V.V. Molkov. Pressure peaking phenomenon: Model validation against unignited release and jet fire experiments. *International Journal of Hydrogen Energy*, 43(19), 9454–9469, 2018. doi: 10.1016/J.IJHYDENE.2018.03.162.

MathWorks. Matlab User Guide(r2020b). *ode45* Apple Hill Drive Natick, MA, 2020.

B.J. McBride, S. Gordon, and M. Reno. *Coefficients for Calculating Thermodynamic and Transport Properties of Individual Species*. Nasa Technical Memorandum, 4513(NASA-TM-4513), 98, NASA, US. Government 1993.

J. A. Vrugt. Markov chain Monte Carlo simulation using the DREAM software package: Theory, concepts, and MATLAB implementation. *Environmental Modelling & Software*, 75, 273–316, 2016. doi: 10.1016/J.ENVSOFT.2015.08.013.

J. Wang, Z. Zhou, K. Lin, C.K. Law, and B. Yang. Facilitating Bayesian analysis of combustion kinetic models with artificial neural network. *Combustion and Flame*, 213, 87–97, 2020. doi: 10.1016/j.combustflame.2019.11.035.

Proceeding B

Pressure peaking phenomena: Large-scale experiments of ignited and unignited hydrogen releases

A.W. Lach and A.V. Gaathaug

This paper was presented at the 13th International Symposium on Hazards, Prevention and Mitigation of Industrial Explosions, ISHPMIE 2020– Virtual Conference, Braunschweig, Germany, 813-826. doi:

[10.7795/810.20200724](https://doi.org/10.7795/810.20200724)

Pressure peaking phenomena: Large-scale experiments of ignited and unignited hydrogen releases

Agnieszka Lach^a, André Vagner Gaathaug^a

^a University of South-Eastern Norway, Porsgrunn, Norway

E-mail: Agnieszka.Lach@usn.no

Abstract

This work aims to validate the pressure peaking phenomenon occurring in constant hydrogen releases, which is important for the safety of enclosures and human beings during accidental releases of ignited and unignited hydrogen. Rapid hydrogen discharge from a tank in confined spaces leads to high overpressures that can cause property damage. This pressure peaking phenomenon (PPP) is defined as an impermanent pressure rise in an enclosure with limited ventilation. PPP is a specific phenomenon for gases lighter than air, especially when a lighter gas is released at a relatively high mass flow rate into an enclosure filled with a denser gas with a relatively small vent area.

The experiments were performed in a large-scale setup consisting of a steel-reinforced container with volume 14.9 m³ and a ventilation area sized from 0.0006 m² to 0.0165 m². The hydrogen was released through a 4 mm round nozzle with varying mass flow rates (\dot{m}), and the overpressure was measured within the enclosure. The aim was to choose parameters that result in a pressure lower than 10–20 kPa, which is accepted as a safe overpressure limit. Experiments were controlled by a pulse generator (a central timing unit), and all data were stored on two oscilloscopes. The \dot{m} was measured during the experiments by a Coriolis-type mass flow meter, and a Kulite pressure transducer (XTM-190) was used to measure the overpressure inside the enclosure. Two different cases were investigated, one with unignited releases of hydrogen and the second with ignited releases. Hydrogen concentration sensors (XEN-5320) were installed on the enclosure walls to measure the hydrogen concentration and temperature change during unignited experiments. For ignited releases, thermocouples were used for temperature measurements. The experimental setup assured no air ingress into the enclosure, a constant ventilation area, and almost constant hydrogen inflow. All the experiments proved the phenomenon and the hazards of hydrogen releases in confined spaces. The maximum pressure occurs at the beginning of the hydrogen release. For unignited releases, the hydrogen concentration continues to increase after the pressure peak. This considerably increases the risk of ignition and thus explosion hazards as well as oxygen depletion leading to asphyxiation. The ignited releases result in much higher overpressures. In this case, the ventilation area had to be increased a minimum of 28 times to keep the pressure below the 10 kPa limit.

Keywords: *hydrogen safety, pressure peak phenomenon, hazards, passive ventilation, large-scale experiments.*

1. Introduction

Hydrogen fuel vehicles are becoming a valuable and attractive zero-emission alternative. Two types of tanks are used for hydrogen storage: 350 bar and 700 bar, each with mandatory mounted pressure relief devices (PRD) (European Parliament, 2010). The PRD provides fast hydrogen release from the tank in the case of a car accident where high temperatures are present. The role of PRDs is to keep the tanks safe from explosion when exposed to fire for extended amounts of time (Sunderland, 2008).

The regulation codes and standards (RCS) do not specify safety orifice diameters for PRDs. The orifice presently used has diameter of 5.08 mm, which results in high mass flow rates (Brennan et al., 2019).

The hydrogen releases from a thermally activated pressure release device (TPRD) with the mentioned diameter will likely be acceptable in open-air scenarios. Nevertheless, the rapid discharge of hydrogen in confined spaces presents additional hazards and must be considered by automobile manufacturers and regulated by the RCS.

The pressure peaking phenomenon occurs for both ignited and unignited releases. Nevertheless, the overpressure reaches different ranges (ignited releases result in much higher overpressures due to the combustion process), and the two cases must be investigated separately. The environmental conditions have an influence on the results; thus, it is worth noting that the unignited release experiments in this work were performed in the summer and the ignited release experiments in the autumn.

The consequences of indoor hydrogen releases differ significantly from outdoor releases and can affect people, structures, and the environment. Many European research projects have focused on those consequences by investigating hydrogen energy systems and related safety issues. Releases in an enclosure with insufficient ventilation can result in the formation of explosive clouds (Papanikolaou et al., 2010). The final report of one of the projects (HyIndoor; Fuster et al., 2017) presented existing knowledge gaps including ventilation solutions. Leakage from the hydrogen fuel tank inside a small enclosure was studied by Gupta et al. (2009) with non-catastrophic conditions. The relationship between the hydrogen discharge ratio and the enclosure ventilation is a crucial parameter to avoid or significantly reduce the risk of the enclosure's collapse. For the safety development of hydrogen applications, those knowledge gaps need to be closed. Consequently, an engineering tool must be developed and distributed among hydrogen safety engineers.

The high mass flow rates of hydrogen releases in confined spaces result in high overpressures. This may create hazards and cause property damage and injury. The rising pressure is called the pressure peaking phenomenon (PPP) and can be defined as "a transient process of pressure change in vented enclosure with a characteristic peak exceeding the steady-state pressure" (Makarov et al., 2018). PPP occurs when introducing a gas with lower density into an enclosure filled with a heavier gas (e.g., hydrogen into air). The phenomenon is pronounced for hydrogen and occurs when the released hydrogen mass flow rate is relatively high and the vent area is relatively small (Makarov et al., 2018). Under those conditions, the molar flow at the vent will consist of a mixture of the gases inside the enclosure. The inflow will only be hydrogen. At the beginning of the hydrogen release, the flow rate at the nozzle is higher than that at the vent area. This will lead to molar accumulation and hence increased pressure inside the enclosure. The overpressure will grow until the molar flows at both openings become equal. Then pressure peak will be reached and the molar flow at the vent area starts to increase, hence the pressure will decrease.

A previous study (Hussein et al., 2018) affirmed that the vent size and hydrogen mass flow rates are major parameters that determine the overpressure in an enclosure. Brennan and Molkov (2018) investigated hydrogen releases with constant and blowdown mass flow rates. The results of their work showed hazards with the TPRD diameters used presently. Their study provided a model that was used to prepare the experiments described in this work. Their study presented a relationship between TPRD diameter, overpressures, concentration, and vent area. Larger orifice diameters result in higher overpressures. Increasing the vent area decreases the maximum overpressure but increases the hydrogen concentration inside the enclosure, hence creating a higher hydrogen concentration at the maximum overpressure. A high level of hydrogen concentration creates hazards of asphyxiation and ignition. The hydrogen tanks designed for cars that are currently in use are type 4 (Stephenson, 2005), with the limitation of being exposed to high temperatures. The exposure time increases with decreasing PRD diameter, which must be taken under consideration. The PPP validation study was made for the first time by Makarov et al. (2018). Their study developed a model for ignited releases

from the TPRD and revealed the risk of much higher overpressures compared to unignited releases. The model consists of the volumetric mass balance of introduced, generated, and combusted gases under the perfect mix assumption based on a stoichiometric evaluation. The adiabatic temperature was included in calculations for the temperature change inside the enclosure. The results from laboratory-scale experiments presented the possibility of a new hazard for garage-like enclosures, as they showed that, in few seconds during ignited hydrogen releases, the enclosure will be destroyed by the overpressure. This issue must be addressed in order to avoid too high pressures from hydrogen releases in confined spaces.

The following study considers hydrogen releases in a confined space with a limited ventilation area. Residential garages and underground parking are the main focus. In Norway, passenger ferries and ships play a significant role in transport traffic, and their use of hydrogen systems and fuel cells provide a promising alternative that reduces greenhouse gas emissions. A risk assessment of a hydrogen-fueled high-speed ferry (Aarskog et al., 2020) showed the need for adjustments to keep risks within acceptable limits. The PPP is relevant for maritime applications as well as any confined space where hydrogen releases may occur. Specifically, proper ventilation systems must be investigated as a part of a risk evaluation. The investigation of hazards from unignited and ignited hydrogen releases at the mentioned conditions is part of the pre-normative research for the safety of hydrogen fuel vehicles and transport through tunnels and similar confined spaces (HyTunnel-CS, project founded by HFC, Horizon2020).

2. Experiments

The experiments were performed in a steel-reinforced container of volume 14.9 m^3 , shown in Fig. 1. The steel-reinforced container has five vents with 80 mm diameter in total, each located at the front and back wall. Four of them are in the lower corners, and the fifth is located in the middle of the front wall (Fig. 1) to the inside of the chamber floor. The fifth vent was used for the hydrogen inlet from a crate of 12x50 l bottles at 200 bar. For the case of ignited releases, a propane pipe was used as an ignition system, described in Section 2.2.

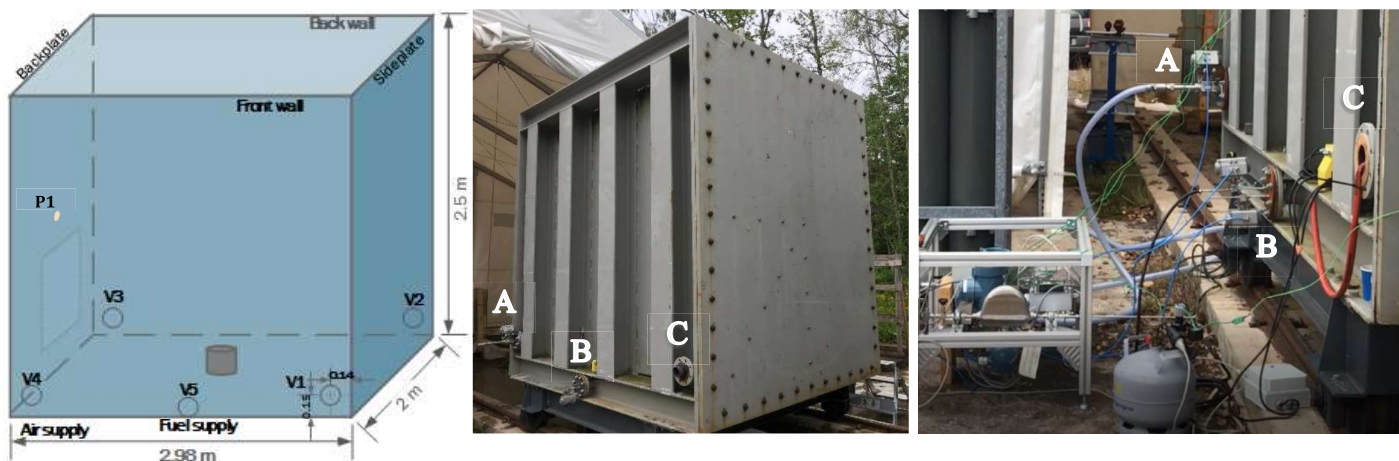


Fig. 1. The steel-reinforced container of volume 14.9 m^3 . (A) Air inlet, (B) hydrogen inlet, (C) ventilation area.

A valve at the bottle crate was used to control the hydrogen pressure. A stainless steel pipe with ID 4 mm connected the bottle crate with the mass flow meter. From the mass flow meter, the pipe was connected to a ball valve before it was connected to the 4 mm release nozzle. The nozzle was placed in the center of the steel-reinforced container's floor to vertically discharge hydrogen inside the chamber. An oscilloscope (Sigma; Fig. 3 and Fig. 5) was used to record the hydrogen mass flow data obtained from the Coriolis-type mass flow meter. The mass flow rates of hydrogen discharge were narrow due to the maximum operating pressure of the mass flow meter (110 bar) and a continuously reducing hydrogen pressure in the bottle stack. The explosion chamber was equipped with a pressure transducer, thermocouples (ignited), and hydrogen sensors (unignited). To measure the overpressure,

the Kulite pressure transducers XTM-190-10A (unignited) and -50A (ignited) were used, mounted 1.5 m above the floor in the middle of the back-plate (P1 in Fig. 1). The overpressure was logged at 25 kHz, which gave a measurement precision of $\sigma = 0.07 \text{ kPa}$. The accuracy was calibrated with a Fluke pressure calibrator. The pressure transducer was connected to an oscilloscope (HBM Gen3i) with a transient recording. A pulse generator was used to control all instrumentation. It was programmed to send the trigger at the same time to both oscilloscopes and the hydrogen release valve. An air fan (Fig. 1, A) was activated after the release of hydrogen was closed. This was done to dilute the hydrogen inside the enclosure after unignited releases and to flush out the hot air after ignited releases.

2.1 Unignited experiments

For unignited releases, only one vent was used for ventilation (V1 in Fig. 1), located 15 cm above the floor. To place the ventilation outlet 20 cm from the ceiling, a 75 mm diameter vertical PVC pipe was installed inside the steel-reinforced container. The cover with the diameter of the desired ventilation area was placed at the end of the PVC pipe (outside the explosion chamber) (Fig. 2).



Fig. 2. The vent with variable area.

Hydrogen concentration measurements were carried out continuously with two wireless XEN-3520 concentration sensors, placed inside the steel-reinforced container during experiments. Due to technical problems for Experiments 6–11, a USB cable was used instead of the wireless connection (measurements at 3 Hz were stored by the laptop computer). One sensor was mounted in the middle of the front wall, 1.24 m above the floor. The second sensor was mounted in the middle of the back plate, 2.85 m above the floor (Fig. 3).

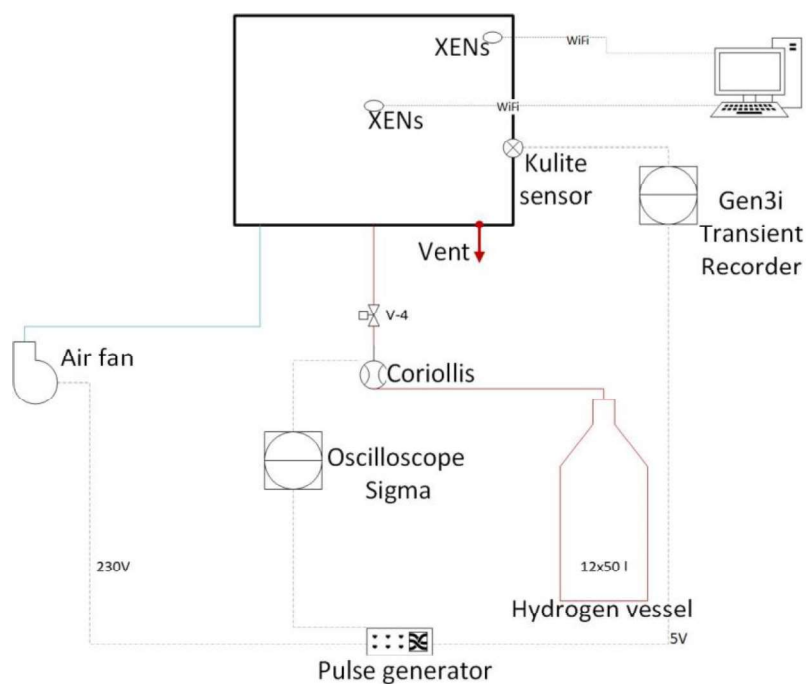


Fig. 3. Unignited setup: Simplified piping and instrumentation diagram (P&ID).

The hydrogen concentration (after the hydrogen discharge was stopped) in the steel-reinforced container reached 13%–62% (depending on the experiment). To ensure the same initial conditions for each experiment, air from the fan was introduced to reduce the hydrogen concentration to less than 2% (without interfering with the applied sealing).

2.2 Ignited experiments

For the ignited releases, a propane pilot flame with a 10 kV spark ignition source controlled by a pulse generator (Fig. 4) was mounted on the hydrogen nozzle. The propane was supplied through a stainless steel pipe with ID 4 mm. The potential pressure increase due to the propane pilot flame was measured to be lower than the precision of the sensor.



Fig. 4. The ignition pilot, located together with hydrogen nozzle.

The ignited hydrogen releases were carried out without hydrogen concentration sensors. The temperature was measured continuously with four thermocouples (Type K Autek-TD20H-KP). Teflon cables were used between the thermocouples and amplifiers, and a PVC-insulated compensation cable was used between oscilloscope and amplifiers. Each thermocouple had a 20 mm compression fitting plug mounted in the chamber walls. Sensors were mounted 0.06 m from the wall to avoid boundary layers. They were mounted at heights 0.035 m, 1.24 m, 1.85 m, and 2.85 m.

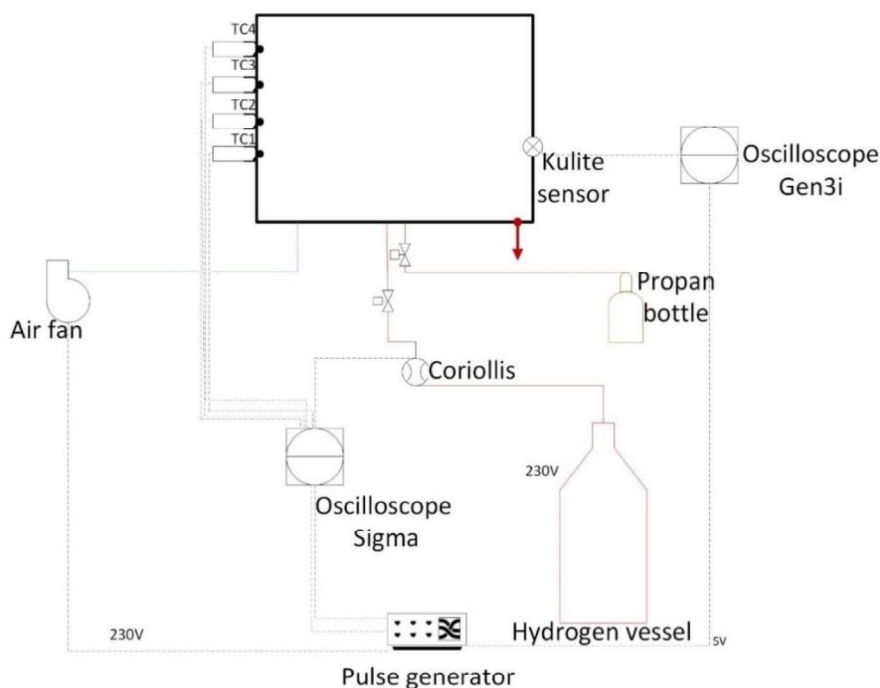


Fig. 5. Ignited setup: A simplified piping and instrumentation diagram (P&ID).

3. Results and discussion

In this chapter, the experiments from unignited and ignited releases will be presented and analyzed.

3.1 Unignited releases

Table 1 lists the measured overpressures (pressure peaks) and maximum concentrations. The pressure peaking phenomenon was observed during all experiments. Due to the limitation of hydrogen discharge described in Section 2, observations of PPP required the implementation of small ventilation areas (Table 1, column 4). The ventilation area was assured constant by applied sealing. The initial pressure in the enclosure was equal to the ambient pressure. Due to technical issues with the XENSensors, no data were stored for Experiments 4 and 5. For Experiments 2 and 3, the temperature data used a format rounding to unity, resulting in large uncertainty. Therefore, the initial temperature for those experiments was assumed to be 293 K. The hydrogen concentration increased until the H₂ discharge was stopped, resulting in maximum values at the end of the H₂ inflow.

Table 1. Results of measured maximum overpressures and hydrogen concentrations for Experiments 2–11. Vertically discharged unignited hydrogen through 4 mm nozzle.

Exp. no.	Setup				Measured	
	T ₀ in enclosure [K]	H ₂ release time [s]	Vent area [m ²]	Mass flow rate [g/s]	Experimental overpressure [kPa]	Experimental max H ₂ conc. [%]
2	293.00*	90	0.0012	1.90	0.42	13
3	293.00*	120	0.0020	3.50	0.51	28
4	293.00*	120	0.0020	9.05	2.86	-
5	293.00*	120	0.0014	9.90	6.45	-
6	296.00	120	0.0014	10.1	6.74	62
7	292.34	180	0.0006	3.05	4.07	35
8	291.94	180	0.0006	3.05	3.96	35
9	293.12	200	0.0006	4.75	8.05	53
10	289.71	200	0.0006	4.20	6.70	47

11	293.57	1000	0.0006	blowdown	7.00	34
----	--------	------	--------	----------	------	----

*Assumed values

The last experiment was performed with a continuously decreasing mass flow rate (blowdown) from a maximum value of 4.85 g/s. The mass flow rate decreased due to the falling pressure inside the hydrogen bottles. This experiment had the longest duration of hydrogen inflow, but the hydrogen concentration data was only stored until 122 s (due to a technical issue). Nevertheless, H₂ concentration data were captured at the time of maximum pressure $t(p_{max})$ (Table 2). The H₂ concentration changes depended on the experimental conditions (\dot{m} and A_v). From Table 2, it can be seen that the concentration at $t(p_{max})$ is higher with higher \dot{m} at the same A_v .

Table 2. Measured hydrogen concentration at max pressure.

Exp. No.	2	3	6	7	8	9	10	11
\dot{m} [g/s]	1.90	3.50	10.10	3.05	3.05	4.75	4.20	4.85 _{blowdown}
A_v [m ²]	0.0012	0.0020	0.0014	0.0006	0.0006	0.0006	0.0006	0.0006
H ₂ % at p_{max}	1.5%	0.2%	24.0%	15.4%	16.0%	25.0%	22.0%	21.5 %
$t(p_{max})$ [s]	10 s	10 s	37 s	80 s	77 s	89 s	89 s	64 s

When $\dot{n}_{in} = \dot{n}_{out}$, the maximum overpressure (p_{max}) is reached. Then, the molar flow at the vent ($\dot{n}_{out} = \dot{m}_{out}/M_{en}$) continues to increase, as it is higher than the molar flow at the nozzle ($\dot{n}_{in} = \dot{m}_{in}/M_{H_2}$). This leads to a decrease in the overpressure. The enclosure volume does not affect the time of maximum overpressure $t(p_{max})$ at a given ventilation area, but \dot{n}_{in} does have an affect (Brennan and Molkov, 2018). As an obvious outcome based on a model description (Lach, 2019), with the same ventilation area and constant enclosure volume, p_{max} will be higher for higher \dot{n}_{in} . Higher \dot{m} increases the time needed to reach the maximum pressure (Fig. 6). This result can be used to estimate the evacuation time and also provides a design criterion for the TPRD diameter.

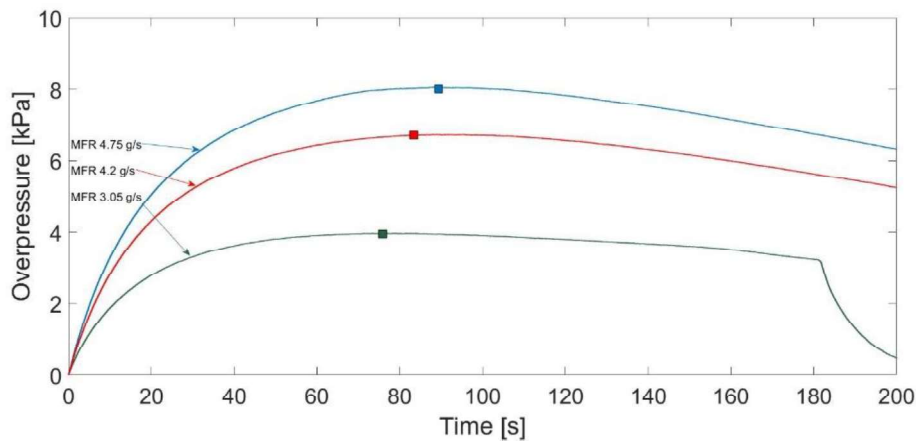


Fig. 6. Experimental overpressures for different \dot{m} at the same ventilation area ($A_v = 0.0006 \text{ m}^2$); pressure peak occurrence (rectangle).

All the experiments showed that the maximum overpressure occurred before the hydrogen concentration reached its maximum (Fig. 7). Increasing the hydrogen concentration increases ignition risks and depletes the oxygen in the container, which is hazardous to human life.

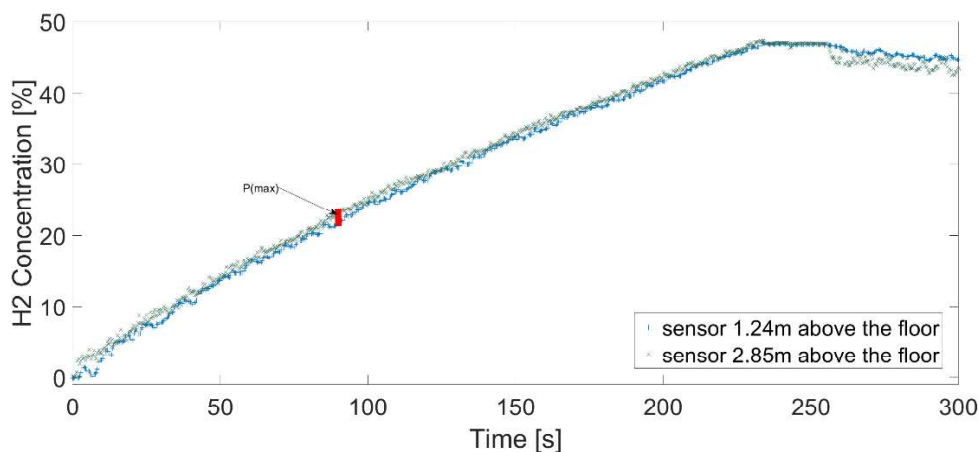


Fig. 7. Hydrogen concentration for Experiment 10. Inflow duration is 200 s, \dot{m} is 4.2 g/s.

As expected, the results showed that higher \dot{m} results in higher p_{max} and a higher hydrogen concentration for the same ventilation area. Experiment 9 had the highest pressure peak among the experiments with $A_v=0.0006 \text{ m}^2$. It also had the highest hydrogen concentration at that point (Table 2).

3.2 Ignited releases

Table 3 lists the results from 31 tests of ignited hydrogen releases in the same steel-reinforced container. The pressure peak phenomenon was successfully demonstrated for hydrogen jet fires. The tests were conducted with different and approximately constant mass flow rates and a combination of three possible vents. Each vent has an area of 0.0055 m^2 . Steel flanges were used to blind the vents to get the desired total ventilation area. The initial pressure in the enclosure was equal to ambient pressure. The temperature and pressure were measured continuously; Table 4 provides the maximum values for overpressures and underpressures and the maximum values for each thermocouple. The initial temperature is the volume-weighted average temperature, measured with thermocouples at the beginning of the experiment. For the first 10 experiments, the air fan was used to flush out hot air and water from the enclosure after the hydrogen jet flame was shut down. This was done prior to opening the door to the enclosure. Due to the observed underpressure after the H_2 release was closed, the air fan was disconnected for the rest of the experiments. This was done to investigate the possible underpressures in the experiments.

Table 3. Experimental results: 31 tests of H_2 releases through a 4 mm nozzle with varying \dot{m} and ventilation area. One open vent = 0.0055 m^2 , two open vents = 0.0109 m^2 , three open vents = 0.0164 m^2 .

Exp no.	Setup				Measured					
	T_0 in enclosure [K]	H_2 release time [s]	Open vent	Mass flow rate [g/s]	Experimental overpressure [kPa]	Experimental underpressure [kPa]	Temperature [°C]			
							T1	T2	T3	T4
1	8	5.0*	1	1.45	4.8	-0.1	9	45	86	85
2	9	10.0*	1	1.37	4.5	-0.3	14	81	128	125
3	10	5.0*	1	3.38	16.7	-0.6	69	119	171	164
4	12	10.0*	1	3.15	15.8	-2.8	141	175	251	225
5	15	10.0*	2	3.14	5.3	-1.1	93	175	270	230
6	15	10.0*	2	3.04	5.0	-1.1	86	176	258	223
7	3	6.0*	2	7.90	22.0	-2.5	166	209	353	319
8	4	6.0*	2	7.50	20.6	-2.3	142	207	348	287
9	6	6.0*	3	8.37	13.9	-2.9	194	242	403	345

10	6	6.0*	3	8.35	13.7	-2.8	192	243	389	332
11	7	7.5	3	8.63	14.7	-3.3	204	249	416	358
12	9	6.0	3	8.90	15.1	-2.3	176	215	372	322
13	8	6.0	3	11.72	21.7	-4.3	244	288	458	408
14	4	6.0	3	11.37	21.1	-3.8	241	274	430	352
15	4	6.0	3	4.00	4.3	-0.5	40	129	202	194
16	4	6.0	3	4.07	4.5	-0.5	45	130	209	190
17	5	6.0	2	11.52	33.3	-3.2	211	263	415	367
18	5	6.0	2	11.47	33.0	-3.4	205	267	414	367
19	5	6.0	1	8.62	48.1	-5.7	194	205	359	300
20	5	7.5	1	8.50	46.5	-8.2	243	247	383	332
21	7	6.0	2	8.52	23.7	-2.0	166	223	333	294
22	7	6.0	2	2.60	4.1	-0.3	12	98	142	139
23	6	15.0	2	2.36	3.5	-1.1	87	174	275	238
24	7	25.0	3	2.38	1.8	-1.0	195	240	368	331
25	5	25.0	3	3.87	4.1	-2.2	315	339	481	435
26	9	20.0	3	6.70	10.1	-4.6	384	467	603	568
27	8	10.0	3	6.65	9.9	-2.7	213	259	433	391
28	9	10.0	2	6.56	16.8	-3.5	219	247	419	369
29	8	20.0	2	6.55	16.7	-8.7	375	474	578	531
30	10	10.0	1	6.65	35.9	-14.1	246	259	392	349
31	9	20.0	1	6.56	35.3	-25.3	366	444	556	522

* The air fan was used after hydrogen release (duration time).

The obtained overpressures show the dependency (with high sensitivity) of hydrogen mass flow rates and ventilation areas (Fig. 8), as was expected based on previous unignited experiments and other PPP studies. The model developed for ignited releases in enclosures (Makarov et al., 2018) simulated

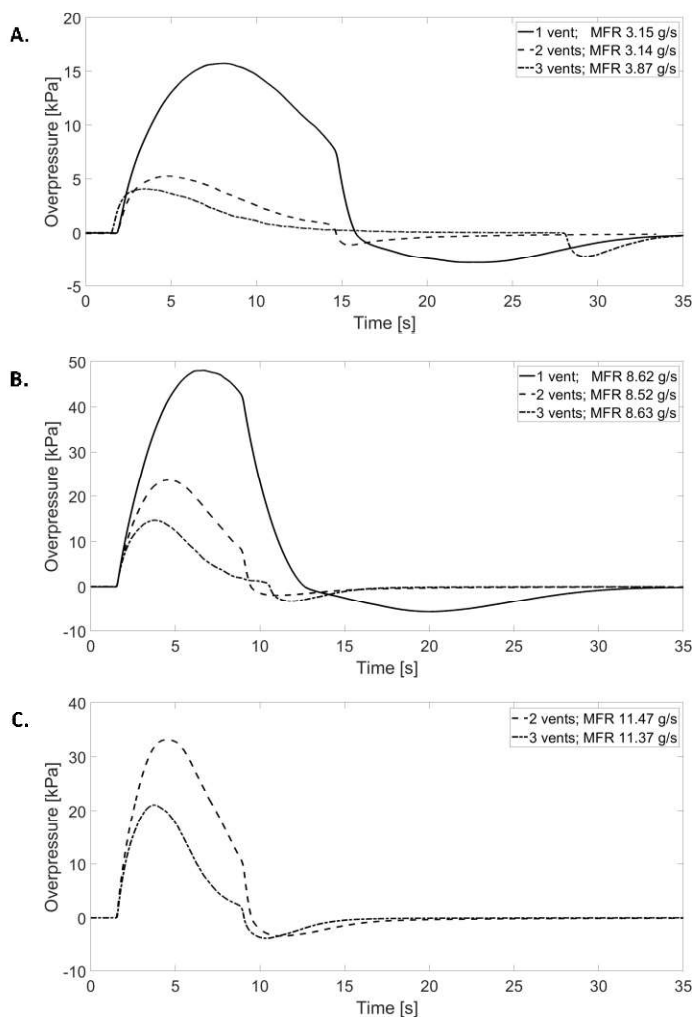


Fig. 8. Overpressures for (A) 3.1–3.9 g/s, (B) ~8.6 g/s, and (C) ~11.4 g/s \dot{m} s at three different ventilation areas, where one open vent = 0.0055 m², two open vents = 0.0109 m², and three open vents = 0.0164 m².

overpressures from a 700 bar tank through a 2 mm nozzle in the 1 m³ enclosure. The model showed that overpressures from ignited hydrogen releases of 107 g/s can be 100 kPa higher with only one brick difference and will destroy the enclosure in less than 10 s.

The experiments from this study showed that, with a higher ventilation area, the overpressures reach lower values and the time of pressure peak ($t(p_{max})$) occurs earlier (Fig. 8). The accepted safe overpressure in enclosures has a threshold of 10–20 kPa (Brennan and Molkov, 2018). During experiments with \dot{m} not higher than 4 g/s, the safe overpressures were obtained with all three ventilation areas ($P_{max} < 20$ kPa); see Fig. 8(A). The ventilation area with two and three open vents gives a pressure below the threshold ($P_{max} < 10$ kPa). For $\dot{m} = 8$ –9 g/s, only three open vents gave overpressures below 20 kPa; see Fig. 8(B). The ventilation area with one open vent showed overpressure over 45 kPa, double the threshold, and further experiments with only one open vent for $\dot{m} \sim 11.5$ g/s have not been performed. For $\dot{m} \sim 11.5$ g/s, the obtained overpressures were over 21 kPa, which is above the thresholds with both ventilation areas (two and three open vents). The pressure peak occurred about 2 to 6 seconds after the hydrogen releases (for unignited experiments, it was 75 to 90 seconds).

For higher ventilation areas, the value of the pressure peak is lower but occurs faster (Fig. 8). This is opposite the results from the unignited experiments, where a higher \dot{m} resulted in a later time for the pressure peak.

In the 14.9 m³ steel-reinforced container with a ventilation area of 0.0165 m² (three open vents), the pressure peak occurs no later than 3 s for each value of tested \dot{m} . This means that the time of maximum pressure ($t(p_{max})$) can be estimated based on ventilation area and enclosure volume (independent of \dot{m}). The pressure drop takes longer than its rise but is still relatively short. The fast pressure drop may cause enclosure collapse and is a danger to the enclosure, surroundings, and human lives.

The comparison of overpressures with hydrogen releases from unignited (Experiment 8) and ignited releases (Experiment 4) are presented in Fig. 9. The hydrogen was released into the same enclosure volume with approximately the same \dot{m} but with different ventilation areas. The hydrogen jet fire resulted in four times higher overpressure than occurred from unignited releases with nine times larger ventilation area.

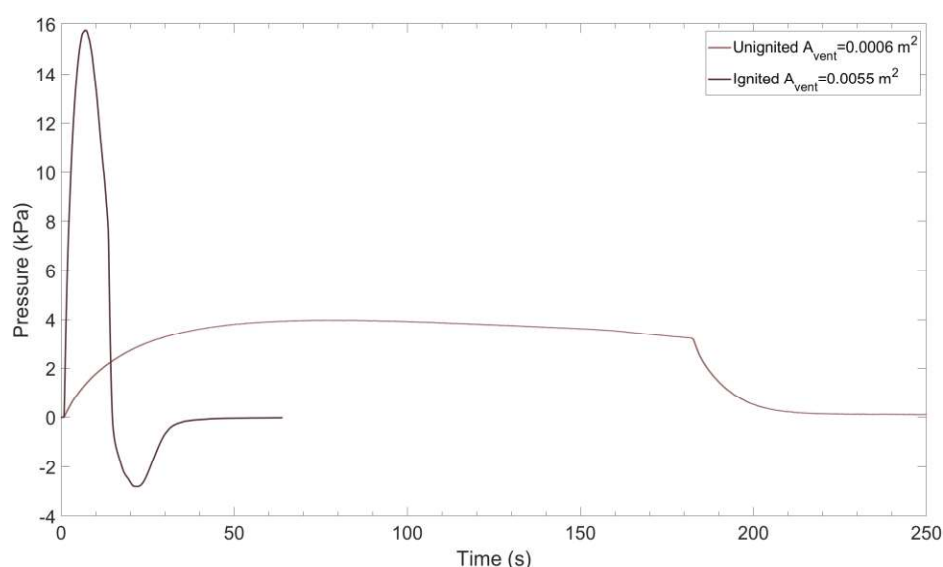


Fig. 9. Pressure peak phenomenon for unignited and ignited releases with $\dot{m} \sim 3.1$ g/s through a 4 mm nozzle.

Hydrogen jet fires cause high overpressure due to the large amount of energy (from the chemical reaction) released in a very short time. Water vapor is the only combustion product. The energy of water formation has the highest influence on the temperature inside the enclosure, hence the overpressure.

The temperature depends on the total amount of energy from combustion and heat loss in the enclosure (as well as the ventilation area):

- The heat loss in the enclosure is the sum of the convective heat loss and the heat loss from vapor condensation at the walls/ceiling. The condensing water increases the heat transfer to the walls. The temperature of the walls is an important factor affecting the condensation rate (Jia et al., 2001) and, at the beginning, was assumed to be equal to the ambient temperature ($\sim 4^{\circ}\text{C}$ for a Norwegian autumn).
- The longer combustion occurred, the higher the maximum temperatures that were obtained (last six experiments).

The pressure peak does not depend on the total amount of burnt hydrogen. It occurs at the beginning of the release of jet fires and drops to a value close to ambient pressure. While combustion continues, the temperatures increase inside the enclosure. After closing the hydrogen release (no jet fire), a rapid decline in the temperature was observed. As a consequence, an underpressure was measured inside

the enclosure. This depended on the total energy released during combustion (total amount of burnt hydrogen) and the change in density inside the enclosure as air from the outside flowed into the enclosure.

The last six experiments investigated the relationship between overpressure and underpressure from the total time of combustion and ventilation area (for the same mass flow rates). The experiments showed that, for the same ventilation area, the pressure peak was the same, independent of the total time of hydrogen combustion (Fig. 10). The underpressure, on the other hand, showed a large dependency on the ventilation area, as also occurred for overpressures and the duration of hydrogen combustion. With a longer combustion duration, the absolute values of the underpressure increased.

Fig. 10 presents the pressure data from the last six experiments. The red curves show the data from the experiments with one open vent, the black curves represent two open vents, and the blue curves are for three open vents. Dashed lines are the short combustion duration experiments (10 s), while the solid line indicates the longer combustion duration (20 s). If we investigate the difference between the overpressures, we see that there is no significant difference between the short and long combustion times. However, the combustion time influences the peak underpressure. In general, longer combustion duration results in a lower absolute pressure in the negative phase.

The two experiments with three open vents show that the difference in underpressure was 1.9 kPa. For the two experiments with two open vents, the difference was 5.2 kPa, and with one open vent, it was 11.2 kPa.

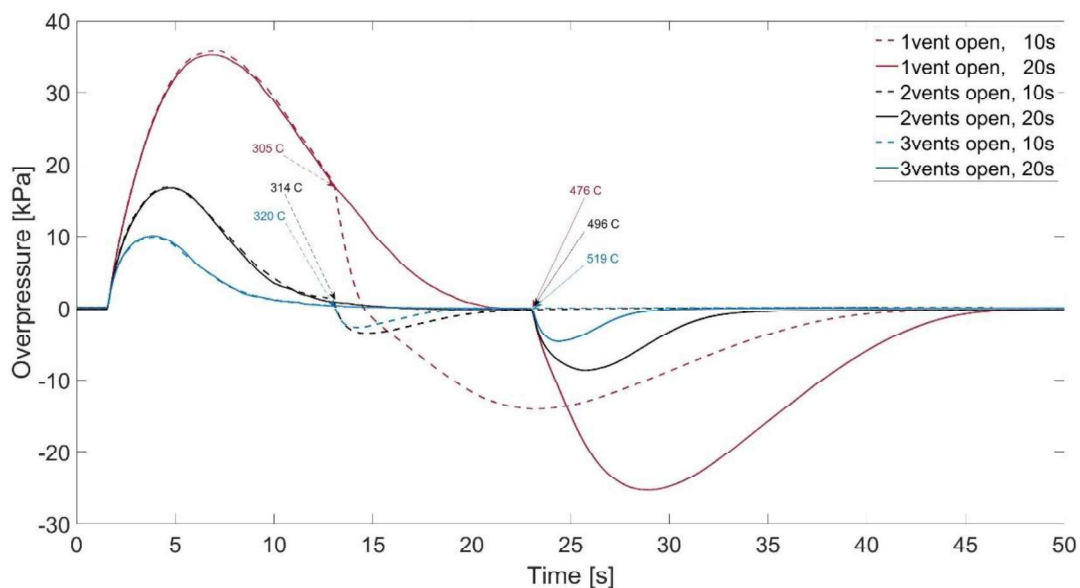


Fig. 10. Overpressures in the 14.9 m³ enclosure during hydrogen releases of 10 s and 20 s with three different ventilation areas at the same $\dot{m} \sim 6.6$ g/s. One open vent = 0.0055 m², two open vents = 0.0109 m², three open vents = 0.0164 m². Experiments 26–31.

4. Conclusions

The pressure peaking phenomenon was validated in large-scale experiments for two cases: ignited and unignited releases:

- Ignited releases result in much higher overpressures, and a larger ventilation area has to be applied.
- With increasing \dot{m} , the value of pressure peak is higher. For ignited releases, it occurs earlier. The opposite results are shown for the unignited experiments, where a higher \dot{m} resulted in a later occurrence for the pressure peak.
- The heat loss is a significant factor and cannot be neglected when designing an engineering tool.

- Ignited releases result in underpressure after closing the hydrogen discharge, creating additional hazards to the enclosure, surroundings, and human lives.

Further investigations into hydrogen releases (ignited and unignited) with a blowdown mass flow type from a 700-bar tank are scheduled for later this year (2020). The heat loss investigation and detailed modeling will be an integral focus of further studies.

Acknowledgments

The authors wish to acknowledge funding from the Fuel Cells and Hydrogen 2 Joint Undertaking (JU) under grant agreement No 826193. The JU receives support from the European Union's Horizon 2020 research and innovation programme and United Kingdom, Germany, Greece, Denmark, Spain, Italy, Netherlands, Belgium, France, Norway, Switzerland.

This work was performed within MoZEES, a Norwegian Centre for Environment-friendly Energy Research (FME), co-sponsored by the Research Council of Norway (project number 257653) and 40 partners from research, industry, and the public sector.

References

- Aarskog, Fredrik G, Olav R Hansen, Trond Strømgren, and Øystein Ulleberg. 2020. "Concept Risk Assessment of a Hydrogen Driven High Speed Passenger Ferry." *International Journal of Hydrogen Energy* 45(2): 1359–72.
<http://www.sciencedirect.com/science/article/pii/S0360319919319846>.
- Brennan, S. et al. 2019. "Pressure Effects of an Ignited Release from Onboard Storage in a Garage with a Single Vent." *International Journal of Hydrogen Energy* 44(17): 8927–34.
<https://www.sciencedirect.com/science/article/pii/S0360319918323541> (April 5, 2019).
- Brennan, Sile, and Vladimir Molkov. 2018. "Pressure Peaking Phenomenon for Indoor Hydrogen Releases." *International Journal of Hydrogen Energy* 43(39): 18530–41.
<https://www.sciencedirect.com/science/article/pii/S0360319918326375> (April 3, 2019).
- European Parliament. 2010. "COMMISSION REGULATION (EU) No 406/2010 of 26 April 2010 Implementing Regulation (EC) No 79/2009 of the European Parliament and of the Council on Type-Approval of Hydrogen-Powered Motor Vehicles." *Official Journal of the European Union* (2).
- Fuster, Béatrice et al. 2017. "Guidelines and Recommendations for Indoor Use of Fuel Cells and Hydrogen Systems." *International Journal of Hydrogen Energy* 42(11): 7600–7607.
- Gupta, Sanjeev, Jerome Brinster, Etienne Studer, and Isabelle Tkatschenko. 2009. "Hydrogen Related Risks within a Private Garage: Concentration Measurements in a Realistic Full Scale Experimental Facility." *International Journal of Hydrogen Energy* 34(14): 5902–11.
<https://www.sciencedirect.com/science/article/pii/S0360319909003759> (March 27, 2019).
- Hussein, H.G. et al. 2018. "Numerical Validation of Pressure Peaking from an Ignited Hydrogen Release in a Laboratory-Scale Enclosure and Application to a Garage Scenario." *International Journal of Hydrogen Energy* 43(37): 17954–68.
<https://www.sciencedirect.com/science/article/pii/S0360319918323784> (April 3, 2019).
- Jia, L. et al. 2001. "Effects of Water Vapor Condensation on the Convection Heat Transfer of Wet Flue Gas in a Vertical Tube." *International Journal of Heat and Mass Transfer* 44(22): 4257–65. <https://www.sciencedirect.com/science/article/pii/S0017931001000825> (January 28, 2020).
- Lach, Agnieszka Weronika. 2019. *Pressure Peaking Phenomena-Unignited Releases. Report Experiments*. USN
- Makarov, D., V. Shentsov, M. Kuznetsov, and V. Molkov. 2018. "Pressure Peaking Phenomenon:

Model Validation against Unignited Release and Jet Fire Experiments.” *International Journal of Hydrogen Energy* 43(19): 9454–69.

<https://www.sciencedirect.com/science/article/pii/S0360319918309911> (April 11, 2019).

Papanikolaou, E.A. et al. 2010. “HySafe SBEP-V20: Numerical Studies of Release Experiments inside a Naturally Ventilated Residential Garage.” *International Journal of Hydrogen Energy* 35(10): 4747–57. <https://www.sciencedirect.com/science/article/pii/S0360319910002715> (April 1, 2019).

Stephenson R. 2005. “Fire Safety of Hydrogen-Fueled Vehicles : System-Level Bonfire Test.” *Ichs* (September).

Sunderland, P. 2008. “Pressure Relief Devices for Hydrogen Vehicles.” *3rd european summer school in hydrogen safety, Belfast, UK*: 1–29.

Proceeding D

**Thermal effects from downwards hydrogen impinging jet flame
– experimental results from high-pressure releases in a carpark**

A.W. Lach, A.V. Gaathaug and K.Vågsæther

This paper was submitted to the 10th International Seminar on Fire and
Explosion Hazards on the 10th January 2022

Thermal effects from downwards hydrogen impinging jet – experimental results from high-pressure releases in a carpark.

Lach A.W* , Vaagsaether K., Gaathaug A.V

University of South-Eastern Norway, Department of Process, Energy and Environmental Technology, Porsgrunn, Vestfold and Telemark, Norway.

**Corresponding author's email: Agnieszka.Lach@usn.no*

ABSTRACT

The study of hydrogen releases from high-pressure storage systems is important for practical applications for 1) hydrogen driving vehicles: technology and safety, and 2) validation of computational fluid dynamic models. The focus of this paper is on accidental releases that occur due to for example a failure of the TPRD (thermal pressure-activated relief device) with immediate ignition. The physics and dynamics of such releases have to be understood and the importance of the resulted effects needs to be implemented into the development of RCS (regulations, codes, and standards) and mitigation systems. In this paper the real scale experimental results are presented. Releases from the hydrogen tank with storage pressure 350 and 700 bar through 0.5 mm and 1.0 mm diameter into a container with an installed forced ventilation system are presented. The thermal effects resulting from a different angle of the TPRD exhaust pipe were tested. The resulting hydrogen jet fires showed direct dependence on the mass flow rates. Higher mass flow rates resulted from the bigger TPRD diameter or higher storage pressure caused higher temperatures in the ventilation pipe and in the container. A more detailed analysis of the thermal consequences related to TPRD size, storage pressure, and ventilation rate is presented. Results from all the experiments showed temperatures below specified in the regulations, 300 °C, in the ventilation pipe. Low temperatures measured at the front of the car and high temperatures behind will be used for the mitigation strategies and first response guidance. Generally decreasing TPRD diameter to 0.5 mm decreased max temperature behind the car from 500 °C to 250 °C from the same storage pressure, and decreasing harm distance.

KEYWORDS: Hydrogen safety, impinging H₂ jet, thermal effects, compressed hydrogen, jet fire,

INTRODUCTION

The change in the transportation system from conventional vehicles (gasoline, diesel, LPG) to zero-emission vehicles (battery/hydrogen driven or hybrid) needs a reevaluation of the mitigation system used today. The consequences of accidental hydrogen releases from a high-pressure tank (commonly used from 200 bar to 700 bar) varied from conventional ones. Hence the Regulation Codes and Standards (RCS) which remain unchanged in many aspects of fire safety engineering need to be reevaluated.

The hydrogen cars are equipped with a thermally activated relief device (TPRD) in order to avoid tank rupture in case of exposure to fire. Other causes of the TPRD activation can be a collision with another car/object or a failure of the TPRD. One of the scenarios (study presented in this work) is that released hydrogen will automatically ignite, creating a jet flame. In closed or semi-closed enclosures the thermal and pressure effects of jet flames are greater than in the open air. The size and direction of the jet flame are determined by the tank pressure; the size of the TPRD opening, and the direction of the released hydrogen.

The experimental investigation described in this paper was focusing on comparing the temperature effects resulting from the turbulent hydrogen jet fires to existing RCS (human factors and principle to the building design). The temperature tolerance limit for unprotected skin (in the literature) varied depending on the water concentration in the atmosphere. The time limits of exposure to convected heat with less than 10% H₂O is 5 min for 115 °C and up to 30 min for 68 °C according to BSI PD 7974-6:2004 and CFWA_E Guidelines No19 [1,2]. The same limits were described in a book of

Fundamentals of Hydrogen Safety Engineering [3]. The temperature limit for the saturated atmosphere is 60 °C for no longer than 30 min. In different sources (ISO/TR 16576:2017 considering open jets) the 45 °C was the pain limit [4]. The study on the skin burns with exposure to hot water resulted in less than 10 min exposure time for 50 °C water temperature causing injury which will not fully recover within 21 days [5]. The same pain limits are given in several sources [6–8].

In a building like a carpark, the temperature limitation is 300 °C classified as class F300 [9,10]. The required ventilation system varied from 3 air changes per hour (ACH) with natural ventilation possibilities (2.5% of the floor area), 6 ACH for carpark which don't have natural ventilation and 10 ACH when the cars in a carpark stay in a queue with running engine.

The prediction of the flame length and resulting thermal effects can be used to increase the effectiveness of fire protection measures. Previous work described mainly vertical and horizontal jets [11–17] while impinging jets are investigated in a few studies [18,19]. The experimental results with turbulent hydrogen jet impinging with the floor from short distances are not available to the authors' knowledge. Experimental investigation of hydrogen jet fires presented in [19] focused on horizontal impinging jets with a barrier wall used as a mitigation technique. The hydrogen jet was impinging 90° with the wall. The most effective mitigation method was to use a three wall (135°) configuration. Experimental results from horizontal high-pressure hydrogen fires [17] were used to validate the simulation of thermal hazards presented by Cirrone et al.[14]. Short time hydrogen releases from 900 bar through 2.0 mm nozzle resulted in temperature from 200 °C to 1500 °C depending on the sensor location.

The TPRD in personal cars is usually placed under the car with a 45° exhaust pipe 25 cm above the floor. The CFD study investigated hydrogen dispersion from impinging jets with the floor from different angles in a carpark and vertical jets [20]. Three TPRD diameters were compared resulting in a smaller flammable cloud from releases through 0.5 mm and 45° compared to higher diameters and releases through 0° and 30°. The simulations were done in a scenario with natural ventilation. The authors continued their investigation on hot gases from ignited hydrogen jets [21]. Results showed that downward hydrogen jet flames through 30° and 45° exhaust pipes were safer for 0.5 mm TPRD diameter and recommendation for experiments was suggested.

In the present article, the investigation of thermal effects resulting from the under-expanded hydrogen jet fire impinged with the floor is presented based on the experimental work. The large-scale carpark geometry and instrumentation setup are described in detail. The goal of this work is to investigate the temperature effects from under-expanded hydrogen jet fires and to develop recommendations for the Regulation Codes and Standards (RCS) for the safe use of hydrogen vehicles in the enclosed transportation system. The study was part of the HYTUNNEL-CS European project sponsored by FCH-JU. The produced experimental data, presented in this work, will be used for benchmarking studies using CFD codes.

The thermal characteristics near the hydrogen jet fire resulting from the activation of TPRD are important for the escape possibilities not only for the passengers of the car but people around as well. The information about temperature effects can be used by firefighters and construction engineers. One of the most important uses of data presented in this work will be to validate the models for the thermal effects resulting from 45° impinging hydrogen jet fires with the floor. To the author's knowledge, no other experimental test on such a impinging jet fires were performed in a underground car park scenarios. The model validation is not part of the work presented in this study.

JET FIRE EXPERIMENTS

In this section, the detailed description of the experimental setup and instrumentation is presented first. Then the results are discussed and analyzed.

Experimental setup

All experiments were carried out in a 40 ft ISO container (summer 2021). The container had isolated walls and inner dimensions of LxWxH: 11.885 x 2.240 x 2.285 m gives a total volume of 60.8 m³ (Fig. 1). The walls and ceiling isolation thickness was approximately 0.07 m. On the floor were mounted cement-based, non-combustible building plates, 6 mm thick. After the first two experiments, two extra layers were added to protect the container floor from burning, those layers were replaced after each second experiment. To compare dimensions, the real-scale carpark/underground parking has the standard 2.25 m minimum free height accordingly to Norwegian Standard [22].



Fig. 1. Container and instrumentations

The table imitating a hydrogen car was scaled against the Toyota Mirai with a scaling factor of 0.4 resulting in dimensions: LxWxH: 1.965 x 0.73 x 0.25 m. The table, further called ‘car’, consists of steel legs and a 1 mm steel plate. The hydrogen outlet was mounted vertically through the steel plate. For the first two experiments, hydrogen was vertically discharged (90°) with a nozzle 230 mm above the floor (Fig. 2 left). For the rest of the experiments, hydrogen was discharged with a 45° nozzle, 180 mm above the floor (Fig. 2 right). All but one experiment were conducted with a 0.5 mm nozzle. The last experiment was conducted with a 1.0 mm nozzle.



Fig. 2. Nozzle: left 90°, right 45°.

A Hexagon type IV hydrogen tank (operating pressure up to 700 bar) with a carbon composite wall was used during all experiments (36.8 l). The hydrogen was compressed from a 200 bar hydrogen pack consisting of 12 hydrogen bottles. All pipes were 6x1.5 mm 316 steel with ID 3.0 mm.

The ventilation outlet with ID 315 mm was located 0.050 m from the ceiling (0.2075 m from the ceiling to centre) on the ventilation wall (Fig. 3). The ventilation pipe consists of two sections, 4 m long in total. One section with 0.315 m diameter pipe with outlet into the container and second section with 0.2 m diameter with airfan at the end. The ventilation was suction-type ventilation provided from an air fan.

Before the hydrogen ignition, a small propane pilot flame was ignited. The hydrogen was released into the propane flame and hence automatically ignited. The thermal effect from the propane flame is assumed to be negligible (propane flame was shut down seconds after hydrogen ignited).

Instrumentation

For the mass flow measurements the coriolis mass flow meter, model HPC010P ultra-high pressure from Emerson Micromotion with connected transmitter model 5700 with a pressure range up to 1043 bar was used during all experiments. The total pipe length from the hydrogen tank to the nozzle was 3.86 m. At the tank outlet, a pressure transmitter ESI model HP1003-1000DE with a pressure range from 0 to 1000 barg was installed. The same type of pressure transmitter was mounted at the outlet of the coriolis mass flow meter.

The airflow rate was controlled by an IRIS 200 damper and voltage speed controller for the fan. The air change per hour (ACH) for the experiments was according to BSI 7346-7:2013 [9]: 10 ACH and 6 ACH. The airflow was measured by the differential pressure of the IRIS 200 damper with the GAMS Sensor differential pressure transmitter model 5266. For the container geometry that means 608 m³/h and 365 m³/h for 10 and 6 ACH respectively.

10 sensors were installed to measure temperature change during experiments: 9 thermocouples inside the container and 1 in the ventilation pipe. All 10 thermocouples were fast response Type ‘K’ thermocouples with grounded hot junction. The sensor locations are presented in Fig. 3 and Table 1.

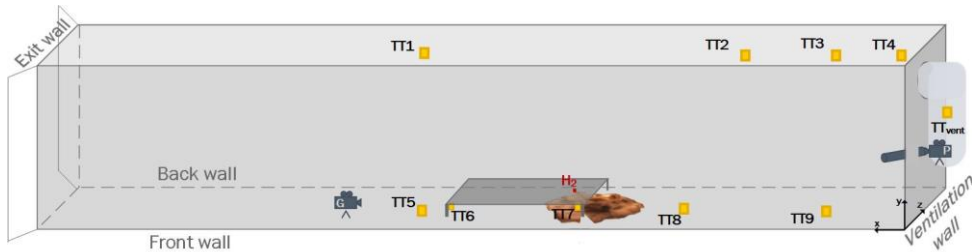


Fig. 3. Thermocouples locations inside the 40 ft container and ventilation pipe.

Four thermocouples (TT1-TT4) were mounted 180 mm from the ceiling along the centre axis ($z=1120$ mm) to measure temperature change under the ceiling and the effect of ventilation rate. Two thermocouples were mounted in the corners under the car (close to the ‘wheels’) at the front (TT6) and in the back (TT7) of the car. Three thermocouples were mounted at the front wall: 735 mm at the front of the car (TT5), and two behind the car: 1190 mm and 3470 mm (TT8 and TT9 respectively) (Fig. 3). The temperature inside the ventilation pipe was measured 510 mm from the top of the pipe and 130 mm from the pipe wall.

Table 1. Location parameters [mm]

	y	x	z
TT1	2105	6250	1120
TT2	2105	2320	1120
TT3	2105	1060	1120
TT4	2105	110	1120
TT5	235	7200	80
TT6	198	6330	868
TT7	200	4600	860
TT8	235	3310	74

TT9	235	1030	80
TTvent	1725		130 inside
Nozzle 45	180	4980	1120
Nozzle 90	230	5000	1120
Table	250	4500	755
outlets	2055	0	1120

^a to the centre

The uncertainty of the instrumentation is listed in Table 2. It's important to notice that measurements from all pressure transmitters and mass flow meter were recorded with a sample rate of 2 kHz and temperature measurements with a sample rate of 50Hz.

Table 2. Instrumentation uncertainty.

Instrument	Uncertainty [%]
ESI Pressure transmitter	$\pm 1\%$ FSO BFS _L ¹
GAMS Differential pressure transmitter	$\pm 1\%$ FS ₂
Mass flow	$\pm 0.2\%$ of flow rate
Thermocouples type K	$\pm 0.75\%$

¹ Full scale output Best Fir Straight Line

² Full scale

Results and discussion

During the experiments, hydrogen was discharged from 350 bar and 700 bar, with 6 and 10 ACH. The nozzle directed 90° vertical downwards, was used in the first 2 experiments (700 bar with both ACH). For experiments 3-8 the nozzle was mounted 45° downwards and backwards (towards the ventilation wall). Table 3 presents: the parameters of the experiments; climatic conditions; initial pressure in the tank and initial mass flow rate and initial mass flow rate estimated with e-laboratory from Net-Tools [23] with under-expanded jet model [11], resulted from experimental initial tank pressure.

Table 3. Parameters of jet fire experiments

Exp Nr	Nozzle angle [°]	Nozzle diameter [mm]	Air change per hour [1/h]	Ambient temp [°C]	Initial tank pressure [bar]	Initial mass flow rate [g/s]	Net-Tools Initial mass flow rate [g/s]	Blowdown duration [s]
1	90	0.5	10	22	708	7.3	6.7	450
2	90	0.5	6	19	695	7.5	6.6	80
3	45	0.5	6	23	357	4.0	3.8	500
4	45	0.5	6	22	698	7.4	6.7	500
5	45	0.5	10	22	690	7.3	6.6	500
6	45	0.5	10	19	357	4.1	3.8	500
7	45	0.5	6	19	360	4.0	3.9	500
8	45	1.0	6	15	357	13	15.2	367

Experiments were recorded with Promon 500 high-speed camera from AOS technologies AG. Video frames from 4 different experiments showing hydrogen jet fires from both diameters, both initial

pressures, and both nozzle angles illustrate the flame development during the blowdown releases (Fig. 4). One layer with a fire-resistance plate was insufficient to protect the floor during experiments with 90° nozzle (the rest experiments had 3 layers). Due to cracks formed in the fire-resistance plates when exposed to the jet fire, the wooden floor beneath them caught fire. The visible fire from the burning floor can be seen after 300 s on Fig. 4, last row. The exp 2 had to be stopped after 80 s due to fire (floor and walls).

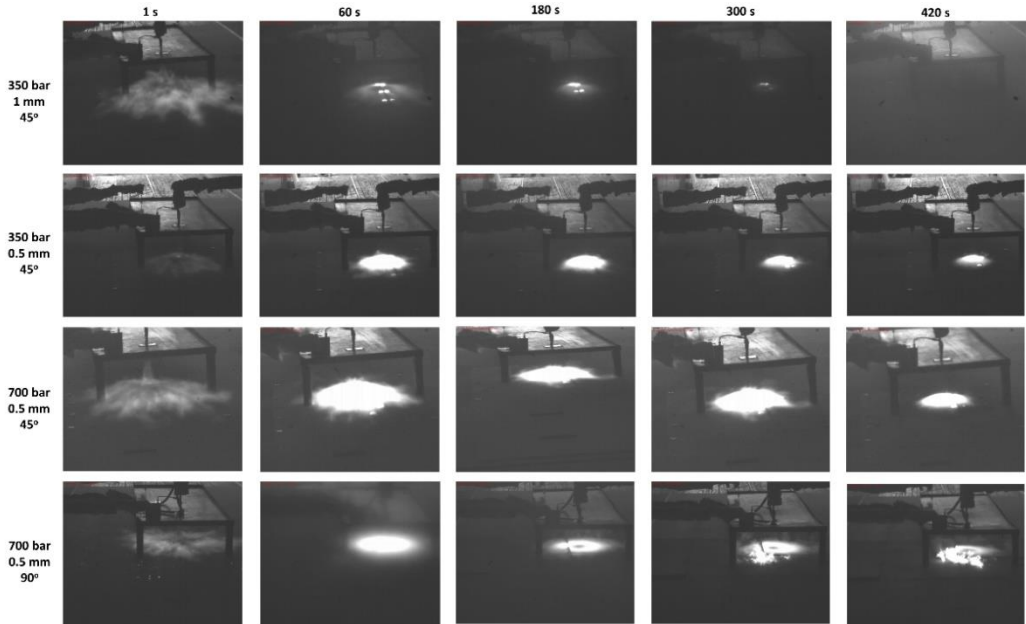


Fig. 4. Flame development from Exp.8 (top row), Exp.7 (second row), Exp.4 (third row), and Exp.1 (bottom row).

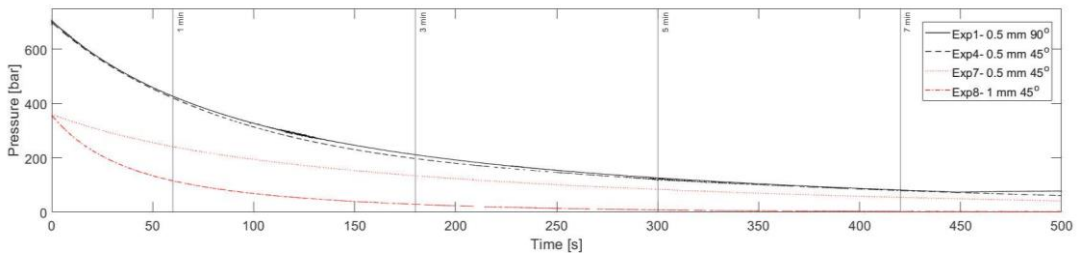


Fig. 5. Tank pressure during blowdown from Exp.1 (solid line), Exp.4 (dashed line), Exp.7 (dotted line), and Exp.8 (dot-dash line).

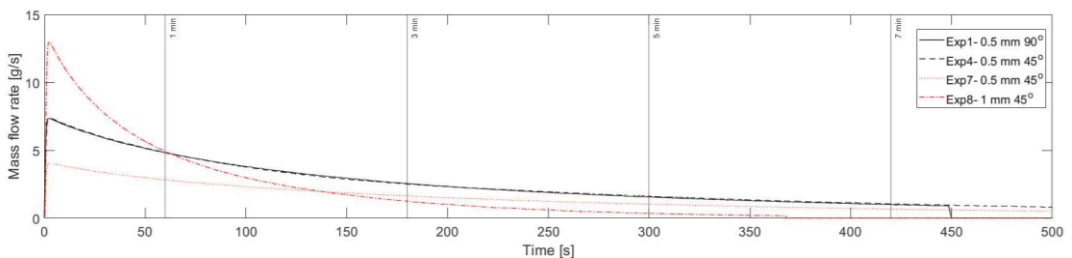


Fig. 6. Hydrogen mass flow rate during blowdown from Exp.1 (solid line), Exp.4 (dashed line), Exp.7 (dotted line), and Exp.8 (dot-dash line).

The hydrogen jet fire length is depending on the mass flow rate (\dot{m}) and nozzle diameter (D) [11,16]. That is why releases from 700 bar through 0.5 mm nozzle and 350 bar through 1 mm nozzle resulted in the largest impingement area. Higher mass flow rates due to higher initial tank pressure and larger nozzle diameter can be seen in Fig. 5 and Fig. 6. The novel dimensionless flame correlation [11] includes the $\dot{m} \propto D^2$ which means the mass flow rate from 350 bar through 1 mm nozzle should have ~16 g/s initial mass flow rate (not 13 g/s as was measured) compared to 4 g/s resulting during releases from 350 bar through 0.5 mm nozzle (confirmed with the results from e-Laboratory – Net-Tools Table 3). The pressure losses in the pipes can be the reason for this discrepancy. The experimental data showed that the variation in the tank pressure and mass flow rate dynamics during blowdown between experiments was low (about 15 bar and 0.09 g/s) for equal initial pressure and nozzle diameter. This can be seen in Fig. 5 and Fig. 6.

The hydrogen is released through higher TPRD diameters faster (Fig. 6) and hence bigger amount of energy is released in a shorter time. The smaller diameter (smaller TPRD diameter) will result in a lower mass flow rate and hence a lower energy rate released during combustion (comparing the same release time).

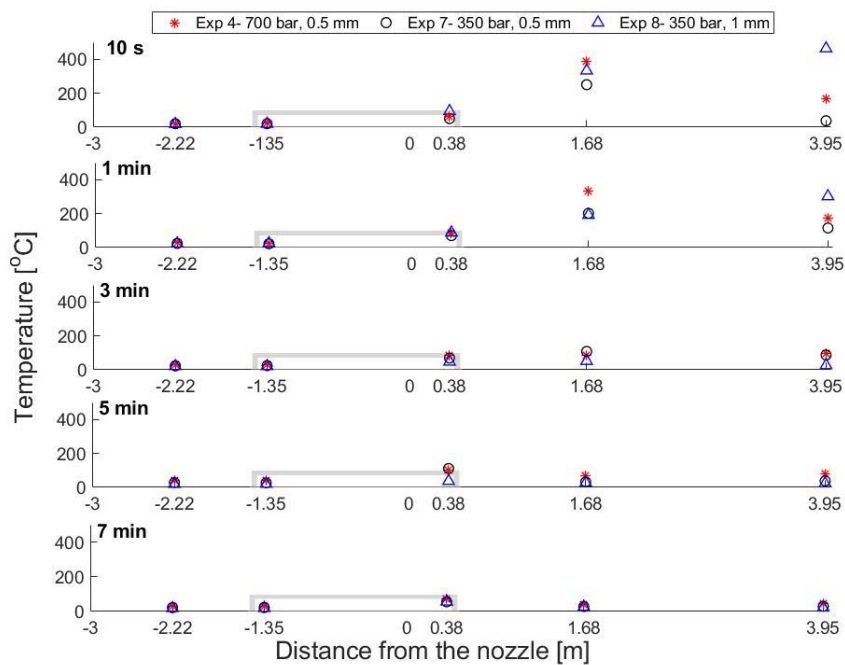


Fig. 7. Comparison of temperature resulted from different initial tank pressure and nozzle diameter (mass flow rates) at five longitudinal positions from the nozzle: TT5(-2.22 m), TT6(-1.35 m), TT7(0.38 m), TT8(1.68 m) and TT9(3.95 m).

The temperature resulted from the releases through 0.5 mm diameter nozzle from 700 bar and 350 bar initial tank pressure and through 1 mm diameter nozzle from 350 bar initial pressure (7.4 g/s- red star, 4.0 g/s- black circle, and 13 g/s- blue triangle respectively) are presented in Fig. 7. All three experiments were performed with the same airflow rate- 6 ACH. On the x-axis, the centre axis longitudinal distance from the nozzle is presented. The temperature at each position at different times is an average temperature in a 0.8 s period (+/- 0.4 s around the given time). Sensors TT6 and TT7, located under the car, in its corners have distances from the nozzle 1.35 m and 0.38 m respectively. The remaining three sensors presented in Fig. 7 were placed at the same height as TT6 and TT7 but on the container walls (inside). The hydrogen jet fire did not increase the temperature in front of the car. This can be seen in the plot of the temperature distribution in Fig 7. The maximum measured

temperature change was 3 °C decreased and 6 °C increased. The change is considered negligible. The temperature measured closest to the jet fire (TT7) was very similar for all three releases and did not exceed 110 °C. Since the hydrogen release during Exp.8 ended after 350 s (the tank was empty) the temperature after 5 min at the distance 0.38 m was lower than from two other experiments at the same time and position.

All those three experiments were performed with a nozzle angle of 45°. That is why the highest temperature was measured behind the car (closer to the ventilation wall). The largest difference between experiments was also measured behind the car. As was expected, and observed from Fig. 4 the highest temperatures were measured for Exp.4 and Exp.8. What distinguishes thermal effects from these two experiments is the location where the highest temperature was measured. For the smaller TPRD diameter (0.5 mm) the highest temperature was measured closer to the car – 1.68 m from the release source and 1.18 from the car for the first 3 min. After that, the temperature measured 3.95 m from the car was close to the temperatures behind the car, and all of them were less than 105 °C. Nevertheless, at both locations, the temperature decreased to 26 degrees after 7 min (Exp.4 and Exp.7). Comparing temperatures measured at 1.68 m location to Exp.8 with releases through 1 mm TPRD diameter, after 10 s the temperature was 50 °C higher for Exp.4 than for Exp.8 but did not exceed 400 °C for any of the experiments. The temperature measured at 3.95 m from the release source was highest for Exp.8 (Fig. 8, TT9). After 10 s the temperature exceeds 450 °C which is almost three times higher than for Exp.4 and 12 higher than Exp.7, at the same position. Nevertheless, the temperature decreased faster than the other two experiments and after 3 min it reached 50 °C and 25 °C at 1.68 m and 3.95 m respectively.

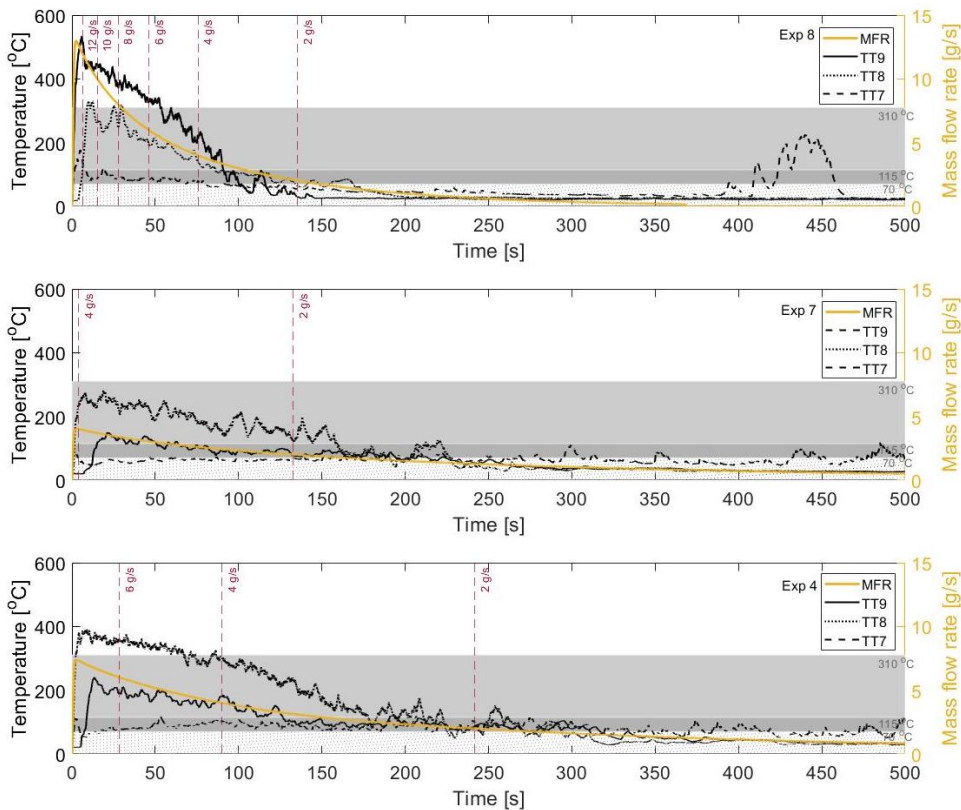


Fig. 8. Temperature behind the TPRD vs time, 0.38 m, 1.68 m and 3.95 m behind the TPRD – TT7, TT8, and TT9 respectively.

The pain limits accordingly to several standards and guidelines [1–3] is 115 °C for no longer than 5 min exposure to convected heat. The 70 °C is considered as no harm limit [21], in other sources is less than 60 °C for 100% saturated air. After 4 min the temperatures presented in Fig. 8 did not exceed 115 °C. Fig. 8 shows that the temperature exceeded the 310 °C harm limit for both Exp.8 (1 min) and Exp.4 (2 min).

The heat transfer to the skin occurs faster in presence of water. While exposure to hot liquid water over 60 °C will cause 2nd-degree burns after 3 s and 3rd-degree burns in 5 s [24]. The tenability limits for hydrogen fire exposure should include the water saturation level in the air since the combustion product consists only of water. The humidity measurements are recommended for the next investigation stage and to be included in the analytical model for the heat transfer to human skin.

The temperature measurements under the ceiling (Fig. 9) showed that hot combustion products were ventilated from the container in both directions: through the vent with forced ventilation and the exit door. The temperature measured at the front and 1.855 m above the car (Fig. 9, TT1) did not differ from temperatures measured closer to the ventilation wall, behind the car (Fig. 9, TT2-TT4).

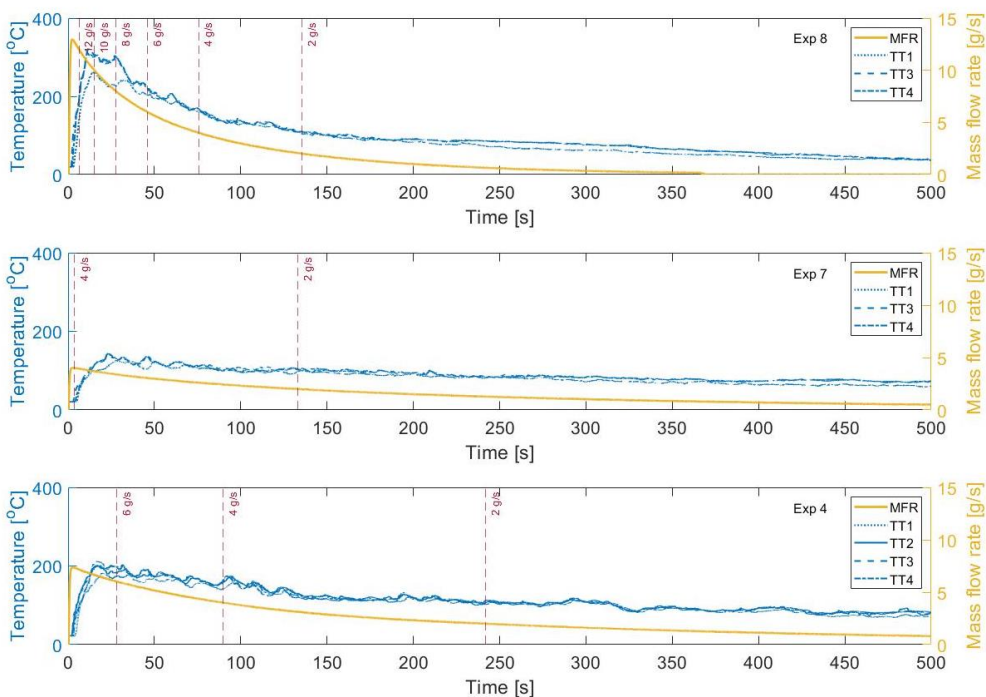


Fig. 9. The temperature under the ceiling vs time.

The temperature under the ceiling did not exceed 300 °C during experiments with 0.5 mm as the limit presented British and Dutch standards [9,10] but is important to notice that the presented temperatures are results from hydrogen jet fires only. The combustion products and their thermal effect from burning car and soundings are not included in the presented experiments.

The 6 and 10 ACH were investigated since they are the minimum requirements given by standards [9] together with the 300 °C maximum temperature in the ventilation criteria. In the BS 2013 the minimum ACH for car parks with natural and forced ventilation is 3 ACH which was considered too low for the geometry used in this work. The effect of forced ventilation is presented in Fig. 10.

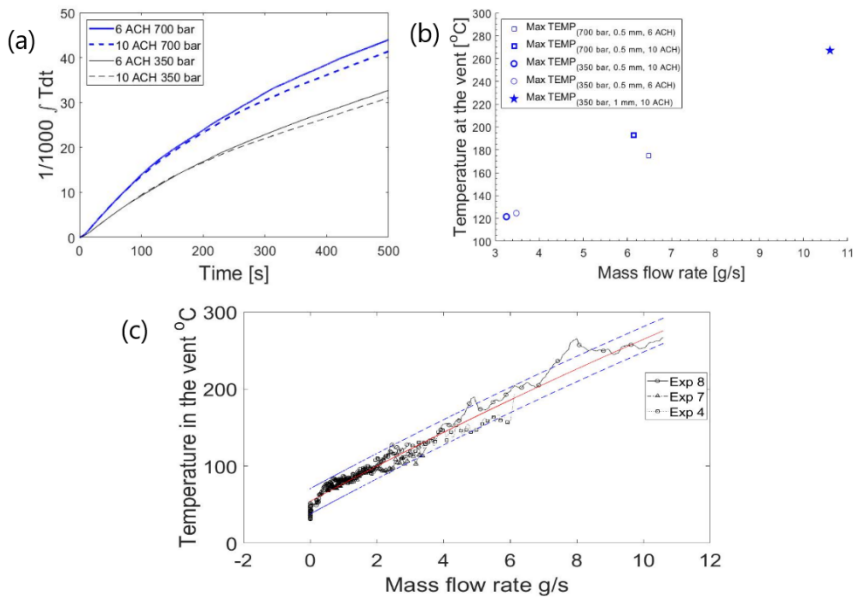


Fig. 10. Temperature effect in the ventilation pipe

Experiments with releases from 350 bar and 700 bar storage pressure (through 0.5 mm 45° nozzle) were used to compare the effect of a forced ventilation system on ventilating hot products through the ventilation pipe. Increasing the ventilation rate from 6 to 10 ACH decreased temperature inside the ventilation pipe by 3.3% and 6.9% for releases through 0.5 mm nozzle from 700 bar and 350 bar respectively (Fig. 10, a). The highest temperature measured in the ventilation pipe was for the experiments with the highest mass flow rate (Fig. 10, b). Which is the outcome of the conclusion that the higher the hydrogen mass flow rate higher the released energy from the combustion. Due to heat loss to the walls in the ventilation pipe, the measured temperatures were ~20 °C lower than temperatures measured under the ceiling (inside the container). That means the temperature in the ventilation pipe did not exceed the maximum requirements given in standards and can also be assumed equal to the temperature of hot products under the ceiling (too simplified calculation purposes). The temperature is depending on the hot products hence the hydrogen mass flow rate. The relation between mass flow rate to the temperature measured from Exp.4, Exp.7, and Exp.8 is presented in Fig. 10, c. Once again results showed the higher the mass flow rate, the higher the temperature. Temperature resulting from given mass flow rate was almost constant, little depended on starting conditions. This can be observed in Fig. 10,c, where the red line presents a first-degree polynomial fit and blue dash lines a 95% prediction interval.

CONCLUSION

In this paper, the authors described the large scale experimental results conducted in June 2021 in Norway. The scenarios with ignited hydrogen releases from 1.0 mm and 0.5 mm TPRD diameter through 90° and 45° exhaust pipe were investigated. The hydrogen was released from the tank (initially 350 bar or 700 bar) into an enclosure imitating a carpark with two ventilation rates: 6 and 10 ACH. The obtained experimental data showed the relation between TPRD diameter and resulted temperature change inside the enclosure and ventilation pipe. The results show that the temperature in the ventilation system increases with the increase of hydrogen mass flow rate i.e. increase in TPRD diameter and/or storage pressure. Nevertheless, the temperature did not exceed 300 °C in the ventilation pipe during releases through both 1.0 mm and 0.5 mm nozzle diameter. The temperature limit under the ceiling was not exceeded during releases from 0.5 mm.

Most of the study focused on the 45° TPRD release. The temperature development around the car, showed a possible safe approach towards the front of the car. The biggest variation in temperature among the experiments was observed behind the car. The increase in TPRD diameter increased the measured temperature at the longest distance from the nozzle. Releases from higher storage pressure through the same TPRD diameter resulted in higher temperatures measured at the same location.

Decreasing the TPRD diameter results in a lower maximum temperature but a longer duration of blowdown. The consequence is an increase in the duration of high temperatures around the car which may cause 1st, 2nd and 3rd burn degrees. A solution concerning all possible consequences is needed in order to ensure safety around the hydrogen personal cars in case of unwanted hydrogen jet flames.

ACKNOWLEDGMENTS

The authors wish to acknowledge funding from the Fuel Cells and Hydrogen 2 Joint Undertaking (JU) under grant agreement No 826193. The JU receives support from the European Union's Horizon 2020 research and innovation programme and United Kingdom. Germany. Greece. Denmark. Spain. Italy. Netherlands. Belgium. France. Norway. Switzerland.

This work was performed within MoZEES, a Norwegian Centre for Environment-friendly Energy Research (FME), co-sponsored by the Research Council of Norway (project number 257653) and 40 partners from research, industry, and the public sector.

REFERENCES

- [1] British Standard PD 7974-6:2004. Application of Fire Safety Engineering Principles to the Design of Buildings. Part 6: Human factors: Life safety strategies — Occupant evacuation, behaviour and condition (Sub-system 6) 2004.
- [2] CFPA-E Guideline No 19:2009 F. Fire safety engineering concerning evacuation from buildings 2009.
- [3] Molkov V. Fundamentals of Hydrogen Safety Engineering I. vol. 4. 2012. <https://doi.org/10.1016/B978-0-08-087872-0.00418-2>.
- [4] ISO/TR 16576:2017. Fire safety engineering — Examples of fire safety objectives, functional requirements and safety criteria 2017.
- [5] Christine Julie Andrews. Validating the relationship between burn temperature, duration of exposure and tissue injury severity for scald burns . The University of Queensland, 2017.
- [6] Loo YL, Haider S, PY YL, Jeffery S. Predictor of the depth of burn injuries: A time and temperature relationship review. *Int J MedicalScience Clin Invent* 2018;5:4119–28. <https://doi.org/10.18535/ijmsci/v5i11.01>.
- [7] Moritz AR, Henriques FC. Studies of Thermal Injury: II. The Relative Importance of Time and Surface Temperature in the Causation of Cutaneous Burns. *Am J Pathol* 1947;23.
- [8] Gottuk, D. R Hall. John, Kazunori, H. Kuligowski, E. Puchovsky, M. Torero, J. Watts J.M. Wieczorek C. SFPE Handbook of Fire Protection Engineering. 5th ed. Springer; n.d.
- [9] BSI Standards Publication BS 7346-7:2013. Components for smoke and heat control systems – Part 7: Code of practice on functional recommendations and calculation methods for smoke and heat control systems for covered car parks 2013.
- [10] Nederlandse praktijkrichtlijn NPR 6095-1 (nl). Smoke and heat control systems - Part 1: Guidelines on design and installation of smoke and heat exhaust installations and smoke control systems in car parks 2012.
- [11] Molkov V, Saffers J-B. Hydrogen jet flames. *Int J Hydrogen Energy* 2013;38:8141–58. <https://doi.org/10.1016/J.IJHYDENE.2012.08.106>.
- [12] Middha P, Hansen OR. CFD simulation study to investigate the risk from hydrogen vehicles in tunnels.

Int J Hydrogen Energy 2009;34. <https://doi.org/10.1016/j.ijhydene.2009.02.004>.

- [13] Palacios A, García W, Rengel B. Flame shapes and thermal fluxes for an extensive range of horizontal jet flames. *Fuel* 2020;279. <https://doi.org/10.1016/j.fuel.2020.118328>.
- [14] Cirrone DMC, Makarov D, Molkov V. Simulation of thermal hazards from hydrogen under-expanded jet fire. *Int J Hydrogen Energy* 2019;44:8886–92. <https://doi.org/10.1016/j.ijhydene.2018.08.106>.
- [15] BOUIX D, SAUZEDDE F, MANICARDI P, MARTIN M, FORERO-MORENO D., STUDER E, et al. FULL-SCALE TUNNEL EXPERIMENTS FOR FUEL CELL HYDROGEN VEHICLES: JET FIRE AND EXPLOSIONS. 9th Int. Conf. Hydrog. Saf., 2021, p. 1197–210.
- [16] Schefer RW, Houf WG, Bourne B, Colton J. Spatial and radiative properties of an open-flame hydrogen plume. *Int J Hydrogen Energy* 2006;31. <https://doi.org/10.1016/j.ijhydene.2005.11.020>.
- [17] Proust C, Jamois D, Studer E. High pressure hydrogen fires. *Int J Hydrogen Energy* 2011;36. <https://doi.org/10.1016/j.ijhydene.2010.04.055>.
- [18] Willoughby DB, Royle M. The interaction of hydrogen jet releases with walls and barriers. *Int J Hydrogen Energy* 2011;36. <https://doi.org/10.1016/j.ijhydene.2010.05.077>.
- [19] Schefer RW, Merilo EG, Groethe MA, Houf WG. Experimental investigation of hydrogen jet fire mitigation by barrier walls. *Int J Hydrogen Energy* 2011;36. <https://doi.org/10.1016/j.ijhydene.2010.04.008>.
- [20] Hussein H, Brennan S, Molkov V. Dispersion of hydrogen release in a naturally ventilated covered car park. *Int J Hydrogen Energy* 2020;45:23882–97. <https://doi.org/https://doi.org/10.1016/j.ijhydene.2020.06.194>.
- [21] Hussein H, Brennan S, Molkov V. Hydrogen Jet Fire from a Thermally Activated Pressure Relief Device (TPRD) from Onboard Storage in a Naturally Ventilated Covered Car Park. *Hydrogen* 2021;2. <https://doi.org/10.3390/hydrogen2030018>.
- [22] Standard Norge NS 3940:2012. Areal- og volumberegninger av bygninger. Calculation of areas and volumes of buildings 2012.
- [23] Karlsruhe Institute of Technology (KIT). Net-Tools e-Laboratory jet parameters model. n.d. https://elab-prod.iket.kit.edu/integrated/jet_parameters/input.
- [24] Antiscald. Burn Exposure Chart 2016. http://antiscald.com/index.php?route=information/information&information_id=15.

Co-Article A

The Pressure Peaking Phenomenon for Ignited Under-Expanded Hydrogen Jets in the Storage Enclosure: Experiments and Simulations for Release Rates of up to 11.5 g/s

D. Cirrone, D. Makarov, A.W. Lach, A.V. Gaathaug and V.Molkov



Published in Energies, December 2021, 15(1): 271, doi:

<https://doi.org/10.3390/en15010271>

Author contribute with experimental setup, planning and execution.

Article

The Pressure Peaking Phenomenon for Ignited Under-Expanded Hydrogen Jets in the Storage Enclosure: Experiments and Simulations for Release Rates of up to 11.5 g/s

Donatella Cirrone ^{1,*}, Dmitriy Makarov ¹, Agnieszka Weronika Lach ² , André Vagner Gaathaug ² and Vladimir Molkov ¹ 

¹ HySAFER Centre, Ulster University, Newtownabbey BT37 0QB, UK; dv.makarov@ulster.ac.uk (D.M.); v.molkov@ulster.ac.uk (V.M.)

² Department of Process, Energy and Environmental Technology, Faculty of Technology, Natural Science and Maritime Science, University of South-Eastern Norway, 3918 Porsgrunn, Norway; Agnieszka.Lach@usn.no (A.W.L.); Andre.V.Gaathaug@usn.no (A.V.G.)

* Correspondence: d.cirrone@ulster.ac.uk

Abstract: This work focuses on the experimental and numerical investigation of maximum overpressure and pressure dynamics during ignited hydrogen releases in a storage enclosure, e.g., in marine vessel or rail carriage, with limited vent size area, i.e., the pressure peaking phenomenon (PPP) revealed theoretically at Ulster University in 2010. The CFD model previously validated against small scale experiments in a 1 m³ enclosure is employed here to simulate real-scale tests performed by the University of South-Eastern Norway (USN) in a chamber with a volume of 15 m³. The numerical study compares two approaches on how to model the ignited hydrogen release conditions for under-expanded jets: (1) notional nozzle concept model with inflow boundary condition, and (2) volumetric source model in the governing conservation equations. For the test with storage pressure of 11.78 MPa, both approaches reproduce the experimental pressure dynamics and the pressure peak with a maximum 3% deviation. However, the volumetric source approach reduces significantly the computational time by approximately 3 times (CFL = 0.75). The sensitivity analysis is performed to study the effect of CFL number, the size of the volumetric source and number of iterations per time step. An approach based on the use of a larger size volumetric source and uniform coarser grid with a mesh size of a vent of square size is demonstrated to reduce the duration of simulations by a factor of 7.5 compared to the approach with inflow boundary at the notional nozzle exit. The volumetric source model demonstrates good engineering accuracy in predicting experimental pressure peaks with deviation from −14% to +11% for various release and ventilation scenarios as well as different volumetric source sizes. After validation against experiments, the CFD model is employed to investigate the effect of cryogenic temperature in the storage on the overpressure dynamics in the enclosure. For a storage pressure equal to 11.78 MPa, it is found that a decrease of storage temperature from 277 K to 100 K causes a twice larger pressure peak in the enclosure due to the pressure peaking phenomenon.

Keywords: the pressure peaking phenomenon; ignited hydrogen releases; jet fire; enclosure; cryogenic releases; experiments; CFD model



Citation: Cirrone, D.; Makarov, D.; Lach, A.W.; Gaathaug, A.V.; Molkov, V. The Pressure Peaking Phenomenon for Ignited Under-Expanded Hydrogen Jets in the Storage Enclosure: Experiments and Simulations for Release Rates of up to 11.5 g/s. *Energies* **2022**, *15*, 271. <https://doi.org/10.3390/en15010271>

Academic Editor: Ali Turan

Received: 30 November 2021

Accepted: 27 December 2021

Published: 31 December 2021

Publisher's Note: MDPI stays neutral with regard to jurisdictional claims in published maps and institutional affiliations.



Copyright: © 2021 by the authors. Licensee MDPI, Basel, Switzerland. This article is an open access article distributed under the terms and conditions of the Creative Commons Attribution (CC BY) license (<https://creativecommons.org/licenses/by/4.0/>).

1. Introduction

The number of fuel cell hydrogen vehicles (FCHV) worldwide is growing and their use in day-to-day life is a reality [1]. A level of safety comparable or higher than fossil fuel vehicles should be provided for FCHV. Thus, all credible incident scenarios involving an FCHV shall be considered and analysed. The parking of a passenger car in a residential garage is a typical scenario. The majority of onboard hydrogen tanks store the gas at elevated pressures of 35–70 MPa [2]. The onboard hydrogen tanks shall be equipped

with non-reclosing thermally-activated pressure relief devices (TPRD), as required by the regulations, e.g., Global Technical Regulation on Hydrogen and Fuel Cell Vehicles (GTR#13) [3], to release hydrogen in the event of a fire and prevent the tank rupture with potentially catastrophic consequences. Similar scenarios include a release in hydrogen storage enclosures on board of trains, ships and planes, compressor rooms, etc.

Releases of hydrogen gas in a confined space with a limited vent size are found to produce pressure dynamics with a distinctive peak that exceeds the steady-state pressure level. This phenomenon is defined as the pressure peaking phenomenon (PPP), and can be observed for gases with density lower than air. The PPP is the most pronounced for hydrogen being the lightest gas of earth. The magnitude of the pressure peak depends mainly on the hydrogen release rate, enclosure vent size and volume. The phenomenon was first revealed and explained theoretically in [4] for unignited hydrogen releases. It was found that the produced pressure peak in an enclosure could be significantly higher than thresholds for the destruction of civil structures of the order of 10–20 kPa. That study analysed a hydrogen release with a constant flow rate through a TPRD of 5.08 mm diameter in a typical 30.4 m³ garage with a single vent of dimensions 10 × 25 cm, which is about a single brick size. Overpressure in the enclosure was simulated to increase up to 50 kPa and 100 kPa for 35 and 70 MPa storage pressures, respectively. After the peak, the pressure decreased tending to a steady-state value. The same authors investigated the PPP following the blowdown of several hydrogen inventories for a variety of release diameters, enclosure vent sizes and enclosure volumes [5]. It was found that a release diameter as low as 0.55 mm would be required for a 5 kg hydrogen inventory at 35 MPa to prevent an overpressure causing major damage and possible collapse of a civil structure with volume 30 m³ and vent size providing a ventilation rate of 0.18 air changes per hour (ACH). Brennan and Molkov provided an engineering tool in a form of nomograms to estimate overpressure in an enclosure following a sustained unignited hydrogen release [6]. The pressure peaking phenomenon is significantly more pronounced for ignited hydrogen releases, i.e., jet fires, as demonstrated in [7], thus requiring a further reduction of TPRD release area to prevent structural damage. It was shown that an unignited hydrogen release through a TPRD diameter of 2 mm from a 70 MPa storage generates the PPP overpressure of 11 kPa acceptable to prevent destruction to a garage. However, the PPP overpressure increased drastically to approximately 200 kPa, when the release from the same TPRD = 2 mm was ignited, resulting in structural damage. Garage vents with an area of up to 4 bricks (10 × 25 cm each) were found to be not sufficient to prevent the structure destruction, conversely to unignited releases. The reduced model to predict the pressure peaking phenomenon dynamics for both unignited and ignited releases was proposed in [7]. The model was validated against experiments on hydrogen releases with a mass flow rate in the range 0.1–1.1 g/s in a comparatively small enclosure with dimensions $H \times W \times L = 1.00 \times 0.98 \times 0.96$ m.

The PPP validation experiments at real scale enclosure for moderate hydrogen storage pressures in the range 2.3–12.4 MPa were performed in the HyTunnel-CS project and described in [8,9]. The PPP tests for unignited hydrogen releases with mass flow rate up to 10.1 g/s were performed in a 2.5 × 2.0 × 2.98 m chamber of approximately 15 m³ volume [8]. The experimental work was complemented by analytical modelling to demonstrate the relationship between ventilation area, enclosure volume and release rate. The same large-scale facility was employed to investigate the PPP for ignited hydrogen releases [9]. For unignited tests, as expected, the measured pressure peak was increasing with the increase of hydrogen mass flow rate, whereas it was seen to decrease for increasing ventilation area. Overall, thirty-one experiments were performed for three different vent areas and hydrogen mass flow rate up to 11.7 g/s (three tests were used in this study with maximum flow rate of 11.5 g/s). The maximum overpressure, recorded at a sensor located on the enclosure wall at 1.49 m above the floor and 1.5 m from the jet fire axis, was approximately 48 kPa. The authors complemented their experimental work with analytical modelling showing a ±2 kPa accuracy.

Computational fluid dynamics (CFD) is a contemporary engineering tool to simulate complex scenarios without restrictive assumptions typical for reduced models. The CFD simulations allow calculation of the thermal load on enclosure surfaces and the hazard distances based on pressure and thermal effects in the external surroundings of the enclosure. A CFD model for simulating the PPP for reacting hydrogen releases was suggested in [10]. The model was based on a RANS approach for turbulence modelling and the eddy dissipation concept (EDC) for combustion. The CFD model was validated against tests in a 1 m³ enclosure for hydrogen mass flow rates of approximately 0.55 and 1.1 g/s. Simulations employed a Courant-Friedrichs-Lewy number ($CFL = (u \cdot \Delta t) / \Delta x$) equal to 7.5, requiring approximately one week to calculate a 2 s pressure transient on a 64-core machine. The computational time would increase to over a month if a $CFL = 1$ was used. It follows that if a similar CFL and space discretization Δx were to be applied for hydrogen releases with higher inlet velocity and longer durations, the required computational time would become not viable for safety engineering assessments. It was assessed that the use of a refined mesh with 4×4 control volumes (CVs) at the notional nozzle exit would require approximately 550 days for a CFL number of 1. The computational study in [10] investigated the significance of different heat transfer mechanisms. The radiative heat transfer was shown to constitute a significant fraction of released energy compared to conductive heat transfer through the enclosure walls, perhaps due to a short time to achieve the PPP for the latter phenomena to make an effect on the simulated overpressures. The validated CFD model was then applied to the real-scale scenario of a garage with dimensions $4.5 \times 2.6 \times 2.6$ m [11]. The vent size was comparatively large of 0.35×0.55 m, whereas the hydrogen release rate into the compartment was approximately 300 g/s through a 3.34 mm diameter TPRD. For unignited releases, the overpressure in the enclosure did not reach harmful levels for people and structure, being below 0.6 kPa. However, the study demonstrated that other hazards arose: the garage was seen to be engulfed in a flammable atmosphere in less than 1 s, while the oxygen depletion reached levels harmful for people. When the jet was ignited, overpressure rose to over 50 kPa, thus reaching the levels of harm for humans and damage for structures following an explosion. Beyond the enclosure vent, the harmful thermal effects for humans associated with the presence of combustion products were seen to reach a hazard distance of 9 m. Simulations were computationally expensive, requiring over a month to calculate pressure dynamics for 1 s when a CFL number equal to 1 was used. This calculation time may not be viable for safety engineering assessments and, as a consequence, increase of CFL up to 10 was applied.

The present study aims to further develop and expand the validation domain of the CFD model [10] for the assessment of pressure effects due to the PPP for hydrogen jet fires in a larger scale garage-like enclosure of 15 m³ volume at moderate hydrogen storage pressures up to 12.4 MPa and mass flow rates up to 11.5 g/s. The simulations using Ulster's CFD model are validated against experiments performed by the University of South-Eastern Norway [9]. The CFD model accounts for gases compressibility, species transport with chemical reactions, radiation heat transfer etc., and as shown in [8,9] requires significant computational power and simulation time. To overcome this issue, for the first time, the CFD model of the PPP uses the volumetric source model for hydrogen release source to significantly reduce the simulation time while maintaining reasonable accuracy. Storage of hydrogen as a cryogenic fluid has the potential to become a popular solution for the H₂ infrastructure, due to its gains in volumetric capacities [12]. As an example, increasing attention has been given to the use of LH₂ in maritime applications to fulfil the objectives for greenhouse gases emissions reduction over the next decades. Maritime applications would require the storage of large quantities of LH₂ in confined spaces. To the authors' knowledge, experimental and numerical studies on the potential of PPP for cryogenic hydrogen releases indoors are currently absent in literature. A better understanding of such phenomenon is crucial for a safer deployment of cryogenic hydrogen infrastructure. In addition to the validation and assessment of the proposed CFD approaches for hydrogen stored at ambient temperature, the present study investigates for the first time the PPP

for cryogenic ignited hydrogen releases. Simulations employ the validated CFD model to assess the effect of storage temperature on the overpressure dynamics in the enclosure.

2. Description of Validation Experiments

The PPP validation experiments were performed by the University of South-Eastern Norway (USN) within the HyTunnel-CS project. Details on the experimental facility and set-up are described in [9]. A total of 31 tests were conducted on ignited hydrogen releases with mass flow rate up to 11.72 g/s in a steel chamber with inner dimensions $2.5 \times 2.0 \times 2.98$ m and 2 cm wall thickness. Figure 1a represents a scheme of the experimental facility. The chamber was equipped with three openings for venting combustion products during experiments (see V1, V2 and V3 in Figure 1a). Vents were circular with a diameter of 80 mm and they were fully closed or opened according to the desired vent area for each test. A further opening for air supply (V4) was equipped with a fan and was designed to ventilate the enclosure in between tests. A fifth opening (V5) was used for inserting the pipes of the fuel supply, i.e., propane for the ignition device and hydrogen for the jet fires. The hydrogen release pipe was located on a 15 cm height stand placed at the centre of the enclosure floor (see Figure 1c). The pipe had a 6 mm length above the stand and internal diameter of 4 mm. The hydrogen was released through the pipe exit with diameter 4 mm into the enclosure. An automatic ball valve was used to control the hydrogen release and provide a quasi-steady-state hydrogen mass flow rate. The measurement of static pressure with a closed valve was considered as the storage pressure (see Table 1). The ignition device was a propane pilot flame (2.1 bar and 6 mm diameter pipe). Ignition had a duration of 2 s and was activated 1 s before the hydrogen release.

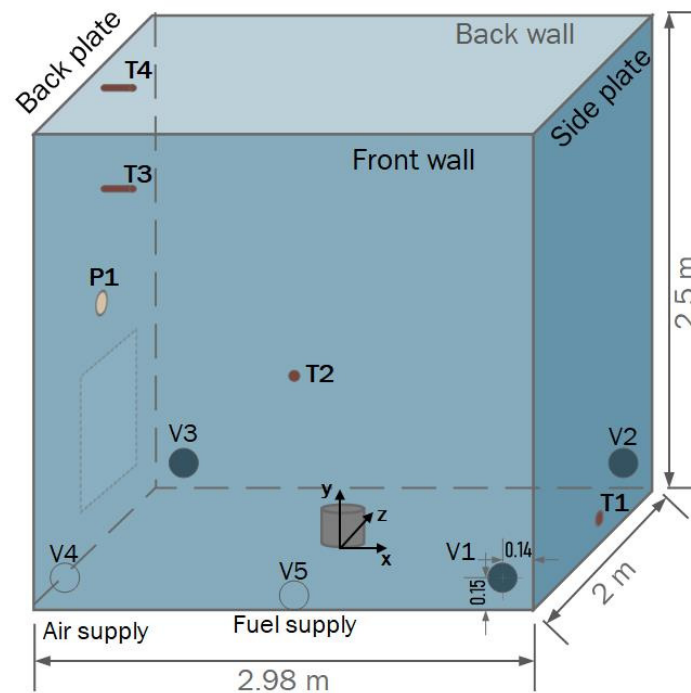
Measurement of pressure in the test chamber was provided by a Kulite pressure transducer located on the enclosure wall at 1.49 m above the floor (P1 in Figure 1). Pressure sensors were not equipped with a silicon layer to further protect readings from the effect of high temperature combustion products. The hydrogen release rate was measured by a Coriolis mass flow rate meter. One thermocouple was placed 6 cm off the side plate at a height of 0.035 m (T1 Figure 1). A second thermocouple was located 6 cm of the front wall at a height of 1.24 m (T2 in Figure 1). Two thermocouples were placed 6 cm off the backplate wall at heights 1.85 and 2.85 m (T3 and T4 in Figure 1). All thermocouples were Type K Autek-TD20H-KP. Ambient pressure and temperature were 101,325 Pa and 277 K, respectively. The initial temperature of the enclosure was given by the average of the four thermocouples T1-T4.

Experiments were performed for mass flow rates (MFR) in the range 1.0–11.7 g/s. The number of open vents was chosen to avoid pressure levels destroying the enclosure. As a consequence, tests with high MFR were performed only for two or three open vents. The maximum pressure was reached in Test 19 (48.1 kPa) with 8.62 g/s hydrogen release and only one open vent.

Three tests with the largest storage pressure and recorded PPP overpressure, and available thermocouples measurements for each of the open vents' scenarios, i.e., 1, 2 or 3 vents open, were selected for CFD model validation in the present study. Table 1 reports the storage pressure, P_S , and hydrogen mass flow rate, \dot{m} , for each of the selected for the simulations tests.

Table 1. The USN experiments for the CFD model validation.

Test No.	Hydrogen Storage Pressure, MPa	Mass Flow Rate, g/s	Number of Open Vents	Maximum Measured Overpressure, kPa
14	11.78	11.37	3	21.1
18	12.46	11.47	2	33.2
19	8.93	8.62	1	48.1



(a)



(b)



(c)

Figure 1. Experimental facility: (a)—sketch of the facility with the location of vents (V1–V3), air supply (V4), fuel supply (V5), pressure transducer (P1) and thermocouples (T1–T4); (b)—picture of the facility front wall; (c)—location of stand with hydrogen release nozzle and propane pilot flame [9].

3. The CFD Model and Numerical Details

3.1. The CFD Model

The basis of the CFD model to simulate the pressure peaking phenomenon for hydrogen jet fires in confined space was developed in [10]. The model was validated against small-scale experiments in a laboratory-scale enclosure of 1 m^3 volume. Here, the model is developed further and the validation domain is expanded to the large-scale garage-like enclosure of 15 m^3 volume. The CFD model employs an implicit pressure-based solver for reacting compressible ideal gas flows. A Reynolds-Averaged Navier–Stokes (RANS) approach is used with the realizable $\kappa\text{-}\epsilon$ sub-model for solving turbulent kinetic energy and turbulence dissipation rate [13]. This turbulence sub-model is selected as it was found to better predict overpressure [10], jet fire temperature and emitted radiation [14], compared to standard $k\text{-}\epsilon$ and RNG $k\text{-}\epsilon$ models. The eddy dissipation concept (EDC) model is used for combustion simulations [15]. The option with chemical mechanisms of 9 species and 18 reactions by a subset of Peters and Rogg’s mechanism [16] was applied. The discrete

ordinates model [17] is applied to account for radiation heat transfer. The main governing equations are presented in [10], and the peculiarities of the CFD model applied in this study are described in sections below.

3.2. Modelling of Hydrogen Release Source

Hydrogen storage pressure in the considered experiments was in the range of 8.93–12.46 MPa. Thus, the release will be in a form of an under-expanded jet, which would lead to a complicated shock waves structure outside the real nozzle.

The notional nozzle (NN) model is the first of two approaches used to model hydrogen jet in the simulations. The diameter of the notional nozzle was calculated using the Ulster's under-expanded jet theory [18], which assumes an isentropic expansion from the stagnation pressure in a storage vessel through the real nozzle and, finally, the jet expansion to the atmospheric pressure through the notional nozzle exit. This theory uses Abel-Noble Equation of State (EOS) to account for the non-ideal behaviour of hydrogen gas at high pressure. The equations for energy and mass conservation are employed in an assumption of a sonic flow to calculate conditions at the notional nozzle exit. Full description of the methodology and equations is available in [18].

The discharge coefficient, C_d , is applied in calculations of notional nozzle exit to account for pressure losses in the piping system and real nozzle compared to the ideal case of no losses with $C_d = 1$. The discharge coefficient can be calculated through the inverse problem method targeting to match the simulated mass flow rate to the measured in an experiment, \dot{m}_{exp} , as follows:

$$\dot{m}_{exp} = C_d \cdot \rho \cdot u \cdot A. \quad (1)$$

where ρ is the hydrogen density at the real nozzle, u is the flow velocity (equal to the speed of sound due to choked flow conditions) and A is the area of the real nozzle ($1.26 \times 10^{-5} \text{ m}^2$). Table 2 presents the calculated notional nozzle parameters that are used as the boundary conditions in the CFD simulations. The discharge coefficient is found to be $C_d = 0.12$ – 0.13 , as a consequence of the friction and minor losses in the piping system, which was approximately 2 m long of 4 mm internal diameter, with a valve, several pipe bends and the mass flow meter.

Table 2. Notional nozzle exit parameters used as hydrogen inlet boundary conditions in simulations *.

Test No.	Mass Flow Rate, g/s	C_d	D_{NN} , mm	T_{NN} , K	U_{NN} , m/s
14	11.37	0.13	11	230.8	1154.5
18	11.47	0.12	11	231.7	1156.6
19	8.62	0.12	9.5	231.7	1156.6

* D_{NN} is the notional nozzle exit diameter, T_{NN} and U_{NN} are the hydrogen temperature and velocity in the notional nozzle exit.

The second approach applied in this study is the modelling of hydrogen release using the so-called volumetric source model. The volumetric sources are applied in equations of conservation of mass, momentum and energy for a selected volume. The source terms for mass, momentum and energy are calculated from the mass flow rate, velocity and temperature at the notional nozzle reported in Table 2. This approach is proved to reduce the calculation time compared to the notional nozzle concept approach. Previous numerical work [18] demonstrated that a volumetric source with size four times the notional nozzle diameter correctly reproduced experiments on unignited hydrogen jets. The present study employs the volumetric source model applied in the space of cubic geometry with a size of 3.8 cm, which corresponds to four times the hydraulic notional nozzle exit diameter for Test No.14.

3.3. Computational Domain and Numerical Grid

The computational domain has dimensions $6.0 \times 3.5 \times 5.0$ m and is shown in Figure 2a. The enclosure is located at a height of 0.5 m from the external ground and at the centre of the domain in other directions. For the first modelling approach, the enclosure solid walls are included in the numerical domain to account for heat transfer to and through them (Figure 2a). The thickness of the rectangular control volumes (CVs) in the solid wall is 2 mm at the inner surface of the enclosure. This increases perpendicularly to the outer wall surface with a growth ratio of 1.1. The inflow boundary corresponds to the notional nozzle exit and is modelled as a square with an area equivalent to that of the round notional nozzle exit. The inflow area was discretised by 2×2 cells. The cell size in the fluid was increased with a maximum cell growth ratio of 1.1. Enlargement of the numerical mesh in the near zone to the release point is shown in Figure 2c. The vents were modelled as squares with dimensions 7×7 cm, with area equivalent to the circular vents used in experiments (4.9×10^{-3} m²). The vent area was discretised by 4×1 cells. The overall CV number in the domain is 575,840. Another numerical grid was built to test simulations sensitivity for the nozzle resolution, i.e., with just 1×1 cell in the nozzle. This numerical grid presents a more refined mesh close to the enclosure walls and contains 636,666 CVs.

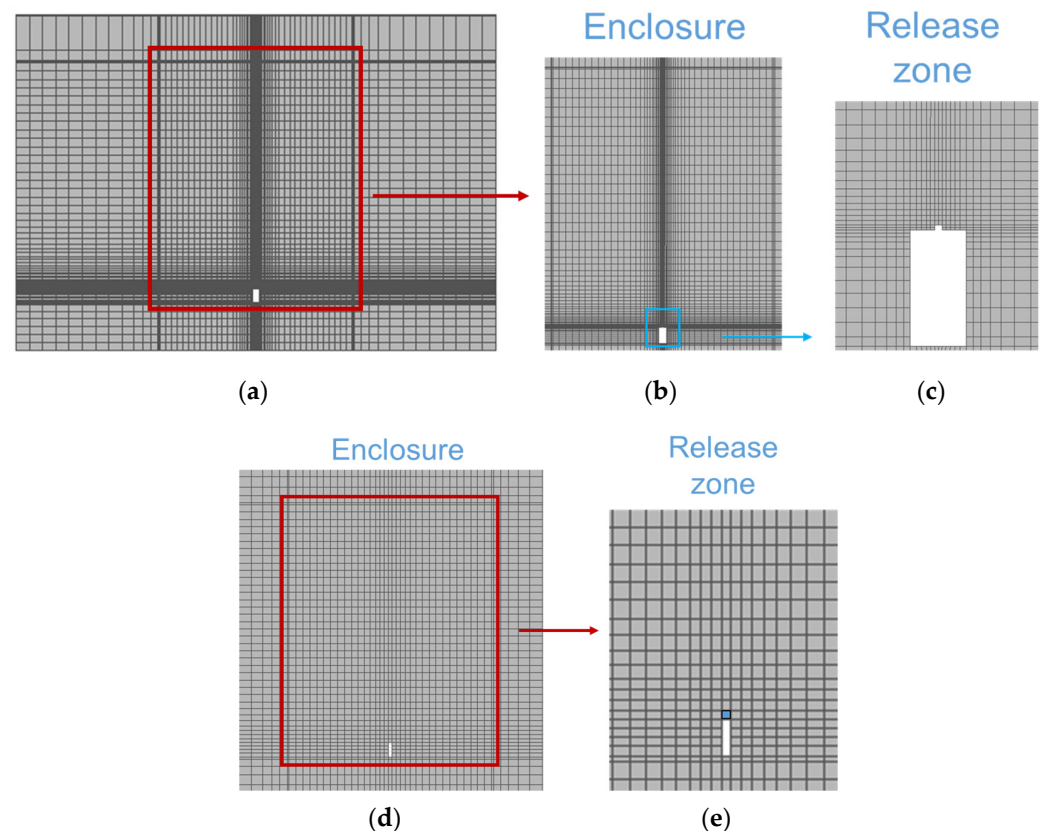


Figure 2. Cross-section of the calculation domain and numerical mesh: inflow boundary for notional nozzle exit approach—(a) total calculation domain, (b) detail of the enclosure, (c) enlargement of the release zone; volumetric source (VS) approach—(d) enclosure, (e) enlargement of the release zone with VS in light blue.

A constant mass flow rate inlet boundary condition is imposed as in the experiments. A turbulent intensity of 25% and turbulent length scale of $0.07D_{not}$ are accepted at the inlet boundary following [14]. Properties for SAE 1010 steel are considered for the solid walls: 59 W/mK for the thermal conductivity, 7832 kg/m³ for the density and 434 J/kgK for the specific heat [19]. The enclosure walls emissivity was taken as 0.94 [20]. The external boundaries are modelled as pressure outlets at ambient temperature and pressure, which

are used as initial conditions in the domain, respectively 101,325 Pa and 277.15 K for Test No.14. The air composition is taken as 0.21 for the mole fraction of O₂ and 0.79 for N₂. The highest velocity in the domain is at the hydrogen release area, where the numerical mesh is characterised by the smallest CV size of approximately 5 mm, thus resulting in the largest CFL number in the calculation domain. Hydrogen temperature and velocity at the release are constant in time. Therefore, in the present case, setting a constant time step during hydrogen release is equivalent to a constant CFL number. The time step is initially set as 0.34 ms which is equivalent to CFL number 50 at the release source. A CFL sensitivity analysis is conducted in Section 4.1 to ensure results independence from the time step (CFL number). The number of iterations per time step is set as 20. Simulations were performed using ANSYS Fluent version 16. However, no difference was observed with results obtained using Fluent version 19.2.

In the second approach for hydrogen release modelling, i.e., the volumetric source model, the numerical grid for the source area employs one cubic cell with a size of 3.8 cm located at the top exit of the release pipe (see Figure 2e). A growth ratio of 1.1 is maintained for the numerical grid within the enclosure. For this case, the heat transfer to and through the solid walls is modelled using a “shell conduction” approach that allows to assess the conductive heat transfer without meshing the wall thickness in the preprocessor. During the solution process, five layers of mock hexa cells are created within the steel wall, starting from a thickness of 2 mm at the inner wall and growing with the ratio of 1.1 in direction of the outer wall surface. The total number of control volumes in the domain was 235,881, thus reducing the CV number more than twice compared to that for the domain with an inflow boundary condition at the notional nozzle exit. Given the larger cell size and smaller velocity at the release source to conserve momentum and energy, a lower CFL is expected compared to the inflow boundary modelling approach for the same time step. However, the use of a coarser grid throughout the enclosure may affect CFL solution convergence. For this reason, a CFL sensitivity analysis is conducted in Section 4.2. Simulations for a volumetric source model were performed using ANSYS Fluent version 19.2.

For both modelling approaches, the discrete ordinates (DO) model was applied with discretisation 5×5 for rays and 3×3 for pixels as suggested in Fluent’s best practices [21]. The least-square cell-based scheme is used for the discretisation of gradients except for pressure gradients. Pressure gradients are discretised using PRESTO! scheme as it was shown to provide better predictions of experiments in [10]. A second-order upwind scheme is used to discretize the convective terms. The CFD approach employs an implicit scheme for time discretization. In the study [10], a 1st order time resolution was seen to give similar results to 2nd order, so it is employed here to reduce computational costs. Simulations employ under-relaxation factors (URFs) of equations in the range 0.3–1.0. These allow to control the update of the computed variables at each iteration for a pressure-based solver. The URFs are defined for each equation as follows: URF = 0.3 for pressure, URF = 0.5 for energy, URF = 0.7 for momentum, URF = 0.75 for density and turbulent viscosity, URF = 0.8 for the turbulent kinetic energy and dissipation rate, URF = 0.85 for the body forces, URF = 0.9 for species and, finally, URF = 1.0 for discrete ordinates. The Chemkin thermodynamic and transport databases are used to describe the species properties [22].

4. Results and Discussion

This section presents the discussion of the results of CFD simulations of the experimentally recorded pressure peaking phenomenon in the large-scale enclosure. The comparison of two different approaches to model the hydrogen release source is mainly focused on the pressure dynamics recorded in the enclosure, which is the primary concern of the safety analysis for such scenarios.

4.1. Inflow Boundary at the Notional Nozzle Exit Approach

The first analysis is focused on the reproduction of the experimental pressure dynamics within the enclosure for Test No.14 by employing the inflow boundary conditions at the

notional nozzle exit. Figure 3 shows the comparison between experimentally recorded pressure transient and simulated pressure dynamics obtained with a different resolution of the nozzle, i.e., 1×1 CV and 2×2 CVs. The simulations with a 2×2 CVs resolution at the notional nozzle exit boundary used time steps (Δt) 0.17 ms and 0.34 ms, which correspond to CFL numbers at the release area of approximately 25 and 50, respectively. Simulated pressure transients were shifted by 1.4 ms, which corresponds approximately to the time needed by the mass flow rate to reach a constant value at the release nozzle in the experiments. The experimental pressure dynamics in the enclosure is well reproduced in simulations with both CFL numbers 25 and 50. The pressure in the enclosure increases as long as the volumetric flow rate of hydrogen entering the chamber is higher than the volumetric flow rate of gases leaving the chamber. The latter increases in time due to two factors: (a) the decrease of density of the gas mixture in the enclosure by the increase of hydrogen fraction, and (b) the increase of pressure in the enclosure to compensate for the growth of pressure due to hydrogen inflow by the increase of gas mixture outflow rate through the enclosure vent. The maximum pressure in the enclosure is reached when the outflow volumetric rate through the vent is equal to the volumetric flow rate of hydrogen into the chamber. Simulations well predict the experimental peak overpressure of 21.1 kPa with an accuracy of 3% for $\Delta t = 0.17$ ms (20.5 kPa) and 5% for $\Delta t = 0.34$ ms (20.1 kPa). Given the negligible difference in the obtained pressure up to 6 s, it is concluded that the time step equal to 0.34 ms can be accepted. Thus, simulation then continued only for $\Delta t = 0.34$ ms, given the associated significant saving of computational time. At approximately 9 s the hydrogen release is stopped (see Figure 3) and maximum velocity in the calculation domain starts to decrease, allowing to gradually increase time step. The time step was doubled five times till it reached 5.4 ms, each time letting the simulation run for 20 time steps before the next time step increase. The time step 5.4 ms is maintained for the rest of the simulation. Figure 3 shows that beyond 9 s, the pressure rapidly decreases reaching negative values. Experimental negative pressure peak is seen to reach approximately -4 kPa, whereas CFD simulation prediction is about -2 kPa. Experimentalists noted that water vapour started condensing at the cold walls of the enclosure. Condensation could affect the pressure dynamics but was not accounted for in the model. This may be a reason for the discrepancy between the simulated and experimental negative pressure transients. Another reason could be the resolution of the vent area.

Figure 4a shows the distribution of hydroxyl (OH) mole fraction in the plane $x = 0$ perpendicular to the enclosure walls in the location of vents. The presence of hydroxyl is an indicator of the location of chemical reactions i.e., the combustion zone in the jet fire. A limit to OH mole fraction equal to 0.001 is generally considered to indicate the most reacting zone and estimate a jet fire flame length [23]. The latter was seen to be consistent with the visible flame length corresponding to the region with temperature in the range 1300–1500 K [24] in the numerical study by [25]. It can be seen that the jet fire hits the enclosure ceiling. With time, the jet fire increases in width and the maximum OH mole fraction decreases, as an indication of a decreased reaction rate due to decreased concentration of air in the enclosure. Figure 4b shows the temperature distribution in the enclosure with time. The high-temperature zone (>1800 K) impinges on the ceiling and the hot combustion products move along the ceiling and then descend along the enclosure walls. By the time 5.4 s, the enclosure starts to be filled up with hot combustion products. This creates potentially harmful conditions for humans by temperature criteria and oxygen depletion. Similar to what observed from the OH mole fraction distribution, the jet fire increases in width (see zone $T > 1300$ K in Figure 4b) and the maximum temperature along the jet axis decreases with time.

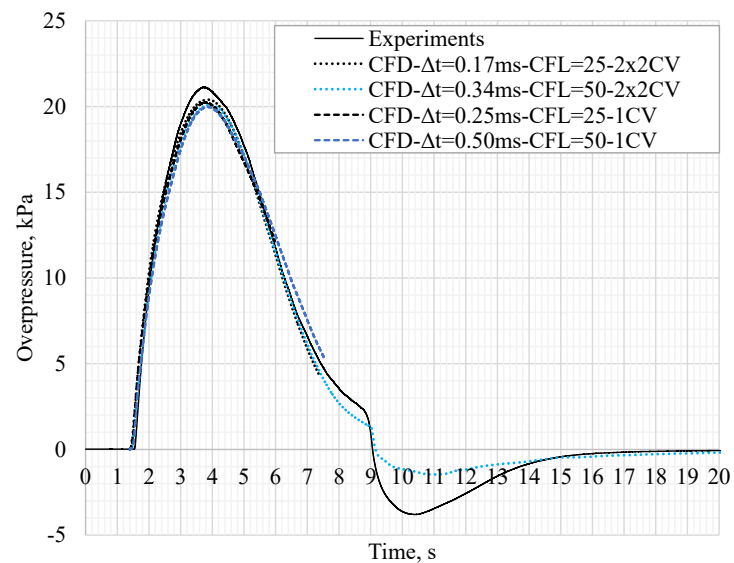


Figure 3. Simulated pressure dynamics in the enclosure with inflow boundary conditions at the notional nozzle exit for different CFL number and nozzle grid refinement (CVs) versus experimental pressure transient for Test No.14 ($P_S = 11.78$ MPa, $\dot{m} = 11.37$ g/s, Number of simulated experimental vents = 3).

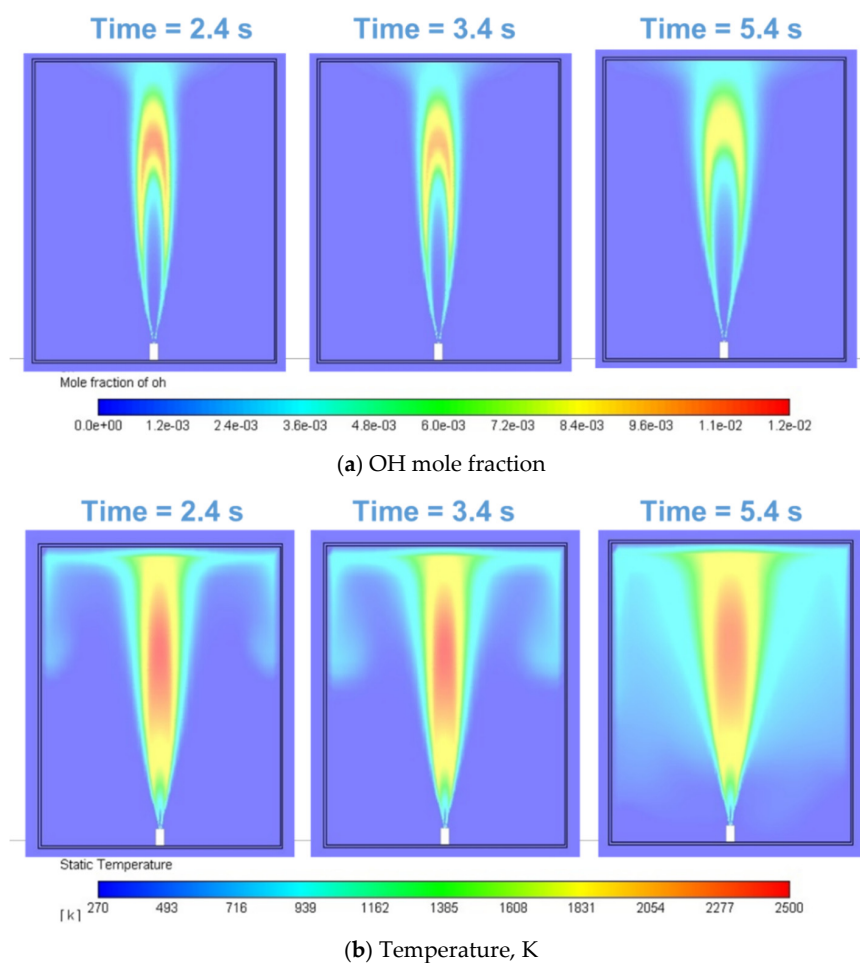


Figure 4. (a) Simulated hydroxyl mole fraction and (b) temperature distributions in the plane $x = 0$ perpendicular to the enclosure walls with vents for Test No.14 ($P_S = 11.78$ MPa, $\dot{m} = 11.37$ g/s, Number of experimental vents = 3), $\Delta t = 0.34$ ms, CFL = 50.

Four experimental thermocouples were located close to the enclosure walls to assess the thermal load on the structure (see Figure 1). The thermocouples were coated with protective Inconel alloy, which would affect their response time due to heat transfer through the Inconel layer. On the other hand, numerical simulations provide the instantaneous “non-inertial” temperature of the hot combustion gases, preventing a direct comparison with experimental measurements and requiring the data manipulation to include heat transfer through the sensors’ Inconel layer. This process may be affected by inaccuracies rendering the comparison not reliable and, for this reason, this analysis is omitted.

The calculation time for simulations of 1 s is approximately 45 h with a time step of 0.34 ms on a 60 CPU workstation. Thus, the calculation time for a complete release simulation is approximately two weeks. The numerical grid employing 1×1 CV to discretise the inflow boundary allows the use of a larger time step while maintaining the same CFL number due to the larger cell size at the release area. Simulations are performed by using a time step equal to 0.5 ms (CFL = 50) or 0.25 ms (CFL = 25). Figure 3 shows the resulting overpressure dynamics for both grids and nozzle resolutions. The maximum variation in the simulated pressure peaks was within 0.5%, confirming the independence of the grid resolution at the inflow boundary for the same CFL number. The simulation time was 30 h for 1 s of hydrogen release, which is not yet sufficient to have a time-efficient and accurate calculation strategy.

4.2. Volumetric Source Model Approach

To further reduce the calculation time without affecting the solution accuracy, a volumetric source model is used to simulate hydrogen release. As the first step, the analysis is conducted to find convergence by CFL number. This was changed in the range 0.37–50.0, which corresponds to the time step range 0.12–16 ms. Figure 5 shows the resulting overpressure dynamics for the CFL number in the range 0.37–3.0. It can be observed that variation in simulated pressure dynamics from experimental measurement decreases with the decrease of CFL. The calculated pressure peaks are 20.37 kPa and 20.86 kPa (approximately 2% relative difference) for CFL numbers 1.5 ($\Delta t = 0.5$ ms) and 0.75 ($\Delta t = 0.25$ ms) respectively. A further decrease of CFL to 0.37 ($\Delta t = 0.125$ ms) results in a pressure peak equal to 21.00 kPa, which is higher by merely 0.7% than the pressure peak for CFL = 0.75. Thus, a CFL = 0.75 is deemed to lead to a converged solution while maintaining an acceptable calculation time of 17 h to simulate 1 s of hydrogen release. With the volumetric source model, the simulations of a test can be completed in approximately 5 days, which is a significant decrease in calculation time compared to the case employing the notional nozzle exit as the inflow boundary (approximately 2 weeks). A CFL = 0.75 is applied for the rest of the simulations. The calculated pressure peak is 20.9 kPa, which agrees well with the experimentally measured peak pressure of 21.1 kPa. Figure 5 shows that the pressure dynamics is reproduced well, even though a slight difference towards the descending phase of the curve can be noticed. Once the release of hydrogen is stopped, the computational time step size was gradually increased with the same procedure as described for the notional nozzle exit inflow boundary modelling approach. Simulated negative overpressure decreases to approximately -3 kPa, whereas about -4 kPa was measured in the experiment. The effect of the number of iterations per time step is assessed by increasing it from 20 to 40. A variation of about 2% in the simulated pressure peak is observed, thus confirming the good accuracy of a solution with 20 iterations per time step. This value is maintained in the simulations.

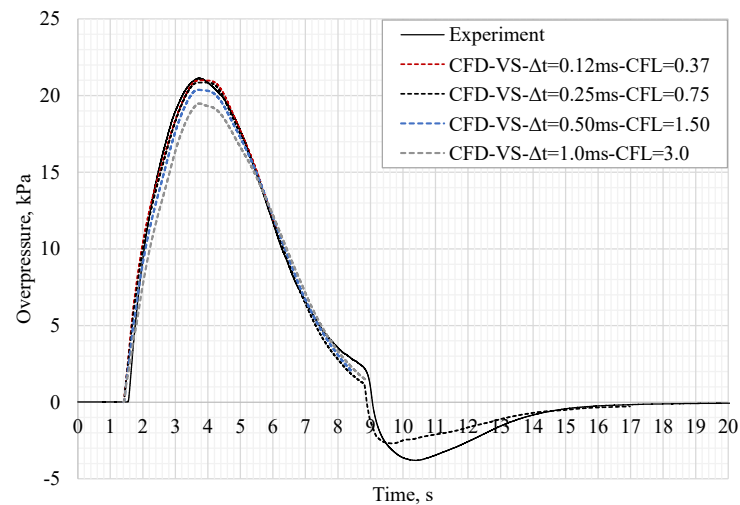


Figure 5. Simulated pressure dynamics in the enclosure and convergence by CFL number with the volumetric source model versus experimental pressure transient for Test No.14 ($P_S = 11.78$ MPa, $\dot{m} = 11.37$ g/s, Number of experimental vents = 3).

The described above CFD model is used then to simulate Tests No.18 and No.19. Figure 6 shows the comparison between the experimental and simulated pressure dynamics in the enclosure. The simulated pressure peak for Test No.18 is 35.10 kPa, which conservatively predicts the experimentally measured 33.22 kPa with 7% accuracy. On the other hand, simulated overpressure in the enclosure for Test No.19 reaches the maximum value of 42.21 kPa, which underpredicts the experimental pressure peak of 48.1 kPa by 14%. This variation is considered to be acceptable in the engineering calculations of such phenomenon. The dynamics and magnitude of the negative pressure phase are well reproduced for both Tests No.18 and No.19. However, it can be observed that the maximum negative pressure for Test No.19 simulation is achieved 4 s earlier than in the experiment. The last is though due to the absence of water vapour condensation in the CFD model.

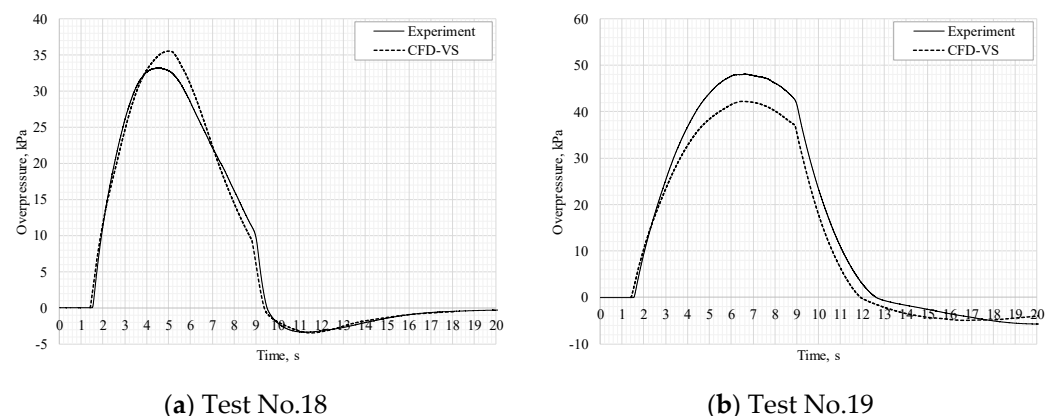


Figure 6. Pressure dynamics in the enclosure: CFD simulations with CFL = 0.75 versus experiments: (a) Test No.18 ($P_S = 12.46$ MPa, $\dot{m} = 11.47$ g/s, Number of experimental vents = 2); (b) Test No.19 ($P_S = 8.93$ MPa, $\dot{m} = 8.62$ g/s, Number of experimental vents = 1).

4.2.1. Effect of Heat Transfer to the Enclosure Walls

The effect of heat transfer on pressure dynamics is assessed by comparing simulations for adiabatic and thermally conductive enclosure walls, see Figure 7. In both cases, radiative heat transfer from the jet fire is included through the DO model. Pressure peak slightly increases from 20.86 kPa to 21.05 kPa when heat losses are not included in the model, which is considered to be a negligible effect on the pressure peak and pressure dynamics.

This result confirms the conclusion drawn in [10] that the heat transfer to the walls has a negligible effect on the positive phase of the overpressure dynamics. The negative phase may be affected by condensation of water vapour at the enclosure walls, which will be dependent on the heat transfer.

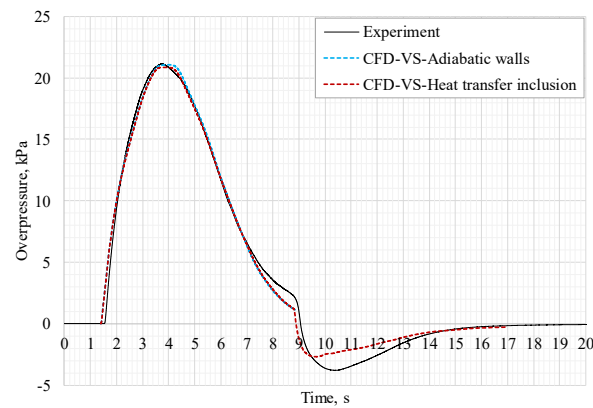


Figure 7. Pressure dynamics in the enclosure for Test No.14 ($P_S = 11.78$ MPa, $\dot{m} = 11.37$ g/s, Number of experimental vents = 3): effect of heat transfer to the enclosure walls.

4.2.2. Time-Efficient Approach of the Uniform Cube-Shaped Control Volumes Grid

The use of a volumetric source model is found, as demonstrated above, to reduce significantly the calculation time by approximately a factor of 3. In this section, a novel and simplified approach is developed to further enhance the time efficiency of calculations while maintaining an acceptable solution accuracy. This is based on the building of a uniform hexahedral grid throughout the calculation domain with the same size as the vent (7 cm square opening). The volumetric source is modelled as a cube with a 7 cm side. This dimension corresponds to approximately eight times the notional nozzle diameter. The CV number in the domain is 317,878. Maintaining the same CFL = 0.75 at the release area for this grid increases time step by three times ($\Delta t = 0.75$ ms). Thus, it is expected to significantly decrease the computational time.

Figure 8a shows the pressure dynamics for Test No.14. A larger volumetric source results in a larger simulated overpressure (22.66 kPa) by approximately 8% relative difference, whereas the negative phase is simulated similarly. The hydrogen mass flow rate provided by the volumetric source (VS) is monitored. Maximum variation of released hydrogen between the two VS sizes, respectively 3.8 and 7.0 cm, is calculated to be within 0.7%. However, even though the hydrogen mass flow rate is maintained nearly the same for both cases, the distribution of hydrogen, combustion products and temperature can vary greatly, affecting as a consequence the composition and density of gases exiting the enclosure and the reached overpressure. A lower volumetric flow rate through the vents is observed for the simplified approach with uniform CV size 7 cm. All the above could be a direct consequence of the application of the volumetric source approach beyond the validity range stated in [18] and the use of a coarser grid. Calculation time is approximately 6 h to simulate 1 s of hydrogen release. With full understanding of the simplified approach limitations, this is seen as a pragmatic way to reduce the calculation time by approximately a factor of 3. Thus, the authors yet consider the simplified approach as valuable for PPP prediction to obtain time efficient calculations. However, it should be highlighted that the reduction of computational time may come at a cost of a lower accuracy of calculations that should be maintained within reasonable for engineering applications precision.

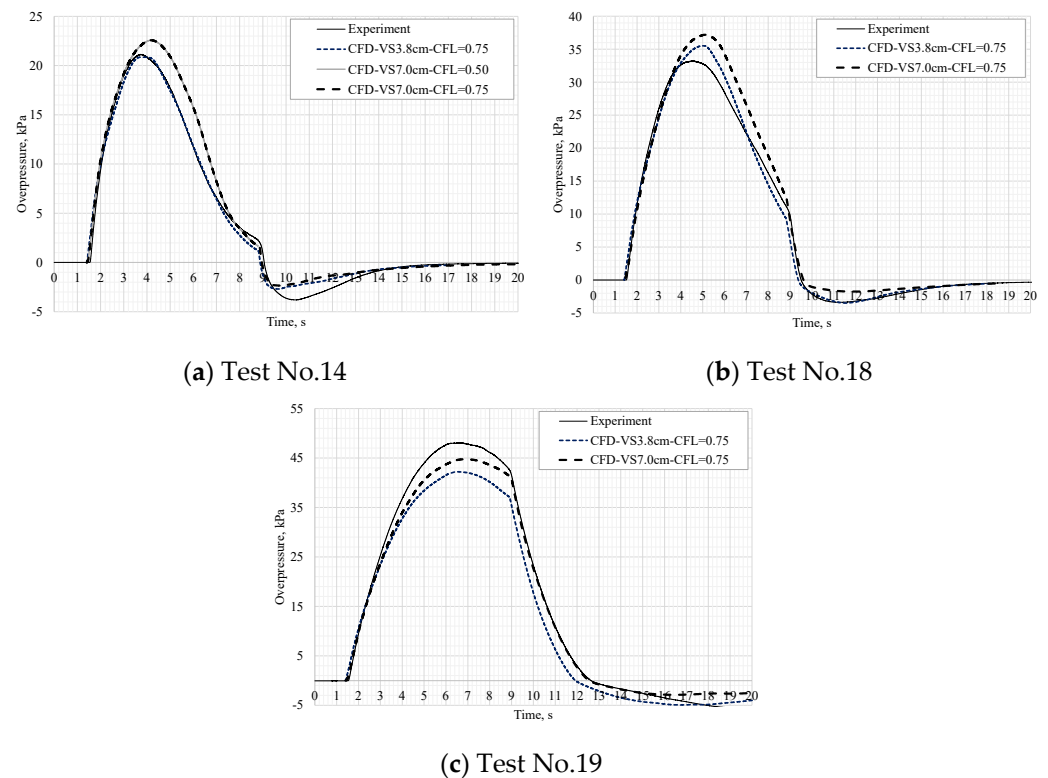


Figure 8. Pressure dynamics in the enclosure for the unified “cube grid” approach (VS7.0 cm): (a) Test No.14 ($P_S = 11.78$ MPa, $\dot{m} = 11.37$ g/s, Number of vents = 3); (b) Test No.18 ($P_S = 12.46$ MPa, $\dot{m} = 11.47$ g/s, Number of vents = 2); (c) Test No.19 ($P_S = 8.93$ MPa, $\dot{m} = 8.62$ g/s, Number of vents = 1).

The CFL independence of a solution for the volumetric source (VS) model with uniform “cube grid” of 7.0 cm size was assessed for Test No.14 for CFL number 0.50 and 0.75 (see Figure 8a). The pressure dynamics is not affected by the CFL number change by 50%. Thus, the CFL = 0.75 was maintained for the simulations using the “cube grid”. Figure 8b,c show the overpressure dynamics for Test No.18 and Test No.19 respectively. Maximum pressure for Test No.18 demonstrates variation by +5.8%, i.e., the increase from 35.10 kPa for a VS size 3.8 cm to 37.20 kPa for VS size 7.0 cm, and the difference of maximum overpressure simulated for VS = 7.0 cm from the experimentally measured value is +11% (conservative). For Test No.19, the simulated overpressure peak with VS = 3.8 cm underestimates experimental measurement by −14%, whereas the case with VS = 7.0 cm differs from experiments by only −7.4%. Conversely to what is observed for Test No.14, the negative pressure in Tests No.18 and No.19 is affected by the change of VS modelling approach, resulting in approximately half of the maximum negative pressure recorded in experiments when the VS = 7.0 cm approach is employed. Simulation results on the maximum overpressure peaks for the two approaches VS = 3.8 cm and VS = 7.0 are summarized and compared to experiments in Table 3.

Table 3. Comparison of the experimentally measured maximum overpressure peaks to simulation results for the employed volumetric source approaches (in brackets relative difference from experiments).

Test No.	Experimental Maximum Overpressure, kPa	Simulated Maximum Overpressure, kPa	
		VS = 3.8 cm	VS = 7.0 cm
14	21.1	20.9 (−1%)	22.7 (+7%)
18	33.2	35.1 (+5%)	37.2 (+11%)
19	48.1	42.2 (−14%)	44.8 (−7%)

The simplified uniform “cube grid” $VS = 7.0$ cm approach is seen to reduce significantly the calculation time by approximately 3 times compared to the $VS = 3.8$ cm approach, and by approximately 7.5 times compared to the previously used notional nozzle exit approach for hydrogen inflow boundary. The accuracy of the maximum simulated overpressure is found to be $\pm 11\%$. This is well within the acceptable engineering accuracy for such complex phenomenon. It can be concluded that the unified “cube grid” $VS = 7.0$ cm approach is a valuable hydrogen safety engineering tool for the assessment of the pressure peaking phenomenon.

Both the inflow boundary at the notional nozzle exit and volumetric source approaches are seen to represent well experiments with storage pressure up to 12.5 MPa and hydrogen mass flow rate up to 11.5 g/s. The validation domain of the CFD model is not limited by storage pressure but is defined by the released mass flow rate, being this the key input for PPP. A release of hydrogen from a storage with pressure 12.5 MPa and TPRD diameter of 4 mm would be equivalent to a release from a 70 MPa storage and 0.65 mm TPRD diameter, as calculated through e-Laboratory developed within NET-Tools project [26] (11.5 g/s for conservative $C_d = 1$). Thus, the conclusions of the present study are valid for current onboard storage systems with such TPRD diameter and the CFD model can be applied for the associated safety assessments.

4.3. Effect of Cryogenic Storage Temperature on the Pressure Peaking Phenomenon

Hydrogen may be stored in cryo-compressed conditions, i.e., storage temperature below 120 K as generally considered for cryogenics [27] and pressure up to 35 MPa [28]. Cryogenic storage pressure below 20 MPa is considered to provide a better gain in gravimetric and volumetric capacities against the energy required for the compression and cooling down of the hydrogen gas. With the increase of storage pressures above 20 MPa, these benefits are seen to reduce [29].

This section assesses the effect of hydrogen storage temperature on the PPP dynamics for the same enclosure and the volumetric source model approach with VS size 3.8 cm and $CFL = 0.75$ (see detailed description in Section 4.2) is used for the cases listed in Table 4. Simulations include the effect of heat transfer through the enclosure walls. The selected scenario is that of Test No.14, i.e., storage pressure 11.78 MPa, nozzle diameter 4 mm and constant hydrogen mass flow rate. All three experimental vents of the enclosure are simulated as fully open. The storage temperature, T_S , is varied from ambient 277 K, as per Test No.14, to an intermediate temperature of 200 K and to cryogenic temperature of 100 K. Four cases of hydrogen releases at a storage temperature lower than atmospheric are simulated and details are given in Table 4 along Test No.14 data. Effect of heat transfer through the release pipe walls is not taken into account to isolate the effect of storage temperature on the pressure peak. Parameters at the notional nozzle exit are calculated as in [30], i.e., through the under-expanded jet theory implementing the NIST database [31] using the Helmholtz Free Energy EOS. The calculated notional nozzle parameters are used to define the source terms in the volumetric source approach. It is considered that the potential for hydrogen phase change during expansion of cryo-compressed hydrogen can be neglected for this range of applications and the CFD model. Table 4 shows that conditions at the notional nozzle exit would be above hydrogen critical point. Furthermore, the volumetric source approach was seen in [32] to well reproduce experimental temperature distribution for a transient hydrogen unignited jet from a storage with initial pressure and temperature equal to 20 MPa and 80 K respectively [33]. Cases 2 and 3 maintain the same storage pressure, pipe diameter of 4 mm and discharge coefficient as per Test No.14. The decrease of temperature causes an increase of released hydrogen mass flow rate from 11.37 g/s for $T_S = 277$ K, to 14.11 g/s for $T_S = 200$ K and 23.16 g/s for $T_S = 100$ K. Cases 4 and 5 consider the effect of storage temperature on the PPP dynamics for scenarios of the same storage pressure and the same mass flow rate as per Case 1 (Test No.14). For releases at ambient temperature, the PPP magnitude depends on the released mass flow rate of hydrogen for unvaried enclosure volume and vent area. This analysis aims at quantifying

the sole effect of cryogenic hydrogen temperature at the release on the combustion products temperature and enthalpy, and, thus, on the resulting maximum overpressure peak. To match the same mass flow rate as in Test No.14 (Case 1) the discharge coefficient is reduced for the Cases 4 and 5 at cryogenic temperatures. This is equivalent to reducing the pipe diameter, as the mass flow rate is proportional to the product of discharge coefficient and pipe cross section area being proportional to diameter squared. The change in calculated notional nozzle diameters, D_{NN} , in cases 4 and 5 is due to the application of NIST EOS which provides larger densities for cryogenic hydrogen compared to the Abel Noble EOS employed for case 1 at ambient temperature.

Table 4. Simulations to assess effect of storage temperature on PPP: storage, release and notional nozzle conditions.

Case	Storage Pressure, MPa	Storage Temperature, K	C_d	Constant Mass Flow Rate H_2 , g/s	D_{NN} , mm	T_{NN} , K	U_{NN} , m/s	Pressure Peak, kPa
1 (Test No.14)	11.78	277	0.13	11.37	11.0	230.8	1154.5	20.95
2	11.78	200	0.13	14.11	10.8	145.0	915.1	26.95
3	11.78	100	0.13	23.16	11.1	67.3	623.3	42.82
4	11.78	200	0.10	11.37	9.7	145.0	915.1	20.51
5	11.78	100	0.06	11.37	7.8	67.3	623.3	19.96

Figure 9 presents the resulting overpressure dynamics for the simulated cases (see Table 4). As expected, Cases 2 and 3 demonstrate a higher pressure peak than for case 1, due to the higher hydrogen mass flow rate (MFR) for the same storage pressure and discharge coefficient but lower storage temperature. The pressure peak recorded for Case 2 with storage temperature $T_S = 200$ K and MFR = 14.11 g/s is 26.95 kPa. The pressure peak increases up to 42.82 kPa for the Case 3 ($T_S = 100$ K, MFR = 23.16 g/s). The higher is the positive pressure peak the higher is the negative pressure peak, which reaches -5.36 kPa.

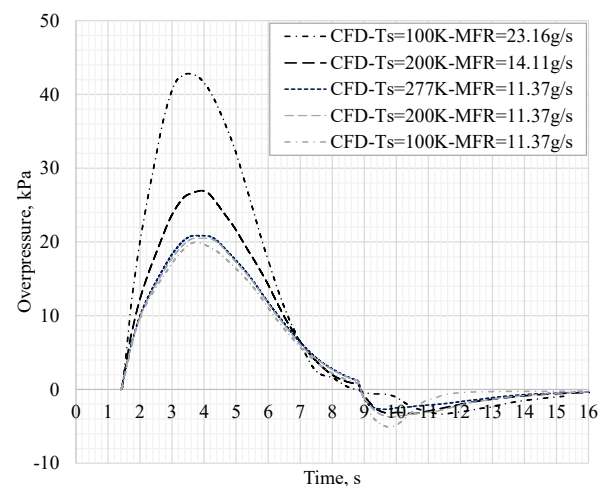


Figure 9. Effect of hydrogen storage temperature on the PPP dynamics in the enclosure with volume of 15 m^3 and three vents with dimensions 7×7 cm.

It is expected that the higher pressure peak for cryogenic releases is associated with a larger difference between the volumetric flow rate entering the enclosure, due to the larger hydrogen MFR and its combustion, and the volumetric flow rate of gases exiting the enclosure through vents. To confirm this generic concept, two limiting cases, i.e., Case 1 ($T_S = 277$ K) and Case 3 ($T_S = 100$ K) are compared. The assessment is based on the PPP theory for ignited hydrogen releases [7]. For the complete combustion of hydrogen in air,

the volumetric flow rate “entering” the enclosure is determined by “competition” between the rate of consumption of cold hydrogen and enclosure air during combustion, and the rate of generation of hot combustion products in reaction at adiabatic flame temperature, T_{ad} . For an arbitrary molar flow rate of hydrogen and assuming an isobaric combustion at atmospheric pressure, the balance of gas volume consumption and generation associated with hydrogen combustion in air can be written as [7]:

$$\dot{V}_{c, in} = \frac{\dot{m}_{H_2}}{M_{H_2}} \frac{RT_{ad}}{P} + \frac{3.76}{2} \frac{\dot{m}_{H_2}}{M_{H_2}} \frac{RT_{ad}}{P} - \frac{(1+3.76)}{2} \frac{\dot{m}_{H_2}}{M_{H_2}} \frac{RT_0}{P} - \frac{\dot{m}_{H_2}}{M_{H_2}} \frac{RT_0}{P} = \frac{\dot{m}_{H_2}}{M_{H_2}} \frac{RT_0}{P} \left(\frac{T_{ad}}{T_0} + \frac{3.76}{2} \frac{T_{ad}}{T_0} - \frac{1+3.76}{2} - 1 \right), \quad (2)$$

where M_{H_2} is the hydrogen molar mass (2 kg/kmol), R is the universal gas constant (8314.4 J/kmol/K) and P is the ambient pressure. T_0 is the initial temperature of the mixture of hydrogen at notional nozzle temperature, T_{NN} , and air at ambient temperature, T_{amb} . The conservation of enthalpy is used to calculate T_0 as follows:

$$c_{p,mix}(m_{H_2} + m_{air})T_0 = c_{p,H_2}m_{H_2}T_{NN} + c_{p,air}m_{air}T_{amb}. \quad (3)$$

Table 5 shows the parameters calculated for the selected Cases 1 and 3. A diffusion flame consumes reactants at a stoichiometric composition, meaning that a mole of hydrogen requires 2.38 mole of air. This corresponds to 1 g of hydrogen, m_{H_2} in Equation (3), consuming 34.8 g of air, m_{air} in Equation (3). Ambient temperature, T_{amb} , is 277 K. The specific heat for air, $c_{p,air}$, is equal to 1010 J/kgK, whereas the specific heat for hydrogen, c_{p,H_2} , is obtained from NIST Chemistry WebBook [31]. Thus, T_0 is calculated as 263.8 K and 228.1 K for T_s equal to 277 K and 100 K, respectively.

Table 5. Effect of storage temperature on combustion parameters and volumetric flow rate balance for limiting cases 1 and 3.

Case	T_s , K	Mass Flow Rate \dot{m}_{H_2} , g/s	T_{NN} , K	T_0 , K	T_{ad} , K	$\frac{\dot{m}_{H_2}}{M_{H_2}} \frac{RT_0}{P}$, m ³ /s	α	$\dot{V}_{c,in}$, m ³ /s
1	277	11.37	230.8	263.8	2370.9	0.123	22.5	2.77
3	100	23.16	67.3	228.1	2351.9	0.217	26.3	5.70

A minor effect of hydrogen storage temperature is observed on T_{ad} , which presents a difference of approximately 20 K. The multiplier $\alpha = \left(\frac{T_{ad}}{T_0} + \frac{3.76}{2} \frac{T_{ad}}{T_0} - \frac{1+3.76}{2} - 1 \right)$ represents the difference between the volumetric flow rate of the unignited release and the ignited release (jet fire) from the same source [7]. The term α increases from 22.5 for $T_s = 277$ K to 26.3 for $T_s = 100$ K. The variation in α and the more significant double increase in mass flow rate for decreasing storage temperature, cause the volumetric flow rate “entering” the enclosure, i.e., the volumetric flow rate resulting from the combustion of the released hydrogen in air, to rise from 2.77 m³/s to 5.70 m³/s. Figure 10 compares the calculated inlet volumetric flow rate resulting from combustion, $\dot{V}_{c,in}$, and the simulated volumetric flow rate exiting the enclosure through the three vents $\dot{V}_{v,out}$. It can be observed that for $T_s = 277$ K, the maximum $\dot{V}_{v,out}$ almost equalises $\dot{V}_{c,in}$. On the other hand, for $T_s = 100$ K, $\dot{V}_{c,in}$ is almost twice the volumetric flow rate going out from the enclosure, and this is the cause for the higher overpressure recorded in the enclosure.

Cases 4 and 5 investigate the effect of only hydrogen storage temperature on the pressure peaking phenomenon while maintaining the same storage pressure and mass of released hydrogen as in Case 1 by reducing the discharge coefficient. Reduction of temperature leads to a slight decrease of pressure peak in the enclosure from 20.95 kPa for $T_s = 277$ K to 20.51 kPa for $T_s = 200$ K and to 19.96 kPa for $T_s = 100$ K if the mass flow rate (11.37 g/s) and the storage pressure (11.78 MPa) are kept the same. This result is expected as a decrease of the hydrogen temperature mixing with air would lead to

a decrease of combustion temperature. As a consequence, after stopping the hydrogen release, combustion products cool down faster for lower hydrogen release temperature. This causes a more pronounced negative pressure as shown in Figure 9.

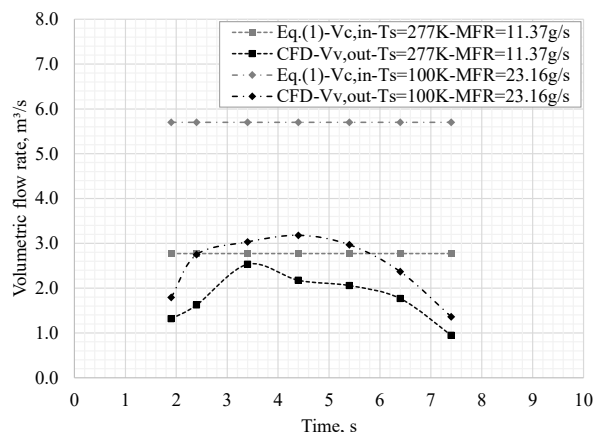


Figure 10. Effect of hydrogen storage temperature on volumetric flow rates entering and exiting the enclosure for the two limiting cases 1 ($T_S = 277$ K) and 3 ($T_S = 100$ K).

It can be concluded that for the same storage pressure and hydrogen mass flow rate (requires, in general case, the decrease of piping diameter for lower temperature), the decrease in storage temperature causes the decrease of enthalpy associated to the entering hydrogen, see Equation (2), and, thus, only a slight reduction of the PPP overpressure in the enclosure. On the other hand, for the same storage pressure, and the same piping system (with the same discharge coefficient) resulting in the increased hydrogen mass flow rate for lower temperature, causes, as a consequence, the increase of the pressure peak in the storage enclosure. As an example, it is observed that for a storage pressure of 11.78 MPa, the hydrogen mass flow rate increases from 11.37 g/s for $T_S = 277$ K to 23.16 g/s for $T_S = 100$ K. Such a variation in mass flow rate leads to a twofold increase in the pressure peak from 20.95 kPa to 42.82 kPa.

5. Conclusions

The *significance* of this work is the development and validation of the time-efficient CFD model as a contemporary engineering tool for hydrogen safety engineering. The unique experiments on the pressure peaking phenomenon (PPP) for ignited hydrogen releases at storage pressures up to 12 MPa in a large-scale 15 m³ enclosure are used to develop and validate the CFD model. The conclusions of the work and CFD model are valid for current onboard storage systems with storage pressure 70 MPa and TPRD diameter up to 0.65 mm.

The *originality* of the study lies in the further development of the CFD model by the application of the volumetric source model capable to drastically improve the time efficiency of computations. Two approaches to model hydrogen release in terms of predictive capability and computational performance are compared: the widely used notional nozzle exit inflow boundary approach and the volumetric source approaches. The volumetric source model allowed a threefold decrease of the simulations time compared to the notional nozzle approach. To further reduce the computational time, a unified size throughout the domain “cube grid” approach employing a volumetric source model was developed. This approach is found to well reproduce the experimental pressure dynamics with $\pm 11\%$ accuracy while reducing the computational time by approximately a factor of 7.5 in comparison to the “standard” notional nozzle exit inflow boundary approach.

The developed and validated CFD model was then applied to assess the effect of hydrogen storage temperature in the range from atmospheric to cryogenic temperatures on the pressure peaking phenomenon. The decrease of storage temperature for the same

storage pressure and discharge coefficient caused an increase in hydrogen mass flow rate, and, thus, a higher overpressure peak. It was found that for the storage pressure of 11.78 MPa, the overpressure peak increased from 20.95 kPa to 42.82 kPa for a temperature drop from 277 K to 100 K. This effect should be accounted for in the design of safety systems for release from cryo-compressed hydrogen storage.

The validation of the CFD model against large-scale experiments underpins the *rigour* of the study. The work expanded the validation domain of the CFD model from enclosures with the free volume of about 1 m³ with release at hydrogen mass flow rates up to 1.1 g/s [10] to the volume of 15 m³ and mass flow rate up to 11.5 g/s in this study with the generation of pressure as large as 48 kPa well above 10–20 kPa that civil structures could withstand. The simulated pressure dynamics and maximum overpressure are found to agree well with experimental data. For example, the deviation of simulations from experimental pressure was within $\pm 5\%$ for Test No.14 with storage pressure of 11.78 MPa and hydrogen mass flow rate of 11.37 g/s. Heat transfer to and through the enclosure walls is found not to affect significantly the resulting overpressure peak, confirming previous observations [10].

Author Contributions: Conceptualization, D.C., D.M. and V.M.; methodology, D.C., D.M. and V.M.; software, D.C.; validation, D.C., D.M. and V.M.; formal analysis, D.C., D.M., V.M., A.W.L. and A.V.G.; investigation, D.C., D.M., V.M., A.W.L. and A.V.G.; resources, D.C., D.M., V.M., A.W.L. and A.V.G.; data curation, D.C., D.M., V.M., A.W.L. and A.V.G.; writing—original draft preparation, D.C.; writing—review and editing, D.C., D.M., V.M., A.W.L. and A.V.G.; visualization, D.C., D.M. and V.M.; supervision, V.M. and D.M.; project administration, V.M. and D.M.; funding acquisition, V.M. All authors have read and agreed to the published version of the manuscript.

Funding: This research has received funding from the Fuel Cells and Hydrogen 2 Joint Undertaking under grant agreement No. 826193 (HyTunnel-CS) and No. 779613 (PRESLHY). The JU receives support from the European Union’s Horizon 2020 research and innovation programme and the United Kingdom, Germany, Greece, Denmark, Spain, Italy, Netherlands, Belgium, France, Norway, Switzerland. The authors would like to acknowledge EPSRC for funding the project Kelvin-2 “Tier 2 High-Performance Computing Services”, EP/T022175/1.

Institutional Review Board Statement: Not applicable.

Informed Consent Statement: Not applicable.

Data Availability Statement: The data presented in this study are publicly available in the cited references.

Conflicts of Interest: The authors declare no conflict of interest. The funders had no role in the design of the study; in the collection, analyses, or interpretation of data; in the writing of the manuscript, or in the decision to publish the results.

References

1. IEA Fuel Cell Electric Vehicle Stock by Segment, 2017–2020. Available online: <https://www.iea.org/data-and-statistics/charts/fuel-cell-electric-vehicle-stock-by-segment-2017-2020> (accessed on 16 December 2021).
2. Veenstra, M.J.; Hobein, B. On-Board Physical Based 70 MPa Hydrogen Storage Systems. *SAE Int. J. Engines* **2011**, *4*, 1862–1871. [CrossRef]
3. United Nations Economic Commission for Europe Global Registry. *Addendum 13: Global technical regulation No. 13. Global Technical Regulation on Hydrogen and Fuel Cell Vehicles*; UNECE: Geneva, Switzerland, 2013.
4. Brennan, S.; Makarov, D.; Molkov, V. Dynamics of Flammable Hydrogen-Air Mixture Formation in an Enclosure with a Single Vent. In Proceedings of the Sixth International Seminar on Fire and Explosion Hazards, Leeds, UK, 11–16 April 2010.
5. Brennan, S.; Molkov, V. Safety assessment of unignited hydrogen discharge from onboard storage in garages with low levels of natural ventilation. *Int. J. Hydrogen Energy* **2013**, *38*, 8159–8166. [CrossRef]
6. Brennan, S.; Molkov, V. Pressure peaking phenomenon for indoor hydrogen releases. *Int. J. Hydrogen Energy* **2018**, *43*, 18530–18541. [CrossRef]
7. Makarov, D.; Shentsov, V.; Kuznetsov, M.; Molkov, V. Pressure peaking phenomenon: Model validation against unignited release and jet fire experiments. *Int. J. Hydrogen Energy* **2018**, *43*, 9454–9469. [CrossRef]
8. Lach, A.W.; Gaathaug, A.V.; Vaagsaether, K. Pressure peaking phenomena: Unignited hydrogen releases in confined spaces—Large-scale experiments. *Int. J. Hydrogen Energy* **2020**, *45*, 32702–32712. [CrossRef]

9. Lach, A.W.; Gaathaug, A.V. Large scale experiments and model validation of Pressure Peaking Phenomena-ignited hydrogen releases. *Int. J. Hydrogen Energy* **2021**, *46*, 8317–8328. [CrossRef]
10. Hussein, H.G.; Brennan, S.; Shentsov, V.; Makarov, D.; Molkov, V. Numerical validation of pressure peaking from an ignited hydrogen release in a laboratory-scale enclosure and application to a garage scenario. *Int. J. Hydrogen Energy* **2018**, *43*, 17954–17968. [CrossRef]
11. Brennan, S.; Hussein, H.G.; Makarov, D.; Shentsov, V.; Molkov, V. Pressure effects of an ignited release from onboard storage in a garage with a single vent. *Int. J. Hydrogen Energy* **2019**, 8927–8934. [CrossRef]
12. DOE. *Technical Assessment: Cryo-Compressed Hydrogen Storage for Vehicular Applications*; 2006. Available online: https://www.energy.gov/sites/default/files/2014/03/f12/cryocomp_report.pdf (accessed on 15 February 2021).
13. Shih, T.H.; Liou, W.W.; Yang, A.; Shabbir, Z. A new eddy-viscosity model for high Reynolds number turbulent flows—Model development and validation. *Comput. Fluids* **1995**, *24*, 227–238. [CrossRef]
14. Cirrone, D.; Makarov, D.; Molkov, V. Thermal radiation from cryogenic hydrogen jet fires. *Int. J. Hydrogen Energy* **2019**, *44*, 8874–8885. [CrossRef]
15. Magnussen, B. On the structure of turbulence and a generalized eddy dissipation concept for chemical reaction in turbulent flow. In Proceedings of the 19th Aerospace Sciences Meeting, St. Louis, MO, USA, 12–15 January 1981.
16. Peters, N.; Rogg, B. *Reduced Kinetic Mechanisms for Applications in Combustion Systems*; Springer: Berlin/Heidelberg, Germany, 1993.
17. Murthy, J.Y.; Mathur, S.R. A finite volume method for radiative heat transfer using unstructured meshes. *36th AIAA Aerosp. Sci. Meet. Exhib.* **1998**, *12*, 313–321. [CrossRef]
18. Molkov, V.; Makarov, V.; Bragin, M.V. Physics and modelling of underexpanded jets and hydrogen dispersion in atmosphere. *Phys. Extrem. States Matter* **2009**, 146–149.
19. Engineers Edge, Thermal Properties of Metals, Conductivity, Thermal Expansion, Specific Heat. Available online: https://www.engineersedge.com/properties_of_metals.htm (accessed on 2 February 2021).
20. Mikron Table of Emissivity of Various Surfaces. Available online: http://www-eng.lbl.gov/~{dw}/projects/DW4229_LHC_detector_analysis/calculations/emissivity2.pdf (accessed on 15 February 2021).
21. Ansys Fluent. *User's Guide*; Ansys Inc.: Canonsburg, PA, USA, 2016.
22. Kee, R.J.; Rupley, F.M.; Miller, J.A.; Coltrin, M.E.; Grcar, J.F.; Meeks, E.; Moffat, H.K.; Lutz, A.E.; Dixon-Lewis, G.; Smooke, M.D.; et al. The Chemkin Thermodynamic Database. In *Chemkin Collection Release 3.6*; Reaction Design: Diego, CA, USA, 2000; ISBN SAND87-8215B.
23. Yates, D. Innovative Solutions to Reduce Separation Distances in On-Board Hydrogen Storage. Ph.D. Thesis, Ulster University, Coleraine, UK, 2016.
24. Schefer, R.; Houf, B.; Bourne, B.; Colton, J. Experimental Measurements to Characterize the Thermal and Radiation Properties of an Open-flame Hydrogen Plume. In Proceedings of the 15th Annual Hydrogen Conference and Hydrogen Expo, Los Angeles, CA, USA, 26–30 April 2004.
25. Cirrone, D.; Makarov, D.; Kuznetsov, M.; Friedrich, A.; Molkov, V. Effect of heat transfer through the release pipe on simulations of cryogenic hydrogen jet fires and hazard distances. In Proceedings of the International Conference on Hydrogen Safety, Edinburgh, Scotland, 21–24 September 2021.
26. *NET-Tools Project Novel Education And Training Tools Based on Digital Applications Related to Hydrogen and Fuel Cell Technology*; European Commission: Brussels, Belgium, 2017.
27. Radebaugh, R. Cryogenics. The MacMillan Encyclopedia of Chemistry. 2002. Available online: https://books.google.com.hk/books?id=RDT-DwAAQBAJ&pg=PA122&lpg=PA122&dq=27.%09Radebaugh,+R.+Cryogenics.+MacMillan+Encycl.+Chem.+2002++,+1%E2%80%933&source=bl&ots=g_TUGwm44h&sig=ACfU3U31tuh2JVSjxrwFonpEBjfyQgEti&hl=zh-TW&sa=X&redir_esc=y&hl=zh-CN&sourceid=cndr#v=onepage&q=27.%09Radebaugh%2C%20R.%20Cryogenics.%20MacMillan%20Encycl.%20Chem.%202002%20%20%2C%201%E2%80%933&f=false (accessed on 15 February 2021).
28. Ahluwalia, R.K.; Peng, J.-K.; Hua, T.Q. Cryo-compressed hydrogen storage. In *Compendium of Hydrogen Energy*; Gupta, R.B., Basile, A., Veziroğlu, T.N., Eds.; Woodhead Publishing: Sawston, UK, 2016; pp. 119–145.
29. Stetson, N.T.; McWhorter, S.; Ahn, C.C. Introduction to hydrogen storage. In *Compendium of Hydrogen Energy*; Gupta, R.B., Basile, A., Veziroğlu, T.N., Eds.; Woodhead Publishing: Sawston, UK, 2016; pp. 3–25.
30. Cirrone, D.; Makarov, D.; Molkov, V. Cryogenic hydrogen jets: Flammable envelope size and hazard distances for jet fire. ID191. In Proceedings of the International Conference on Hydrogen Safety, Adelaide, Australia, 24–26 September 2019.
31. NIST Chemistry WebBook, Thermophysical Properties of Fluid Systems. Available online: <https://webbook.nist.gov/chemistry/fluid/> (accessed on 15 April 2021).
32. Giannisi, S.G.; Venetsanos, A.G.; Cirrone, D.; Molkov, V.; Ren, Z.; Wen, J.; Friedrich, A.; Veser, A. Cold hydrogen blowdown release: An inter-comparison study. ID112. In Proceedings of the 9th International Conference on Hydrogen Safety, Edinburgh, UK, 21–23 September 2021.
33. Veser, A.; Friedrich, A.; Kuznetsov, M.; Jordan, T.; Kotchourko, N. Hydrogen blowdown release experiments at different temperatures in the discha-facility. In Proceedings of the 9th International Conference on Hydrogen Safety, Edinburgh, UK, 21–24 September 2021; pp. 442–454.

Errata

1. Page 13.

Added a missing reference for Molkov et al [27]

2. Page 45. (not included in the text)

The uncertainties data given in Table 6 are given by a manufacturers

Doctoral dissertation no. 130

2022

Hydrogen safety in confined spaces

Dissertation for the degree of Ph.D

Agnieszka Weronika Lach

ISBN: 978-82-7206-677-1 (print)

ISBN: 978-82-7206-678-8 (online)

usn.no

